UNIVERSITÉ DE LIÈGE
Faculté des Sciences Appliquées

The Fast Multipole Method for Electromagnetic Field Computation in Numerical and Physical Hybrid Systems

Ruth VÁZQUEZ SABARIEGO
Ingénieur Civil en Télécommunications
de l'Université de Vigo (Espagne)

Thèse présentée en vue de l'obtention
du grade de Docteur en Sciences Appliquées

Octobre 2004

Acknowledgment

First of all, I wish to thank Professor W. Legros and Dr. P. Dular for the opportunity they gave me to do research in excellent conditions and with great freedom in the Department of Electrical Engineering and Computer Science of the University of Liège. I extend my gratitude to the Belgian government that finances the Inter-University Attraction Poles research project P5/34 (Computational electromagnetics for electrical power applications and interactions with information technology devices), in the frame of which this work has been carried out.

I also thank Professor J. Destiné (University of Liège), Professor L. Dupré (Ghent University), Professor A. Genon (University of Liège), Professor A. Kost (Technical University of Cottbus), Professor F. Piriou (University of Lille) and Professor B. Vanderheyden (University of Liège) for accepting to be members of my thesis committee.

The deeply enriching experience that I have enjoyed during the last four years at the research Unit of Applied Electricity (ELAP) is largely due to the people that have shared my daily life, assisted and influenced me and my work. Their contribution has been invaluable both personally and professionally. In particular, I am deeply indebted to Professor J. Gyselinck and Dr. P. Dular for the countless hours spent advising my research and their involvement in our common works. Further credit goes to Dr. C. Geuzaine who, even across the Ocean, is always ready to provide assistance.

Finally, I want to warmly thank my friends, my colleagues and my Flemish 'foster' family who have helped me get over my homesickness and make life enjoyable even in those periods when research was fruitless. They are simply far too many to mention here.

Most of all, I am very grateful to my parents, my brother and my partner, Johan. Their love and support have been a great source of encouragement and strength to me.

¡Muchísimas gracias a todos!

Liège, October 2004 Ruth Vázquez Sabariego

List of Symbols

Alphanumeric symbols

$\mathbb{R}^3$	: Three-dimensional oriented Euclidean space
$\mathbb{R}^2$	: Two-dimensional oriented Euclidean space
$\underline{x} = (x, y, z)$	: Point $\in \mathbb{R}^3$
$\underline{x} = (x, y)$	: Point $\in \mathbb{R}^2$
$\imath$	: Imaginary unit
$L^2(\Omega)$, $\boldsymbol{L}^2(\Omega)$	: Spaces of square integrable scalar and vector fields over Ω
$H^p(\Omega)$, $\boldsymbol{H}^p(\Omega)$	: pth order Sobolev spaces of scalar and vector fields over Ω
$\boldsymbol{H}(\mathrm{curl}; \Omega)$	: Stream function space $\{\underline{v} \in \boldsymbol{L}^2(\Omega) : \mathrm{curl}\, \underline{v} \in \boldsymbol{L}^2(\Omega)\}$
$\boldsymbol{H}(\mathrm{div}; \Omega)$	: Flux space $\{\underline{v} \in \boldsymbol{L}^2(\Omega) : \mathrm{div}\, \underline{v} \in L^2(\Omega)\}$
$W^p(\Omega)$	: Discrete subspace of $H^1(\Omega)$, $\boldsymbol{H}(\mathrm{curl}; \Omega)$, $\boldsymbol{H}(\mathrm{div}; \Omega)$ and $L^2(\Omega)$ for $i = 0, \ldots, 3$ respectively
$\underline{h}$	: Magnetic field (A/m)
$\underline{b}$	: Magnetic flux density (T)
$\underline{e}$	: Electric field (V/m)
$\underline{d}$	: Electric flux density (C/m^2)
$\underline{j}$	: Electric current density (A/m^2)
$\underline{j}$	: Equivalent magnetic current density (V/m^2)
q	: Electric charge density (C/m^3)
$\underline{m}$	: Magnetisation (A/m)
$\underline{p}$	: Electric polarisation (C/m^2)
$\underline{a}$	: Magnetic vector potential (Wb/m)
$\underline{f}$	: Electric vector potential (C/m)
v	: Electric scalar potential (V)
c	: Speed of light in vacuum ($= 1/\sqrt{\epsilon_0 \mu_0} = 2.99792458\, 10^8$ m/s)
t	: Time (s)
f	: Frequency (Hz)
k	: Wavenumber (m^{-1})
G	: Green function
J_m	: Bessel function of the first kind and order m
Y_m	: Bessel function of the second kind and order m (Weber's function)
$H_m^{(1)}$	: Hankel function of the first kind and order m
$H_m^{(2)}$	: Hankel function of the second kind and order m
j_m	: Spherical Bessel function of the first kind and order m
y_m	: Spherical Bessel function of the second kind and order m

$h_m^{(1)}$: Spherical Hankel function of the first kind and order m
$h_m^{(2)}$: Spherical Hankel function of the second kind and order m
P_l : Legendre polynomial of order l
P_l^m : Associated Legendre function of the first kind degree l and order m
Y_l^m : Spherical harmonic function related to P_l^m
$\mathcal{N}$, $\mathcal{E}$, $\mathcal{F}$, $\mathcal{V}$: Sets of nodes, edges, faces and elements

Greek symbols

Ω : Bounded open set of $\mathbb{R}^3$
Γ : Boundary of Ω ($= \partial\Omega$)
φ : Magnetic scalar potential (A)
σ : Electric conductivity (S/m)
μ : Magnetic permeability (H/m)
μ_0 : Magnetic permeability of vacuum ($= 4\pi\,10^{-7}$ H/m)
μ_r : Relative magnetic permeability ($= \mu/\mu_0$)
ν : Magnetic reluctivity $\nu = 1/\mu$
ϵ : Electric permittivity (F/m)
ϵ_0 : Electric permittivity of vacuum ($\simeq 8.854187817\,10^{-12}$ F/m)
ϵ_r : Relative electric permittivity ($= \epsilon/\epsilon_0$)
χ_m : Magnetic susceptibility
χ_e : Electric susceptibility (F/m)
ω : Angular frequency (Hza)
λ : Wavelength (m)
η : Intrinsic impedance (Ω)
η_0 : Intrinsic impedance of vacuum ($\eta_0 = \sqrt{\mu_0/\epsilon_0} \simeq 120\pi\,\Omega$)

Abbreviations

FEM : Finite element method
IEM : Integral equation method
BEM : Boundary element method
MoM : Method of Moments
FMM : Fast multipole method
EFIE : Electric field integral equation
MFIE : Magnetic field integral equation
CFIE : Combined field integral equation
PEC : Perfectly electric conductor
MEMS : Microelectromechanical Systems

Operators

∂ : Boundary operator
$^{\mathrm{C}}$: Complement

∂_x, ∂_y, ∂_z	: Space derivatives
∂_t	: Time derivative
grad	: Gradient
curl	: Curl
div	: Divergence
dim	: Dimension
$\mathcal{K}$	: Nullspace (kernel)
$\mathcal{D}$	: Domain
$\mathcal{R}$	: Range (codomain)
$\times$	: Vector product
$\cdot$	: Scalar product
$\| \|_K$	: Norm on the domain K
$\Re$, $\Im$	: Real and imaginary parts

Contents

List of Figures

List of Tables

Introduction

Contents

Motivation

Computational electromagnetics is a discipline that connects physics, mathematics, computer science and various application fields. Its purpose is the modelling of electromagnetic systems, i.e. transposing the physical phenomena, completely characterised by Maxwell's equations and the constitutive relations, into a matrix system that will be solved by means of a computer.

Maxwell's theory is valid over a broad range of frequencies and large length scales. There is a continuous quest of modelling techniques that allow to handle accurately increasingly complex structures. These techniques can be roughly classified in two big families:

- ✓ Partial differential equation (PDE) methods, such as the finite difference (FD) method or the finite element (FE) method, solve directly the partial differential equations (PDEs) associated to the electromagnetic problem. The differential form of Maxwell's equations are local relations that must be satisfied by the electromagnetic field at every point in space.

- ✓ Integral equation (IE) methods, such as the boundary element (BE) method or the Method of Moments (MoM), solve for the sources of an electromagnetic field rather than the field itself. The starting point is therefore to obtain a source-field relationship in the form of an integro-differential operator working on the source terms. The integral equation is then obtained by enforcing the appropriate boundary conditions.

The main advantage of differential-equation based methods is their ability to handle arbitrary, inhomogeneous, and nonlinear materials. This ability stems from

the fact that every point in space needs to be discretised. The FE method, contrary to the FD method, uses inherently unstructured meshes what makes it very attractive for solving PDEs on complex geometries [Jonhson, 1987]. Furthermore, automatic mesh adaptation is relatively straightforward [Babuska & Rheinboldt, 1979]. PDE methods yield a sparse system matrix with $\mathcal{O}(N)$ nonzero elements where N is the number of degrees of freedom of the discretised problem at hand. Explicit mechanisms are required to truncate the computational domain when these methods are used for the analysis of open-region problems. Indeed, the magnetic and electric field cannot be neglected far away from the structure under study. Several techniques have been proposed by different authors. The simplest one consists in approximating the infinite domain by a sufficiently large closed domain. In low frequency problems it is frequent to use spatial transformations to reduce an open infinite region to a closed one [Brunotte *et al.*, 1992]. The application of absorbing boundary conditions (ABCs) [Chew, 1995] or a perfectly matched layer (PML) [Berenger, 1994; Fang & Wu, 1995] is more common in scattering problems. Of course, all these truncation strategies constitute a source of errors. A natural choice to rigorously account for the space extending to infinity would be the coupling with an IE method [Zienkiewicz *et al.*, 1977].

IE-based techniques usually involve a smaller number of unknowns than PDE solvers because only the surfaces (contours) of the considered bodies must be discretised. Moreover, boundary conditions at infinity are implicitly accounted for by the Green function and the surrounding space extending to infinity is thus taken into account exactly. BE methods are very popular for the numerical solution of electrostatic or magnetostatic problems with linear, homogeneous media embedded in free space. They are less suitable for nonlinear analysis and eddy current problems. To handle nonlinear material, the BE method can be extended with a volume integral equation or coupled with the FE method. Hybrid FE-BE models are particularly suited for solving open electromagnetic field problems that comprise nonlinear media and movement [Forsman & Kettunen, 1997; Kurz *et al.*, 1998; Fetzer *et al.*, 1999; Barmada *et al.*, 2000; Rischmüller *et al.*, 2000; Fetzer *et al.*, 2000]. They are extensively used for quasi-stationary and scattering problems [Yuan *et al.*, 1990; Jin *et al.*, 1991; Volakis *et al.*, 1997].

However, IE techniques have one significant disadvantage: the matrix of the system of equations is fully populated. The associated memory requirement is at least $O(N^2)$. Additionally, the computational labour may be excessive when solving the matrix either by a direct method (e.g. LU decomposition) or by an iterative technique (e.g. conjugate gradient techniques (CG) or Krylov subspace techniques). The LU decomposition requires $\mathcal{O}(N^3)$ operations and $\mathcal{O}(N^2)$ memory storage. An iterative method requires $\mathcal{O}(N^2)$ operations per iteration, and in general the number of iterations grows with the size of the problem. This significantly limits the size of the problem to be handled.

This disadvantage can be overcome if the linear system of equations is solved iteratively, e.g. by means of GMRES [Saad & Schultz, 1986], in conjunction with a so-called fast method. Methods that perform a matrix-vector multiplication in $\mathcal{O}(N^p)$ operations, with p significantly lower than 2, are called fast methods. In

the literature, three main methods are defined to be fast in this sense: the fast multipole method (FMM) [Rokhlin, 1985; Greengard & Rokhlin, 1987b; Rokhlin, 1990; Engheta *et al.*, 1992; Rokhlin, 1993], the wavelet-based method [Beylkin *et al.*, 1991; Alpert *et al.*, 1993; Kim *et al.*, 1996] and the impedance matrix location method (IML)[Canning, 1990; Canning, 1993].

The FMM, whose study, development and enhancement constitute the aim of this work, is the most popular one. Originally developed for the evaluation of fields in particle systems [Greengard & Rokhlin, 1987a], the FMM method was adapted to the solution of integral equations, both the Laplace equation [Rokhlin, 1985; Greengard & Rokhlin, 1987b; Greengard & Rokhlin, 1988] and the Helmholtz equation [Rokhlin, 1990; Rokhlin, 1993]. Besides reducing the computational cost in every iteration, the FMM brings about a less costly assembly of the system matrix.

The FMM has been successfully and extensively applied to BE models in both high frequency [Song & Chew, 1995; Burkholder & Kwon, 1996] and low frequency problems [Nabors *et al.*, 1992; Buchau *et al.*, 2000]. With regard to hybrid FE-BE models, the FMM had been solely used in scattering applications [Lu & Jin, 1996; Bindiganavale & Volakis, 1997; Eibert *et al.*, 2000; Sheng & Yung, 2002].

Goal of this work

This work contributes to the modelling of electromagnetic phenomena in two-dimensional and three-dimensional structures by hybrid FE-BE or pure BE techniques accelerated by the FMM. The application of the FMM to problems from low frequency (electrostatics, magnetostatics, magnetodynamics, ...) to high frequency (scattering, radiation, ...) in 2D and 3D dimensions is aimed at. With this purpose, an important part of the time devoted to the realisation of this work has been spent on implementing and testing a complete software package. The following strategy has been followed:

- ✓ Conceive an efficient data structure specially adapted to the application of the FMM and easy to integrate into a general software environment: GetDP [GetDP, 1997–2004]. GetDP (a General environment for the treatment of Discrete Problems) was developed by P. Dular and C. Geuzaine in the Department of Electrical Engineering and Computer Sciences of the University the Liège.

- ✓ Implement the geometrical tools (grouping strategy, group centres, neighbour and far groups, ...) and mathematical tools (Green functions and their multipole expansions, incorporation in the iterative solver) required for applying the FMM to the solution of an electromagnetic problem.

- ✓ Design a new truncation method for the multipole expansions that further reduces the computational cost and memory requirements.

- ✓ Analyse hybrid FE-BE problems that may comprise eddy currents, saturation, movement and deformations.

Outline

The present text is organised into five chapters. In Chapter 1, the equations governing electromagnetic phenomena are shortly reminded. The continuous mathematical structure is presented, i.e. the function spaces to which the unknown fields and potentials belong. Some electromagnetic models are studied. The general framework required for the discretisation procedure of fields and potentials is introduced as well.

Chapter 2 deals with the establishment of continuous formulations. Two sets of weak formulations are elaborated. Special attention is paid to the coupling with integral methods.

The bases of integral equations are established in Chapter 3. The developments herein focus on high frequency problems.

Chapter 4 describes the Fast Multipole Method (FMM) for both the Laplace and Helmholtz Green equations. Some aspects relative to the problems involving movement are considered. An adaptive truncation scheme for the Laplace Green function is introduced. Particular attention is paid to its application in conjunction with an iterative method, and to the computational cost and memory requirements.

Some test problems are presented in Chapters 5 and 6. Hybrid FE-BE and pure BE formulations are considered. Though software tools have been implemented for both low and high frequency problems, the original contributions mainly concern low frequency problems. The test cases illustrate the possibilities of the developed software tools and lead to their validation.

Finally, some conclusions are drawn. The efficiency of the FMM is discussed. Some future research lines are pointed out.

Original contributions

This work mainly contributes to the application of the FMM to low frequency problems. Our efforts have been focused on the analysis of different hybrid FE-BE models comprising eddy currents, nonlinearities and movement.

The FMM has been extensively used in scattering applications. Hence, our contribution herein is reduced. The multipole expansions of the Helmholtz Green functions, required for scattering problems, are presented in an original way. Some scattering test cases have been studied in Chapter 6.

Hereafter, a list of contributions that we believe original is drawn up. References to papers published in the frame of this thesis are also cited.

- ✓ An adaptive truncation scheme for the 2D Laplace Green function is elaborated (see Section 4.3.1). This scheme significantly contributes to the computation time savings achieved with the fast multipole method, particularly when dealing with moderate sized problems. To the best of our belief, the FMM is applied for the first time to a hybrid FE-BE eddy current problem in [Sabariego *et al.*, 2004a].

- ✓ The FMM taking movement into account in 2D is considered. Updating the acceleration data (aggregation, disaggregation and translation) for every new position of the moving parts is proved to be simple and computationally cheap (see Section 4.3.1.4). The resolution of a 2D electromechanical problem by means of a hybrid FE-BE model accelerated with the FMM is elaborated in [Sabariego *et al.*, 2003]. The mechanical equation, the saturation (nonlinearity of the material) and the voltage supply (electrical coupling) are taken into account. The application of the FMM to problems comprising movement does not seem to appear in the literature so far. The first accelerated hybrid models involving nonlinearities are reported in [Balasubramanian & Shanker, 2002; Mayergoyz *et al.*, 2003; Sabariego *et al.*, 2003].

- ✓ An adaptive truncation scheme for the 3D Laplace Green function is developed (see Section 4.3.1). The application of the FMM to a 3D problem with movement is treated in Section 4.3.2.4. An electrodynamic levitation device is modelled in [Sabariego *et al.*, 2004d]. Results are compared with measurements. To the best of our knowledge, it is the first time that a 3D hybrid problem comprising movement is solved by applying FMM. A passive and active shielding problem is studied in [Sabariego *et al.*, 2004c] by means of an accelerated 3D finite element-boundary element model. Results are compared with measurements and with results obtained with a 2D FE model.

- ✓ The FMM is further tested on a microelectromechanical (MEMS) device. A pure BE electrostatic problem coupled to a FE elasticity problem is considered in [Sabariego *et al.*, 2004b]. The results are compared with those obtained by some commercial software.

The presented truncation scheme could be straightforwardly extended to the high frequency case.

Chapter 1

Electromagnetic models

Contents

1.1 Introduction

The equations governing macroscopic electromagnetic phenomena are Maxwell's equations [Stratton, 1941; Harrington, 1961; Balanis, 1988]. They consist of a set of coupled first-order partial differential equations interrelating the various components of electric and magnetic fields. The set of four equations can be written in the

three-dimensional Euclidean space $\mathbb{R}^3$ as [1]

$$\operatorname{curl} \underline{h} - \partial_t \underline{d} = \underline{j}, \tag{1.1}$$

$$\operatorname{curl} \underline{e} + \partial_t \underline{b} = 0, \tag{1.2}$$

$$\operatorname{div} \underline{b} = 0, \tag{1.3}$$

$$\operatorname{div} \underline{d} = q, \tag{1.4}$$

where the four vectors $\underline{h}$, $\underline{e}$, $\underline{b}$, $\underline{d}$ are called the magnetic field (A/m), the electric field (V/m), the magnetic flux density (T) and the electric flux density (C/m^2), respectively. The electric charge density q and the current density $\underline{j}$ are the source terms in these equations. Note that the current density $\underline{j}$ is due to different sources (e.g. in conductors the current density is considered to be proportional to the electric field $\sigma\underline{e}$; in generators the source current density $\underline{j}_s$ can be considered as imposed). These equations have been written employing the SI units, the system of electromagnetic units used in this thesis.

Maxwell's brilliant contribution in 1865 [Maxwell, 1891] was the addition of the displacement current $\partial_t \underline{d}$ in Ampère's law ($\operatorname{curl} \underline{h} = \underline{j}$). The presence of this term means that a changing electric field causes a magnetic field. This necessary modification is crucial for rapidly fluctuating fields. Without it there would be no electromagnetic radiation. The generalised Ampère law (1.1) is thus consistent for time-dependent fields. It constitutes together with Faraday's law (1.2) the electromagnetic coupling equations. Electric and magnetic Gauss' laws (1.4)–(1.3) are called equations of conservation. Implicit in Maxwell's equations is the equation of conservation of electric charge, indeed, (1.1) and (1.4) imply

$$\operatorname{div} \underline{j} + \partial_t q = 0. \tag{1.5}$$

If $\underline{j}$ is given for any time, the charge q can be obtained by integrating (1.5) with respect to time. Analogously, Gauss' law (1.3) can be deduced from (1.2) if an initial zero divergence of the magnetic induction is assumed.

If the average electromagnetic properties of a medium are described by a macroscopic magnetisation $\underline{m}$ and electric polarisation $\underline{p}$, the magnetic flux density $\underline{b}$ and the electric flux density $\underline{d}$ are given by

$$\underline{b} = \mu_0(\underline{h} + \underline{m}), \tag{1.6}$$

$$\underline{d} = \epsilon_0 \underline{e} + \underline{p}, \tag{1.7}$$

which are the magnetic and electric constitutive laws, respectively. Further discussion on more general constitutive relations is found in the following section.

Given q, $\underline{j}$, $\underline{m}$, $\underline{p}$ and proper initial values for $\underline{e}$ and $\underline{h}$ at the initial time instant $t = t_0$, the system (1.1)–(1.7) determines $\underline{h}$, $\underline{e}$, $\underline{b}$, $\underline{d}$ for any other time instant t [Bossavit, 1993].

[1] See page i for the definition of symbols.

1.1.1 Constitutive relations

In vacuum and media where the presence of applied electromagnetic field causes no reaction, we have $\underline{m} = 0$ and $\underline{p} = 0$. These systems are thus described by the constants $\mu_0 = 4\pi\,10^{-7}\,\mathrm{H/m}$ and $\epsilon_0 = 1/(\mu_0 c^2)\,\mathrm{F/m}$, where c is the speed of light in vacuum.

In all other media, when field-matter interaction occurs, the system (1.1)–(1.4) can be solved if $\underline{d}$ and $\underline{h}$ are known in terms $\underline{e}$ and $\underline{b}$. These connections are known as constitutive relations,

$$\underline{h} = \underline{h}(\underline{e}, \underline{b})\,, \tag{1.8}$$

$$\underline{d} = \underline{d}(\underline{e}, \underline{b})\,, \tag{1.9}$$

and for conducting media, there is the generalised Ohm law,

$$\underline{j} = \underline{j}(\underline{e}, \underline{b})\,. \tag{1.10}$$

The connections are not necessarily simple and may be nonlinear, may depend on past history (hysteresis), etc. Explicit forms can be found by experimentation or deduced from atomic considerations. In most materials, the polarisation $\underline{p}$ and the magnetisation $\underline{m}$ suffice to summarise the response of the media. This approximation often permits to describe very accurately the macroscopic behaviour of the considered systems [Jackson, 1998]. There is a tremendous diversity in the electric and magnetic properties of the matter, especially in crystalline solids, with ferroelectric and ferromagnetic materials having nonzero $\underline{p}$ or $\underline{m}$ in the absence of applied fields, as well as more ordinary dielectric, diamagnetic and paramagnetic substances. The discipline that deals with the study of all these properties is solid-state physics [Kittel, 1996].

The first constitutive law (1.8) expresses an approximate relation between the magnetisation $\underline{m}$ and the magnetic field $\underline{h}$ in magnetic materials [Jiles, 1991].

Paramagnetic and diamagnetic materials are characterised by a linear law

$$\underline{m} = \chi_m \underline{h}\,, \quad \underline{b} = \mu \underline{h} \tag{1.11 a,b}$$

with $\mu = (1 + \chi_m)\mu_0$, where the magnetic susceptibility χ_m is positive or negative, respectively. It can be a tensor in the case of anisotropic materials. For most bodies, χ_m is too small to matter in numerical simulations ($\chi_m \backsim 10^{-4}$ for Al or Cu).

Ferromagnetic metals (such as Fe, Co, Ni) and their alloys are the exception with susceptibilities up to 10^5. They present a nonlinear and hysteretic behaviour. In practice, the linear law $\underline{b} = \mu \underline{h}$ is often accepted as valid if $|\underline{b}| < 1$ T.

For permanent magnets [Lacroux, 1989], a convenient law is

$$\underline{m} = \chi_m \underline{h} + \underline{h}_m\,, \tag{1.12}$$

which considers a nonzero permanent magnetic field $\underline{h}_m$ supported by the magnet and independent of the local magnetic field $\underline{h}$. However, this law is limited to the

normal working conditions of magnets, which means that $\underline{h}$ and $\underline{b}$ have opposite direction and are not too large. Introducing (1.12) in (1.6), we get

$$\begin{aligned}\underline{b} &= \mu_0(\underline{h} + \chi_m \underline{h} + \underline{h}_m) \\ &= \mu_0(1+\chi_m)\underline{h} + \mu_0 \underline{h}_m \\ &= \mu_0 \mu_r \underline{h} + \mu_0 \underline{h}_m \\ &= \mu \underline{h} + \mu_0 \underline{h}_m, \end{aligned} \tag{1.13}$$

where μ and $\mu_r = 1 + \chi_m$ are the magnetic permeability and the relative magnetic permeability of the material, respectively.

The second constitutive law (1.9) refers to polarisable materials (dielectrics), where charges are too strongly bound to move from their initial position, but loose enough to be pulled a little off their equilibrium when the material is embedded in a macroscopic electric field. It states a simple relation between the polarisation and the electric field

$$\underline{p} = \chi_e \underline{e} + \underline{p}_e. \tag{1.14}$$

Again, the electric susceptibility χ_e can be a tensor to describe an anisotropic behaviour. A permanent polarisation $\underline{p}_e$ is considered for materials exhibiting a permanent polarisation independent of the electric field, such as electrets. Introducing (1.14) in (1.7), we get

$$\begin{aligned}\underline{d} &= \epsilon_0 \underline{e} + \chi_e \underline{e} + \underline{p}_e \\ &= (\epsilon_0 + \chi_e)\underline{e} + \underline{p}_e \\ &= \epsilon_0 \epsilon_r \underline{e} + \underline{p}_e \\ &= \epsilon \underline{e} + \underline{p}_e, \end{aligned} \tag{1.15}$$

where ϵ and $\epsilon_r = 1 + \chi_e/\epsilon_0$ are the electric permittivity and the relative electric permittivity of the material, respectively.

The last constitutive law (1.10), known as Ohm's law, is valid for conductors and generators. In the former, the current density is considered to be proportional to the electric field. In the latter, the source current density $\underline{j}_s$ can be taken as imposed and independent of the local electromagnetic field. It reads

$$\underline{j} = \sigma \underline{e} + \underline{j}_s\,. \tag{1.16}$$

The conductivity σ is always positive (or equal to zero for insulators), and can be a tensor, in order to take an anisotropic behaviour into account. Note that this relation is only valid for nonmoving conductors; for a conductor moving at speed $\underline{v}$, (1.16) becomes $\underline{j} = \sigma(\underline{e} + \underline{v} \times \underline{b}) + \underline{j}_s$.

In case of simple hysteresis models or when the material characteristics are frequency dependent, it is useful to introduce a Fourier transform with respect to the frequency. Constitutive laws thus appear in the form of convolution products. These

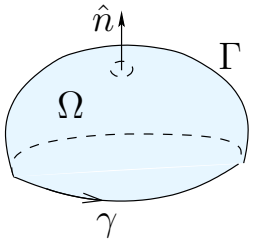

Figure 1.1: Orientation of the closed contour γ

kinds of problems are linear but they have memory, i.e. the value of a field at a given instant depends on the values of another field at that given instant and at precedent instants.

When the dependences in the constitutive equations cannot be considered as linear (e.g. in ferromagnetic materials), or when it is necessary to consider other physical parameters influencing the physical characteristics (e.g. thermal and mechanical effects [Henrotte, 2000]), one should consider σ, ϵ and μ as functions of the fields, which leads to the resolution of a nonlinear problem, with or without memory.

Memoryless linear materials are characterised by constant values of μ, ϵ and σ in (1.13), (1.15) and (1.16), respectively. All the test cases studied and solved belong to this class (see Chapters 5 and 6).

1.1.2 Boundary conditions

Maxwell's equations (1.1)–(1.4) are differential equations that apply locally at each point in space-time. By means of the Stokes and divergence theorems, they can be cast in an integral form. Applying the Stokes theorem to the generalised Ampère law (1.1) and Faraday's law (1.2) we get the corresponding integral equations,

$$\oint_\gamma \underline{h}\,\mathrm{d}\gamma = \int_\Gamma \left(\underline{j} + \partial_t \underline{d}\right) \cdot \hat{n}\,\mathrm{d}\Gamma\,, \tag{1.17}$$

$$\oint_\gamma \underline{e}\,\mathrm{d}\gamma = -\int_\Gamma \partial_t \underline{b} \cdot \hat{n}\,\mathrm{d}\Gamma\,, \tag{1.18}$$

with γ a closed contour, Γ an open surface spanning γ and $\hat{n}$ the unit normal on Γ pointing in the direction given by the right-hand side rule from the sense of the integration around the contour γ (see Figure 1.1).

Let Ω be a finite volume in the three-dimensional Euclidean space $\mathbb{R}^3$, Γ the closed surface bounding it, and $\hat{n}$ the outward unit normal (see Figure 1.1). Then the divergence theorem applied to (1.3) and (1.4) yields

$$\oint_\Gamma \underline{b} \cdot \hat{n}\,\mathrm{d}\Gamma = 0\,, \tag{1.19}$$

$$\oint_\Gamma \underline{d} \cdot \hat{n}\,\mathrm{d}\Gamma = \int_\Omega \rho_v\,\mathrm{d}\Omega\,, \tag{1.20}$$

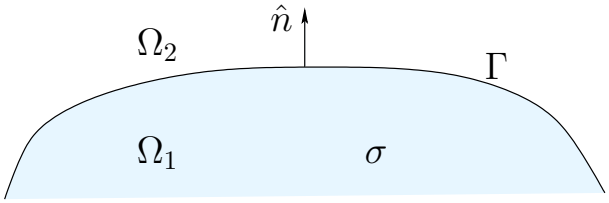

Figure 1.2: Schematic diagram of boundary surface between different media. The boundary region is assumed to carry idealised surface charge and current densities ρ_s and $\underline{j}_s$

where ρ_v is the volume charge density. Equation (1.19) implies that there is no net flux of $\underline{b}$ through a closed surface Γ. Equation (1.20) indicates that the flux of $\underline{d}$ through the surface Γ equals the charge contained inside.

Electromagnetic fields present a discontinuous behaviour at some material interfaces. They are therefore no differentiable. The integral equations (1.17)–(1.20) can be used for deducing the so-called boundary or transmission conditions, i.e. a relationship of normal and tangential components of the fields on either side of an interface between different media.

Let us consider the boundary surface Γ between two continuous media Ω_1 and Ω_2 represented in Figure 1.2. The unit normal $\hat{n}$ on Γ points from Ω_1 to Ω_2. Surface charge and current densities ρ_s and $\underline{j}_s$ can exist on Γ. The transmission conditions can be written as

$$\hat{n} \times (\underline{h}_2 - \underline{h}_1)|_\Gamma = \underline{j}_s \,, \tag{1.21}$$

$$\hat{n} \times (\underline{e}_2 - \underline{e}_1)|_\Gamma = 0 \,, \tag{1.22}$$

$$\hat{n} \cdot (\underline{b}_2 - \underline{b}_1)|_\Gamma = 0 \,, \tag{1.23}$$

$$\hat{n} \cdot (\underline{d}_2 - \underline{d}_1)|_\Gamma = \rho_s \,, \tag{1.24}$$

where the subscripts 1 and 2 refer to fields on the side of the boundary surface in Ω_1 and Ω_2, respectively. These expressions are simply obtained by application of the integral forms of Maxwell's equations to particular surfaces and volumes crossing the interface Γ. Details on their deduction can be found in [Bossavit, 1998a].

Equation (1.21) implies that the tangential component of $\underline{h}$ is discontinuous by an amount equal to the magnitude of the surface current density and whose direction is parallel to $\underline{j}_s \times \hat{n}$. From (1.22), we can see that the tangential component of $\underline{e}$ across an interface is continuous.

The relation between the normal components of $\underline{b}$ and $\underline{d}$ on either side of the interface is expressed by (1.23) and (1.24). The normal component of $\underline{b}$ is continuous and the discontinuity of the normal component of $\underline{d}$ at any point is equal to the surface charge density at that point.

The boundary or transmission conditions (1.21)–(1.24) are useful for solving Maxwell's equations in different regions and then connecting the solutions to obtain the fields throughout all space.

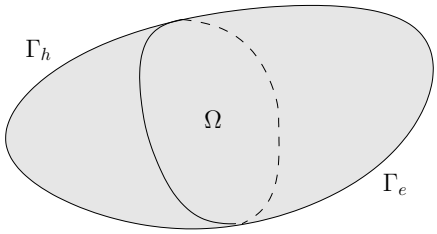

Figure 1.3: Bounded open domain Ω in $\mathbb{R}^3$ with boundary $\Gamma = \Gamma_h \cup \Gamma_e$

1.2 Continuous mathematical structure

We consider a bounded open domain Ω in $\mathbb{R}^3$ with boundary Γ (see Figure 1.3).

Maxwell's equations (1.1)–(1.7) govern the spatial distribution of vector fields (magnetic field $\underline{h}$, electric field $\underline{e}$, magnetic vector potential $\underline{a}$, ...) or scalar fields (electric scalar potential v, magnetic scalar potential φ, ...) in Ω. These fields can be expressed in terms of differential forms, e.g. $\underline{h}$ and $\underline{e}$ are 1-forms; $\underline{b}$ and $\underline{j}$ are 2-forms. This means that the circulations of $\underline{h}$ and $\underline{e}$ along paths are physically meaningful and that the fluxes of $\underline{b}$ and $\underline{j}$ through surfaces are physically meaningful as well. Moreover, three differential operators grad, curl and div appear in (1.1)–(1.7).

A mathematical structure that can welcome partial differential equations must be defined. More specifically, we shall precisely characterise the domains of definition of the differential operators, which are function spaces of vector and scalar fields defined in Ω.

1.2.1 Helmholtz decomposition

The solutions of (1.1)–(1.4) belong to spaces of square integrable scalar and vector fields $L^2(\Omega)$ and $\boldsymbol{L}^2(\Omega)$ (see Appendix A).

The Helmholtz decomposition of $\boldsymbol{L}^2(\Omega)$ into five mutually orthogonal subspaces, widely treated in the literature [Bossavit, 1988a; Kettunen *et al.*, 1998], is crucial to establishing and discretising the continuous formulations.

Figure 1.4 represents the algebraic-differential structure known as the de Rham complex. The horizontal axes represent the spaces $L^2(\Omega)$ and $\boldsymbol{L}^2(\Omega)$ on four levels (0, 1, 2 and 3 for $L^2(\Omega)$, $\boldsymbol{L}^2(\Omega)$, $\boldsymbol{L}^2(\Omega)$ and $L^2(\Omega)$, respectively). Subdivisions of these axes represent their subspaces. Note that the axis on level 2 is exactly the inverted axis on level 1 (i.e. levels 1 and 2 correspond to the same space $\boldsymbol{L}^2(\Omega)$). The arrows between the levels represent the application of the corresponding operators grad, curl and div (i.e. the ends of two arrows determining a subspace and its image).

The subspaces $\mathcal{H}^1(\Omega)$ and $\mathcal{H}^2(\Omega)$ depicted in Figure 1.4 are used in the construction of the continuous formulations and posterior discretisation. $\mathcal{H}^1(\Omega)$ includes the elements with a null curl that are not gradients. It has a finite dimension that equals the number of loops if there exist cutting surfaces [Bossavit, 1988a] in a bounded open set Ω of $\mathbb{R}^3$, the boundary of which is denoted $\partial\Omega = \Gamma$. $\mathcal{H}^2(\Omega)$ is the set of elements with a zero divergence which are not curls. The dimension of $\mathcal{H}^2(\Omega)$ is also

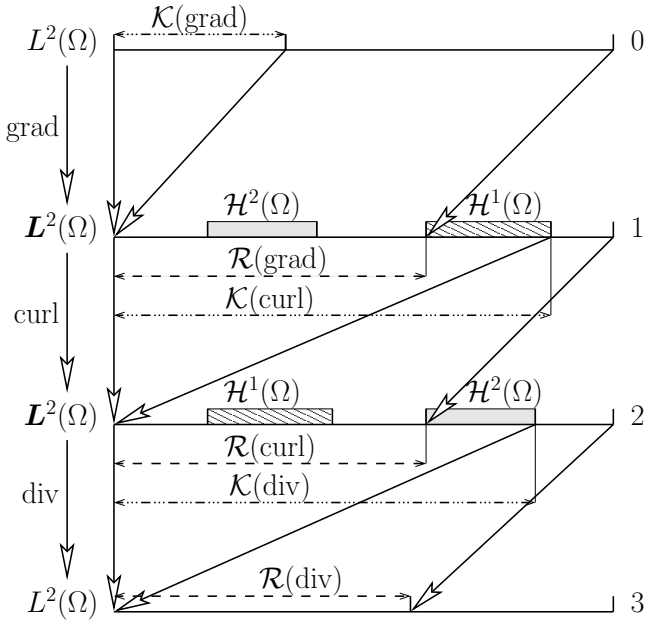

Figure 1.4: De Rham complex in three dimensions over Ω – domain, range and kernel of operators grad, curl and div

finite and equals the number of cavities in Ω. These subspaces are defined as

$$\mathcal{H}^1(\Omega) = \left\{ \underline{u} \in \boldsymbol{L}^2(\Omega) : \operatorname{curl} \underline{u} = 0, \operatorname{div} \underline{u} = 0, \underline{n} \cdot \underline{u}\big|_\Gamma = 0 \right\}, \tag{1.25}$$

$$\mathcal{H}^2(\Omega) = \left\{ \underline{u} \in \boldsymbol{L}^2(\Omega) : \operatorname{curl} \underline{u} = 0, \operatorname{div} \underline{u} = 0, \underline{n} \times \underline{u}\big|_\Gamma = 0 \right\}. \tag{1.26}$$

The domains of the differential operators (grad, curl and div) are defined in a restrictive way, i.e. they are defined as subspaces of $L^2(\Omega)$ and $\boldsymbol{L}^2(\Omega)$ satisfying appropriate boundary conditions [Bossavit, 1989]. The domain, range and kernel of these differential operators (see Appendix A.1.2) in (1.1)–(1.4) are also depicted in Figure 1.4.

1.2.2 Tonti diagram

Let Γ_h and Γ_e denote two complementary parts of the boundary Γ of Ω (see Figure 1.3), so that

$$\Gamma = \Gamma_h \cup \Gamma_e \quad \text{and} \quad \Gamma_h \cap \Gamma_e = \emptyset, \tag{1.27}$$

where scalar fields u_h or u_e, or the trace of vector fields $\underline{u}_h$ or $\underline{u}_e$, are imposed, respectively.

The basic continuous structure is formed by two dual de Rham complexes (see Appendix A.1.3), put into correspondence in the following Tonti diagram [Bossavit,

1988b; Bossavit, 1989]:

$$\begin{array}{ccc} H_h^1(\Omega) & \longrightarrow & L^2(\Omega) \\ \downarrow{\scriptstyle \mathrm{grad}_h} & & \uparrow{\scriptstyle \mathrm{div}_e} \\ \boldsymbol{H}_h(\mathrm{curl};\Omega) & \longrightarrow & \boldsymbol{H}_e(\mathrm{div};\Omega) \\ \downarrow{\scriptstyle \mathrm{curl}_h} & & \uparrow{\scriptstyle \mathrm{curl}_e} \\ \boldsymbol{H}_h(\mathrm{div};\Omega) & \longrightarrow & \boldsymbol{H}_e(\mathrm{curl};\Omega) \\ \downarrow{\scriptstyle \mathrm{div}_h} & & \uparrow{\scriptstyle \mathrm{grad}_e} \\ L^2(\Omega) & \longrightarrow & H_e^1(\Omega) \end{array} \tag{1.28}$$

Both complexes (1.28) will be referred to as either primal or dual depending on the formulation we are dealing with (e.g. the complex on the left is the primal complex for magnetic field conforming formulations, but the dual complex for magnetic flux density conforming formulations).

The domains of the operators grad_h, curl_h and div_h are given by

$$H_h^1(\Omega) = \{u \in L^2(\Omega) : \mathrm{grad}\, u \in \boldsymbol{L}^2(\Omega), u|_{\Gamma_h} = u_h\}, \tag{1.29}$$
$$\boldsymbol{H}_h(\mathrm{curl};\Omega) = \{\underline{u} \in \boldsymbol{L}^2(\Omega) : \mathrm{curl}\, \underline{u} \in \boldsymbol{L}^2(\Omega), \underline{n} \times \underline{u}|_{\Gamma_h} = \underline{n} \times \underline{u}_h\}, \tag{1.30}$$
$$\boldsymbol{H}_h(\mathrm{div};\Omega) = \{\underline{u} \in \boldsymbol{L}^2(\Omega) : \mathrm{div}\, \underline{u} \in L^2(\Omega), \underline{n} \cdot \underline{u}|_{\Gamma_h} = \underline{n} \cdot \underline{u}_h\}, \tag{1.31}$$

and the domains of the operators grad_e, curl_e and div_e by

$$H_e^1(\Omega) = \{u \in L^2(\Omega) : \mathrm{grad}\, u \in \boldsymbol{L}^2(\Omega), u|_{\Gamma_e} = u_e\}, \tag{1.32}$$
$$\boldsymbol{H}_e(\mathrm{curl};\Omega) = \{\underline{u} \in \boldsymbol{L}^2(\Omega) : \mathrm{curl}\, \underline{u} \in \boldsymbol{L}^2(\Omega), \underline{n} \times \underline{u}|_{\Gamma_e} = \underline{n} \times \underline{u}_e\}, \tag{1.33}$$
$$\boldsymbol{H}_e(\mathrm{div};\Omega) = \{\underline{u} \in \boldsymbol{L}^2(\Omega) : \mathrm{div}\, \underline{u} \in L^2(\Omega), \underline{n} \cdot \underline{u}|_{\Gamma_e} = \underline{n} \cdot \underline{u}_e\}. \tag{1.34}$$

By applying Green's formulae (see Appendix A.3), it is easy to prove the adjoint operators of grad_h, curl_h and div_h are $\mathrm{grad}_h^* = -\mathrm{div}_e$, $\mathrm{curl}_h^* = \mathrm{curl}_e$ and $\mathrm{div}_h = -\mathrm{grad}_e$, respectively. Assuming homogeneous boundary conditions (i.e. for which the traces u_h, $\underline{n} \times \underline{u}_h$, $\underline{n} \cdot \underline{u}_h$, u_e, $\underline{n} \times \underline{u}_e$ or $\underline{n} \cdot \underline{u}_e$ vanish on Γ_h and Γ_e, respectively) , these adjoint operators verify

$$(\mathrm{grad}_h\, u, \underline{v}) = (u, \mathrm{grad}_h^*\, \underline{v}) = (u, -\mathrm{div}_e\, \underline{v}), \quad \forall u \in \mathcal{D}(\mathrm{grad}_h), \forall \underline{v} \in \mathcal{D}(\mathrm{grad}_h^*)\,, \tag{1.35}$$
$$(\mathrm{curl}_h\, \underline{u}, \underline{v}) = (\underline{u}, \mathrm{curl}_h^*\, \underline{v}) = (\underline{u}, \mathrm{curl}_e\, \underline{v}), \quad \forall \underline{u} \in \mathcal{D}(\mathrm{curl}_h), \forall \underline{v} \in \mathcal{D}(\mathrm{curl}_h^*)\,, \tag{1.36}$$
$$(\mathrm{div}_h\, \underline{u}, v) = (\underline{u}, \mathrm{div}_h^*\, v) = (\underline{u}, -\mathrm{grad}_e\, v), \quad \forall \underline{u} \in \mathcal{D}(\mathrm{div}_h), \forall v \in \mathcal{D}(\mathrm{div}_h^*)\,. \tag{1.37}$$

Assuming homogeneous boundary conditions, we obtain spaces parallel to the domains of the differential operators defined above, that will serve as function spaces for the test functions used in weak formulations. For the sake of conciseness, these spaces are denoted by $H_h^{10}(\Omega)$, $\boldsymbol{H}_h^0(\mathrm{curl};\Omega)$, $\boldsymbol{H}_h^0(\mathrm{div};\Omega)$, $H_e^{10}(\Omega)$, $\boldsymbol{H}_e^0(\mathrm{curl};\Omega)$ and $\boldsymbol{H}_e^0(\mathrm{div};\Omega)$.

Maxwell's equations (1.1)–(1.4) together with the constitutive relations (1.13), (1.15) and (1.16) fit naturally in (1.28). Indeed, vector fields like the magnetic field $\underline{h}$

or the electric field $\underline{e}$, for which it is physically meaningful to compute the circulation along a contour, belong to $\boldsymbol{H}(\mathrm{curl};\Omega)$ and correspond to differential forms of degree one (1-forms). Vector fields like the magnetic flux density $\underline{b}$ or the current density $\underline{j}$, for which it is physically meaningful to compute the flux across a surface, belong to $\boldsymbol{H}(\mathrm{div};\Omega)$ and correspond to differential forms of degree two (2-forms). Similarly, scalar fields like the electric potential $\varphi \in \mathcal{H}^1(\Omega)$ or the electric charge density $q \in L^2(\Omega)$, which are evaluated locally or integrated over a volume, correspond to differential forms of degree zero and three (0-forms and 3-forms). The function spaces appropriate to the fields $\underline{h}$, $\underline{d}$, $\underline{j}$, $\underline{e}$ and $\underline{b}$ are thus:

$$\underline{h} \in \boldsymbol{H}_h(\mathrm{curl};\Omega), \quad \underline{d}, \underline{j} \in \boldsymbol{H}_h(\mathrm{div};\Omega),$$
$$\underline{e} \in \boldsymbol{H}_e(\mathrm{curl};\Omega), \quad \text{and} \quad \underline{b} \in \boldsymbol{H}_e(\mathrm{div};\Omega).$$

They constitute the domains of definition of the differential operators that can be applied to these fields. These domains of definition account for the boundary conditions; the physical constraint of finite energy is satisfied as well.

Considering the fields $\underline{h}$, $\underline{d}$, $\underline{j}$, $\underline{e}$ and $\underline{b}$ and their respective function spaces, the equations, the constitutive relations and the boundary conditions can thus be summarised in a Tonti diagram (1.28). The equations appear vertically on both sides of the diagram, and can be considered to have a purely geometrical character. The constitutive relations appear horizontally, and have no associated geometrical notion. What concerns the boundary conditions, they are directly taken into account in the domains of definitions of the differential operators. Note that the Tonti diagram (1.28) can be generalised for time-varying problems by adding a third dimension. The electrostatic, magnetostatic and magnetodynamic models will be considered in the following section. These three applications fit naturally in (1.28).

At the discrete level and for a given formulation, it is not possible to satisfy exactly both sides of the Tonti diagram and the constitutive relations. Formulations which respect the left-hand side of the Tonti diagram are called magnetic field conforming ($\underline{h}$-conforming); formulations which respect the right-hand side of the Tonti diagram are called magnetic flux density conforming ($\underline{b}$-conforming). Both types of formulations have advantages and disadvantages. The $\underline{h}$-conforming formulations allow to satisfy exactly Ampère's law. Using the $\underline{b}$-conforming formulations, Faraday's law will be exactly satisfied.

A multiplicity of partial differential equation models [Bossavit, 1989; Henrotte, 2000; Meys, 1999] can be expressed by structures like (1.28).

1.3 Models

Concrete electromagnetic problems in electromagnetism rarely require the solution of the general Maxwell equations (1.1)–(1.7). Different simplifications are possible and generate different models. Among them, it is worth mentioning the following:

- ✓ harmonic state,

- ✓ steady-state problems (electrostatics, magnetostatics...),
- ✓ eddy currents theory (magnetodynamics).

1.3.1 Harmonic state

Maxwell's equations can be solved in the frequency domain when the excitation is sinusoidal in time and if all the constitutive laws are linear [Schelkunoff, 1964; Ramo *et al.*, 1984]. In that case, any solution field can also be described by a sinusoidal variation as

$$f(\underline{x},t) = f_m(\underline{x})\cos(\omega t + \varphi(\underline{x})), \tag{1.38}$$

where $\omega = 2\pi f$ is the angular frequency of the excitation, and $\varphi(\underline{x})$ is a phase angle (in radians) which can be position dependent.

The complex formalism consists in defining this physical field as the real part of a complex field, i.e.:

$$f(\underline{x},t) = \Re(f_m(\underline{x})e^{\imath(\omega t+\varphi(\underline{x}))}) = \Re(f_p(\underline{x})e^{\imath\omega t}), \tag{1.39}$$

where $\imath = \sqrt{-1}$ denotes the imaginary unit and $f_p(\underline{x}) = f_m(\underline{x})e^{\imath\varphi(\underline{x})} = f_r(\underline{x}) + \imath f_i(\underline{x})$ is called a phasor having real and imaginary parts $f_r(\underline{x})$ and $f_i(\underline{x})$.

If all physical fields are assumed to be phasors as in (1.39), Maxwell's equations (1.1)–(1.4) in frequency domain read

$$\operatorname{curl}\underline{h} - \imath\omega\underline{d} = \underline{j}, \tag{1.40}$$
$$\operatorname{curl}\underline{e} + \imath\omega\underline{b} = 0, \tag{1.41}$$
$$\operatorname{div}\underline{b} = 0, \tag{1.42}$$
$$\operatorname{div}\underline{d} = q. \tag{1.43}$$

Note that through (1.39), the time derivative operator becomes a product by the factor $\imath\omega$.

1.3.2 Steady-state problems

The electromagnetic phenomena are considered as time-independent, i.e. $\partial_t\underline{d} = 0$ and $\partial_t\underline{b} = 0$. Maxwell's equations and the constitutive relations (1.1)–(1.7) can be decoupled into two independent systems that model electrostatic and magnetostatic phenomena, respectively.

1.3.2.1 Electrostatics

Electrostatics refers to the phenomena involving time-independent distributions of charges and fields. In this case, $\partial_t\underline{b} = 0$, and thus $\operatorname{curl}\underline{e} = 0$. The set of Maxwell's equations (1.1)–(1.4) together with the electric constitutive law (1.7) are reduced to

$$\operatorname{curl}\underline{e} = 0\,, \quad \operatorname{div}\underline{d} = q\,, \quad \underline{d} = \epsilon\,\underline{e}. \tag{1.44 a–c}$$

From equation (1.44 a) it follows that $\underline{e}$ is the gradient of a scalar function v, the electric scalar potential:

$$\underline{e} = -\text{grad}\, v\,. \tag{1.45}$$

Combining (1.45) and (1.44 b), a Poisson equation is obtained:

$$-\,\text{div}\,(\epsilon\,\text{grad}\, v) = q\,. \tag{1.46}$$

In charge-free regions, the electric scalar potential v satisfies the Laplace equation:

$$-\,\text{div}\,(\text{grad}\, v) = -\Delta v = 0\,. \tag{1.47}$$

Appropriate boundary conditions are required to ensure a physically meaningful solution for the Poisson (or Laplace) equation. The Dirichlet boundary condition consists in specifying the potential on a surface. The Neumann boundary condition specifies the electric field (normal derivative of the potential) on the surface.

When $\epsilon = \epsilon_0$ throughout space, the electric scalar potential v in terms of the electric charge density q is given by

$$v(\underline{x}) = \frac{1}{4\pi\epsilon_0}\int_{\mathbb{R}^3}\frac{q(\underline{y})}{|\underline{x}-\underline{y}|}d\underline{y}\,. \tag{1.48}$$

The electrostatic model fits naturally in the Tonti diagram (1.28). The unknown fields $\underline{d} \in \boldsymbol{H}_h(\text{div};\Omega)$ and $\underline{e} \in \boldsymbol{H}_e(\text{curl};\Omega)$ solutions of (1.44) together with the constitutive law (1.15), and the electric scalar potential $v \in H^1_e(\Omega)$, which verifies (1.45), can be introduced in (1.28). The electrostatic Tonti diagram is given by

$$\begin{array}{ccc} & & 0 \\ & & \uparrow \text{curl}_e \\ \underline{d} & \underline{d} = \epsilon\underline{e} & \underline{e} \\ \downarrow \text{div}_h & & \uparrow \text{grad}_e \\ q & & v \end{array} \tag{1.49}$$

Note that the electric scalar potential v is placed at a level lower than the field it originates.

1.3.2.2 Magnetostatics

In a similar way, considering $\partial_t \underline{d} = 0$ in Maxwell's equations (1.1)–(1.4) and the magnetic constitutive law (1.6), we have for the magnetostatic case

$$\text{curl}\,\underline{h} = \underline{j}, \quad \text{div}\,\underline{b} = 0 \quad \text{and} \quad \underline{b} = \mu\underline{h}\,. \tag{1.50 a–c}$$

The current density $\underline{j} = \underline{j}_s$ is given in some regions and determines $\underline{b}$ and $\underline{h}$ in the whole space. Permanent magnets can be considered as another source if the magnetic constitutive relation $\underline{b} = \mu\underline{h}$ is rewritten as in (1.13).

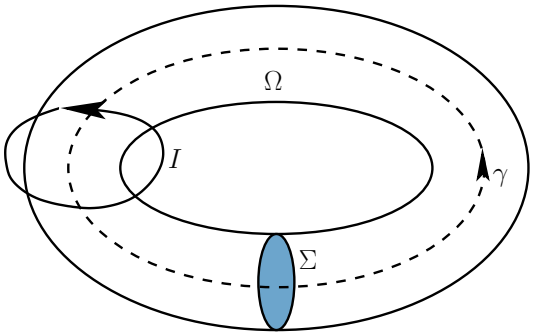

Figure 1.5: Toroidal domain Ω, a multiply connected domain

Under certain conditions, the magnetic field $\underline{h}$ and the magnetic flux density $\underline{b}$ can be expressed in terms of a magnetic scalar potential φ and a magnetic vector potential $\underline{a}$, respectively. The use of these auxiliaries reduces considerably the computational cost.

If a field $\underline{h}_s$ is defined in Ω as

$$\operatorname{curl} \underline{h}_s = \underline{j}_s \,, \tag{1.51}$$

and if the associated field $\underline{h}_r$ is defined such as $\underline{h} = \underline{h}_s + \underline{h}_r$, then this field $\underline{h}_r$ can be derived from a magnetic scalar potential φ, i.e.

$$\underline{h}_r = -\operatorname{grad} \varphi. \tag{1.52}$$

The source magnetic field obeying (1.51) is not unique. Assuming $\mu = \mu_0$ everywhere in Ω (all magnetic materials are removed from the domain), the one calculated by Biot-Savart law [Jackson, 1998] at any point $\underline{x}$ of Ω,

$$\underline{h}_s(\underline{x}) = \frac{1}{4\pi} \int_{\mathbb{R}^3} \frac{\underline{j}_s(\underline{y}) \times (\underline{x} - \underline{y})}{|\underline{x} - \underline{y}|^3} d\underline{y} \,, \tag{1.53}$$

verifies $\operatorname{div} \underline{h}_s = 0$. This condition is an implicit gauge.

In this case, the field $\underline{h}_r$ is due to the magnetisation of the magnetic materials and is called the reaction field (and φ is called the reaction potential).

Note that on account of (1.52), the continuity of the tangential component of the magnetic field is ensured if the scalar potential is continuous. Equation (1.52) implies that the line integral of $\underline{h}_r$ along a curve γ from points $\underline{x}$ to $\underline{y}$ equals the difference between the scalar potentials at the extremes of the curve, i.e.

$$\int_\gamma \underline{h}_r \, \mathrm{d}\gamma = \int_\gamma -\operatorname{grad} \varphi \, \mathrm{d}\gamma = \varphi_x - \varphi_y \,. \tag{1.54}$$

When the curve is closed, $\underline{x} \equiv \underline{y}$, the circulation of $\underline{h}_r$ vanishes ($\varphi_x = \varphi_y$). This is the case of a torus crossed by a wire carrying a current (see Figure 1.5).

By reason of Ampère's law (1.1), this circulation (1.54) cannot be zero. Equation (1.52) is only valid if a cut Σ, on which a discontinuity of potential is imposed, can be defined [Dautray & Lions, 1988; Bossavit, 1988a].

The zero divergence ensured by (1.53) is not mandatory. In fact, a whole family of $\underline{h}_s$ verifying (1.51) exists. The field $\underline{h}_s$ with $\operatorname{div} \underline{h}_s = 0$ is the only physical field of those. It can be useful to choose other fields in this family and impose a gauge. The so-called generalised source magnetic fields have no physical meaning. The generalised magnetic field $\underline{h}_s$ will be chosen equal to zero everywhere outside the conductors, except in the vicinity of their associated cuts [Dular *et al.*, 1997].

Taking into account (1.50 b), the magnetic flux density $\underline{b}$ can be derived from a vector potential $\underline{a}$ such that

$$\underline{b} = \operatorname{curl} \underline{a}. \tag{1.55}$$

However this vector potential is not unique. In fact, if $\underline{a}' = \underline{a} + \operatorname{grad} f$ then $\operatorname{curl} \underline{a}' = \operatorname{curl} \underline{a}$ (where f is an arbitrary function). A gauge is necessary to ensure the uniqueness of $\underline{a}$. A possible gauge is the Coulomb gauge [Biró & Preis, 1989]

$$\operatorname{div} \underline{a} = 0\,, \tag{1.56}$$

which implies the continuity of the normal component of the vector potential $\underline{a}$. Other gauges can be envisaged. Let us consider the condition

$$\underline{a} \cdot \underline{w} = 0\,, \tag{1.57}$$

where $\underline{w}$ is a vector field with open field lines that can connect any pair of points in the domain under study [Albanese & Rubinacci, 1990]. If $\underline{a}_1$ and $\underline{a}_2$ verify $\operatorname{curl} \underline{a}_1 = \operatorname{curl} \underline{a}_2$ and then $\operatorname{curl} \delta\underline{a} = \operatorname{curl} (\underline{a}_1 - \underline{a}_2) = 0$. Moreover, if $\underline{a}_1$ and $\underline{a}_2$ satisfy also (1.57), then $\delta\underline{a} \cdot \underline{w} = 0$, and it holds

$$\int_{\gamma_{xy}} \delta\underline{a}\, \mathrm{d}\gamma = \int_{\gamma_{xy}} \operatorname{grad} f\, \mathrm{d}\gamma = f(\underline{y}) - f(\underline{x}) = 0, \quad \forall \underline{y}, \underline{x} \in \Omega\,, \tag{1.58}$$

where γ_{xy} is a path along the field lines of $\underline{w}$. This shows that the function f is constant and that $\delta\underline{a} = \operatorname{grad} f = 0$, i.e. $\underline{a}_1 = \underline{a}_2$. Condition (1.57) is thus a gauge condition.

If $\mu = \mu_0$ throughout space, the magnetic vector potential $\underline{a}$ can be expressed as

$$\underline{a}(\underline{x}) = \frac{\mu_0}{4\pi} \int_{\mathbb{R}^3} \frac{\underline{j}(\underline{y})}{|\underline{x} - \underline{y}|} d\underline{y}\,. \tag{1.59}$$

The magnetostatic model fits naturally in the Tonti diagram (1.28). The unknown fields $\underline{h} \in \boldsymbol{H}_h(\operatorname{curl}; \Omega)$, $\underline{j} \in \boldsymbol{H}_h(\operatorname{div}; \Omega)$ and $\underline{b} \in \boldsymbol{H}_e(\operatorname{div}; \Omega)$, solutions of (1.50) together with the constitutive law (1.13), and the potentials $\varphi \in H^1_h(\Omega)$ and $\underline{a} \in \boldsymbol{H}_e(\operatorname{curl}; \Omega)$, which verify (1.52) and (1.55), respectively, can be introduced in (1.28). The magnetostatic Tonti diagram is presented in (1.60). Note that the potentials are placed at a level lower than the field they originate. The function spaces $H^1_h(\Omega)$, $\boldsymbol{H}_h(\operatorname{curl}; \Omega)$, $\boldsymbol{H}_h(\operatorname{div}; \Omega)$, $\boldsymbol{H}_e(\operatorname{curl}; \Omega)$ and $\boldsymbol{H}_e(\operatorname{div}; \Omega)$ have been defined in

Section 1.2.2 and contain the boundary conditions applicable to the fields on the complementary parts Γ_h and Γ_e of the domain Ω (see Figure 1.3).

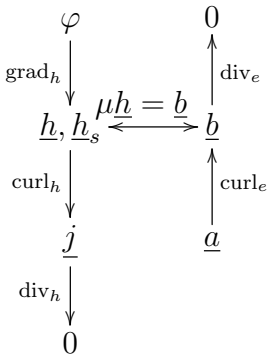

(1.60)

1.3.3 Magnetodynamics: eddy current theory

In this model, the displacement currents $\partial_t \underline{d}$ in (1.1) are negligible. This approximation is valid when the wavelength $\lambda = c/f$ is much greater than the characteristic size of Ω. Maxwell's equations (1.1)–(1.4) can thus be particularised to

$$\operatorname{curl} \underline{e} = -\partial_t \underline{b}, \quad \operatorname{curl} \underline{h} = \underline{j}, \quad \operatorname{div} \underline{b} = 0\,. \tag{1.61 a–c}$$

The system is then completed with the constitutive relations (1.13) and (1.16) in conducting regions Ω_c, i.e.

$$\underline{b} = \mu \underline{h}\,, \quad \underline{j} = \sigma \underline{e}\,. \tag{1.62 a,b}$$

Given initial and boundary conditions, the magnetic field $\underline{h}$, the current density $\underline{j}$, the electric field $\underline{e}$ and the magnetic flux density $\underline{b}$ suffice to characterise an electromagnetic state. However, potentials help to reduce the computational cost associated with the resolution of the magnetodynamic formulations.

In nonconducting regions Ω_c^{C}, the magnetic field $\underline{h}$ is decomposed (since $\underline{j} = 0$ in Ω_c^{C}) as

$$\underline{h} = \underline{h}_s + \underline{h}_r, \quad \text{with} \quad \operatorname{curl} \underline{h}_s = \underline{j}_s \quad \text{and} \quad \operatorname{curl} \underline{h}_r = 0\,, \tag{1.63}$$

and the reaction field $\underline{h}_r$ can be derived from a magnetic scalar potential φ,

$$\underline{h}_r = -\operatorname{grad} \varphi. \tag{1.64}$$

Considering (1.61 c), analogously to the magnetostatic case, the magnetic flux density $\underline{b}$ can be derived from a magnetic vector potential $\underline{a}$ that verifies

$$\underline{b} = \operatorname{curl} \underline{a}. \tag{1.65}$$

Equation (1.2) implies that $\operatorname{curl}(\underline{e} + \partial_t \underline{a}) = 0$, which leads to the definition of an electric scalar potential v such that

$$\underline{e} = -\partial_t \underline{a} - \operatorname{grad} v. \tag{1.66}$$

As in the magnetostatic case, a gauge condition has to be defined in order to ensure the uniqueness of the vector potential. Again the gauges (1.56) and (1.57), defined

in Section 1.3.2.2, are valid [Biró & Preis, 1989; Albanese & Rubinacci, 1990]. An implicit gauge in Ω_c is provided by setting the electric scalar potential v to zero in the conducting regions. This leads to the generalisation of the so-called modified magnetic vector potential formulation [Emson & Simkin, 1983; Kameari, 1990].

The magnetodynamic model can also be fitted in the Tonti diagram (1.28) presented in Section 1.2.2. The unknown fields $\underline{h} \in \boldsymbol{H}_h(\mathrm{curl};\Omega)$, $\underline{j} \in \boldsymbol{H}_h(\mathrm{div};\Omega)$, $\underline{b} \in \boldsymbol{H}_e(\mathrm{div};\Omega)$ and $\underline{e} \in \boldsymbol{H}_e(\mathrm{curl};\Omega)$ (solutions of the system constituted by (1.61) and the constitutive laws (1.13) and (1.16)) and the potentials $\varphi \in H^1_h(\Omega)$, $\underline{a} \in \boldsymbol{H}_e(\mathrm{curl};\Omega)$ and $v \in H^1_e(\Omega)$ (verifying (1.64), (1.65) and (1.66), respectively) can be introduced in (1.28). The function spaces $H^1_h(\Omega)$, $\boldsymbol{H}_h(\mathrm{curl};\Omega)$, $H^1_e(\Omega)$, $\boldsymbol{H}_e(\mathrm{curl};\Omega)$ and $\boldsymbol{H}_e(\mathrm{div};\Omega)$, defined in Section 1.2.2, contain the boundary conditions applicable to the fields on the complementary boundaries Γ_h and Γ_e of Ω.

The magnetodynamic Tonti diagram (where the time derivative has been abstracted) is then

$$
\begin{array}{ccc}
\varphi & & 0 \\
\downarrow{\scriptstyle \mathrm{grad}_h} & & \uparrow{\scriptstyle \mathrm{div}_e} \\
\underline{h} & \xleftrightarrow{\ \mu\underline{h} = \underline{b}\ } & \underline{b} \\
\downarrow{\scriptstyle \mathrm{curl}_h} & & \uparrow{\scriptstyle \mathrm{curl}_e} \\
\underline{j}, \underline{d} & \xleftrightarrow{\ \underline{j} = \sigma\underline{e}\ } & \underline{e}, \underline{a} \\
\downarrow{\scriptstyle \mathrm{div}_h} & & \uparrow{\scriptstyle \mathrm{grad}_e} \\
q & & v
\end{array}
\tag{1.67}
$$

1.4 Discrete mathematical structure

The aim of this section is to present the general framework required for the discretisation of the formulations presented in Chapter 2. The discretisation process consists in replacing the continuous spaces $\mathcal{H}^1(\Omega)$, $\boldsymbol{H}(\mathrm{curl};\Omega)$, $\boldsymbol{H}(\mathrm{div};\Omega)$ and $L^2(\Omega)$ by some discrete subspaces. The structure of the complexes in (1.28) should be preserved. A finite element (FE) method is a discretisation method in which discrete subspaces with piecewise elements are defined on discretised domains [Jonhson, 1987].

The theory of mixed finite elements (curl-conforming and div-conforming finite elements) has been extensively covered in the literature, e.g. for computational electromagnetics [Mur & de Hoop, 1985; Webb & Forghani, 1993].

The introduction of the Whitney elements by Bossavit in 1988 [Bossavit, 1988b] was a great step forward. Whitney elements are the finite element interpolating functions that correspond to the discrete differential forms, the Whitney forms. Whitney forms are a family of differential forms on a mesh (e.g. a mesh of tetrahedra) defined in such a way that p-forms are determined by their integrals on p-simplices ($p = 0$ for nodes, 1 for edges, etc.).

The sequence of Whitney elements was originally developed for tetrahedra [Bossavit, 1998b]. A generalisation for hexahedral basis functions has been presented

in [Welij, 1985; Kameari, 1990; Dular *et al.*, 1994] and for prismatic basis functions in [Dular *et al.*, 1994]. The accuracy of interpolation has been increased by introducing high order hierarchical finite elements [Webb & Forghani, 1993; Ren & Ida, 2000; Geuzaine *et al.*, 1999a].

1.4.1 Conformity

We assume scalar basis functions or vector basis functions whose components are polynomials. We can define four types of finite elements depending on their class:

- ✓ Conforming finite elements (in $\mathcal{H}^1(\Omega)$) interpolate scalar fields that are continuous across any interface. These elements are referred to as nodal elements because their degrees of freedom are (commonly) associated with the nodes of the element. This type of elements may be used to discretise the magnetic scalar potential φ or the electric scalar potential v.
- ✓ Curl-conforming finite elements (in $\boldsymbol{H}(\mathrm{curl};\Omega)$) ensure the continuity of the tangential component of the field. These elements are referred to as edge elements, since their degrees of freedom are associated with the edges of the element. Curl-conforming finite elements may be used to discretise the magnetic field $\underline{h}$, the magnetic vector potential $\underline{a}$ or the electric field $\underline{e}$.
- ✓ Div-conforming finite elements (in $\boldsymbol{H}(\mathrm{div};\Omega)$) ensure the continuity of the normal component of the interpolated field. These elements are often referred to as face elements, since their degrees of freedom are associated with the faces of the element. Div-conforming elements may be used to discretise the magnetic flux density $\underline{b}$, the current density $\underline{j}$ or the electric flux density $\underline{d}$.
- ✓ Finite elements in $L^2(\Omega)$ do not impose any continuity between elements on the interpolated field. These elements are often called volume elements, since their degrees of freedom are always associated with the volume of the element. They may be used to discretise the electric charge density ρ.

1.4.2 The Whitney elements

We consider a mesh of Ω formed by geometrical elements, e.g. a tetrahedral mesh. The sets of nodes, edges, faces and elements are denoted $\mathcal{N}$, $\mathcal{E}$, $\mathcal{F}$, $\mathcal{V}$, respectively. A geometrical element is denoted $\mathcal{G}$. A node is identified by n or its index i. Analogously, an edge is denoted by e or the indexes of its two nodes i, j; a face is denoted by f or the indexes of its nodes i, j, k (tetrahedral mesh).

Consider a node i and a point $u \in \mathcal{G}$ sharing node i. Let $\varsigma_i(u)$ be the barycentric weight of u with respect to node i in $\mathcal{G}$. With the convention that $\varsigma_i(u) = 0$ in other cases, we obtain a continuous piecewise linear function ς_i.

The Whitney elements of order p are expressed as [Bossavit, 1988b]

$$\underline{w}_{i_0,\cdots,i_p} = p! \sum_{j=0}^{p} (-1)^j \varsigma_{i_j} \operatorname{grad} \varsigma_{i_0} \times \cdots \times \operatorname{grad} \varsigma_{i_{j-1}} \times \operatorname{grad} \varsigma_{i_{j+1}} \times \cdots \times \operatorname{grad} \varsigma_{i_p} \,. \quad (1.68)$$

Now, we can define Whitney elements of degree $p = 0, 1, 2, 3$ (nodal elements, edge elements, face elements and volume elements, respectively) as

- ✓ Nodal elements are piecewise linear continuous elements. They are well suited for the discretisation of scalar fields. From (1.68), the nodal element reads

$$w_n(u) = \varsigma_i(u)\,. \tag{1.69}$$

  The value of w_n is 1 at node n, 0 at the other nodes of $\mathcal{G}$. The function w_n is continuous across faces.

- ✓ Edge elements can approximate 1-forms such as $\underline{h}$ and $\underline{e}$. Their degrees of freedom are the circulations of the field along the edges of the mesh. From (1.68), the edge element is defined by the vector field

$$\underline{w}_e = \varsigma_i \operatorname{grad}\varsigma_j - \varsigma_j \operatorname{grad}\varsigma_i\,. \tag{1.70}$$

  The circulation of $\underline{w}_e$ is 1 along edge e, 0 along the other edges of $\mathcal{G}$. The tangential component of $\underline{w}_e$ is continuous across faces.

- ✓ Face elements are well suited for discretising 2-forms such as $\underline{b}$ and $\underline{j}$ (normal component continuous across medium interfaces). Their degrees of freedom are the fluxes of the field through the faces of the mesh. From (1.68), the face element is given by the vector field

$$\underline{w}_f = 2\left(\varsigma_i \operatorname{grad}\varsigma_j \times \operatorname{grad}\varsigma_k - \varsigma_j \operatorname{grad}\varsigma_i \times \operatorname{grad}\varsigma_k + \varsigma_k \operatorname{grad}\varsigma_i \times \operatorname{grad}\varsigma_j\right). \tag{1.71}$$

  The flux of $\underline{w}_f$ is 1 across face f, 0 across the other faces of $\mathcal{G}$. The normal component of $\underline{w}_f$ is continuous across faces.

- ✓ Volume elements are piecewise constant functions. Their degree of freedom is the integration over its volume. They are suitable for the discretisation of densities like the electric charge density q. From (1.68), the volume element is

$$\begin{aligned}\underline{w}_v = 6\,(&\varsigma_i \operatorname{grad}\varsigma_j \times \operatorname{grad}\varsigma_k \times \operatorname{grad}\varsigma_l - \varsigma_j \operatorname{grad}\varsigma_i \times \operatorname{grad}\varsigma_k \times \operatorname{grad}\varsigma_l + \\ &\varsigma_k \operatorname{grad}\varsigma_i \times \operatorname{grad}\varsigma_j \times \operatorname{grad}\varsigma_l - \varsigma_l \operatorname{grad}\varsigma_i \times \operatorname{grad}\varsigma_j \times \operatorname{grad}\varsigma_k)\,.\end{aligned} \tag{1.72}$$

  The sum of $\underline{w}_v$ is 1 over the volumen of $\mathcal{G}$, 0 over other volumes.

Note that Whitney elements are functions (if $p = 0$ or 3) or vector fields (if $p = 1$ or 2) associated with p-simplices.

1.4.3 The Whitney complex

We call $W^p(\mathcal{G})$ the finite dimensional subspace generated by taking linear combinations of p-Whitney elements built on $\mathcal{G}$. These finite dimensional subspaces satisfy the property of conformity (see Section 1.4.3), i.e.

$$W^0(\mathcal{G}) \subset H^1(\mathcal{G}), \tag{1.73}$$

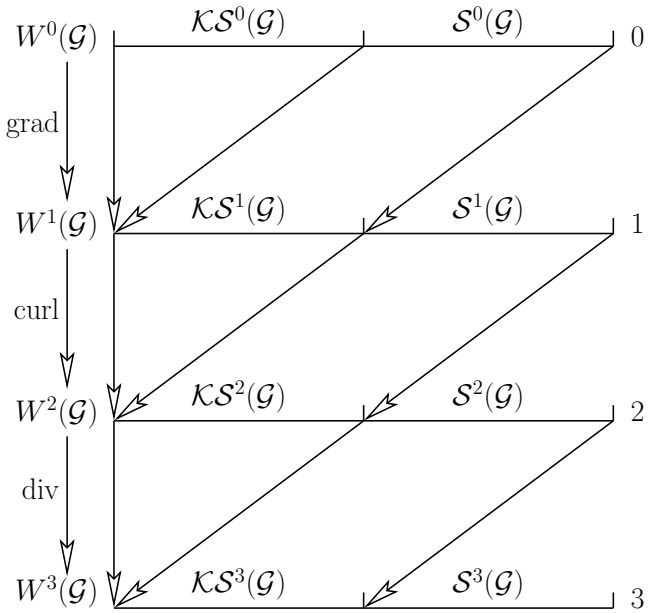

Figure 1.6: The Whitney complex: de Rham complex for discrete subspaces

$$W^1(\mathcal{G}) \subset \boldsymbol{H}(\mathrm{curl};\mathcal{G}), \tag{1.74}$$
$$W^2(\mathcal{G}) \subset \boldsymbol{H}(\mathrm{div};\mathcal{G}), \tag{1.75}$$
$$W^3(\mathcal{G}) \subset L^2(\mathcal{G}). \tag{1.76}$$

Let $\mathcal{S}$ be the local function spaces for the four types of mixed elements (see Section 1.4.2) built on a geometrical element $\mathcal{G}$. Function spaces can be decomposed into the kernel of the associated differential operator (grad, curl and div respectively) and its orthogonal complement, i.e.:

$$W^p(\mathcal{G}) = \mathcal{KS}^p(\mathcal{G}) \oplus \mathcal{S}^p(\mathcal{G}), \quad p = 0, \ldots, 2\,.$$

By the Poincaré lemma [Dautray & Lions, 1988], the differential operators grad, curl and div are isomorphisms of $\mathcal{S}^1(\mathcal{G})$ onto $\mathcal{KS}^1(\mathcal{G})$, $\mathcal{S}^1(\mathcal{G})$ onto $\mathcal{KS}^2(\mathcal{G})$ and $\mathcal{S}^2(\mathcal{G})$ onto $\mathcal{KS}^3(\mathcal{G})$, respectively.

The fields whose curl or divergence vanishes in $\mathcal{G}$ can thus be expressed as the gradient or the curl of some other fields. Therefore, the sequence

$$W^0(\mathcal{G}) \xrightarrow{\text{grad}} W^1(\mathcal{G}) \xrightarrow{\text{curl}} W^2(\mathcal{G}) \xrightarrow{\text{div}} W^3(\mathcal{G})$$

formed by the local spaces is exact (see Section A.1.3). The decomposition is summed up on the de Rham complex shown in Figure 1.6, which should be compared with Figure 1.4. The sequence in the continuous case is not exact due to the loops and cavities in Ω.

Chapter 2

Continuous formulations, coupling with integral equations

Contents

2.1 Introduction

In the Chapter 1, the continuous electromagnetic field problems are cast in a continuous mathematical structure. Then, the continuous spaces are replaced by discrete spaces that allow for the discretisation of fields and potentials. In this chapter, we

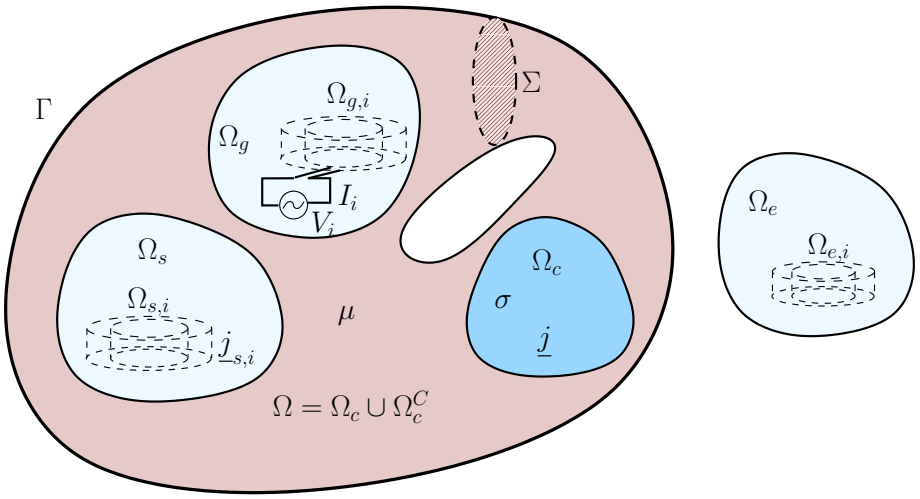

Figure 2.1: Bounded domain Ω with boundary Γ

express the continuous electromagnetic problems in continuous formulations suitable for their discretisation thanks to these discrete spaces.

First we describe the general problem. Assumptions about its geometry and electromagnetic properties are formulated. Then we establish the classical weak formulations [Bossavit, 1998a]. The formulations that in the discrete case retain the tangential continuity of the magnetic field $\underline{h}$ are called magnetic field conforming formulations ($\underline{h}$-conforming formulations), and those which imply the normal continuity of the magnetic flux density $\underline{b}$ are referred to as magnetic flux density conforming formulations ($\underline{b}$-conforming formulations). The coupling of these continuous formulations with the integral equations is elaborated as well. The hybrid $\underline{b}$-conforming formulation is founded on [Bossavit & Vérité, 1982; Bossavit & Vérité, 1983]; the hybrid $\underline{b}$-conforming formulation is based on [Ren *et al.*, 1990; Ren *et al.*, 1992].

2.2 Description of a general problem

Our goal is solving Maxwell's equations and the constitutive relations (1.1)–(1.7) in a bounded open set $\Omega \in \mathbb{R}^3$ with boundary Γ and characterised by $\sigma \geq 0$, $\epsilon \geq \epsilon_0$ and $\mu > 0$. The domain Ω can be split in a conducting region Ω_c ($\sigma > 0$) and a nonconducting one $\Omega_c^C = \Omega \backslash \Omega_c$. The outward normal unit vector is denoted $\hat{n}$. Such a configuration is depicted in Figure 2.1.

The boundary Γ may consist of $c+1$ closed surfaces Γ_i, $i = 0, \ldots, c$, which implies that there are c cavities in Ω. The region Ω may also contain l loops, if there exist l cutting surfaces Σ_i (called cuts), $i = 1, \ldots, l$, inside Ω that make Ω homologically simple [Kotiuga, 1987; Bossavit, 1988a]. It should be noted that a homologically simple domain is not necessarily simply connected [Bossavit *et al.*, 1989].

The sources of the electromagnetic field are inductors defined by local magnitudes

(current density) or global magnitudes (voltages and currents), and can be located inside or outside Ω (see Figure 2.1).

Ω_e denotes the set of all inductor domains $\Omega_{e,i}$, $i = 1, \ldots, e$ located outside Ω. The field generated by these external sources is determined a priori.

The sources inside Ω are confined in Ω_s and Ω_g, which are subsets of Ω defined in the two following sections.

2.2.1 Inductors Ω_s

Ω_s comprises the set of inductor domains $\Omega_{s,i}$, $i = 1, \ldots, s$, carrying an imposed current density $\underline{j}_s$. We assume $\Omega_s \subset \Omega_c^{\mathrm{C}}$. Stranded inductors (winding of N_i turns) belong to this class. Such inductors are modelled by defining a source magnetic field $\underline{h}_s$ that verifies

$$\begin{cases} \operatorname{curl} \underline{h}_s = \underline{j}_s & \text{in } \Omega_s \\ \operatorname{curl} \underline{h}_s = 0 & \text{in } \Omega_s^{\mathrm{C}} \end{cases}. \tag{2.1}$$

The lack of uniqueness of $\underline{h}_s$ allows for some flexibility for its computation (see Section 1.3.2.2).

We consider now that the stranded inductor supply is a generator imposing a global current or voltage. Hence, $\underline{j}_s$ is a priori unknown. In this case, we have independent source fields $\underline{h}_{s,i}$ linked to each inductor $\Omega_{s,i}$ that verify

$$\begin{cases} \operatorname{curl} \underline{h}_{s,i} = \underline{j}_{s,i} & \text{in } \Omega_{s,i} \\ \operatorname{curl} \underline{h}_{s,i} = 0 & \text{in } \Omega_{s,i}^{\mathrm{C}} \end{cases}, \tag{2.2}$$

with $\underline{j}_{s,i}$ the equivalent current density of a unit current flowing in the N_i turns of the ith inductor in Ω_s [Dular *et al.*, 1999].

2.2.2 Generators Ω_g

Ω_g comprises the set of generators $\Omega_{g,i}$ (sources of electromotive force) $i = 1, \ldots, g$, where either a global voltage V_i or a global current I_i is imposed. In case of circuit coupling, V_i and I_i are a priori unknown. Each $\Omega_{g,i}$ is either a subset of Ω_c or Ω_c^{C}.

An idealised generator $\Omega_{g,i}$ is shown in Figure 2.3. It is actually a source of electromotive force between two electrodes very close to each other.

Different kinds of inductors can be connected to these generators. We distinguish $\Omega_s \subset \Omega_c^{\mathrm{C}}, \Omega_m \subset \Omega_c$ and $\Omega_f \subset \Omega_c$ composed of stranded, massive and foil windings, respectively.

Each $\Omega_{g,i}$ has an associated voltage V_i and current I_i flowing through one of the electrodes $\Gamma_{g,i}$ (see Figure 2.3). For massive inductors Ω_m, the electric field $\underline{e}$ in $\Omega_{g,i}$ is considered as known and its circulation along any path $\gamma_{g,i}$ from one electrode to the other in $\Omega_{g,i}$ is thus the applied voltage V_i [Dular *et al.*, 2000], i.e.

$$\int_{\gamma_{g,i}} \underline{e} \cdot d\underline{l} = V_i \quad \text{and} \quad \int_{\Gamma_{g,i}} \hat{n} \cdot \underline{j}\, ds = I_i. \tag{2.3 a,b}$$

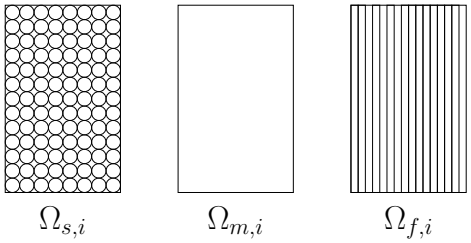

Figure 2.2: Cuts of a stranded, massive and foil inductor, $\Omega_{s,i}$, $\Omega_{m,i}$ and $\Omega_{f,i}$

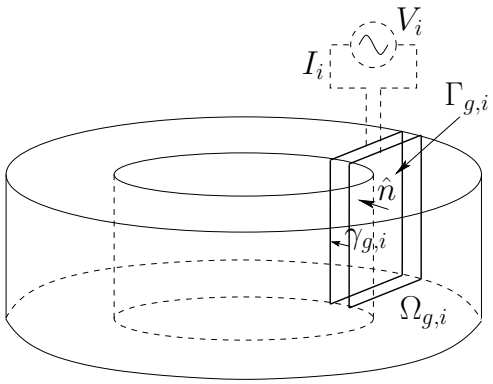

Figure 2.3: Model of an inductor with a source of electromotive force $\Omega_{g,i}$

For stranded inductors Ω_s or foil windings Ω_f, equation (2.3 a) becomes the sum of the circulations of $\underline{e}$ for all the wires or foils, and the number of turns of the winding N_i is incorporated into (2.3) as [Dular *et al.*, 2000]

$$\sum_{j=1}^{N_i} \int_{\gamma_{g,i,j}} \underline{e} \cdot d\underline{l} = V_i \quad \text{and} \quad \int_{\Gamma_{g,i}} \hat{n} \cdot \underline{j}\, ds = N_i I_i, \tag{2.4 a,b}$$

where $\gamma_{g,i,j}$ is a path in $\Omega_{g,i}$ connecting the jth wire to the corresponding electrodes. Moreover, for all kinds of inductors, the following local conditions must be satisfied

$$\hat{n} \times \underline{e}\big|_{\partial\Omega_{g,i}} = 0 \quad \text{and} \quad \hat{n} \cdot \underline{j}\big|_{\partial\Omega} \begin{cases} m,i \\ s,i \\ f,i \end{cases} = 0.$$

2.3 Magnetic field conforming formulations

2.3.1 Magnetodynamics

We consider the magnetodynamic problem in $\mathbb{R}^3$ that has been described in Section 1.3.3 and represented in Figure 2.1. The particularised Maxwell's equations (1.61) together with the constitutive relations (1.13) and (1.16) establish the system to be solved.

In order to satisfy Ampère's law (1.61 b) in a strong sense, we take $\underline{h} \in \boldsymbol{H}_h(\mathrm{curl};\Omega)$ and $\underline{j} \in \boldsymbol{H}_h(\mathrm{div};\Omega)$. This is equivalent to verifying the left-hand

side of the Tonti diagram (1.67) in a strong sense. Moreover, satisfying exactly the constitutive relations (1.13) and (1.16) implies placing $\underline{b} \in \boldsymbol{H}_e(\mathrm{div};\Omega)$ and $\underline{e} \in \boldsymbol{H}_e(\mathrm{curl};\Omega)$. Faraday's law (1.61 a) can only be verified approximately. The $\underline{h}$-conforming formulation is obtained from the weak form (see Appendix A.3) of Faraday's law (1.61 a) as

$$\partial_t(\underline{b},\underline{h}')_\Omega + (\mathrm{curl}\,\underline{e},\underline{h}')_\Omega = 0, \quad \forall \underline{h}' \in \boldsymbol{H}^0_h(\mathrm{curl};\Omega), \tag{2.5}$$

where $\underline{h}' \in \boldsymbol{H}^0_h(\mathrm{curl};\Omega)$ [Dular *et al.*, 1999] is a field of test functions independent of time (see Section 1.2.2 for the definition of the function spaces). Applying the Green formula of type curl-curl (A.25) to the second term in (2.5), we have

$$\partial_t(\underline{b},\underline{h}')_\Omega + (\underline{e},\mathrm{curl}\,\underline{h}')_\Omega + \langle \hat{n}\times\underline{e},\underline{h}'\rangle_{\Gamma_e} = 0, \quad \forall \underline{h}' \in \boldsymbol{H}^0_h(\mathrm{curl};\Omega). \tag{2.6}$$

Let us introduce now the magnetic constitutive relation (1.13) in (2.6) to obtain:

$$\partial_t(\mu\underline{h},\underline{h}')_\Omega + (\underline{e},\mathrm{curl}\,\underline{h}')_\Omega + \langle \hat{n}\times\underline{e},\underline{h}'\rangle_{\Gamma_e} = 0, \quad \forall \underline{h}' \in \boldsymbol{H}^0_h(\mathrm{curl};\Omega). \tag{2.7}$$

Ampére's law can be also written in integral form with a test field $\underline{j}'$ as

$$(\mathrm{curl}\,h,\underline{j}')_\Omega = (\underline{j},\underline{j}')_\Omega, \quad \forall \underline{j}' \in \boldsymbol{H}^0_h(\mathrm{div};\Omega). \tag{2.8}$$

Introducing Ohm's law (1.16) in (2.8), we obtain

$$(\mathrm{curl}\,h,\underline{j}')_\Omega = (\sigma\underline{e},\underline{j}')_{\Omega_c} + (\underline{j}_s,\underline{j}')_{\Omega_s}, \quad \forall \underline{j}' \in \boldsymbol{H}^0_h(\mathrm{div};\Omega). \tag{2.9}$$

Equations (2.7) and (2.9) constitute a mixed $\underline{h}$-$\underline{e}$ formulation where only the conformity of $\underline{h}$ is ensured. The numerical solution of this formulation is not obvious.

In order to obtain an expression that depends only on $\underline{h}$, we combine Ohm's law (1.16) with Ampère's law (1.61 b), $\mathrm{curl}\,\underline{h} = \underline{j} = \sigma\underline{e}$ in Ω_c, and we have thus

$$\partial_t(\mu\underline{h},\underline{h}')_\Omega + (\sigma^{-1}\mathrm{curl}\,\underline{h},\mathrm{curl}\,\underline{h}')_{\Omega_c} + (\underline{e},\mathrm{curl}\,\underline{h}')_{\Omega_c^{\mathrm{C}}} + \langle \hat{n}\times\underline{e},\underline{h}'\rangle_{\Gamma_e} = 0, \quad \forall \underline{h}' \in \boldsymbol{H}^0_h(\mathrm{curl};\Omega). \tag{2.10}$$

The general expression of the magnetic field $\underline{h}$ in Ω is

$$\underline{h} = \underline{h}_s + \underline{h}_r, \tag{2.11}$$

with $\underline{h}_s$ a source magnetic field in Ω_s and $\underline{h}_r$ the reaction magnetic field in Ω_c, which is indeed the unknown of our problem. Let us consider an imposed current density $\underline{j} = \underline{j}_s$ in the inductors Ω_s. A source magnetic field $\underline{h}_s$ fulfils (2.1) (see Section 1.3.2.2 for discussion on the uniqueness of $\underline{h}_s$). Since

$$\begin{cases} \mathrm{curl}\,\underline{h} = \underline{j}_s & \text{in } \Omega_s \\ \mathrm{curl}\,\underline{h} = 0 & \text{in } \Omega_c^{\mathrm{C}}\backslash\Omega_s \end{cases}, \tag{2.12}$$

it reads

$$\mathrm{curl}\,\underline{h}_r = 0 \quad \text{in } \Omega_c^{\mathrm{C}}. \tag{2.13}$$

The test field $\underline{h}'$ in the weak form (2.6) has been chosen in a subspace of $\boldsymbol{H}_h^0(\mathrm{curl};\Omega)$ for which $\mathrm{curl}\,\underline{h}'_r = 0$ in Ω_c^{C}, with $\underline{h}' = \underline{h}'_s + \underline{h}'_r$. The third term of (2.10) is thus cancelled outside Ω_s and equation (2.10) can be rewritten as

$$\partial_t(\mu\underline{h},\underline{h}')_\Omega + (\sigma^{-1}\mathrm{curl}\,\underline{h},\mathrm{curl}\,\underline{h}')_{\Omega_c} + (\sigma^{-1}\underline{j}_s,\mathrm{curl}\,\underline{h}')_{\Omega_s} + \langle\hat{n}\times\underline{e},\underline{h}'\rangle_{\Gamma_e} = 0,$$
$$\forall\underline{h}' \in \boldsymbol{H}_h^0(\mathrm{curl};\Omega) \quad \text{with} \quad \mathrm{curl}\,\underline{h}'_r = 0 \text{ in } \Omega_c^{\mathrm{C}} \quad \text{and} \quad \underline{h}' = \underline{h}'_s + \underline{h}'_r. \tag{2.14}$$

Note that this formulation does not allow to determine the electric field in the nonconducting regions Ω_c^{C}. The trace of the electric field $\hat{n}\times\underline{e}$ is subject to a natural boundary condition on the boundaries Γ_e of the domain Ω. This boundary condition can adopt several forms:

- ✓ The trace of the electric field can be locally specified. For instance, when applying a homogeneous Neumann boundary condition the symmetry condition of perpendicular current or zero magnetic flux is imposed, i.e. $\hat{n}\times\underline{e}\big|_{\Gamma_e} = 0$ implies $\hat{n}\cdot\underline{b}\big|_{\Gamma_e} = 0$.
- ✓ The trace of the electric field can appear in local implicit boundary conditions, which is the case for the treatment of thin structures [Geuzaine *et al.*, 1999b; Geuzaine, 2001].
- ✓ The trace can be a field for which only associated global quantities are known (i.e. a functional of $\hat{n}\times\underline{e}$). This can be employed for the modelling of massive, stranded and foil winding inductor [Dular *et al.*, 1997; Dular *et al.*, 1998; Dular *et al.*, 1999; Dular *et al.*, 2000].
- ✓ The traces can appear in the definition of an integral operator for the coupling with an integral formulation and they become the local unknowns of the problem. This is developed in Section 2.6.1.

2.3.2 Magnetostatics

The magnetostatic problem can be seen as a simplification of the magnetodynamic problem treated in the previous section. Herein all time dependent variation is neglected. We study the magnetostatic problem in $\mathbb{R}^3$ that has been described in Section 1.3.2.2. We have to solve the system (1.50).

In order to satisfy (1.50 a) in a strong sense, we take $\underline{h} \in \boldsymbol{H}_h(\mathrm{curl};\Omega)$ and $\underline{j} \in \boldsymbol{H}_h(\mathrm{div};\Omega)$. The left-hand side of the Tonti diagram (1.60) is consequently satisfied in a strong sense.

The starting point is the weak form of (1.50 b), i.e.

$$(\mathrm{div}\,\underline{b},\varphi')_\Omega = 0, \quad \forall\varphi' \in H_h^{10}(\Omega). \tag{2.15}$$

Let us consider the Green formula of type grad-div (A.23) in Ω applied to the fields $\underline{b}$ and φ', it reads

$$(\underline{b},-\mathrm{grad}\,\varphi')_\Omega + \langle\hat{n}\cdot\underline{b},\varphi'\rangle_{\Gamma_e} = 0, \quad \forall\varphi' \in H_h^{10}(\Omega). \tag{2.16}$$

In order to satisfy the left-hand side of the Tonti diagram (1.60) in a strong sense, we first introduce (1.11 b) into (2.16) to obtain

$$(\mu \underline{h}, -\text{grad}\,\varphi')_\Omega + \langle \hat{n} \cdot \underline{b}, \varphi' \rangle_{\Gamma_e} = 0, \quad \forall \varphi' \in H_h^{10}(\Omega). \tag{2.17}$$

Then, decomposing $\underline{h} \in \boldsymbol{H}(\text{curl}; \Omega)$ by (2.11) in the same way as in Section 2.3.1, we can derive the reaction field $\underline{h}_r$ from a scalar potential φ such that $\underline{h}_r = -\text{grad}\,\varphi$ everywhere in Ω. Of course, if the domain Ω is multiply connected, the scalar potential φ is a priory multivalued. Cuts must be introduced to avoid the multiplicity of φ [Bossavit, 1988a]. The weak form (2.17) can then be written as

$$(\mu\,(\underline{h}_s - \text{grad}\,\varphi), -\text{grad}\,\varphi')_\Omega + \langle \hat{n} \cdot \underline{b}, \varphi' \rangle_{\Gamma_e} = 0, \quad \forall \varphi' \in H_h^{10}(\Omega). \tag{2.18}$$

2.4 Magnetic flux density conforming formulations

2.4.1 Magnetodynamics

Let us consider the magnetodynamic problem in $\mathbb{R}^3$ defined in Section 1.3.3. We want to solve the system formed by the particularised Maxwell's equations (1.61) and the constitutive relations (1.16) and (1.13).

In order to satisfy Faraday's law (1.61 a) in a strong sense, we take $\underline{b} \in \boldsymbol{H}_e(\text{div}; \Omega)$ and $\underline{e} \in \boldsymbol{H}_e(\text{curl}; \Omega)$. Both constitutive laws (1.16) and (1.13) are exactly verified as well. The right-hand side of Tonti diagram (1.67) is then satisfied in a strong sense. From a discrete point of view this is equivalent to placing $\underline{h} \in \boldsymbol{H}_e(\text{div}; \Omega)$ and $\underline{j} \in \boldsymbol{H}_e(\text{curl}; \Omega)$, what implies that Ampère's law (1.61 b) holds approximately.

The starting point is the weak form of Ampère's law (1.61 b):

$$(\text{curl}\,\underline{h}, \underline{a}')_\Omega = (\underline{j}, \underline{a}')_\Omega, \quad \forall \underline{a}' \in \boldsymbol{H}_e^0(\text{curl}; \Omega)\,, \tag{2.19}$$

where the field $\underline{a}'$ is a field of test functions independent of time. Applying the Green formula of type curl-curl (A.25) in Ω to the fields $\underline{h}$ and $\underline{a}'$ in (2.19), we obtain

$$(\underline{h}, \text{curl}\,\underline{a}')_\Omega + \langle \underline{n} \times \underline{h}, \underline{a}' \rangle_{\Gamma_h} = (\underline{j}, \underline{a}')_\Omega, \quad \forall \underline{a}' \in \boldsymbol{H}_e^0(\text{curl}; \Omega)\,. \tag{2.20}$$

We first introduce the constitutive relations (1.11 b) and (1.16) in the weak form (2.20) in order to fulfil both Faraday's and Gauss's law in a strong sense, i.e. the right-hand side of the Tonti diagram (1.67) is satisfied in a strong sense. The weak form reads

$$\begin{aligned}(\mu^{-1}\underline{b}, \text{curl}\,\underline{a}')_\Omega + \langle \underline{n} \times \underline{h}, \underline{a}' \rangle_{\Gamma_h} = (\sigma \underline{e}, \underline{a}')_{\Omega_c} + (\underline{j}_s, \underline{a}')_{\Omega_s}, \\ \forall \underline{a}' \in \boldsymbol{H}_e^0(\text{curl}; \Omega).\end{aligned} \tag{2.21}$$

Let us introduce the magnetic vector potential $\underline{a}$ and the electric scalar potential v, verifying (1.65) and (1.66), in (2.21). We get

$$\begin{aligned}&(\mu^{-1}\text{curl}\,\underline{a}, \text{curl}\,\underline{a}')_\Omega + (\sigma\,\partial_t \underline{a}, \underline{a}')_{\Omega_c} + (\sigma\,\text{grad}\,v, \underline{a}')_{\Omega_c} \\ &+\langle \underline{n} \times \underline{h}, \underline{a}' \rangle_{\Gamma_h} = (\underline{j}_s, \underline{a}')_{\Omega_s}\,, \qquad \forall \underline{a}' \in \boldsymbol{H}_e^0(\text{curl}; \Omega).\end{aligned} \tag{2.22}$$

The electric scalar potential v is only defined in the conducting regions Ω_c. The magnetic vector potential $\underline{a}$ is solely defined as a single-valued field in the conducting regions Ω_c. A gauge condition has to be imposed everywhere else (see Sections 1.3.3 and 1.3.2.2).

The weak formulation (2.22) implies, by taking $\underline{a}' = \operatorname{grad} v'$ as a test function, that

$$(\sigma\, \partial_t \underline{a}, \operatorname{grad} v')_{\Omega_c} + (\sigma \operatorname{grad} v, \operatorname{grad} v')_{\Omega_c} = \langle \underline{n} \cdot \underline{j}, v' \rangle_{\Gamma_g}, \quad \forall v' \in H_e^{10}(\Omega_c), \tag{2.23}$$

where Γ_g is the part of the boundary of Ω_c carrying a current. In fact, the formulation (2.23) is the weak form of $\operatorname{div} \underline{j} = 0$ in Ω_c.

The trace of the magnetic field $\underline{n} \times \underline{h}$ is subject to an inherent boundary condition on the boundaries Γ_h of the domain Ω . This boundary condition can take several forms:

- ✓ The trace of the magnetic field can be locally specified. This is the case for a homogeneous Neumann boundary condition, e.g. imposing a symmetry condition of "zero crossing current" ($\underline{n} \times \underline{h}\big|_{\Gamma_h} = 0 \Rightarrow \underline{n} \cdot \operatorname{curl} \underline{h}\big|_{\Gamma_e} = 0 \Rightarrow \underline{n} \cdot \underline{j}\big|_{\Gamma_e} = 0$).
- ✓ The trace of the magnetic field can appear in local implicit boundary conditions, such as those established for the treatment of thin structures [Geuzaine *et al.*, 1999b; Geuzaine, 2001].
- ✓ The trace can be a field for which only associated global quantities are known. This is employed in the modelling of the treatment of massive, stranded and foil winding inductors [Dular *et al.*, 2000].
- ✓ The traces can appear in the definition of an integral operator for the coupling with an integral formulation and they constitute then local unknowns of the problem. This is developed in Section 2.6.2.

2.4.2 Magnetostatics

As in Section 2.3, the magnetostatic problem can be seen as a particularisation of the magnetodynamic problem for which all time dependent variation has been neglected. We study the magnetostatic problem in $\mathbb{R}^3$ that has been described in Section 1.3.2.2. We have to solve system (1.50).

In order to satisfy Faraday's law (1.61 a) in a strong sense, we take $\underline{b} \in \boldsymbol{H}_e(\operatorname{div}; \Omega)$. The constitutive law (1.11 b) is also exactly verified. The right-hand side of Tonti diagram (1.60) is thus satisfied in a strong sense.

Let us start by writing a weak form of (1.50 a), i.e.

$$(\operatorname{curl} \underline{h}, \underline{a}')_{\Omega} = (\underline{j}, \underline{a}')_{\Omega}, \quad \forall \underline{a}' \in \boldsymbol{H}_e^0(\operatorname{curl}; \Omega). \tag{2.24}$$

Considering the Green formula of type curl-curl (A.25) in Ω applied to the fields $\underline{h}$ and $\underline{a}'$ in (2.24), and taking into account that $\underline{j} = \underline{j}_s \in \Omega_s$, we obtain

$$(\underline{h}, \operatorname{curl} \underline{a}')_{\Omega} + \langle \hat{n} \times \underline{h}, \underline{a}' \rangle_{\Gamma_h} = (\underline{j}_s, \underline{a}')_{\Omega_s}, \quad \forall \underline{a}' \in \boldsymbol{H}_e^0(\operatorname{curl}; \Omega). \tag{2.25}$$

In order to satisfy the right-hand side of the Tonti diagram (1.60) in a strong sense, we first introduce (1.11 b) into (2.25) to obtain

$$(\mu^{-1}\underline{b}, \operatorname{curl}\underline{a}')_{\Omega} + \langle \hat{n} \times \underline{h}, \underline{a}' \rangle_{\Gamma_h} = (\underline{j}_s, \underline{a}')_{\Omega_s}, \quad \forall \underline{a}' \in \boldsymbol{H}^0_e(\operatorname{curl}; \Omega). \tag{2.26}$$

The field $\underline{b} \in \boldsymbol{H}(\operatorname{div}; \Omega)$ can be derived from a vector potential $\underline{a}$ such that $\underline{b} = \operatorname{curl}\underline{a}$ everywhere in Ω, the weak form (2.26) can be written as

$$(\mu^{-1}\operatorname{curl}\underline{a}, \operatorname{curl}\underline{a}')_{\Omega} + \langle \hat{n} \times \underline{h}, \underline{a}' \rangle_{\Gamma_h} = (\underline{j}_s, \underline{a}')_{\Omega_s}, \quad \forall \underline{a}' \in \boldsymbol{H}^0_e(\operatorname{curl}; \Omega). \tag{2.27}$$

2.5 2D magnetic flux density conforming formulation

The two-dimensional magnetic flux density ($\underline{b}$-) conforming formulations elaborated hereafter will be employed in the numerical test cases of Chapter 5.

2.5.1 Magnetodynamics

We consider now the $\underline{b}$-conforming formulation of a magnetodynamic problem in $\mathbb{R}^2$. Complex notation is adopted in this section for denoting the sinusoidal time variation of frequency f and pulsation $\omega = 2\pi f$ (see Section 1.3.1).

In this 2D case, the z-component of the magnetic field vector $\underline{h}$ and the magnetic flux density vector $\underline{b}$ vanish. The current density $\underline{j} = j_s(x, y)\underline{1}_z$ is given in a domain Ω_s and directed along the z-axis.

The problem is formulated in terms of the magnetic vector potential $\underline{a} = a(x, y)\,\underline{1}_z$ in Ω and the equivalent current layer $\underline{q} = q(\xi)\,\underline{1}_z$ on Γ_h [Geuzaine *et al.*, 2001].

For any continuous potential a, (1.61 a) and (1.61 c) are fulfilled on account of

$$\underline{b} = \operatorname{curl}\underline{a} = \underline{1}_z \times \operatorname{grad} a\,, \quad \underline{e} = -\imath\omega\underline{a}\,. \tag{2.28}$$

Ampère's law (1.61 b) in the frequency domain is written in terms of $a(x, y)$ as

$$\operatorname{curl}\underline{h} = -\operatorname{div}\left(\mu^{-1}\operatorname{grad} a\right)\underline{1}_z + \sigma\imath\omega\underline{a}\,. \tag{2.29}$$

The weak form of (2.29) is given by

$$\begin{aligned}&(\mu^{-1}\operatorname{grad} a, \operatorname{grad} a')_{\Omega} + (\sigma\,\imath\omega a, a')_{\Omega_c} = \\ &(j_s, a')_{\Omega_s} + \langle \mu^{-1}\partial_n a, a' \rangle_{\Gamma_h}\,, \qquad \forall a' \in H^{10}_e(\Omega)\end{aligned} \tag{2.30}$$

where the test function a' is independent of time. Note that the magnetodynamic problem in $\mathbb{R}^2$ is reduced to a scalar problem.

2.5.2 Magnetostatics

A magnetostatic problem in $\mathbb{R}^2$ can be seen as a particular case of the magnetodynamic problem described in Section 2.5.1. Its treatment is analogous. The $\underline{b}$-conforming formulation of a two-dimensional magnetostatic problem is thus determined by the weak form of Ampère's law.

The weak form of Ampère's law (2.29) is now given by

$$(\mu^{-1}\mathrm{grad}\, a, \mathrm{grad}\, a')_\Omega = (j_s a, a')_{\Omega_s} + \langle \mu^{-1}\partial_n a, a'\rangle_{\Gamma_h}\,, \qquad \forall a' \in H_e^{10}(\Omega) \tag{2.31}$$

where the test function a' is independent of time.

2.6 Coupling with integral formulations

2.6.1 Hybrid $\underline{h}$-conforming formulations

Let us consider the $\underline{h}$-conforming formulation for the magnetodynamic case elaborated in Section 2.6.1.

When dealing with open boundary problems, the surface term $\langle \hat{n}\times\underline{e}, \underline{h}'\rangle_{\Gamma_e}$ in (2.14) is not fixed a priori and constitutes an unknown of the problem. This surface term can be reduced to $\partial_t\langle \hat{n}\cdot\underline{b}, \varphi'\rangle_{\Gamma_e}$ on account of

$$\begin{aligned}\langle \hat{n}\times\underline{e}, \underline{h}'\rangle_{\Gamma_e} &= -\langle \hat{n}\times\underline{e}, \mathrm{grad}\,\varphi'\rangle_{\Gamma_e} = \\ &= -\langle \hat{n}, \varphi\,\mathrm{curl}\,\underline{e}\rangle_{\Gamma_e} + \langle \hat{n}, \mathrm{curl}\,(\varphi'\underline{e})\rangle_{\Gamma_e} = \langle \partial_t(\hat{n}\cdot\underline{b}), \varphi'\rangle_{\Gamma_e}\,.\end{aligned} \tag{2.32}$$

The coupling of the FE model with the BE model is actually done through this surface integral (2.32). We choose an exterior hybrid formulation described in [Geuzaine *et al.*, 2001], i.e. the FE method is used in a domain Ω with boundary Γ_e while the BE method takes into account the exterior space $\mathbb{R}^3\backslash\Omega$. A boundary operator, that relates the trace of the magnetic flux density $\underline{b}$ on the boundary Γ_e and a magnetic scalar potential φ in the domain $\mathbb{R}^3\backslash\Omega$, is defined. A classical magnetic field conforming hybrid FE-BE method is thus obtained [Bossavit & Vérité, 1982; Bossavit & Vérité, 1983].

Let us consider an exterior inductor domain Ω_e in which a source current density $\underline{j}_e$ exists (see Section 2.2). The magnetic field $\underline{h}$ can thus be decomposed into a source magnetic field $\underline{h}_e$ generated by the source current and a reduced magnetic field $\underline{h}_r$ derived from a scalar potential $\varphi \in H_h^1(\Omega)$ as in (1.63), i.e.

$$\underline{h} = \underline{h}_e + \underline{h}_r = \underline{h}_e - \mathrm{grad}\,\varphi. \tag{2.33}$$

The exterior domain $\mathbb{R}^3\backslash\Omega$ may contain l loops. In this case, l cuts have to be introduced in $\mathbb{R}^3\backslash\Omega$ in order to make the scalar potential φ single-valued. Another possibility consists in writing the FE-BE coupling directly in terms of the magnetic field as presented in [Ren *et al.*, 1992].

We define the following integral operator:

$$\mathcal{P}(q) = \int_{\Gamma_e} q(\underline{y})\, G(\underline{x},\underline{y})\,\mathrm{d}\underline{y} \quad \text{with} \quad G(\underline{x},\underline{y}) = \frac{1}{4\pi|\underline{x}-\underline{y}|}, \tag{2.34 a,b}$$

where q is an equivalent magnetic charge on Γ_e, and G is the three-dimensional Laplace Green function. The normal derivative of (2.34 a) in a point $\underline{x}$ on Γ_e is given by

$$\hat{n} \cdot \operatorname{grad} \mathcal{P}(q) = \frac{1}{2}\, q + \int_{\Gamma_e} q\, \hat{n} \cdot \operatorname{grad} G(\underline{x}, \underline{y})\ \mathrm{d}\underline{y}\,, \tag{2.35}$$

where $\hat{n}$ represents the exterior normal to $\mathbb{R}^3 \backslash \Omega$ (or the interior normal to Ω).

The scalar potential φ and its normal derivative in a point $\underline{x}$ on Γ_e can be expressed as [Bossavit, 1998a]

$$\varphi(\underline{r}) = \mu^{-1}\, \mathcal{P}(q)\,, \tag{2.36}$$

$$\hat{n} \cdot \operatorname{grad} \varphi(\underline{r}) = \mu^{-1} \hat{n} \cdot \operatorname{grad} \mathcal{P}(q)\,. \tag{2.37}$$

There are different ways of establishing the FE-BE coupling [Ren *et al.*, 1988]. Among all the possible schemes, it is worth mentioning the collocation method [Brebbia & Walker, 1980] and the variational method [Bossavit & Vérité, 1982] which is adopted in the present work.

The surface term in (2.14) thus becomes

$$\partial_t \langle \hat{n} \cdot \underline{b}, \varphi' \rangle_{\Gamma_e} = -\partial_t \langle \hat{n} \cdot \operatorname{grad} \mathcal{P}(q), \varphi' \rangle_{\Gamma_e} + \partial_t \langle \mu \hat{n} \cdot \underline{h}_e, \varphi' \rangle_{\Gamma_e}\,. \tag{2.38}$$

Introducing (2.38) in (2.14), we obtain the coupled expression

$$\begin{aligned} &\partial_t (\mu \underline{h}, \underline{h}')_\Omega + (\sigma^{-1} \operatorname{curl} \underline{h}, \operatorname{curl} \underline{h}')_{\Omega_c} + (\sigma^{-1} \underline{j}_s, \operatorname{curl} \underline{h}')_{\Omega_s} \\ &- \partial_t \langle \hat{n} \cdot \operatorname{grad} \mathcal{P}(q), \varphi' \rangle_{\Gamma_e} + \partial_t \langle \mu \hat{n} \cdot \underline{h}_e, \varphi' \rangle_{\Gamma_e} = 0\,, \\ &\forall \underline{h}' \in \boldsymbol{H}^0_h(\operatorname{curl}; \Omega) \quad \text{with} \quad \operatorname{curl} \underline{h}'_r = 0 \text{ in } \Omega_c^{\mathrm{C}} \quad \text{and} \quad \underline{h}' = \underline{h}'_s + \underline{h}'_r\,. \end{aligned} \tag{2.39}$$

Beware that now the normal $\hat{n}$ points outward the domain Ω.

The weak form of (2.36) reads

$$\langle \varphi, q' \rangle_\Gamma = \langle \mu^{-1} \mathcal{P}(q), q' \rangle_\Gamma, \quad \forall q' \in H^{10}_h(\Gamma_e)\,, \tag{2.40}$$

where $H^{10}_h(\Gamma_e)$ is the function space defined on Γ_e which contains the basis functions for q and the test function q'.

Applying the Galerkin method to the equations (2.39) and (2.40), the system of equations of the hybrid model is obtained. Edge basis functions (1.70) are employed for $\underline{h}$, resulting in sparse blocks in the system matrix. The terms comprising the integral operator $\mathcal{P}(q)$ (2.34) give dense blocks. Let us consider, e.g. , the fully populated block $\boldsymbol{M}$ due to the right-hand side of (2.40).

On the basis of the discretisation of Γ, N_q interpolation functions $\beta_l(\underline{r})$ are defined for the equivalent magnetic charge q and their coefficients q_l are assembled in the column matrix $\boldsymbol{Q}$:

$$q(\underline{r}) = \sum_{l=1}^{N_q} q_l\, \beta_l(\underline{r}) \quad \text{and} \quad \boldsymbol{Q} = \left[\ q_1\ \ \ldots\ \ q_{N_q}\ \right]^T\,. \tag{2.41}$$

The elements of $\boldsymbol{M}$ are therefore given by

$$M_{k,l} = \frac{1}{\mu} \oint_\Gamma \beta_k \left(\oint_\Gamma \beta_l \, G \, \mathrm{d}\Gamma \right) \mathrm{d}\Gamma \ . \tag{2.42}$$

The double integration is a critical and time-consuming stage for the assembly of the BE blocks, especially when numerical integration is used. The number of Gauss integration points required for accurately evaluating the self-interactions is high (see Section 3.5). If plane triangular elements and piecewise constant basis functions (1.72) or linear basis functions (1.69) are used for $q(\underline{r})$, the inner integral in (2.42) can be evaluated analytically [Graglia, 1993]. The outer integration can be performed adaptively with numerical Gauss integration.

When using the magnetostatic formulation in Section 2.3.2, integral operators for the treatment of open boundary problems, taking (2.32) into account, are introduced analogously.

2.6.2 Hybrid $\underline{b}$-conforming formulations

We consider the $\underline{b}$-conforming formulations for magnetodynamic case developed in Section 2.4.1.

For open boundary problems, the surface term $\langle \underline{n} \times \underline{h}, \underline{a}' \rangle_{\Gamma_h}$ in (2.22) is not fixed a priori and constitutes an unknown of the problem. Using the exterior hybrid approach as in Section 2.6.1, we introduce a boundary operator relating the trace of the magnetic field on the boundary Γ_h and the magnetic vector potential $\underline{a}$ in the exterior domain $\mathbb{R}^3 \backslash \Omega$, which leads in a natural way to a classical magnetic flux density hybrid finite element and boundary element method [Ren *et al.*, 1990; Ren *et al.*, 1992].

The magnetic flux density $\underline{b}$ in $\mathbb{R}^3 \backslash \Omega$ can be decomposed as

$$\underline{b} = \underline{b}_e + \underline{b}_r = \underline{b}_e + \operatorname{curl} \underline{a}, \tag{2.43}$$

where $\underline{b}_e$ is a source magnetic flux density (e.g. determined by the Biot-Savart law) due to the source current $\underline{j}_e$ in the exterior inductor domain Ω_e, and $\underline{b}_r$ is a reduced magnetic flux density derived from the magnetic vector potential $\underline{a}$.

Let us define the integral operator $\underline{\mathcal{A}}(\underline{q})$ as

$$\underline{\mathcal{A}}(\underline{q}) = \int_{\Gamma_h} \underline{q}(\underline{y}) \, G(\underline{x}, \underline{y}) \, \mathrm{d}\underline{y} \quad \text{with} \quad G(\underline{x}, \underline{y}) = \frac{1}{4\pi |\underline{x} - \underline{y}|}, \tag{2.44 a,b}$$

where the source $\underline{q}$ is an equivalent magnetisation current and G is the three-dimensional Laplace Green function.

The normal derivative of (2.44 a) in a point $\underline{x}$ on Γ_h is given by

$$\hat{n} \times \operatorname{curl} \underline{\mathcal{A}}(\underline{q}) = \frac{1}{2} \underline{q}(\underline{x}) + \int_{\Gamma_h} \hat{n}(\underline{x}) \times (\operatorname{grad} G(\underline{x}, \underline{y}) \times \underline{q}(\underline{y})) \, d\underline{y} \, . \tag{2.45}$$

The vector potential can then be expressed as

$$\underline{a}(\underline{x}) = \mu\, \underline{\mathcal{A}}(\underline{q})\,, \tag{2.46}$$

and its derivative at a point $\underline{x}$ on Γ_h can be expressed as [Bossavit, 1998a]

$$\hat{n} \times \operatorname{curl} \underline{a}(\underline{x}) = \mu\, \hat{n} \times \operatorname{curl} \underline{\mathcal{A}}(\underline{q})\,. \tag{2.47}$$

The FE-BE coupling is achieved through the surface term $\langle \hat{n} \times \underline{h}, \underline{a}' \rangle_{\Gamma_h}$ in (2.22). A relation between $\hat{n} \times \underline{h}$ and $\underline{a}$ on Γ_h must be found. We adopt a variational formulation with $\underline{q} \in \boldsymbol{H}^0_e(\mathrm{div}; \Gamma_h)$ and $\underline{a} \in \boldsymbol{H}^0_e(\mathrm{curl}; \Gamma_h)$. The surface term in (2.22) becomes

$$\langle \hat{n} \times \underline{h}, \underline{a}' \rangle_{\Gamma_h} = \langle \hat{n} \times \operatorname{curl} \underline{\mathcal{A}}(\underline{q}), \underline{a}' \rangle_{\Gamma_h} + \langle \mu^{-1} \hat{n} \times \underline{b}_e, \underline{a}' \rangle_{\Gamma_h}, \quad \forall \underline{a}' \in \boldsymbol{H}^0_e(\mathrm{curl}; \Gamma_h). \tag{2.48}$$

Introducing (2.48) in (2.22) we get

$$\begin{aligned}(\mu^{-1} \operatorname{curl} \underline{a}, \operatorname{curl} \underline{a}')_\Omega + (\sigma\, \partial_t \underline{a}, \underline{a}')_{\Omega_c} + (\sigma \operatorname{grad} v, \underline{a}')_{\Omega_c} + \langle \hat{n} \times \operatorname{curl} \underline{\mathcal{A}}(\underline{q}), \underline{a}' \rangle_{\Gamma_h} \\ + \langle \mu^{-1} \hat{n} \times \underline{b}_e, \underline{a}' \rangle_{\Gamma_h} = (\underline{j}_s, \underline{a}')_{\Omega_s} \qquad \forall \underline{a}' \in \boldsymbol{H}^0_e(\mathrm{curl}; \Omega).\end{aligned} \tag{2.49}$$

The system of equations of the hybrid model is completed with the weak form of (2.46) that reads:

$$\langle \underline{a}, \underline{q}' \rangle_{\Gamma_h} = \langle \mu \underline{\mathcal{A}}(\underline{q}), \underline{q}' \rangle_{\Gamma_h}, \quad \forall \underline{q}' \in \boldsymbol{H}^0_e(\mathrm{div}; \Gamma_h)\,, \tag{2.50}$$

where $\boldsymbol{H}^0_e(\mathrm{div}; \Gamma_h)$ is the function space that contains the basis functions for both $\underline{q}$ and $\underline{q}'$.

It is important to note that the equivalent magnetisation current $\underline{q}$, analogously to $\underline{a}$, is not unique and a gauge condition has to be applied (see Sections 1.3.3 and 1.3.2.2) in order to ensure its uniqueness. The source $\underline{q}$ should be gauged in the same way as the vector potential $\underline{a}$ [Kettunen *et al.*, 1999; Geuzaine, 2001].

When employing the magnetostatic case in Section 2.3.2, integral operators for the treatment of unbounded domains are incorporated analogously.

2.6.3 2D Hybrid $\underline{b}$-conforming formulations

We combine the BE method with the $\underline{b}$-conforming formulation of a magnetodynamic case described in Section 2.5.1.

The FE-BE coupling is done through the surface integral $\langle \mu^{-1} \partial_n a, a' \rangle_{\Gamma_h}$ in (2.30). Note that the term $\mu^{-1} \partial_n a$ is the tangential component of the magnetic field $h_t = \mu^{-1} b_t = \mu^{-1} \partial_n a = \mu^{-1} \hat{n} \cdot \operatorname{grad} a$, where $\hat{n}$ is the unit normal vector on Γ_h pointing into Ω.

Let us introduce the two-dimensional integral operator $\mathcal{A}(q)$ as

$$\mathcal{A}(q) = \int_{\Gamma_h} q(\underline{y})\, G(\underline{x}, \underline{y})\, \mathrm{d}\underline{y} \quad \text{with} \quad G(\underline{x}, \underline{y}) = -\frac{1}{2\pi} \ln |\underline{x} - \underline{y}|, \tag{2.51 a,b}$$

with $\underline{x} \in \mathbb{R}^2 \backslash \Omega$, $\underline{y} \in \Gamma_h$, and the function G the two-dimensional Laplace Green function. The equivalent magnetisation current $\underline{q} = q(\xi)\,\underline{1}_z$ on Γ_h is directed along the z-axis.

Particularising (2.45) for the two-dimensional case, one can show [Bossavit, 1998a; Geuzaine *et al.*, 2001] that on the boundary Γ_h and within Ω, it holds that

$$\partial_n \mathcal{A}(q) = \frac{1}{2}\, q + \int_{\Gamma_h} q(\underline{y})\, \hat{n} \cdot \operatorname{grad} G(\underline{x}, \underline{y})\, \mathrm{d}\underline{y}\,. \tag{2.52}$$

The magnetic potential a and its normal derivative can be expressed in terms of the integral operator (2.51) and (2.52), respectively, as

$$a = \mu \mathcal{A}(q)\,, \quad \partial_n a = \mu \partial_n \mathcal{A}(q)\,. \tag{2.53 a,b}$$

The weak form of (2.53 a) reads:

$$\langle a, q' \rangle_{\Gamma_h} = \langle \mu \mathcal{A}(q), q' \rangle_{\Gamma_h}\,, \quad \forall q' \in H_e^{10}(\Gamma_h)\,. \tag{2.54}$$

Introducing (2.53 b) in (2.30), we obtain

$$\begin{aligned} &(\mu^{-1} \operatorname{grad} a, \operatorname{grad} a')_\Omega + (\sigma\, \partial_t a, a')_{\Omega_c} = \\ &(j_s a, a')_{\Omega_s} + \langle \partial_n \mathcal{A}(q), a' \rangle_{\Gamma_h}\,, \qquad \forall a' \in H_e^{10}(\Omega)\,. \end{aligned} \tag{2.55}$$

On the basis of the discretisation of Ω and Γ_h, N_a real basis functions $\alpha_j(x, y)$ and N_q real basis functions $\beta_l(\xi)$ are defined for the vector potential $a(x, y)$ and the equivalent current layer $q(\xi)$ respectively:

$$a(x, y) = \sum_{j=1}^{N_a} a_j\, \alpha_j(x, y) \quad \text{and} \quad q(\xi) = \sum_{l=1}^{N_q} q_l\, \beta_l(\xi)\,. \tag{2.56}$$

The complex coefficients a_j and q_l are assembled in the column matrices $\boldsymbol{A}$ and $\boldsymbol{Q}$:

$$\boldsymbol{A} = \begin{bmatrix} a_1 & \dots & a_{N_a} \end{bmatrix}^T \quad \text{and} \quad \boldsymbol{Q} = \begin{bmatrix} q_1 & \dots & q_{N_q} \end{bmatrix}^T\,. \tag{2.57}$$

The complete hybrid system of algebraic equations is obtained by employing the N_a real basis functions $\alpha_i(x, y)$ as test functions in (2.55) and the N_q real basis functions $\beta_k(\xi)$ as test functions in (2.54). The resulting system of $N_a + N_q$ complex equations of the hybrid model can thus be written as:

$$\begin{bmatrix} \boldsymbol{S} + \imath w \boldsymbol{T} & \boldsymbol{C} \\ \boldsymbol{D}^T & \boldsymbol{M} \end{bmatrix} \begin{bmatrix} \boldsymbol{A} \\ \boldsymbol{Q} \end{bmatrix} = \begin{bmatrix} \boldsymbol{J} \\ 0 \end{bmatrix}\,, \tag{2.58}$$

where $\boldsymbol{S}$ and $\boldsymbol{T}$ are sparse $N_a \times N_a$ FE matrices, $\boldsymbol{C}$ and $\boldsymbol{D}$ are partially dense $N_a \times N_q$ matrices and $\boldsymbol{M}$ is a full $N_q \times N_q$ BE matrix. Their elements are given by

$$S_{i,j} = \int_\Omega \mu^{-1}\, \operatorname{grad} \alpha_i \cdot \operatorname{grad} \alpha_j\, \mathrm{d}\Omega\,, \tag{2.59}$$

$$T_{i,j} = \int_{\Omega_c} \sigma\, \alpha_i\, \alpha_j \,\mathrm{d}\Omega\,, \tag{2.60}$$

$$C_{i,l} = \oint_{\Gamma_h} \alpha_i \left(\frac{1}{2}\beta_l + \oint_{\Gamma_h} \beta_l\, \partial_n G \,\mathrm{d}\Gamma_h \right) \mathrm{d}\Gamma_h\,, \tag{2.61}$$

$$D_{j,k} = \oint_{\Gamma_h} \alpha_j \beta_k \,\mathrm{d}\Gamma_h\,, \tag{2.62}$$

$$M_{k,l} = \mu \oint_{\Gamma_h} \beta_k \left(\oint_{\Gamma_h} \beta_l\, G \,\mathrm{d}\Gamma_h \right) \mathrm{d}\Gamma_h\,. \tag{2.63}$$

The $N_a \times 1$ column matrix $\boldsymbol{J}$ follows from the imposed current density in Ω_s:

$$J_i = \int_{\Omega_s} j_s\, \alpha_i \,\mathrm{d}\Omega\,. \tag{2.64}$$

For the magnetostatic counterpart described in Section 2.5.2, the introduction of the integral operator for unbounded domains is done in the same way.

Introducing (2.53 b) in (2.31), we obtain

$$(\mu^{-1}\mathrm{grad}\, a, \mathrm{grad}\, a')_\Omega = (j_s a, a')_{\Omega_s} + \langle \partial_n \mathcal{A}(q), a' \rangle_{\Gamma_h}\,, \qquad \forall a' \in H_e^{10}(\Omega)\,. \tag{2.65}$$

Applying the same discretisation scheme as for the magnetodynamic case described above, the complete hybrid system of algebraic equations reads

$$\begin{bmatrix} \boldsymbol{S} & \boldsymbol{C} \\ \boldsymbol{D}^T & \boldsymbol{M} \end{bmatrix} \begin{bmatrix} \boldsymbol{A} \\ \boldsymbol{Q} \end{bmatrix} = \begin{bmatrix} \boldsymbol{J} \\ 0 \end{bmatrix}\,, \tag{2.66}$$

where $\boldsymbol{S}$ is a sparse $N_a \times N_a$ FE matrix, $\boldsymbol{C}$ and $\boldsymbol{D}$ are partially dense $N_a \times N_q$ matrices and $\boldsymbol{M}$ is a full $N_q \times N_q$ BE matrix. The definition of their elements is given in (2.59), (2.61), (2.62) and (2.63). Note that as all time dependent variation has been neglected, the resulting system is real.

Chapter 3

Basic theory of Integral equations

Contents

3.1 Introduction

Integral equation techniques solve for the sources of an electromagnetic field rather than for the field itself. The starting point is therefore to obtain a source-field

relationship in the form of an integro-differential operator working on the source terms. Indeed, Maxwell's equations (1.1)–(1.4) relate electromagnetic fields to their electromagnetic sources, i.e. currents and charges. The integral equation is obtained by enforcing the appropriate boundary conditions and a discretisation scheme is used to solve the equation numerically.

The method of moments (MoM) [Harrington, 1993] is the most popular discretisation scheme for scattering and radiation problems. The unknown source is expanded in terms of N known basis functions. A matrix system is then obtained by choosing a set of N test functions and enforcing the residual to be orthogonal to the test functions. All basis functions interact with all other basis functions and the matrix produced by the MoM is thus a full matrix. The memory needed to store this matrix scales as $\mathcal{O}(N^2)$ and the CPU time as $\mathcal{O}(N^3)$ or $\mathcal{O}(N^2)$ with a direct and an iterative equation solver, respectively. The MoM is particularly advantageous for configurations involving homogeneous regions and open regions since only the boundaries need to be discretised. However, the MoM is also used to solve volume integral equations for inhomogeneous regions.

In the nineties, the fast multipole method (FMM) [Rokhlin, 1990; Coifman *et al.*, 1993] has been introduced to enhance the MoM scheme. The memory requirement and CPU time scale as $\mathcal{O}(N^{1.5})$ for the single level case and as $\mathcal{O}(N \log N)$ for multilevel implementations. The FMM will be discussed in detail in Chapter 4.

This chapter is organised as follows. In Section 3.2, we discuss the way of establishing an integral equation by means of the equivalence principle and we derive expressions of the electric and magnetic fields as a function of auxiliary potential functions. The projection method known as the method of moments (MoM), very popular for solving scattering problems, is presented in Section 3.3. Particular attention is paid to the Galerkin testing scheme and the choice of basis functions. Some often encountered examples of integral equations are given in Section 3.4. Finally, Section 3.5 briefly deals with the problem of singularities in IE methods.

3.2 Integral equations

The treatment presented hereafter illustrates some basic principles of integral formulations. We deliberately omit any further details. A more extensive treatment can be found in many works, e.g. those of [Balanis, 1988] and [Peterson *et al.*, 1998].

3.2.1 The equivalence principle

The derivation of an integral equation begins with the application of an appropriate equivalence principle [Harrington, 1961; Balanis, 1988]. This allows the problem to be reduced to that of sources (currents or charges) radiating in a homogeneous medium and the integral equation is derived by enforcing the appropriate boundary conditions (see Section 1.1.2). This general principle is illustrated below by way of two complementary examples.

Assume that a homogeneous object Ω_1 (ϵ_1, μ_1, σ_1) is present in free space and excited by an incident field. The unknown fields are $\underline{e}$ and $\underline{h}$. The surface equivalence principle can be used to establish an equivalent problems where $\underline{e}$ and $\underline{h}$ remain unchanged outside Ω_1 but become zero inside.

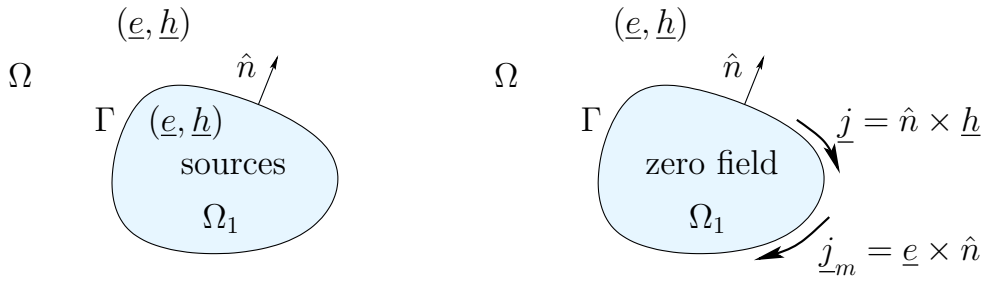

Figure 3.1: The equivalence principle: the equivalent electric and magnetic currents, $\underline{j}$ and $\underline{j}_m$, produce the same field external to Γ as the original sources

The discontinuity of the fields must be offset by placing equivalent electric and magnetic surface currents on the surface of the object (see Section 1.1.2). These equivalent surface currents are

$$\underline{j} = \hat{n} \times \underline{h}\,, \quad \underline{j}_m = \underline{e} \times \hat{n}\,, \tag{3.1}$$

where $\hat{n}$ is the outward unit normal (see Figure 3.1). The sources in (3.1) radiate in a homogeneous medium.

We consider now the equivalent problem with unknown fields $\underline{e}$ and $\underline{h}$ inside Ω_1 and zero field outside. Again it is required to place equivalent surface currents on the surface Γ. These currents are the same as those in (3.1) except that $\hat{n}$ is the inward unit normal. Since the field is zero outside, the free space region can be filled with a material characterised by ϵ_1, μ_1 and σ_1.

The exterior and interior equivalent problems described above can be combined by imposing tangential continuity of $\underline{e}$ and $\underline{h}$ on the surface of Ω_1 which yields two coupled integral equations with the unknown currents $\underline{j}$ and $\underline{j}_m$.

3.2.2 Source-field relationships

Integral equations in electromagnetics are derived by specifying the sources radiating in a homogeneous medium and requiring the generated field. An alternative approach consists in considering the scattered fields as derived from auxiliary functions known as potentials. While it is possible to calculate the electric and magnetic fields, $\underline{e}$ and $\underline{h}$, directly from the electric and magnetic source current densities, $\underline{j}$ and $\underline{j}_m$, it is often simpler to calculate the auxiliary magnetic and electric vector potential functions first, $\underline{a}$ and $\underline{f}$, and then determine $\underline{e}$ and $\underline{h}$. The magnetic and electric vector potentials $\underline{a}$ and $\underline{f}$ are, as it will be clear, generated by $\underline{j}$ and $\underline{j}_m$.

Let us consider a certain homogeneous volume Ω with boundary surface Γ characterised by ϵ, μ, σ.

We derive the expression of the fields as a function of $\underline{a}$ and $\underline{f}$ by considering two complementary cases:

- ✓ $\underline{j} \neq 0$ and $\underline{j}_m = 0$, we obtain $\underline{e}_a$ and $\underline{h}_a$ where the subscript a indicates the field due to the magnetic vector potential $\underline{a}$;
- ✓ $\underline{j} = 0$ and $\underline{j}_m \neq 0$, we obtain $\underline{e}_f$ and $\underline{h}_f$ where the subscript f indicates the field due to the electric vector potential $\underline{f}$.

The total fields are then obtained by the superposition of the individual fields due to $\underline{a}$ and $\underline{f}$, i.e.

$$\underline{e} = \underline{e}_a + \underline{e}_f \,, \tag{3.2}$$

$$\underline{h} = \underline{h}_a + \underline{h}_f \,. \tag{3.3}$$

3.2.2.1 Electric and magnetic fields due to an electric current source

We assume $\underline{j} \neq 0$ and $\underline{j}_m = 0$. Since (1.42) is always true, we can introduce a magnetic vector potential $\underline{a}$ verifying

$$\underline{b}_a = \operatorname{curl} \underline{a} \,. \tag{3.4}$$

Substituting (3.4) in Faraday's law (1.41), we obtain

$$\operatorname{curl} (\underline{e}_a + \imath\omega\underline{a}) = 0 \,. \tag{3.5}$$

From the vector identity

$$\operatorname{curl} (-\operatorname{grad} v) = 0$$

and (3.5), it follows that

$$\underline{e}_a = -\operatorname{grad} v - \imath\omega\underline{a} \,, \tag{3.6}$$

where v represents an electric scalar potential.

Taking the curl on both sides of (3.4), considering the magnetic constitutive relation (1.11 b) and using the vector identity

$$\operatorname{curl}\operatorname{curl} \underline{a} = \operatorname{grad}\operatorname{div} \underline{a} - \Delta\underline{a} \,,$$

we can write for a homogeneous medium

$$\mu\operatorname{curl} \underline{h}_a = \operatorname{grad}\operatorname{div} \underline{a} - \Delta\underline{a} \,. \tag{3.7}$$

Introducing Ampére's law (1.40) and the electric constitutive relation (1.15) in (3.7) leads to

$$\mu\underline{j} + \imath\omega\mu\epsilon\underline{e}_a = \operatorname{grad}\operatorname{div} \underline{a} - \Delta\underline{a} \,. \tag{3.8}$$

Substituting (3.6) into (3.8), we obtain

$$\Delta\underline{a} + k^2\underline{a} = -\mu\underline{j} + \operatorname{grad} (\operatorname{div} \underline{a} + \imath\omega\mu\epsilon v) \,, \tag{3.9}$$

where $k = \omega\sqrt{\mu\epsilon} = 2\pi/\lambda$ is referred to as the wavenumber; λ is the wavelength. In order to simplify (3.9), we impose the so-called Lorentz condition, i.e.

$$\operatorname{div} \underline{a} = -\imath\omega\mu\epsilon v \,. \tag{3.10}$$

From (3.9) and (3.10), we obtain the inhomogeneous Helmholtz equation

$$\Delta \underline{a} + k^2 \underline{a} = -\mu \underline{j}\,, \tag{3.11}$$

whose solution Γ is the magnetic vector potential $\underline{a}$. If $\underline{j}$ is confined within a surface Γ, it reads

$$\underline{a}(\underline{r}) = \mu \int_{\Gamma} \underline{j}(\underline{r}')\, G(\rho)\, \mathrm{d}\Gamma'\,, \tag{3.12}$$

where $G(\rho)$ is the three-dimensional Helmholtz Green function,

$$G(\rho) = \frac{e^{-\imath k \rho}}{4\pi\rho}\,, \tag{3.13}$$

which depends on the distance $\rho = |\underline{r} - \underline{r}'|$ between the source point $\underline{r}'$ and the observation point $\underline{r}$. For two-dimensional problems, the Helmholtz Green function is given by

$$G_{2D}(\rho) = \frac{1}{4\imath} H_0^{(2)}(k\rho)\,, \tag{3.14}$$

with $H_0^{(2)}$ is the Hankel function of second kind and order 0.

In addition, (3.6) reduces to

$$\underline{e}_a = -\imath\omega \underline{a} - \frac{\imath}{\omega\mu\epsilon} \mathrm{grad}\,(\mathrm{div}\,\underline{a})\,. \tag{3.15}$$

3.2.2.2 Electric and magnetic field due to a magnetic current source

The essential difference between electric and magnetic currents is the nonexistence of magnetic charges in nature. There is thus no free magnetic charge and no magnetic current. Equivalent magnetic currents $\underline{j}_m$ arise when using the equivalence theorem. This equivalent magnetic current is introduced in Faraday's law (1.41) as

$$\mathrm{curl}\,\underline{e} + \imath\omega \underline{b} = -\underline{j}_m\,. \tag{3.16}$$

The field generated by an equivalent magnetic current in a homogeneous region, with $\underline{j} = 0$ but $\underline{j}_m \neq 0$, must satisfy from (1.43) $\mathrm{div}\,\underline{d} = 0$. Therefore, $\underline{e}_f$ considering (1.15) can be expressed as

$$\underline{e}_f = -\frac{1}{\epsilon} \mathrm{curl}\,\underline{f}\,. \tag{3.17}$$

Introducing (3.17) in Ampére's law (1.40), and taking into account the vector identity

$$\mathrm{curl}\,(-\mathrm{grad}\,\varphi) = 0\,,$$

it follows that

$$\underline{h}_f = -\mathrm{grad}\,\varphi - \imath\omega \underline{f}\,, \tag{3.18}$$

where φ represents a magnetic scalar potential.

Taking the curl of (3.17) and considering (3.16) leads to

$$-\underline{j}_m - \imath\omega\mu\underline{h}_f = \frac{1}{\epsilon}(\operatorname{grad}\operatorname{div}\underline{f} - \Delta\underline{f})\,. \tag{3.19}$$

The substitution of (3.18) into (3.19) reduces it to

$$\Delta\underline{f} + k^2\underline{f} = -\epsilon\underline{j}_m + \operatorname{grad}(\operatorname{div}\underline{f} + \imath\omega\mu\epsilon\varphi)\,. \tag{3.20}$$

In order to simplify (3.20), we choose

$$\operatorname{div}\underline{f} = -\imath\omega\mu\epsilon\varphi\,. \tag{3.21}$$

From (3.20) and (3.21), we obtain thus the following inhomogeneous Helmholtz equation

$$\Delta\underline{f} + k^2\underline{f} = -\epsilon\underline{j}_m\,, \tag{3.22}$$

whose solution is the electric vector potential $\underline{f}$. If $\underline{j}_m$ is confined within a surface Γ, it reads

$$\underline{f}(\underline{r}) = \epsilon\int_\Gamma \underline{j}_m(\underline{r}')\,G(\rho)\,\mathrm{d}\Gamma'\,. \tag{3.23}$$

Besides, the expression of the magnetic field in function of $\underline{f}$ is

$$\underline{h}_f = -\imath\omega\underline{f} - \frac{\imath}{\omega\mu\epsilon}\operatorname{grad}(\operatorname{div}\underline{f})\,. \tag{3.24}$$

The total fields (3.2) and (3.3) are thus given by

$$\underline{e} = \underline{e}_a + \underline{e}_f = -\imath\omega\underline{a} - \frac{\imath}{\omega\mu\epsilon}\operatorname{grad}(\operatorname{div}\underline{a}) - \frac{1}{\epsilon}\operatorname{curl}\underline{f}\,, \tag{3.25}$$

$$\underline{h} = \underline{h}_a + \underline{h}_f = -\imath\omega\underline{f} - \frac{\imath}{\omega\mu\epsilon}\operatorname{grad}(\operatorname{div}\underline{f}) + \frac{1}{\mu}\operatorname{curl}\underline{a}\,. \tag{3.26}$$

Another useful representation is the mixed potential form in which both vector and scalar potentials are used. The electric and magnetic scalar potentials, v and φ, read

$$v(\underline{r}) = \frac{1}{\epsilon}\int_\Gamma q(\underline{r}')\,G(\rho)\,\mathrm{d}\Gamma'\,, \tag{3.27}$$

$$\varphi(\underline{r}) = \frac{1}{\mu}\int_\Gamma q_m(\underline{r}')\,G(\rho)\,\mathrm{d}\Gamma'\,, \tag{3.28}$$

with q and q_m the electric and magnetic surface charge density, respectively. Note that the only unknowns are the currents $\underline{j}$ and $\underline{j}_m$ which are related to the respective charge densities q and q_m through the equation of conservation (1.5). In the frequency domain, it is given by

$$\operatorname{div}\underline{j} = -\imath\omega q\,. \tag{3.29}$$

The electric and magnetic fields, (3.25) and (3.26), can then be written as

$$\underline{e} = -\imath\omega\underline{a} - \operatorname{grad} v - \frac{1}{\epsilon}\operatorname{curl}\underline{f}\,, \tag{3.30}$$

$$\underline{h} = -\imath\omega\underline{f} - \operatorname{grad}\varphi + \frac{1}{\mu}\operatorname{curl}\underline{a}\,. \tag{3.31}$$

3.3 The method of moments (MoM)

The method of moments (MoM) [Harrington, 1993] is a discretisation scheme for equations of the form

$$\mathcal{L}f = g\,, \tag{3.32}$$

where $\mathcal{L}$ is a linear integro-differential operator, g is a known excitation function and f is the unknown response function to be determined. Typical examples of such equations are the EFIE (3.49), the MFIE (3.62) and the CFIE (3.66). The first step in the MoM is to expand the unknown function f as a linear combination of N basis functions f_n, defined in the same domain as f. The approximation is

$$f = \sum_{n=1}^{N} c_n f_n\,, \tag{3.33}$$

where c_n are unknown coefficients. The basis functions f_n are chosen so that each $\mathcal{L}f_n$ can be conveniently evaluated (in closed form or numerically). The residual, considering the linearity of $\mathcal{L}$, is defined as

$$r_N = g - \mathcal{L}\sum_{n=1}^{N} c_n f_n = g - \sum_{n=1}^{N} c_n \mathcal{L}f_n\,. \tag{3.34}$$

The residual is forced to be orthogonal to another N-dimensional subspace spanned by a set of functions w_m, $m = 1, 2, \cdots, N$. This condition is expressed as

$$\langle w_m, r_N \rangle = 0, \quad m = 1, 2, \cdots, N\,. \tag{3.35}$$

The functions w_n are known as test or weight functions.

Inserting (3.34) in (3.35), the following matrix equation is obtained:

$$\boldsymbol{M}\underline{i} = \underline{v}\,, \tag{3.36}$$

where the elements of the impedance matrix $\boldsymbol{M}$ and the excitation vector $\underline{v}$ are given by

$$M_{m,n} =< w_m, \mathcal{L}f_n >\,, \quad v_m =< w_m, g > \ . \tag{3.37 a,b}$$

The elements i_n of $\underline{i}$ are the coefficients in (3.33). The MoM does not guarantee that the coefficients i_n are optimal. If the test functions are poorly chosen, the residual might have components outside the space spanned by the test functions. In general, this is avoided if the test functions can accurately represent both g and $\sum_{n=1}^{N} c_n \mathcal{L}f_n$. This requires that w_n is in the range of $\mathcal{L}$ [Sarkar, 1985].

3.3.1 Galerkin method

The EFIE and MFIE operators presented in Sections 3.4.1 and 3.4.2 have the same domain and range [Hsiao & Kleinman, 1997]. This suggests that the choice

$$w_n = f_n \tag{3.38}$$

might be good. The orthogonality condition in (3.35) becomes

$$\langle f_m, r_N \rangle = 0, \quad m = 1, 2, \cdots, N\,. \tag{3.39}$$

This special case, in which the basis functions coincide with the test functions, is actually the Galerkin method.

Many authors have stated that the Galerkin method does not contribute to a better performance of the MoM, and that basis and test functions can be chosen independently, e.g. [Harrington, 1993]. However, it was shown in [Wandzura, 1991] that the Galerkin method presents a better convergence for scattering computations. Although the Galerkin approach is optimal for far field computations, other testing schemes might perform equally well. Indeed, the error in the surface current depends on the choice of the basis functions and not on the choice of the test functions [Peterson *et al.*, 1996]. Nevertheless, the error in scattering fields depends on both the basis and test functions.

3.3.2 Basis functions

In the previous section, a testing scheme that relates the test functions to the basis functions is presented. The discussion was general and nothing was said about the specific choice of basis functions. In this section, we consider different kinds of basis functions and their properties.

Basis functions can be classified into entire-domain or subsectional basis functions. Entire-domain basis functions are defined on the entire-domain, e.g. the surface Γ (3.50). This is generally not practical for 3D problems. They are rarely used. An exception is a wire antenna where the domain is one-dimensional and a Fourier expansion of the current has proved efficient [Sarkar *et al.*, 1985].

Subsection basis functions are defined on a subdomain of the object. This subdomains are often referred to as patches and usually taken as triangles or quadrilaterals. Well known examples of such subsectional basis functions are the rooftop basis functions for triangles in [Rao *et al.*, 1982] and the rooftop basis functions for quadrilaterals in [Glisson & Wilton, 1980]. The rooftop basis functions for triangles are often referred to as the Rao-Wilton-Glisson (RWG) basis functions. They provide a piecewise linear expansion of the surface current, i.e. the current is expanded in terms of first order polynomials. High order basis functions are subsectional basis functions that provide a piecewise polynomial expansion of second, third, or even higher order. The high order expansion allows the size of the element to be increased and the overall number of basis functions to be decreased in comparison with a first order expansion [Graglia *et al.*, 1997].

Divergence-conforming basis functions impose normal continuity of a vector quantity between neighbouring elements and are suitable for expansion of the surface current in a MoM solution. The enforced continuity avoids buildup of line charges at the boundary between adjacent patches.

Many authors have tried to find the most suitable basis functions for a specific problem [Sarkar, 1985; Sarkar *et al.*, 1985; Gürel *et al.*, 1999; Aksun & Mittra,

1993]. These works illustrate that the choice of basis functions is always a trade-off between different properties. The four factors mentioned in [Harrington, 1993] that can be used to choose a suitable set of basis functions are:

- ✓ the accuracy of the solution desired,
- ✓ the ease of evaluation of the matrix elements,
- ✓ the size of the matrix that can be inverted,
- ✓ the condition number of the matrix.

It is worth noticing that the basis functions commonly used in the MoM community can be directly related to the basis functions in the FEM community [Graglia *et al.*, 1997]. Recognising these relation has two main benefits:

- ✓ The high order basis functions for MoM computations are readily available through the work done in FEM [Geuzaine *et al.*, 1999a; Ren & Ida, 2000; Bossavit, 2002; Geuzaine, 2001].
- ✓ The recently proposed loop-star basis functions [Vecchi, 1999; Lee *et al.*, 2003] are similar to the tree-cotree decomposition in the vector finite element methods. Analogously to the tree-cotree decomposition in FEM, the loop-star splitting allows to obtain reliable MoM solutions in the low frequency limit. This low frequency instability also results in deteriorating the condition number when smaller elements are used in MoM computations.

We consider in particular the RWG and the thin wire basis functions related to edge element and nodal element basis functions, respectively.

3.3.2.1 Relation between RWG basis functions and edge element basis functions

The usual description of the RWG basis functions for triangles is shown in Figure 3.2. The RWG vector basis function associated with the common edge of triangles T^+

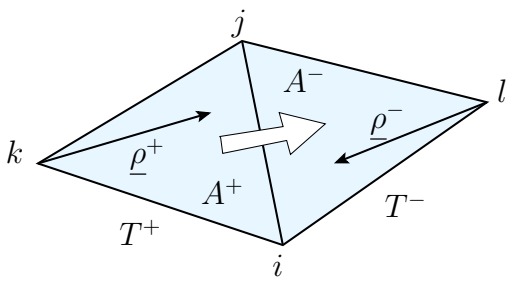

Figure 3.2: Triangle pair and geometrical parameters for the RWG basis function

and T^- can be written as

$$\underline{f}_{i,j}^{T}(\underline{r}) = l_{i,j} \begin{cases} \dfrac{\underline{\rho}^+}{2A^+}, & \underline{r} \in T^+ \\ \dfrac{-\underline{\rho}^-}{2A^-}, & \underline{r} \in T^- \\ 0 & \text{, elsewhere} \end{cases}, \tag{3.40}$$

where A^+ and A^- are the area of triangles T^+ and T^-, respectively. The length of the common edge is $l_{i,j}$ and the local vectors $\underline{\rho}^+$ and $\underline{\rho}^-$ are defined with regard to the vertex opposite to the common edge as in Figure 3.2. Furthermore, we have

$$\operatorname{div} \underline{f}_{i,j}^{T}(\underline{r}) = l_{i,j} \begin{cases} \dfrac{1}{A^+}, & \underline{r} \in T^+ \\ \dfrac{-1}{A^-}, & \underline{r} \in T^- \\ 0, & \text{elsewhere} \end{cases}. \tag{3.41}$$

An edge is mostly shared by two triangles. Beware additional unknowns need to be assigned when an edge is shared by more than two triangles.

The usual description of edge elements in FEM is shown in Figure 3.3. The edge

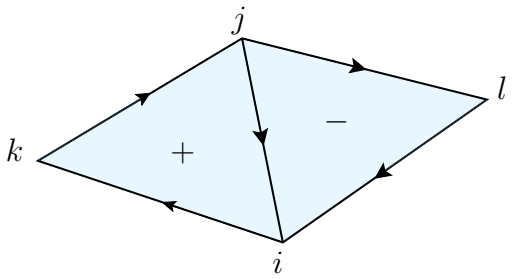

Figure 3.3: Edge elements for triangular FEM

element basis function (1.70) associated with edge i, j is defined by

$$\underline{w}_{i,j} = \varsigma_i \operatorname{grad} \varsigma_j - \varsigma_j \operatorname{grad} \varsigma_i \tag{3.42}$$

where ς_i is the centroid coordinates of vertex i. The RWG basis function, $\underline{f}_{i,j}^{S}$, and the edge element basis function, $\underline{w}_{i,j}$, are related by

$$\underline{f}_{i,j}^{T}(\underline{r}) = l_{i,j} \begin{cases} \hat{n}^+ \times \underline{w}_{i,j}(\underline{r}), & \underline{r} \in T^+ \\ \hat{n}^- \times \underline{w}_{i,j}(\underline{r}), & \underline{r} \in T^- \end{cases}, \tag{3.43}$$

where $\hat{n}^+$, $\hat{n}^-$ are the unit normals to triangles T^+, T^-, respectively.

3.3.2.2 Relation between thin wire basis functions and nodal element basis functions

Basis functions suitable for representing currents induced in thin wires (the surface current density presents a dominant axial component [Balanis, 1997]) are given by

$$\underline{f}_i^S(\underline{r}) = \begin{cases} \dfrac{\underline{\rho}^+}{l^+}, & \underline{r} \in S^+ \\ \dfrac{-\underline{\rho}^-}{l^-}, & \underline{r} \in S^- \\ 0, & \text{elsewhere} \end{cases}, \tag{3.44}$$

where l^+, l^- are the lengths of the segments S^+, S^-, and the local vectors $\underline{\rho}^+$ and $\underline{\rho}^-$ are defined as in Figure 3.4. Note that they are associated with node i. The

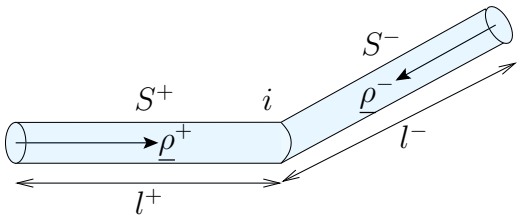

Figure 3.4: Segment pair and geometrical parameters for thin wire basis functions

divergence of (3.44) is calculated analytically as

$$\operatorname{div} \underline{f}_i^S(\underline{r}) = \begin{cases} \dfrac{1}{l^+}, & \underline{r} \in S^+ \\ \dfrac{-1}{l^-}, & \underline{r} \in S^- \\ 0, & \text{elsewhere} \end{cases}. \tag{3.45}$$

The nodal element basis functions w_i (1.69) associated with node i are linear basis functions with unit value at node i and zero elsewhere, i.e.

$$w_i = \varsigma_i \,. \tag{3.46}$$

It is easy to find a relation between the thin wire basis functions f_i^S (3.44) and the nodal element basis function w_i associated with node i. This relation reads

$$\underline{f}_i^S(\underline{r}) = \begin{cases} \hat{t}^+ \cdot w_i(\underline{r}), & \underline{r} \in S^+ \\ \hat{t}^- \cdot w_i(\underline{r}), & \underline{r} \in S^- \end{cases}, \tag{3.47}$$

where $\hat{t}^+$, $\hat{t}^-$ are the unit tangent vectors on S^+, S^- and have the same origin as $\underline{\rho}^+$, $\underline{\rho}^-$.

3.4 Some examples of integral equations

3.4.1 Electric field integral equation (EFIE) for PEC

Following the equivalence principle (see Section 3.2.1), it is easy to derive the EFIE for closed perfectly electric conductors (PEC) in free space. The surface equivalence principle is applied to remove the PEC object, leaving only an electric surface current $\underline{j}$ on its surface Γ radiating in free space. The field $\underline{e}$ is given by the sum of an incident field $\underline{e}_i$, which exists at a given location independently of the PEC object, and a scattered field $\underline{e}_s$ caused by the electric surface current on the PEC object. The magnetic surface current $\underline{j}_m$ is zero to satisfy $\hat{n} \times \underline{e} = 0$, i.e. the tangential field must vanish on Γ,

$$\hat{n} \times \underline{e}(\underline{r}) = \hat{n} \times (\underline{e}_i(\underline{r}) + \underline{e}_s(\underline{r})) = 0\,, \quad \underline{r} \in \Gamma\,. \tag{3.48}$$

It is useful to express the EFIE as

$$\hat{n} \times \left(\underline{e}_i + \mathcal{L}_e \underline{j}\right) = 0\,. \tag{3.49}$$

The linear operator $\mathcal{L}_e \underline{j}$ can be derived by substituting (3.12) and (3.27) in (3.30) and considering the equation of continuity $\operatorname{div} \underline{j} = -\imath\omega q$. It reads

$$\mathcal{L}_e \underline{j} = \imath\omega\mu \int_\Gamma \underline{j}(\underline{r}')\, G(\rho)\, \mathrm{d}\Gamma' - \frac{1}{\imath\omega\epsilon} \operatorname{grad} \int_\Gamma \left(\operatorname{div} \underline{j}(\underline{r}')\right)\, G(\rho)\, \mathrm{d}\Gamma'\,, \quad \underline{r} \in \Gamma\,. \tag{3.50}$$

This form of the EFIE (3.49) is known as the mixed potential formulation. Integral equations in the form of (3.49) are referred to as Fredholm integral equations of the first kind since the unknown quantity only appears inside the integral [Delves & Walsh, 1974].

The EFIE, derived above for a closed PEC object, is also valid for an open PEC such as an infinitely thin plate. This can be seen by taking the limit as a closed object with finite thickness collapses into an infinitely thin object. The electric surface current is the average of the currents on the two sides of the infinitely thin object. The current component orthogonal to the edge of a thin object must vanish at the edge. The outward normal $\hat{n}$ in (3.49) is not uniquely defined for an infinitely thin object but can be chosen as either of the two normals on the surface Γ.

In order to discretise the EFIE for PEC (3.49), we express it as a function of the magnetic vector potential (3.12) and the electric scalar potential (3.27) as

$$\hat{n} \times \underline{e}_i(\underline{r}) = \hat{n} \times (\imath\omega\underline{a} + \operatorname{grad}\varphi)\,, \quad \underline{r} \in \Gamma\,, \tag{3.51}$$

or simply

$$\underline{e}_{i,t}(\underline{r}) = (\imath\omega\underline{a} + \operatorname{grad}\varphi)_t\,, \quad \underline{r} \in \Gamma\,, \tag{3.52}$$

where the subscript t denotes to the tangential component of the electric field.

Let us apply the Galerkin method to (3.52) with the RWG basis functions (3.40) defined in the Section 3.3. It yields

$$\imath\omega\langle \underline{a}, \underline{f}_m\rangle_\Gamma + \langle \operatorname{grad}\varphi, \underline{f}_m\rangle_\Gamma = \langle \underline{e}_i, \underline{f}_m\rangle_\Gamma\,, \quad 1 \le m \le N. \tag{3.53}$$

Taking into account the divergence theorem on a closed surface,

$$\int_\Gamma \operatorname{grad}\varphi \cdot \underline{f}_m \, \mathrm{d}\Gamma = -\int_\Gamma \varphi \operatorname{div} \underline{f}_m \, \mathrm{d}\Gamma \,, \tag{3.54}$$

and approximating the fields and potentials at the triangle centroids $\underline{r}_m^{c\pm}$ of each basis function, (3.53) reduces to a linear system of equations, $1 \leq m, n \leq N$:

$$l_m \left[\imath\omega \left(\underline{a}_{mn}^{c+} \cdot \frac{\underline{\rho}_m^{c+}}{2} - \underline{a}_{mn}^{c-} \cdot \frac{\underline{\rho}_m^{c-}}{2} \right) + \varphi_{mn}^{c-} - \varphi_{mn}^{c+} \right] i_n = l_m \left[\underline{e}_i \left(\underline{r}_m^{c+} \right) \cdot \frac{\underline{\rho}_m^{c+}}{2} - \underline{e}_i \left(\underline{r}_m^{c-} \right) \cdot \frac{\underline{\rho}_m^{c-}}{2} \right] , \tag{3.55}$$

where for a pair of triangles T_m^+, T_m^- with a common edge l_m, $\underline{\rho}^{c+}$ and $\underline{\rho}^{c-}$ are local position vectors with origin at the vertices of T_m^+, T_m^- opposite to l_m (see Figure 3.2). This system can be expressed as a matrix equation (3.36), where $\boldsymbol{M}$ is a complex symmetric and dense $N \times N$ matrix, $\underline{v}$ denotes the voltage vector and $\underline{i}$ contains the currents (degrees of freedom) flowing across the inner edges of the triangles. $\underline{i}$ and $\underline{v}$ are column vectors with N elements.

The elements of $\boldsymbol{M}$ and $\underline{v}$ are given by

$$M_{m,n} = l_m \left[\imath\omega \left(\underline{a}_{mn}^{c+} \cdot \frac{\underline{\rho}_m^{c+}}{2} - \underline{a}_{mn}^{c-} \cdot \frac{\underline{\rho}_m^{c-}}{2} \right) + \varphi_{mn}^{c-} - \varphi_{mn}^{c+} \right] , \tag{3.56}$$

$$v_m = l_m \left[\underline{e}_i \left(\underline{r}_m^{c+} \right) \cdot \frac{\underline{\rho}_m^{c+}}{2} - \underline{e}_i \left(\underline{r}_m^{c-} \right) \cdot \frac{\underline{\rho}_m^{c-}}{2} \right] , \tag{3.57}$$

where the magnetic vector potential and the electric scalar potential on the centroids are defined, respectively, as

$$\underline{a}_{mn}^{c\pm} = \frac{\mu}{4\pi} \int_\Gamma \underline{f}_n \left(\underline{r}' \right) \frac{e^{-\imath k R_m^{c\pm}}}{R_m^{c\pm}} \, \mathrm{d}\Gamma', \tag{3.58}$$

$$\varphi_{mn}^{c\pm} = -\frac{1}{4\pi\imath\omega\epsilon} \int_\Gamma \operatorname{div} \underline{f}_n \left(\underline{r}' \right) \frac{e^{-\imath k R_m^{c\pm}}}{R_m^{c\pm}} \, \mathrm{d}\Gamma' \,, \tag{3.59}$$

with $R_m^{c\pm} = |\underline{r}_m^{c\pm} - \underline{r}'|$ distance between the element centroid and a source point $\underline{r}'$.

3.4.2 Magnetic field integral equation (MFIE) for PEC

The MFIE for PEC objects is derived analogously to the EFIE. The surface equivalence principle (see Section 3.2.1) is used to remove the PEC object which leaves only electric surface currents radiating in free space. These electric currents maintain the correct field source outside Γ and a zero field inside. Therefore, the MFIE described below is referred to as the exterior MFIE. The boundary condition for the magnetic field on Γ is

$$\hat{n} \times \underline{h}(\underline{r}) = \hat{n} \times (\underline{h}_i(\underline{r}) + \underline{h}_s(\underline{r})) = 0 \quad \underline{r} \in \Gamma \,. \tag{3.60}$$

Using (3.12) and (3.26) in (3.60) yields

$$\hat{n} \times \underline{h}_i(\underline{r}) = \underline{j}(\underline{r}) - \hat{n} \times \left(\operatorname{curl} \int_\Gamma \underline{j}(\underline{r}') \, G(\rho) \, \mathrm{d}\Gamma' \right), \quad \underline{r} \in \Gamma \,. \tag{3.61}$$

The curl operator can be moved inside the integral by using the results in Appendix C. This leads to

$$\hat{n} \times \underline{h}_i(\underline{r}) = \frac{\underline{j}(\underline{r})}{2} + \hat{n} \times \left(\int\!\!\!\!\!\!- _\Gamma \underline{j}(\underline{r}') \times \operatorname{grad} G(\rho) \, \mathrm{d}\Gamma' \right), \quad \underline{r} \in \Gamma \,, \tag{3.62}$$

where the bar across the integral sign indicates that the point $\underline{r}' = \underline{r}$ is excluded from the integration. The expression in (3.62) is the most common form of the exterior MFIE and is valid for a smooth surface. For more general surfaces, the term $\frac{\underline{j}(\underline{r})}{2}$ should be replaced by $\frac{\phi}{4\pi} \underline{j}(\underline{r})$ where ϕ is the exterior solid angle at $\underline{r}$ [Peterson *et al.*, 1998]. The interior MFIE differs from (3.62) by the sign of the term $\frac{\underline{j}(\underline{r})}{2}$. When implementing the MFIE, it is advantageous to use the following identity:

$$\hat{n} \times \left(\underline{j}(\underline{r}') \times \operatorname{grad} G(\rho) \right) = \frac{G(\rho)}{\rho} \left(\frac{1}{\rho} + \imath k \right) \left[\hat{n} \cdot \underline{\rho} \; \underline{j}(\underline{r}') - \left(\hat{n} \cdot \underline{j}(\underline{r}') \, \underline{\rho} \right) \right] . \tag{3.63}$$

The expression (3.63) is weakly singular whereas the integrand in (3.62) is strongly singular[1]. Note also that (3.63) vanishes if the observation point $\underline{r}$ is located in the plane of the surface current.

The MFIE may be written in the shorter notation

$$\left(\frac{1}{2} \mathcal{I} + \mathcal{L}_m \right) \underline{j} = \hat{n} \times \underline{h}_i \,, \tag{3.64}$$

where $\mathcal{I}$ is the identity operator and $\mathcal{L}_m$ is a compact operator [Peterson *et al.*, 1998]. Integral equations that can be written as (3.64) are known as Fredholm equations of the second kind. Getting a stable numerical solution from those equations is easier than from integral equations of the first kind [Delves & Walsh, 1974].

The MFIE was derived for closed objects. Unfortunately, it is not applicable to open surfaces unless the currents on each side of the open surface are left as independent unknowns. This leads to a more complicated numerical solution and doubles the number of unknowns in comparison to the EFIE.

3.4.3 Combined field integral equation (CFIE) for PEC

Unfortunately, for a closed object, the EFIE and the MFIE fail to provide a unique solution for all frequencies [Chew, 1995; Peterson *et al.*, 1998]. The nonuniqueness is caused by homogeneous (also called spurious) solutions, i.e. solutions that fulfil the boundary conditions with a zero incident field. Physically, the spurious solutions of

[1] Integrals with singularities can be classified as weakly singular, strongly singular or hypersingular. For $\rho \to 0$ the integrands behave as ρ^{-1}, ρ^{-2} and ρ^{-3}, respectively

the EFIE are the resonant modes of a PEC cavity. A cavity made of a perfectly magnetic conductor supports similar resonant magnetic surface currents. The spurious solutions of the MFIE can be interpreted as the electric currents induced by the resonant magnetic currents. These solutions are nonphysical and radiate a nonzero field outside the object. In [Peterson, 1990] the numerical consequences of spurious solutions and some possible corrections are studied. The uniqueness of the solution of the EFIE and MFIE is then not guaranteed at interior resonance frequencies. It is particularly troublesome for large objects due to a large probability of hitting a resonance frequency.

The most common method to deal with this problem is the combined field integral equation (CFIE) which uses a linear combination of the MFIE and EFIE to provide a unique stable solution [Mautz & Harrington, 1978]. This linear combination is given by

$$\text{CFIE} = \alpha\,\text{EFIE} + (1-\alpha)\eta\,\text{MFIE} \tag{3.65}$$

or in operator form

$$\alpha\mathcal{L}_e\underline{j} + (1-\alpha)\eta\left(\frac{1}{2}\mathcal{I} + \mathcal{L}_m\right)\underline{j} = \alpha\,(\hat{n}\times\underline{e}_i) + (1-\alpha)\eta\,(\hat{n}\times\underline{h}_i)\,, \tag{3.66}$$

where α is a real number between 0 and 1 and $\eta = \sqrt{\mu/\epsilon}$ is the intrinsic impedance of the medium. Usually, $0.2 < \alpha < 0.8$ is a good choice. The EFIE and the MFIE have the same resonance frequencies but their null spaces differ. The CFIE has no spurious solutions and is a second kind integral equation [Rao & Wilton, 1990]. It is easy to implement if the EFIE and MFIE solutions are already available.

3.4.4 Electrostatic scalar potential integral equation

In electrostatics (see Section 1.3.2.1), the electric field is time-independent and there is no equivalent magnetic current. Equation (3.25) is reduced to

$$\underline{e} = -\text{grad}\,v\,, \tag{3.67}$$

where

$$v(\underline{r}) = \frac{1}{\epsilon}\int_\Gamma q(\underline{r}')\,G(\rho)\,\mathrm{d}\Gamma'\,, \quad G(\rho) = \frac{1}{4\pi\rho}\,, \tag{3.68}$$

with $G(\rho)$ the three-dimensional Laplace Green function. Note that (3.68) is a particularisation of (3.27) for the static case.

We consider an electrostatic problem in $\mathbb{R}^3$. A set of conductors are embedded in multiple homogeneous isotropic dielectrics and set to fixed potentials.

The equivalence principle is applied so that the conductors can be replaced by the electric charge density q_c on their surfaces and the homogeneous dielectrics by the polarisation charge q_p. The total charge on the interface conductor-dielectric Γ_C is given by the sum of both types of charges. Analogously, on the surface Γ_D between two dielectrics the total charge is the sum of the polarisation charge due to both dielectrics [Rao *et al.*, 1984].

The electrostatic scalar potential integral equation is established from the boundary condition (1.24), which implies that the discontinuity of the normal component of $\underline{d}$ at any point of the boundary equals the surface charge density at that point.

The electric field $\underline{e}$ as $\underline{r}$ approaches an interface between two media can be expressed as [Rao *et al.*, 1984]:

$$\underline{e}^{\pm}(\underline{r}) = \pm\,\hat{n}\frac{q(\underline{r})}{2\epsilon_0} + \frac{1}{4\pi\epsilon_0}\,\langle \operatorname{grad} G(\rho), q(\underline{r}')\rangle_{\Gamma}\,, \tag{3.69}$$

where $\pm$ refers to both sides of the interface, $\hat{n}$ points from the first to the second media (i.e. from $-$ to $+$).

When dealing with a conductor to dielectric interface, we have a particular case. As inside the conductor $\underline{e}^{-} = 0$, considering (3.69), it follows that $\underline{e}^{+}$ on the surface of the conductor is given by

$$\underline{e}^{+}(\underline{r}) = \hat{n}\frac{q(\underline{r})}{\epsilon_0}\,. \tag{3.70}$$

The normal component of $\underline{d}$ must be continuous at a dielectric to dielectric interface. Taking into account the dielectric constitutive relation (1.7) and the fact that there is no electric charge at such interface, we can write

$$\hat{n}\cdot\epsilon_1\underline{e}^{+}(\underline{r}) = \hat{n}\cdot\epsilon_2\underline{e}^{-}(\underline{r})\,. \tag{3.71}$$

The surfaces of conductors and dielectrics $\Gamma = \Gamma_C \cup \Gamma_D$ are discretised with plane triangles. The surface charge density q is assumed to be e.g. piecewise constant.

From (1.24) and (3.69), we obtain the following system of N linear equations

$$\boldsymbol{M}\boldsymbol{Q} = \boldsymbol{B}, \tag{3.72}$$

where $\boldsymbol{Q} = \left[\; q_1 \;\ldots\; q_N \;\right]^T$ contains the charge densities on the elements and $\boldsymbol{B} = \left[\; b_1 \;\ldots\; b_N \;\right]^T$ depends on the boundary conditions. For an element on the surface of a conductor Γ_C, the entry in $\boldsymbol{B}$ is the imposed and fixed potential; for an element on the interface between two dielectrics Γ_D, the entry in $\boldsymbol{B}$ is zero. The elements of the dense nonsymmetric matrix $\boldsymbol{M}$ when k is an element on a conductor are given by

$$M_{k,l} = \frac{1}{\epsilon_0}\oint_{\Gamma_l} G(\rho_k)\,\mathrm{d}\Gamma'\,, \tag{3.73}$$

with G the 3D Laplace Green function (2.34 b) and ρ_k the distance between a source point $\underline{r}'$ (on $\Gamma_l \in \Gamma$) and an observation point $\underline{r}_k$ (on Γ_C). Considering the continuity of the normal component of the electric flux density (1.44 c) at the dielectric-to-dielectric interface Γ_D, the elements of $\boldsymbol{M}$ if k is an element on Γ_D read:

$$M_{k,l} = \begin{cases} \dfrac{\epsilon_{k2}-\epsilon_{k1}}{\epsilon_0(\epsilon_{k1}+\epsilon_{k2})}\displaystyle\oint_{\Gamma_l} \operatorname{grad} G(\rho_k)\cdot\hat{n}_k\,\mathrm{d}\Gamma', & k \neq l\,, \\[2ex] \dfrac{1}{2\epsilon_0}\,, & k = l\,, \end{cases} \tag{3.74}$$

where $\hat{n}_k$ is the outward normal unit vector pointing into the dielectric with permittivity ϵ_{k2}. The integrals in (3.73) and (3.74) can be evaluated analytically [Graglia, 1993].

3.5 Singularities

IE techniques require the evaluation of double integrals having singular kernels. Indeed, the Green functions (2.34 b), (2.51 b), (3.13) and (3.14), exhibit integrable singularities when a source point coincides with an observation point, i.e. $r = |\underline{x} - \underline{y}| = 0$. They depend on $1/r$ and their gradients on $1/r^3$.

To numerically solve surface (contour) integral equations by application of a BE method, like the MoM (see Section 3.3), the geometry is usually divided into patches (segments) of simple shape on which expansion functions for the scalar and/or vector unknowns can be defined in a simple way.

The accuracy of the solution of an IE problem depends strongly on the integral calculation [Fetzer *et al.*, 1997]. Different approaches can be followed:

- ✓ Use a numerical scheme based on a big number of integration points, e.g. Gauss quadrature scheme [Golub & Welsch, 1969]. Albeit employing many integration points, the precision is not guaranteed.

- ✓ Use a singularity removal technique. For a given patch T, it consists in splitting the integral over the patch T into two integrals over $T - T_\varepsilon$ and T_ε. The integral over $T - T_\varepsilon$ is evaluated numerically and the integral over T_ε is evaluated at the limit $\varepsilon \to 0$ [Rao, 1980; Wilton *et al.*, 1984].

- ✓ Use an analytical formula. The expressions can become quite lengthy to write and evaluate, but benefit from the fact that they will be exact. In [Graglia, 1987; Graglia, 1993; Davey, 1989; Arcioni *et al.*, 1997], the problem of integrating on a plane triangle the constant or linear functions times the Green functions and their gradients is treated. They proposed different analytical expressions for the integral of $1/r$ over a plane triangle, i.e. a closed form for the Laplace Green function is given.

  For the Helmholtz Green function, the integrand is split into a well behaved function with a defined value when $r \to 0$ and the singular term $1/r$, i.e.

$$\frac{e^{\imath kr}}{r} = \frac{e^{\imath kr} - 1}{r} + \frac{1}{r}\,. \tag{3.75}$$

  The well behaved function can be numerically integrated while the singular part is dealt analytically. Its gradient is treated analogously. We have implemented the analytical integration of linear or constant basis functions times the singular kernels $1/r$ and grad $1/r$ on a plane triangle proposed by Graglia in [Graglia, 1993].

Chapter 4

Fast multipole method

Contents

4.1 Introduction

The number of unknowns N arising when discretising integral equations is relatively small since only surface discretisation for 3D problems (contour discretisation for 2D problems) is required. But in return, since the kernels of the integral operators are non-local, the discretisation leads to a dense system matrix $\boldsymbol{M}$. Solving a dense $N \times N$ matrix with a direct solver, such as the LU decomposition, is an $\mathcal{O}(N^3)$ procedure. The resolution can be performed by means of an iterative method, such as a conjugate gradient type algorithm. Each iteration typically requires the computation of a couple of scalar products and at least one matrix-vector multiplication. Since the matrix $\boldsymbol{M}$ is dense, the number of operations is $\mathcal{O}(N^2)$ per iteration.

Using second kind integral equations and an appropriate preconditioner [Van der Vorst & Dekker, 1988; Chen, 1998; Beatson *et al.*, 1999], the number of iterations can be controlled. But the major task in order to get an efficient electromagnetic solver consists in implementing a fast matrix-vector multiplication routine. Methods that perform the matrix-vector multiplication in $\mathcal{O}(N^p)$ operations, with p significantly lower than two, are called *fast methods*. In the literature three main methods are reported to be fast in this sense. The fast multipole method (FMM) [Rokhlin, 1985; Greengard & Rokhlin, 1987b; Rokhlin, 1990; Engheta *et al.*, 1992; Rokhlin, 1993], which constitutes the focus of this work, is the most popular one. The two others are the wavelet-based method [Beylkin *et al.*, 1991; Alpert *et al.*, 1993; Kim *et al.*, 1996] and the impedance matrix location method [Canning, 1990; Canning, 1993]. The two latter methods use special basis functions (e.g. wavelet-type basis functions) which localise the important interactions to only a small number of elements within the matrix $\boldsymbol{M}$. Then, a threshold procedure (small elements are approximated by zero) is applied in order to obtain a sparse approximation of $\boldsymbol{M}$.

The FMM provides a nearly optimal reduction in the memory requirements and computation time associated to those integral methods. The main feature of the FMM is a special approximation of the fundamental solution to the Laplace and Helmholtz equations. Originally developed for particle simulations involving a large number of particles [Greengard & Rokhlin, 1987a], the method was then adapted to the solution of boundary integral equations, both the Laplace equation [Rokhlin, 1985; Greengard & Rokhlin, 1987b; Greengard & Rokhlin, 1988] and the Helmholtz equation [Rokhlin, 1990; Rokhlin, 1993]. It is applied repeatedly to candidate solution vectors of an iterative method such as the conjugate gradient algorithm (CG) [Van der Vorst & Dekker, 1988] or the generalised minimum residual (GMRES) algorithm [Saad & Schultz, 1986]. Convergence analyses are provided in [Petersen *et al.*, 1995a; Petersen *et al.*, 1995b] for the Laplace equation and in [Labreuche, 1998; Koc *et al.*, 1999; Song & Chew, 2001; Darve, 2000] for the Helmholtz equation. The computational cost can be reduced with the best algorithms down to $\mathcal{O}(N)$ and $\mathcal{O}(N \log N)$ in the Laplace and Helmholtz cases, respectively.

The layout of this chapter is as follows. In Section 4.2, we give a general description of the functioning of the method and comment briefly on some common geometrical tools. The complex mathematics behind the FMM are discussed in Sections 4.3 and 4.4 for the Laplace and Helmholtz Green equations, both two- and

three-dimensional cases are considered. We dwell on the mathematical trickery of the FMM which is the matrix-vector multiplication. The application of this method to problems with movement does not seem to appear in the literature so far. Some aspects relative to the use of FMM in such cases are discussed.

4.2 Main ideas of the FMM

The complex mathematics behind the FMM is presented in detail in [Rokhlin, 1985; Greengard & Rokhlin, 1987b] for the Laplace Green equation and in [Rokhlin, 1990; Rokhlin, 1993] for the Helmholtz Green equation. Hereafter, a simplified version with more physical intuition is presented.

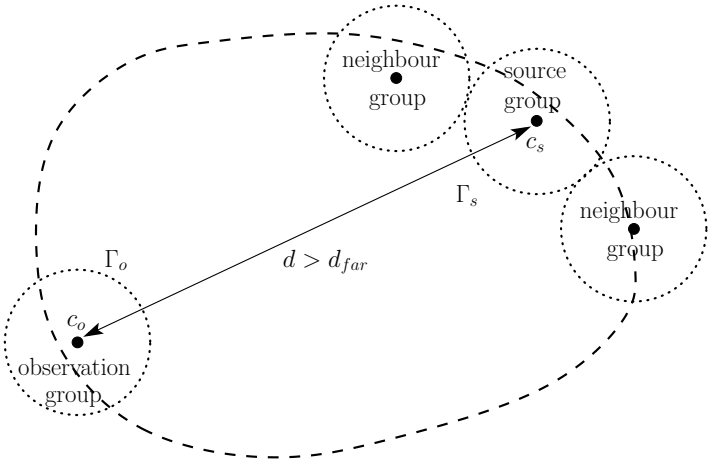

Figure 4.1: Two-dimensional representation of a source FMM group Γ_s with centre c_s, its neighbour groups and a distant observation group Γ_o with centre c_o on Γ

The FMM reduces the computational cost by spatially decomposing the boundary Γ (a surface in $\mathbb{R}^3$ and a contour in $\mathbb{R}^2$) of the electromagnetic domain Ω into N_g groups of elements Γ_g, $\Gamma = \bigcup_{g=1}^{N_g} \Gamma_g$, with $\Gamma_g \bigcap \Gamma_i = \varnothing$ if $g \neq i$. Note that the groups Γ_g are indeed portions of the boundary Γ.

The key is to replace a group of elements characterised by a given source, current or charge (distributed or not, equivalent or not), with another reference element (referred to as centre) that embodies the sources of the whole group. The approximation is valid for the so-called far or distant groups. In practice, this centre is located roughly at the geometrical centre of the considered group Γ_g and may or not be on the boundary Γ. A pair of groups (a source group Γ_s and an observation group Γ_o) are said to be far or distant if the distance between their centres is greater than a given distance d_{far}. Otherwise, they are referred to as neighbour groups. This is illustrated in Figure 4.1. Mathematically, these sources are conveniently represented by means of the multipole expansions of the Green functions.

The FMM comprises thus three fundamental operations:

- ✓ *Aggregation*: The sources in each source group Γ_s are jointly treated as a single clustered source, and the field of the equivalent source is approximated by a

multipole expansion at the centre of the group. This representation is only valid outside the group.

- ✓ *Translation*: For each pair of sufficiently distant source and observation groups, Γ_s and Γ_o, the aggregate multipole expansion at the centre of the source group Γ_s can be represented as an analytical partial field expansion at the centre of the observation group Γ_o, i.e. it consists in translating an aggregate multipole expansion to an observation group Γ_o. The translation is only valid inside a domain including all the elements of the observation group.

- ✓ *Disaggregation*: The aggregate and translated multipole representation of the field is redistributed to all the elements of the observation group Γ_o, i.e. the field is evaluated. This operation is valid inside a domain comprising all the elements of the observation group Γ_o.

For neighbour groups the direct contribution must be calculated in the conventional way to evaluate the field. Therefore, the field at any particular element is the sum of the contributions of M multipoles of each of the far groups and the direct contribution of the neighbour groups.

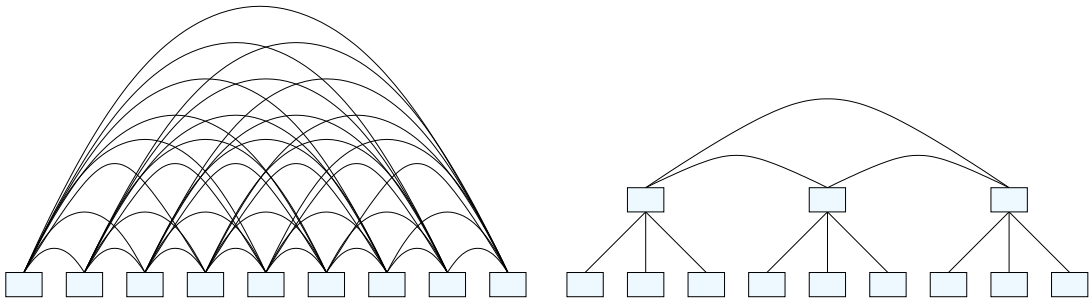

Figure 4.2: a. N source elements and N observation elements interacting directly with each other; b. N source elements and N observation elements interacting thorough a three-stage process

Summarising, a multiplication is effected through three separate procedures: from element source to source group centre, from centre of the source group to that of the observation group and from the observation group center to the observation element. Therefore, the number of interactions is reduced with respect to the normal procedure (see Figure 4.2).

4.2.1 Clustering algorithm

The division in groups of the problem is crucial for the successful and efficient application of the FMM algorithm [Greengard & Rokhlin, 1987b; Buchau *et al.*, 2003; Barakat & Webb, 2004].

The simplest way to achieve the FMM groups is to build a quadtree (2D) or an octree (3D), i.e. to perform a hierarchical subdivision of the body. For the 3D

case, assume that the body to be analysed is enclosed in a fictitious cubical box that is recursively divided into eight boxes. A box that is subdivided into smaller boxes is termed the *parent* of the *child* boxes that result from the operation. Empty subcubes are discarded. For an $n+1$ level scheme, this subdivision proceeds n times. A quadtree structure is generated analogously. Figure 4.3 represents four levels of a quadtree data structure.

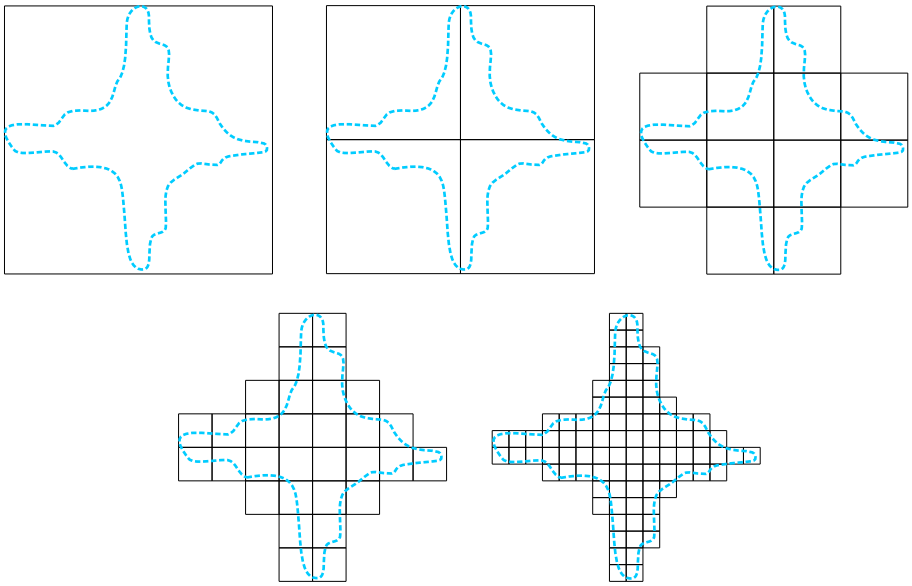

Figure 4.3: Four level of quadtree structure

In addition, an existing quadtree/octree structure can be exploited to initialise complicated block preconditioning techniques. It is possible to employ the small decoupled matrix inverses as a preconditioner in the iterative solution of the entire problem [Nabors *et al.*, 1994; Forsman *et al.*, 1995].

An alternative clustering algorithm is described in [Barakat & Webb, 2004]. The concept is to merge groups that are closest to each other into higher level groups in order to maximise the relative distance between the latter.

We adopt the last level of the quadtree/octree structure as group distribution. This work is thus focused on the application of a so-called single level FMM. A multilevel FMM takes advantage of the quadtree/octree clustering algorithm and deals with groups of groups.

4.2.2 Fast matrix-vector product

The aim of the FMM is accelerating the multiplication of the system matrix $\boldsymbol{M}$ (arising from a BE method) by a trial vector $\boldsymbol{Q}$ within an iterative process. With

this purpose, the system matrix $\boldsymbol{M}$ can be formally approximated as

$$\boldsymbol{M} \;\approx\; \boldsymbol{M}^{near} + \boldsymbol{M}^{far} \;=\; \boldsymbol{M}^{near} + \underbrace{\sum_{o=1}^{N_g}\sum_{s=1}^{N_g}}_{\Gamma_o,\,\Gamma_s \text{ far}} \boldsymbol{M}^{far}_{o,s} \,. \tag{4.1}$$

The matrix $\boldsymbol{M}^{near}$ comprises the near field interactions. It is computed following the normal procedure in the BE method and stored with a sparse storage scheme.

The power of the FMM lies on the matrix $\boldsymbol{M}^{far}$ which accounts for the far field interactions. Indeed, the FMM speeds up the matrix-vector product $\boldsymbol{M}^{far}\boldsymbol{Q}$.

For every distant pair of source and observation groups, Γ_s and Γ_o, we have a matrix $\boldsymbol{M}^{far}_{o,s}$ that can be further decomposed into the disaggregation data matrix $\boldsymbol{M}^{\mathcal{D}}_{o}$ for a group Γ_o, the translation data matrix $\boldsymbol{M}^{\mathcal{T}}$ for a pair of groups Γ_o and Γ_s and the aggregation data matrix $\boldsymbol{M}^{\mathcal{A}}_{s}$ for a group Γ_s, i.e.

$$\underbrace{\sum_{o=1}^{N_g}\sum_{s=1}^{N_g}}_{\Gamma_o,\,\Gamma_s \text{ far}} \boldsymbol{M}^{far}_{o,s} = \sum_{o=1}^{N_g} \boldsymbol{M}^{\mathcal{D}}_{o} \sum_{\substack{s=1 \\ \Gamma_o,\,\Gamma_s \text{ far}}}^{N_g} \boldsymbol{M}^{\mathcal{T}} \boldsymbol{M}^{\mathcal{A}}_{s} \,. \tag{4.2}$$

Group by group, the field produced by the source in the considered group is aggregated into its centre by $\boldsymbol{M}^{\mathcal{A}}_{s}$. This aggregate field is then subsequently translated to the centres of all the far groups by $\boldsymbol{M}^{\mathcal{T}}$, and finally the aggregate and translated field is disaggregated into the degrees of freedom of the far groups thanks to $\boldsymbol{M}^{\mathcal{D}}_{o}$.

Note that the matrix $\boldsymbol{M}^{far}$ itself is never built. During the FMM assembly stage, the required complex matrices $\boldsymbol{M}^{\mathcal{D}}_{o}$, $\boldsymbol{M}^{\mathcal{T}}$ and $\boldsymbol{M}^{\mathcal{A}}_{s}$ are calculated and stored. The integrations appearing in the computation of $\boldsymbol{M}^{\mathcal{D}}_{o}$ and $\boldsymbol{M}^{\mathcal{A}}_{s}$ (this will be clear in the following sections) can be performed numerically by means of a quadrature scheme, e.g. a Gauss quadrature scheme. As we are dealing with far interactions, there is no singularity problem (see Section 3.5) and a reduced number of integration points suffices.

In practice, the FMM can be integrated in a computational software as an independent block. Its functioning in GetDP [GetDP, 1997–2004] is summarised in the flow chart depicted in Figure 4.4. We denote the FMM block as FMM pre-processing.

The first step in the FMM block is splitting the problem into groups and calculating their centres. Then, the neighbour and far groups are determined for each group. If the distance between the centres of two groups is greater than d_{far}, they are said to be far groups, otherwise they are neighbour groups. Using information from the conventional pre-processing (such as the basis functions, the degrees of freedom (Dof), ...), the FMM data matrices are thus computed and stored: an aggregation data matrix $\boldsymbol{M}^{\mathcal{A}}_{s}$ and a disaggregation data matrix $\boldsymbol{M}^{\mathcal{D}}_{o}$ for each group, and a translation data matrix $\boldsymbol{M}^{\mathcal{T}}$ for every pair of far groups. Assuming a constant number of degrees of freedom per group L, and a number of multipoles M,

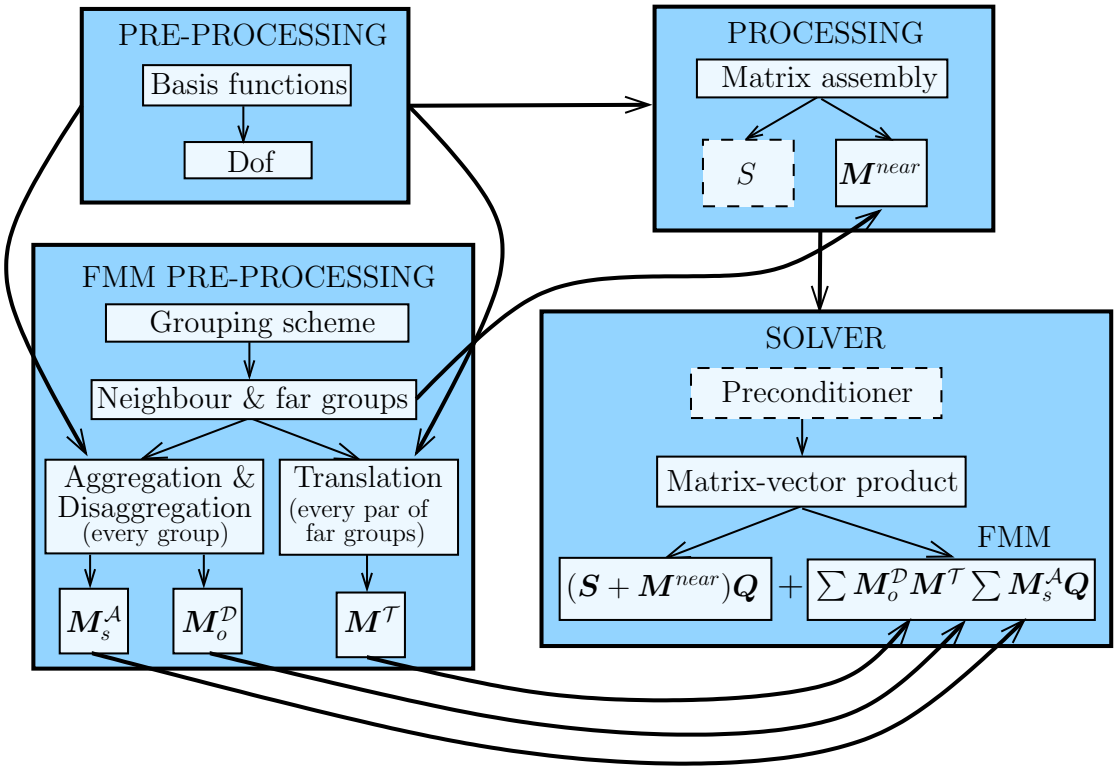

Figure 4.4: Flow chart showing the integration and functioning of the FMM in the computational software GetDP [GetDP, 1997–2004] (the discontinuous line indicates an optional block)

the dimensions of the matrices $\boldsymbol{M}_s^{\mathcal{A}}$, $\boldsymbol{M}^{\mathcal{T}}$ and $\boldsymbol{M}_o^{\mathcal{D}}$ are $M \times L$, $M \times M$ and $L \times M$, respectively.

In the processing step, the full system matrix is assembled. In the general case, we can consider a sparse matrix $\boldsymbol{S}$ due to e.g. a FE model or/and to a circuit coupling. The matrix $\boldsymbol{M}^{near}$ accounts for solely the near field interactions of the BE model. The computation of this latter matrix requires the neighbour groups determined in the so-called FMM pre-processing.

Once the processing is finished, the solver (in our case [SPARSKIT, 1999]) starts an iterative process that performs the multiplication of $\boldsymbol{S}+\boldsymbol{M}^{near}$ by a trial vector $\boldsymbol{Q}$ in every iteration. The FMM intervenes adding the contribution of the far groups given by $\sum_{o=1}^{N_g} \boldsymbol{M}_o^{\mathcal{D}} \sum_{s=1}^{N_g} \boldsymbol{M}^{\mathcal{T}} \boldsymbol{M}_s^{\mathcal{A}}$ in every iteration. The preconditioning of the iterative solver is often required to reduce the number of iterations. In this case, the preconditioning is based on the sparse matrix comprising only the BE near-field interactions (and the FE contribution when dealing with hybrid formulations) [Buchau & Rucker, 2002].

Note that in some coupled problems (e.g. problems with movement), the FMM data may require to be totally or partially updated.

4.3 FMM applied to Laplace equations

The FMM was applied to the solution of two-dimensional potential problems by Rokhlin in [Rokhlin, 1985]. An extension to three-dimensional problems was presented in [Greengard & Rokhlin, 1987b].

An application of a multilevel FMM to solve electrostatic problems with Dirichlet boundary conditions was reported in [Nabors & White, 1991]. Later the same authors proposed an extension to compute problems with Neumann boundary conditions as well [Nabors & White, 1992]. They numerically differentiated the potential to compute the electric flux density at the boundaries with Neumann boundary conditions. A more general approach with analytical differentiations is presented in [Buchau *et al.*, 2000]. The FMM has also been combined with the BE method with higher order elements and the Galerkin method [Buchau *et al.*, 2001]. A preconditioner based on the near-field interactions matrix suitable for the iterative solution of a FMM accelerated BE problem is proposed in [Nabors *et al.*, 1994; Buchau & Rucker, 2002]. In [Apalkov & Visscher, 2003] the FMM is applied to a periodic system.

This section deals with the application of a single level FMM to Laplace equations.

4.3.1 Two-dimensional Laplace Green function

4.3.1.1 Multipole expansion

The 2D Laplace Green function is given by

$$G(\rho) = -\frac{1}{2\pi} \ln \rho \,, \tag{4.3}$$

with $\rho = |\underline{r}_o - \underline{r}_s|$ the distance between a source point $\underline{r}_s$ and an observation point $\underline{r}_o$.

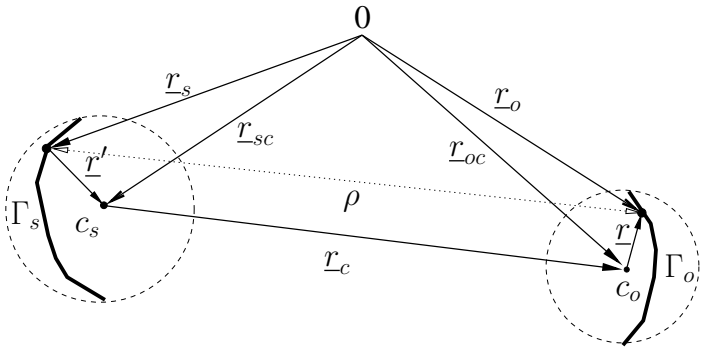

Figure 4.5: Two-dimensional representation of distant FMM groups Γ_s and Γ_o on Γ with respective centres c_s and c_o

Let $\underline{r}_s$ be in a source group Γ_s with centre $\underline{r}_{sc}$ and $\underline{r}_o$ be in an observation group source Γ_o with centre $\underline{r}_{oc}$. We define the following vectors $\underline{r} = \underline{r}_o - \underline{r}_{oc} = (r, \phi)$,

$\underline{r}_c = \underline{r}_{oc} - \underline{r}_{sc} = (r_c, \phi_c)$ and $\underline{r}' = \underline{r}_{sc} - \underline{r}_s = (r', \phi')$, as shown in Figure 4.5. Vectors are expressed in cylindrical coordinates throughout. Omitting the factor $-1/2\pi$, the 2D Laplace Green function (4.3) is then expanded as [Rokhlin, 1985][1]:

$$\ln \rho = \Re \left(\sum_{u=0}^{\infty} \sum_{v=0}^{\infty} \mathcal{D}_u \left(\underline{r} \right) \mathcal{T}_{u,v} \left(\underline{r}_c \right) \mathcal{A}_v \left(\underline{r}' \right) \right) \tag{4.4}$$

with

$$\mathcal{D}_u \left(\underline{r} \right) = r^u \, e^{\imath u \phi}, \tag{4.5}$$

$$\mathcal{T}_{u,v} \left(\underline{r}_c \right) = \begin{cases} \ln \left(r_c \right) & \text{if} \quad u = 0 \quad \text{and} \quad v = 0 \,, \\ \dfrac{-(u+v-1)!}{u! \, v! \, r_c^{u+v} \, e^{\imath (u+v) \phi_c}} & \text{if} \quad u \neq 0 \quad \text{or} \quad v \neq 0 \,, \end{cases} \tag{4.6}$$

$$\mathcal{A}_v \left(\underline{r}' \right) = r'^v \, e^{\imath v \phi'} \,. \tag{4.7}$$

In practice, the multipole expansion (4.4) must be truncated by considering $0 \leq u \leq P$ and $0 \leq v \leq P$, where the truncation number P is sufficiently large to limit the error to a prescribed value ε:

$$\left| \ln \rho - \Re \left(\sum_{u=0}^{P} \sum_{v=0}^{P} \mathcal{D}_u \left(\underline{r} \right) \mathcal{T}_{u,v} \left(\underline{r}_c \right) \mathcal{A}_v \left(\underline{r}' \right) \right) \right| < \varepsilon. \tag{4.8}$$

The truncation number, introduced by Rokhlin in [Rokhlin, 1985] and commonly adopted in the literature, is taken by $P = \log_2(1/\varepsilon)$. However, as will be shown, if the distance between the source point and its group centre and the distance between the observation point and its group centre are small compared to the distance d between the two group centres, a smaller number of terms suffices.

A more economic law takes those distances into account. Let us denote by R_s the maximum distance between a source point in a source group and its centre, by R_o the maximum distance between an observation point in an observation group and its centre, by ϕ_s the local angle formed by $\underline{r}'$ and the line joining the group centers and by ϕ_o the local angle formed by $\underline{r}$ and the line joining the group centers (see Figure 4.6). The truncation number depends on two angles, ϕ_s and ϕ_o, and three distances R_s, R_o and d. We eliminate the angular dependency by considering the most restrictive case (which implies a higher truncation number), i.e. $\phi_s = \phi_o = 0$. This novel truncation method is referred to as the adaptive truncation scheme.

The value of P as a function of R_o/d and R_s/d for $\varepsilon = 10^{-6}$ and $\varepsilon = 10^{-9}$ is depicted in Figures 4.7 and 4.8, respectively. It can be seen that in both cases $P = \log_2(1/\varepsilon)$ corresponds to $R_o/d = R_s/d = 0.35$.

In order to apply the FMM to (2.61), the expansion of $\operatorname{grad} G$ is necessary as well. It can be straightforwardly obtained by deriving (4.5) with respect to the coordinates of the observation point, i.e.

$$\operatorname{grad} \mathcal{D}_u \left(\underline{r} \right) = \left(\partial_{x_o} \mathcal{D}_u \left(\underline{r} \right), \partial_{y_o} \mathcal{D}_u \left(\underline{r} \right) \right) = \left(\partial_x \mathcal{D}_u \left(\underline{r} \right), \partial_y \mathcal{D}_u \left(\underline{r} \right) \right) = \tag{4.9}$$

[1] Beware the complex expressions in the FMM expansions are not related to the harmonic regime described in Section 1.3.1.

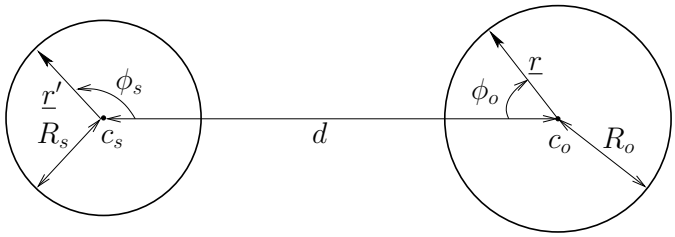

Figure 4.6: Geometrical parameters that determine the truncation number: the local angles ϕ_s and ϕ_o, the distances R_s, R_o and d

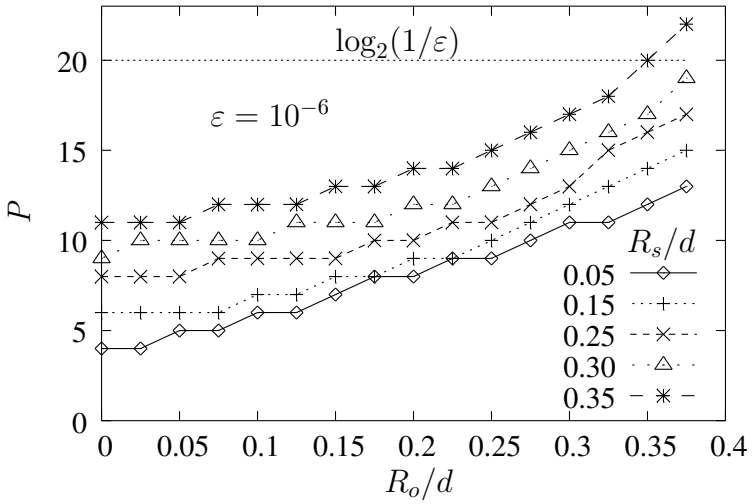

Figure 4.7: Truncation number $P(R_o/d, R_s/d, \varepsilon)$ for $\varepsilon = 10^{-6}$, 2D case

$$= \left(u r^{u-1}\, e^{\imath(u-1)\phi},\; u r^{u-1}\, e^{\imath(u-1)\phi + \imath\pi/2} \right) . \tag{4.10}$$

The process to follow is then analogous.

4.3.1.2 Fast matrix-vector product

Two groups Γ_s and Γ_o are said to be far groups if $R_s/d < \tau$ and $R_o/d < \tau$, where d is the distance between the group centres and where τ is sufficiently small (and certainly $\tau < 1/2$).

We analyse the particular two-dimensional hybrid $\underline{b}$-formulation developed in Section 2.6.3. The application to any other formulation is straightforward. The approximation of the matrix $\boldsymbol{M}$ in (2.58) can be formally written as in (4.1), and analogously for the matrix $\boldsymbol{C}$.

Let us consider the degrees of freedom q_k and q_l of $q(\xi)$ with associated basis functions $\beta_k(\xi)$ and $\beta_l(\xi)$ that are nonzero on the respective far groups Γ_o and Γ_s. Truncating and substituting (4.4) in (2.63), the contribution to the corresponding element in $\boldsymbol{M}^{far}$ is given by

$$\left(\boldsymbol{M}^{far}_{o,s}\right)_{k,l} = \Re\left(\sum_{u=0}^{P} \boldsymbol{M}^{\mathcal{D}}_{o,k,u} \sum_{v=0}^{P} \boldsymbol{M}^{\mathcal{T}}_{u,v}\, \boldsymbol{M}^{\mathcal{A}}_{s,l,v} \right), \tag{4.11}$$

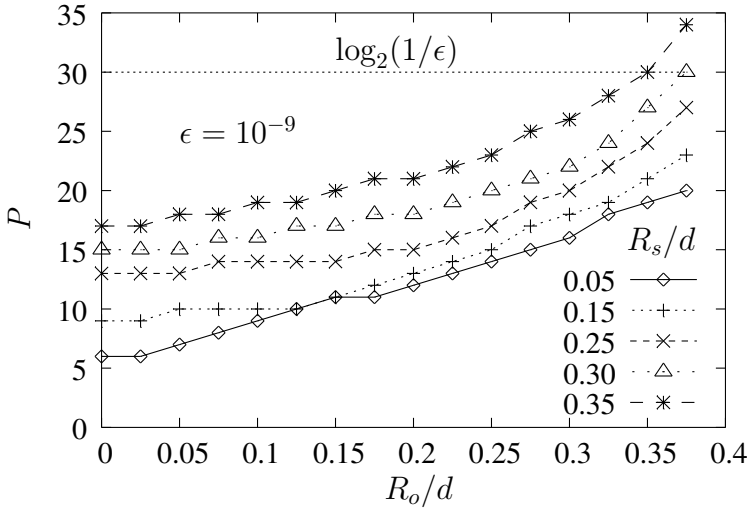

Figure 4.8: Truncation number $P(R_o/d, R_s/d, \varepsilon)$ for $\varepsilon = 10^{-9}$, 2D case

with

$$\boldsymbol{M}^{\mathcal{D}}_{o,k,u} = \int_{\Gamma_o} \beta_k \mathcal{D}_u\left(\underline{r}\right) \mathrm{d}\Gamma\,, \quad \boldsymbol{M}^{\mathcal{A}}_{s,l,v} = \int_{\Gamma_s} \beta_l \mathcal{A}_v\left(\underline{r}'\right) \mathrm{d}\Gamma\,, \tag{4.12 a,b}$$

$$\text{and} \quad \boldsymbol{M}^{\mathcal{T}}_{u,v} = -\frac{1}{2\pi\nu_0} \mathcal{T}_{u,v}\left(\underline{r}_c\right)\,. \tag{4.13}$$

As explained in Section 4.2.2, the goal of the formal decomposition (4.11) is accelerating the multiplication of $\boldsymbol{M}^{far}$ by a trial vector $\boldsymbol{Q}$, required for the iterative solution of the system of algebraic equations (2.58).

In case of straight line elements and piecewise constant basis functions, the integrals in (4.12) can be evaluated analytically considering

$$\int_{\underline{r}_1}^{\underline{r}_2} |\underline{r}_c - \underline{r}|^u \; e^{\imath(u+1)\phi_{r_c r}} \mathrm{d}r \;=\; \frac{|\underline{r}_c - \underline{r}_1|^{u+1}\, e^{\imath(u+1)\phi_{r_c r_1}} - |\underline{r}_c - \underline{r}_2|^{u+1}\, e^{\imath(u+1)\phi_{r_c r_2}}}{u+1}\,.$$

4.3.1.3 Operational count

The total operational count is estimated as follows. We assume that the total number of unknowns N is divided evenly into N_g groups with $L = N/N_g$ unknowns each and that each group has n neighbour groups (a group is neighbour of itself). The number of operations involved in finding the interactions within neighbour groups is nL^2N_g. The computation of (4.12 b) for multipole expansions truncated at order P and N_g groups requires $N_g(P+1)L$ operations (see Figure 4.9[2]). The translations (4.13) for N_g^2 source-observation pairs of groups need $N_g^2(P+1)^2$ operations. Finally, the reconstruction of the fields at the receiving groups (4.12 a) amounts to $N_g(P+1)L$ operations (see Figure 4.10). The total operational count is thus

$$nL^2N_g + 2N_g(P+1)L + N_g^2(P+1)^2\,. \tag{4.14}$$

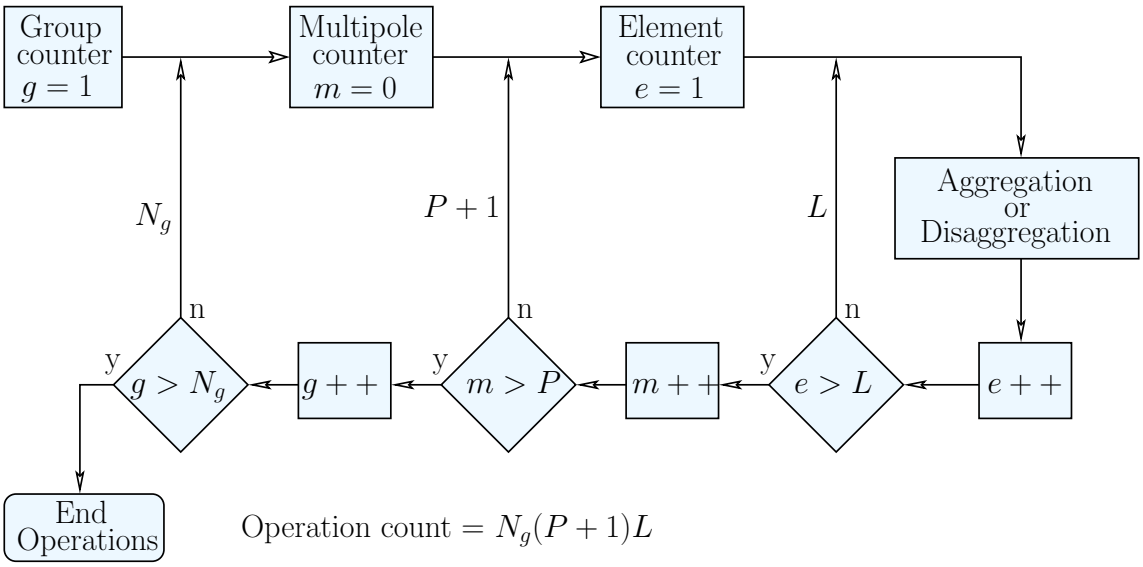

Figure 4.9: Sequence of operations to be performed for the computation of either the aggregation or disaggregation data

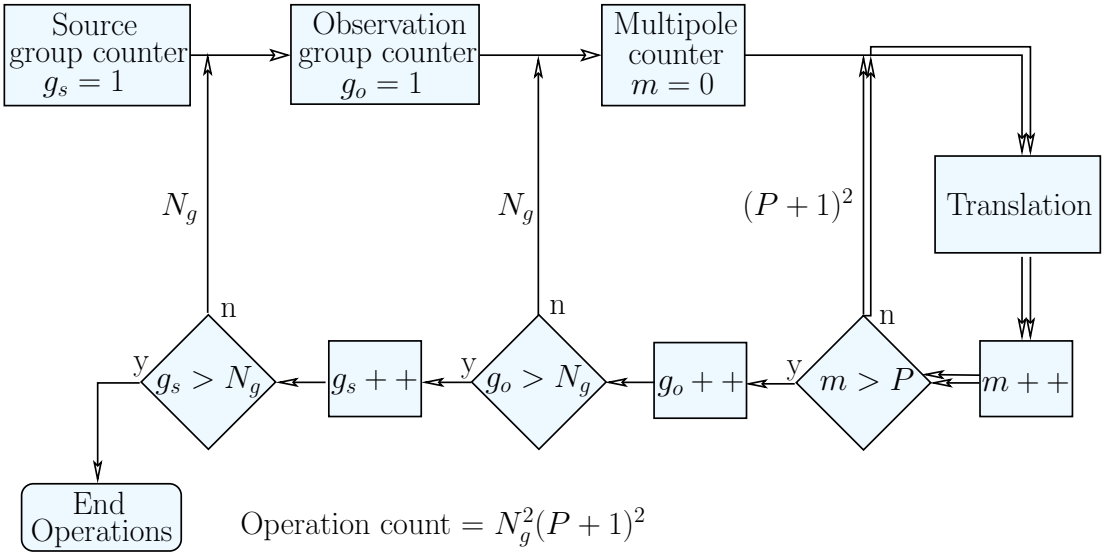

Figure 4.10: Sequence of operations to be performed for the computation of the translation data

Note that the computational cost depends on $(P+1)^2$. Consequently, the product $\boldsymbol{M}^{far}\boldsymbol{Q}$ is further accelerated by means of the adaptive truncation scheme following the law $P = P(R_s/d, R_o/d, \varepsilon)$ shown in Figures 4.7 and 4.8. For the $\boldsymbol{M}^{\mathcal{D}}$ and $\boldsymbol{M}^{\mathcal{A}}$ data of a given group, the truncation number P considered during the FMM assembly stage is determined by its closest far group (the closer the group the higher P), $P = P_{max}$. For the $\boldsymbol{M}^{\mathcal{T}}$ data, the truncation number P is determined by the

[2]In this flow chart, for the sake of simplicity, we have assumed that the number of unknowns equals the number or elements per group. Usually, this is not the case

two groups Γ_s and Γ_o involved in the translation, $P = P_{so}$. During the iterative process, the aggregation step for a given source group is carried out with $P = P_{max}$, while $P = P_{so}$ suffices for the translation and disaggregation steps.

4.3.1.4 Taking movement into account

The analysis is restricted to rigid bodies. In a hybrid FE-BE model, some blocks of the complete system matrix may be time dependent due to the movement (BE part) and magnetic saturation (FE part). Those blocks have to be recalculated every time step.

When applying the FMM, the decomposition in groups $\Gamma = \bigcup_{g=1}^{N_g} \Gamma_g$ is preserved during movement. Expressing the ratio of the new distance p between an element in a group and its group centre (either observation or source) to the previous one $p-1$ as:

$$\frac{\underline{r}^p}{\underline{r}^{p-1}} = e^{\imath(\phi^p - \phi^{p-1})} = e^{\imath\Delta\phi^p}\,, \qquad \frac{\underline{r}'^p}{\underline{r}'^{p-1}} = e^{\imath(\phi'^p - \phi'^{p-1})} = e^{\imath\Delta\phi'^p}\,, \tag{4.15 a,b}$$

and the ratio of the new complex distance between two group centres to the previous one as:

$$\frac{\underline{r}_c^p}{\underline{r}_c^{p-1}} = \frac{r_c^p}{r_c^{p-1}} e^{\imath(\phi_c^p - \phi_c^{p-1})} = \frac{r_c^p}{r_c^{p-1}} e^{\imath\Delta\phi_c^p}\,, \tag{4.16}$$

it is easy to find the relations between the previous and the new FMM data. Indeed, taking into account the relations (4.15) and (4.16), from (4.12) and (4.13), it follows:

$$\boldsymbol{M}_{o,k,u}^{\mathcal{D}^p} = \boldsymbol{M}_{o,k,u}^{\mathcal{D}^{p-1}}\ e^{\imath u\Delta\phi^p}\,, \quad \boldsymbol{M}_{s,l,v}^{\mathcal{A}^p} = \boldsymbol{M}_{s,l,v}^{\mathcal{A}^{p-1}}\ e^{\imath u\Delta\phi'^p}\,, \tag{4.17}$$

$$\text{and} \quad \boldsymbol{M}_{u,v}^{\mathcal{T}^p} = \boldsymbol{M}_{u,v}^{\mathcal{T}^{p-1}} \left(\frac{r_c^{p-1}}{r_c^p}\right)^{u+v} e^{\imath(u+v)\Delta\phi_c^p}\,. \tag{4.18}$$

This way, the integrals (4.12) do not have to be reevaluated. For updating the disaggregation, aggregation and translation data, a product of the previous data with the corresponding exponential factor suffices. In the particular case of purely translational movement, $\Delta\phi^p = \Delta\phi'^p = 0$ for every p, the disaggregation and aggregation data do not vary. Only the translation data have to be modified.

4.3.2 Three-dimensional Laplace Green function

4.3.2.1 Multipole expansion

The 3D Laplace Green function is given by

$$G(\rho) = \frac{1}{4\pi\rho}\,, \tag{4.19}$$

with $\rho = |\underline{r}_o - \underline{r}_s|$ the distance between a source and an observation point.

Let Γ_s be a source group with centre $\underline{r}_{sc}$ and a source point $\underline{r}_s$, and Γ_o an observation group with centre $\underline{r}_{oc}$ and an observation point $\underline{r}_o$. We define the vectors

in $\mathbb{R}^3$ $\underline{r} = \underline{r}_o - \underline{r}_{oc} = (r, \theta, \phi)$, $\underline{r}_c = \underline{r}_{oc} - \underline{r}_{sc} = (r_c, \theta_c, \phi_c)$ and $\underline{r}' = \underline{r}_{sc} - \underline{r}_s = (r', \theta', \phi')$ as shown in Figure 4.5. Vectors are expressed in spherical coordinates throughout. Omitting the factor $1/4\pi$, the 3D Laplace Green function (4.19) is expanded as [Rokhlin, 1985]:

$$\frac{1}{\rho} = \Re\Big(\sum_{m=0}^{\infty} \sum_{n=-m}^{m} \sum_{u=0}^{\infty} \sum_{v=-u}^{u} \mathcal{D}_{m,n}\left(\underline{r}\right) \mathcal{T}_{m+u,n+v}\left(\underline{r}_c\right) \mathcal{A}_{u,v}\left(\underline{r}'\right) \Big) , \tag{4.20}$$

with

$$\mathcal{D}_{m,n}\left(\underline{r}\right) = \frac{r^m \, \mathcal{L}_m^n(\theta, -\phi)}{(m+n)!} , \tag{4.21}$$

$$\mathcal{T}_{m+u,n+v}\left(\underline{r}_c\right) = \frac{(m+u-(n+v))!}{r_c^{m+u+1}} \, \mathcal{L}_{m+u}^{n+v}(\theta_c, \phi_c) , \tag{4.22}$$

$$\mathcal{A}_{u,v}\left(\underline{r}'\right) = \frac{r'^u \, \mathcal{L}_u^v(\theta', -\phi')}{(u+v)!} , \tag{4.23}$$

where $\mathcal{L}_m^n(\theta, \phi) = P_m^n\left(\cos\theta\right) e^{\imath n \phi}$ and P_m^n is the Legendre function of degree m and order n. Note that this expansion is based on the addition theorem for spherical harmonics (see Appendix B.6.1).

In practice, the multipole expansion (4.20) must be truncated by taking $0 \leq m \leq P$ and $0 \leq u \leq P$, where the truncation number P must be sufficiently large to limit the error to a prescribed value ε:

$$\left| \frac{1}{\rho} - \Re \left(\sum_{m=0}^{P} \sum_{n=-m}^{m} \sum_{u=0}^{P} \sum_{v=-u}^{u} \mathcal{D}_{m,n}\left(\underline{r}\right) \mathcal{T}_{m+u,n+v}\left(\underline{r}_c\right) \mathcal{A}_{u,v}\left(\underline{r}'\right) \right) \right| < \varepsilon. \tag{4.24}$$

In most cases, the conventional choice $P = \log_2(1/\varepsilon)$ [Rokhlin, 1985] is too conservative. Indeed, if $r' \ll r_c$ and $r \ll r_c$, a smaller number of terms suffices.

A more economic law takes those distances into account. Strictly, also the local spherical angles (θ', ϕ') and (θ, ϕ) intervene in the computation of the truncation number. Analogously to the two-dimensional case, we consider the worst case in which the observation and source points are closer to each other and aligned with the group centers. Let us consider the radii of the source and observation groups, $R_s = \max_{\Gamma_s}(r')$, $R_o = \max_{\Gamma_o}(r)$, and the distance between their centres $d = r_c$. The minimum value of P as a function of R_o/d and R_s/d for $\varepsilon = 10^{-6}$ and $\varepsilon = 10^{-9}$ is depicted in Figures 4.11 and 4.12. This novel truncation method is referred to as the adaptive truncation scheme.

The function grad G can be expanded in a similar way. It suffices to derive (4.21) with respect to the coordinates of the observation point $\underline{r}_o = (x_o, y_o, z_o)$. Taking into account that $\underline{r} = \underline{r}_o - \underline{r}_{oc} = (x_o - x_{oc}, y_o - y_{oc}, z_o - z_{oc}) = (x, y, z)$, we can write

$$\operatorname{grad} \mathcal{D}_{m,n}\left(\underline{r}\right) = \left(\partial_{x_o} \mathcal{D}_{m,n}, \partial_{y_o} \mathcal{D}_{m,n}, \partial_{z_o} \mathcal{D}_{m,n}\right) = \left(\partial_x \mathcal{D}_{m,n}, \partial_y \mathcal{D}_{m,n}, \partial_z \mathcal{D}_{m,n}\right) \tag{4.25}$$

with

$$\partial_x \mathcal{D}_{m,n} = \frac{r^{m-2}}{(m+n)!} \left[\mathcal{L}_m^n(\theta, -\phi) \left(\frac{\imath n y r^2}{x^2 + y^2} + mx \right) - \partial_x P_m^n \, \frac{xz \sin\theta \, e^{-\imath n \phi}}{\sqrt{x^2 + y^2}} \right] , \tag{4.26}$$

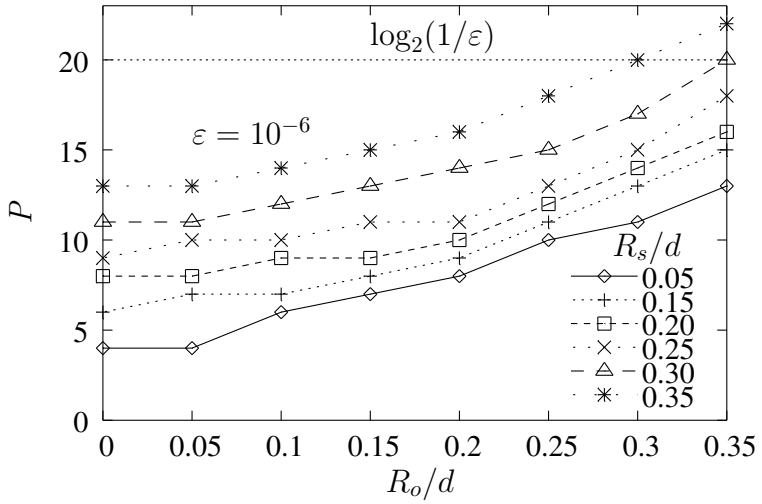

Figure 4.11: Truncation number $P(R_o/d, R_s/d, \varepsilon)$ for $\varepsilon = 10^{-6}$, 3D case

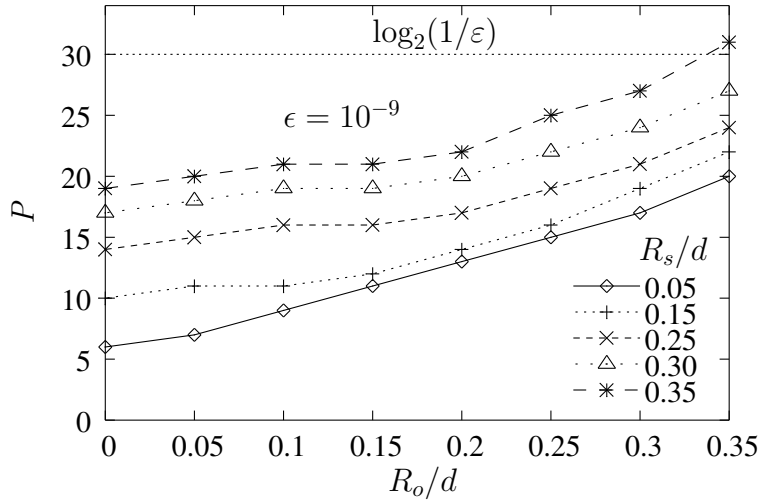

Figure 4.12: Truncation number $P(R_o/d, R_s/d, \varepsilon)$ for $\varepsilon = 10^{-9}$, 3D case

$$\partial_y \mathcal{D}_{m,n} = \frac{r^{m-2}}{(m+n)!}\left[\mathcal{L}_m^n(\theta,-\phi)\left(\frac{-\imath n x r^2}{x^2+y^2}+my\right) - \partial_y P_m^n \frac{yz\sin\theta\, e^{-\imath n\phi}}{\sqrt{x^2+y^2}}\right], \quad (4.27)$$

$$\partial_z \mathcal{D}_{m,n} = \frac{r^{m-2}}{(m+n)!}\left[\mathcal{L}_m^n(\theta,-\phi)\, mz + \partial_z P_m^n \sqrt{x^2+y^2}\,\sin\theta\, e^{-\imath n\phi}\right]. \quad (4.28)$$

The partial derivatives of P_m^n are calculated by means of the recursive formula (B.35). Other relations concerning the Legendre polynomials and functions are also defined in Appendix B.

4.3.2.2 Fast matrix-vector product

Analogously to the two-dimensional case studied in Section 4.3.1.2, two groups Γ_s and Γ_o are said to be far groups if $R_s/d < \tau$ and $R_o/d < \tau$, where d is the distance between the group centres and where τ is sufficiently small (and certainly $\tau < 1/2$).

We consider, e.g. the three-dimensional hybrid $\underline{h}$-conforming formulation described in Section 2.6.1. Any other formulation will be treated analogously. The dense blocks due to the BE part and in particular $\boldsymbol{M}$ (2.42) can be formally written as in (4.1).

Let us consider the degrees of freedom q_k and q_l of q with associated basis functions $\beta_k(\underline{r}_o)$ and $\beta_l(\underline{r}_s)$ that are nonzero on the respective far groups Γ_o and Γ_s. Truncating and substituting (4.20) in (2.42), the contribution to the corresponding element $\left(\boldsymbol{M}^{far}_{o,s}\right)_{k,l}$ in $\boldsymbol{M}^{far}$ is given by

$$\Re\left(\sum_{m=0}^{P}\sum_{n=-m}^{m}\boldsymbol{M}^{\mathcal{D}}_{o,k,m,n}\sum_{u=0}^{P}\sum_{v=-u}^{u}\boldsymbol{M}^{\mathcal{T}}_{m+u,n+v}\boldsymbol{M}^{\mathcal{A}}_{s,l,u,v}\right), \tag{4.29}$$

with

$$\boldsymbol{M}^{\mathcal{D}}_{o,k,m,n}=\int_{\Gamma_o}\beta_k\mathcal{D}_{m,n}\,\mathrm{d}\Gamma\,,\quad \boldsymbol{M}^{\mathcal{A}}_{s,l,u,v}=\int_{\Gamma_s}\beta_l\mathcal{A}_{u,v}\,\mathrm{d}\Gamma\,, \tag{4.30 a,b}$$

and

$$\boldsymbol{M}^{\mathcal{T}}_{m+u,n+v}=\frac{1}{4\pi\mu}\mathcal{T}_{m+u,n+v}\,. \tag{4.31}$$

The goal of formally splitting $\boldsymbol{M}$ (2.42) into $\boldsymbol{M}^{near}$ and $\boldsymbol{M}^{far}$ (4.29) is speeding up the multiplication of $\boldsymbol{M}^{far}$ by a trial vector $\boldsymbol{Q}$, which is required for solving the system of algebraic equations (2.39) and (2.40) (see Section 4.2.2).

4.3.2.3 Operational count

The total operational count is estimated as follows. We assume that the total number of unknowns N is divided evenly into N_g groups with $L = N/N_g$ unknowns each and that each group has n neighbour groups (a group is neighbour of itself). The number of operations involved in finding the interactions within neighbour groups is nL^2N_g. The numerical evaluation of the aggregation and disaggregation, (4.30 b) and (4.30 a), for N_g groups and multipole expansions truncated at order P requires $2N_g(P+1)(2P+1)L$ operations. The translation (4.31) for N_g^2 source-observation pairs of groups amounts to $N_g^2(P+1)^2(2P+1)^2$. The total operational count is thus

$$nL^2N_g+2N_g(P+1)(2P+1)L+N_g^2(P+1)^2(2P+1)^2\,. \tag{4.32}$$

The adaptive truncation scheme following the law $P = P(R_s/d, R_o/d, \varepsilon)$ shown in Figures 4.11 and 4.12 is clearly advantageous when examining (4.32). This way, the matrix-vector product $\boldsymbol{M}^{far}\boldsymbol{Q}$ is further accelerated.

For the $\boldsymbol{M}^{\mathcal{D}}$ and $\boldsymbol{M}^{\mathcal{A}}$ data of a given group, the truncation number P considered during the FMM assembly stage is determined by its closest far group, $P = P_{max}$. For the $\boldsymbol{M}^{\mathcal{T}}$ data, the truncation number P is determined by the two groups Γ_s and Γ_o involved in the translation, $P = P_{so}$. During the iterative process, the aggregation step is carried out with $P = P_{max}$, while $P = P_{so}$ suffices for the translation and disaggregation.

As a rule of thumb, the optimum value of τ lies in the interval $[1/4, 1/5]$, i.e. an observation group Γ_o is far from a source group Γ_s if it is outside the sphere of radius $R_{far} \in [3R_s, 4R_s]$ with origin the centre of Γ_s. The upper limit corresponds to $\tau \leq 1/5$, or, according to Figure 4.11, to a maximum truncation number $P_{max} = 10$ for $\varepsilon = 10^{-6}$, while the classical law leads to $P = \log_2(1/\varepsilon) = 20$.

4.3.2.4 Taking movement into account

The analysis is restricted to rigid bodies, the boundaries of which constitute the BE domain. The decomposition in groups $\Gamma = \bigcup_{g=1}^{N_g} \Gamma_g$ is preserved during movement.

For a given position p, we define the vectors $\underline{r}^p = \underline{r}^p_o - \underline{r}^p_{oc} = (r, \theta^p, \phi^p)$, $\underline{r}^p_c = \underline{r}^p_{oc} - \underline{r}^p_{sc} = (r^p_c, \theta^p_c, \phi^p_c)$ and $\underline{r}'^p = \underline{r}^p_{sc} - \underline{r}^p_s = (r', \theta'^p, \phi'^p)$ analogously to those shown in Figure 4.5. It is easy to find the relations between the previous $p-1$- and the new p- FMM data. Indeed, from (4.30) and (4.31), it follows:

$$\boldsymbol{M}^{\mathcal{D}^p}_{o,k,m,n} = \boldsymbol{M}^{\mathcal{D}^{p-1}}_{o,k,m,n} \frac{\mathcal{L}^m_n(\theta^p, -\phi^p)}{\mathcal{L}^m_n(\theta^{p-1}, -\phi^{p-1})}, \tag{4.33}$$

$$\boldsymbol{M}^{\mathcal{T}^p}_{m+u,n+v} = \boldsymbol{M}^{\mathcal{T}^{p-1}}_{m+u,n+v} \left(\frac{r^p_c}{r^{p-1}_c}\right)^{m+u+1} \frac{\mathcal{L}^{n+v}_{m+u}(\theta^p_c, \phi^p_c)}{\mathcal{L}^{n+v}_{m+u}(\theta^{p-1}_c, \phi^{p-1}_c)}, \tag{4.34}$$

$$\boldsymbol{M}^{\mathcal{A}^p}_{s,l,u,v} = \boldsymbol{M}^{\mathcal{A}^{p-1}}_{s,l,u,v} \frac{\mathcal{L}^v_u(\theta'^p, -\phi'^p)}{\mathcal{L}^v_u(\theta'^{p-1}, -\phi'^{p-1})}. \tag{4.35}$$

This way, the integrals (4.30) do not have to be reevaluated. For updating the disaggregation, aggregation and translation data, a multiplication of the previous data with the corresponding factor suffices. In the particular case of purely translational movement, only the translation data have to be modified.

4.4 FMM applied to Helmholtz equations

The first application of the FMM to electromagnetic scattering problems was reported in [Engheta *et al.*, 1992] for two-dimensional problems and in [Coifman *et al.*, 1993] for three-dimensional cases. Improvements and variants have been contributed in subsequent publications. The ray-propagation fast multipole algorithm (RPFMA) [Wagner & Chew, 1994], the fast far-field approximation (FAFFA) [Lu & Chew, 1995; Brennan & Cullen, 1998] and a high-frequency asymptotic version [Burkholder & Kwon, 1996] introduce a windowed translation operator based on geometrical optics (GO). Indeed, the translation operator has a strong 'main beam' in the direction from source to observation group, favouring plane waves which propagate close to this direction. In [Lu & Chew, 1994; Song & Chew, 1995; Song *et al.*, 1997; Song & Chew, 1998; Sheng *et al.*, 1998; Geng *et al.*, 2001], the multilevel fast multipole algorithm (MLFMA) is presented, in which the operational count is further reduced by nesting groups withing groups. An hybrid FAFFA-MLFMA algorithm is proposed in [Chew *et al.*, 2002]. An incomplete LU preconditioner for FMM implementation is described in [Sertel & Volakis, 2000].

Our study concerns the single level FMM.

4.4.1 Two-dimensional Helmholtz Green function

4.4.1.1 Multipole expansion

The fundamental solution for the Helmholtz equation in two dimensions [Harrington, 1961] is given by

$$G(\rho) = \frac{1}{4\imath} H_0^{(2)}(k\rho), \tag{4.36}$$

where $k = \frac{2\pi}{\lambda}$ is the wavenumber, $H_0^{(2)}$ is the Hankel function of the second kind and order 0, $\rho = |\underline{r}_o - \underline{r}_s|$ is the distance between a source point $\underline{r}_s$ and an observation point $\underline{r}_o$. The distance ρ can be expressed in function of $\underline{r}_c$, $\underline{r}$ and $\underline{r}'$ as $\rho = |\underline{r}_c + \underline{r} + \underline{r}'|$ (see Figure 4.5).

The addition theorem for Hankel functions [Harrington, 1961] (see Appendix B.6.2) is used to expand the Hankel function in (4.36) as

$$H_0^{(2)}(k\rho) = H_0^{(2)}(k|\underline{r}_c + \underline{r} + \underline{r}'|) = \sum_{m=-\infty}^{\infty} J_m(k|\underline{r} + \underline{r}'|) H_m^{(2)}(k\underline{r}_c) e^{\imath m(\phi_c - \phi_{rr'})}, \tag{4.37}$$

where ϕ_c and $\phi_{rr'}$ are the angles that $\underline{r}_c$ and $\underline{r} + \underline{r}'$ form with the x-axis, respectively, and is valid for $r_c > |\underline{r} + \underline{r}'|$.

Next, we consider a Fourier integral form of the Bessel function,

$$J_m(k|\underline{r} + \underline{r}'|) = \frac{1}{2\pi} \int_0^{2\pi} e^{-\underline{k}(\underline{r} + \underline{r}') - \imath m(\phi - \phi_{rr'} + \pi/2)} \mathrm{d}\phi, \tag{4.38}$$

where $\underline{k} = k(\cos\phi, \sin\phi)$.

Omitting the factor $1/\imath 4$ and applying (4.37) and (4.38), we can expand the 2D Helmholtz Green function (4.36) as [Rokhlin, 1990; Burkholder & Kwon, 1996]:

$$H_0^{(2)}(k\rho) = \sum_{m=-\infty}^{\infty} \int_0^{2\pi} \mathcal{D}(\underline{r})\, \mathcal{T}_m(\underline{r}_c)\, \mathcal{A}(\underline{r}')\, \mathrm{d}\phi, \tag{4.39}$$

with

$$\mathcal{D}(\underline{r}) = e^{-\imath \underline{k}\,\underline{r}}, \quad \mathcal{T}_m(\underline{r}_c) = H_m^{(2)}(kr_c) e^{-\imath m(\phi - \phi_c + \pi/2))}, \quad \mathcal{A}(\underline{r}') = e^{-\imath \underline{k}\,\underline{r}'}. \tag{4.40 a–c}$$

The multipole expansion (4.39) is exact. It must be truncated to a finite number of terms. The truncation $-M/2 \leq m \leq M/2$ must be sufficient to achieve the desired accuracy and convergence (the error decreases with M). In fact, once a sufficiently large number of multipoles M is considered, the accuracy of the approximation increases super-algebraically, i.e. faster than any negative power of M [Rokhlin, 1990]. In this reference, an optimal and semi-empirical fit is given for the case of two-dimensional scattering problems. The truncation is determined by the maximum radius R of the circles enclosing the groups as

$$M/2 = kR. \tag{4.41}$$

Obviously, the integral over $[0, 2\pi]$ must be discretised. For this, we use the trapezoidal rule, i.e. for any function f, we write

$$\frac{1}{2\pi}\int_0^{2\pi} f(\phi)\mathrm{d}\phi \approx \frac{1}{N_d}\sum_{n=1}^{N_d} f(\phi_n), \tag{4.42}$$

where $\phi_n = \frac{2\pi n}{N_d}$, and $N_d = M + 1$. The choice of N_d follows from the sampling theorem [Rokhlin, 1990; Lu & Chew, 1993].

Hence the discretised approximated form of (4.39) reads,

$$H_0^{(2)}(k\rho) \approx \frac{1}{N_d}\sum_{n=1}^{N_d} \mathcal{D}_n(\underline{r})\,\mathcal{T}_{m,n}(\underline{r}_c)\,\mathcal{A}_n(\underline{r}') \tag{4.43}$$

with

$$\mathcal{D}_n(\underline{r}) = e^{-\imath \underline{k}_n \underline{r}} = e^{-\imath \underline{k}_n (\underline{r}_o - \underline{r}_{oc})} = e^{-\imath k r \cos(\phi-\phi_n)}, \tag{4.44}$$

$$\mathcal{T}_{m,n}(\underline{r}_c) = \sum_{m=-M/2}^{M/2} H_m^{(2)}(kr_c) e^{-\imath m(\phi_n - \phi_c + \pi/2))} = \tag{4.45}$$

$$= \sum_{m=-M/2}^{M/2} H_m^{(2)}(k|\underline{r}_{oc} - \underline{r}_{sc}|) e^{-\imath m(\phi_n - \phi_c + \pi/2))},$$

$$\mathcal{A}_n(\underline{r}') = e^{-\imath \underline{k}_n \underline{r}'} = e^{-\imath \underline{k}_n (\underline{r}_{sc} - \underline{r}_s)} = e^{-\imath k r' \cos(\phi' - \phi_n)}, \tag{4.46}$$

and $\underline{k}_n = k(\cos\phi_n, \sin\phi_n)$, $n = 1, \cdots, N_d$, is the propagation vector of the nth plane wave.

This multipole approximation (4.43) converges rapidly outside any circle with diameter D containing all the sources (group) and separated from it by at least one wavelength.

The plane wave expansion of (4.39) and its discretised version (4.43) incorporate plane waves propagating in all directions with 360° coverage. However, for a given pair of groups Γ_s and Γ_o and from a high frequency asymptotic point of view, only plane waves propagating close to the direction of $\underline{r}_c$ are expected to contribute strongly to the fields in the observation group. This becomes particularly clear when the groups are widely separated. Using the large argument form of the Hankel function (see Appendix B.1), it is easy to show that for widely separated groups ($r_c \gg 2R$) equation (4.40 b) reduces to

$$\mathcal{T}(\underline{r}_c) \sim \sqrt{\frac{\imath 2}{\pi k r_c}}\, e^{-\imath k r_c} \frac{\sin[(M+1)(\phi - \phi_c)/2]}{\sin[(\phi - \phi_c)]}. \tag{4.47}$$

This function clearly shows a strong main beam for ϕ close to ϕ_c and a highly oscillatory and slowly decaying sidelobe region [Wagner & Chew, 1994]. The translation operator can thus be interpreted as a plane wave filter which selects plane wave components propagating at angles close to $\underline{r}_c$ and attenuates plane waves propagating

at wide angles. An interesting asymptotic evaluation of the translation operator is presented in [Burkholder & Kwon, 1996]. Herein, a windowing function is defined by identifying the geometrical optics lit region of the translator operator, which is evaluated asymptotically using the method of steepest descents [Clemmow, 1950].

The function $\operatorname{grad} G$ can be expanded in a similar way. It suffices to derive (4.44) with respect to the coordinates of the observation point $\underline{r}_o = (x_o, y_o)$. Taking into account that $\underline{r} = \underline{r}_o - \underline{r}_{oc} = (x_o - x_{oc}, y_o - y_{oc}) = (x, y)$, we can write

$$\operatorname{grad} \mathcal{D}_n(\underline{r}) = (\partial_{x_o} \mathcal{D}_n, \partial_{y_o} \mathcal{D}_n) = (\partial_x \mathcal{D}_n, \partial_y \mathcal{D}_n) \,, \tag{4.48}$$

with

$$\partial_x \mathcal{D}_n = -\imath k \, \cos\phi_n \, e^{-\imath k r \cos(\phi - \phi_n)} \,, \qquad \partial_y \mathcal{D}_n = -\imath k \, \sin\phi_n \, e^{-\imath k r \cos(\phi - \phi_n)} \,. \tag{4.49}$$

4.4.1.2 Fast matrix-vector product

Analogously to the Laplace cases treated in Sections 4.3.1.2 and 4.3.2.2 for the Laplace Green equations, the system matrix (3.37 a) can be formally expressed as in (4.1).

Let us consider the degrees of freedom $\underline{j}_k$ and $\underline{j}_l$ of $\underline{j}_s$ associated with the basis functions (3.44) $\underline{\beta}_k(\underline{r}_o)$ and $\underline{\beta}_l(\underline{r}_s)$ that are nonzero vectors on the respective far groups Γ_o and Γ_s. For the sake of simplicity, we restrict the formal decomposition hereafter to the EFIE case (3.49) and in particular to the term that depends on (4.36). Its contribution to $\boldsymbol{M}^{far}$ is denoted $\left(\boldsymbol{M}^{far}_{o,s}\right)_{k,l}$ and obtained by applying (4.43), it reads

$$\Re\left(\sum_{n=1}^{N_d} \boldsymbol{M}^{\mathcal{D}}_{o,k,n} \sum_{m=-M/2}^{M/2} \boldsymbol{M}^{\mathcal{T}}_{m,n} \boldsymbol{M}^{\mathcal{A}}_{s,l,n} \right), \tag{4.50}$$

with

$$\boldsymbol{M}^{\mathcal{D}}_{o,k,n} = \int_{\Gamma_o} \underline{\beta}_k \mathcal{D}_n \, \mathrm{d}\Gamma \,, \quad \boldsymbol{M}^{\mathcal{A}}_{s,l,n} = \int_{\Gamma_s} \underline{\beta}_l \mathcal{A}_n \, \mathrm{d}\Gamma \,, \tag{4.51 a,b}$$

and

$$\boldsymbol{M}^{\mathcal{T}}_{m,n} = \frac{w\mu}{4} \mathcal{T}_{m,n} \,. \tag{4.52}$$

Note that contribution of the term in (3.49) with $\operatorname{grad} G$ would be obtained in a similar way, and then added to (4.50).

The objective of (4.50) is again to speed up the product $\boldsymbol{M}^{far}\boldsymbol{Q}$ within an iterative process (see Section 4.2.2).

4.4.1.3 Operational count

The power of the FMM lies in the fact that there is a one-to-one correspondence between the plane wave spectral components of the source group and the plane wave coefficients of the observation group.

The total operational count involved in the FMM for one matrix-vector multiplication is estimated as follows. Let us assume that the total number of unknowns

N is equally distributed in $N_g = N/L$ groups (L is then the number of unknowns per group) and that there are n nearby groups (in general, two or more depending on the geometry). A group is neighbour of itself. $\boldsymbol{M}^{\mathcal{T}}_{m,n}$ (4.52) translates the mth plane wave of group Γ_s to the mth plane wave of group Γ_s.

The number of operations involved in finding the interactions within the source group and between the n adjacent nearest-neighbour groups (see Figure 4.1) is $nL^2N_g = nLN$. To numerically evaluate (4.51 b) for N_d directions and N_g groups requires $N_dLN_g \approx c_1LN$ operations, where $N_d \approx c_1L$ satisfies the sampling theorem (c_1 constant) [Rokhlin, 1990; Bindiganavale & Volakis, 1996]. The number of plane wave translations (4.52) for N_g^2 source-observation pairs of groups is $N_dN_g^2 \approx c_1N^2/L$. Finally, the plane wave reconstruction of the fields at the receiving groups (4.51 a) requires $N_dLN_g \approx c_1LN$. The total estimated operational count is then

$$c_1N^2/L + c_2LN \tag{4.53}$$

where $c_2 = n + (n-1)c_1$. Minimising with respect to L yields to an operational count of $\mathcal{O}(N^{1.5})$ for $L \approx \sqrt{N}$, what implies $N_g = \sqrt{N}$.

4.4.2 Three-dimensional Helmholtz Green function

4.4.2.1 Multipole expansion

The three-dimensional Helmholtz Green function

$$G(\rho) = \frac{e^{-\imath k\rho}}{4\pi\rho}\,, \tag{4.54}$$

can be expanded by means of the addition theorems for spherical Bessel and Hankel functions [Coifman *et al.*, 1993] (see Appendix B.6.2). Omitting the factor $1/4\pi$, we have

$$\frac{e^{-\imath k\rho}}{\rho} = -\imath k\sum_{m=0}^{\infty}(-1)^m(2m+1)j_m(k|\underline{r}+\underline{r}'|)h_m^{(2)}(kr_c)P_m((\underline{r}+\underline{r}')\cdot\underline{r}_c)\,, \quad |\underline{r}+\underline{r}'| < \rho \tag{4.55}$$

where we have taken into account that the direct path source to observation point can be decomposed as $\underline{\rho} = \underline{r}_o - \underline{r}_s = \underline{r}' + \underline{r}_c + \underline{r}$ (see Figure 4.5), j_m is the spherical Bessel function of order m, $h_m^{(2)}$ is the spherical Hankel function of the second kind and order m and P_m is the Legendre polynomial of order m. These special functions are defined in Appendix B.

Let us consider the expansion of the product $j_m\,P_m$ appearing in equation (4.55) as a surface integral over the unit sphere Γ_{Sph} of propagating plane waves (spectral integral):

$$(-\imath)^m 4\pi j_m(k|\underline{r}+\underline{r}'|)P_m\left((\underline{r}+\underline{r}')\cdot\underline{r}_c\right) = \int_{\Gamma_{Sph}} e^{-\imath\underline{k}\cdot(\underline{r}+\underline{r}')}P_m(\hat{k}\cdot\underline{r}_c)\mathrm{d}s\,, \tag{4.56}$$

where $\hat{k}$ is the unit position vector on Γ_{Sph} and $\underline{k} = k\hat{k}$

Using this identity and interchanging the orders of the summation and integration, the expansion (4.55) can be rewritten as

$$\frac{e^{-\imath k\rho}}{\rho} = \int_{\Gamma_{Sph}} \mathcal{D}\left(\underline{r}\right) \mathcal{T}_m\left(\underline{r}_c\right) \mathcal{A}\left(\underline{r}'\right) \mathrm{d}s\,, \tag{4.57}$$

with

$$\mathcal{D}\left(\underline{r}\right) = e^{-\imath \underline{k}\,\underline{r}}\,, \tag{4.58}$$

$$\mathcal{T}_m\left(\underline{r}_c\right) = \frac{-\imath k}{4\pi} \sum_{m=0}^{\infty} (-\imath)^m (2m+1) h_m^{(2)}(kr_c) P_m(\hat{k}\cdot\underline{r}_c)\,, \tag{4.59}$$

$$\mathcal{A}\left(\underline{r}'\right) = e^{-\imath \underline{k}\,\underline{r}'}\,. \tag{4.60}$$

Again, the exact multipole expansion (4.57) must be truncated. The truncation $0 \le m \le M$ must be sufficient to achieve the desired accuracy and convergence. An excellent empirical fit [Rokhlin, 1993; Coifman *et al.*, 1993] for the number of multipoles required for single precision (8 digit precision) is

$$M = kD + 5\ln\left(kD + \pi\right), \tag{4.61}$$

where D is the maximum diameter of the circles enclosing the groups. For double precision (16 digits) this is

$$M = kD + 10\ln\left(kD + \pi\right). \tag{4.62}$$

Furthermore, the N_d directions $\hat{k}$ on the unit sphere Γ_{Sph} must be sufficient to give a quadrature rule that is exact for all spherical harmonics of order $m < 2M$. A simple method [Rokhlin, 1993] for accomplishing this is to pick polar angles θ that are zeros of $P_M(\cos\theta)$, and azimuthal angles ϕ to be $2M$ equally spaced points. Thus, for this choice of $\hat{k} = (\sin\theta\cos\phi, \sin\theta\sin\phi, \cos\theta)$, the number of directions equals $N_d = 2M^2$. If more efficient quadrature rules for the sphere (e.g. those described in [McLaren, 1963]) are used, then $N_d \approx 4/3M^2$.

Applying the truncation to (4.57), we can expressed the approximated expansion as

$$\frac{e^{-\imath k\rho}}{\rho} \approx \sum_{n=1}^{N_d} \mathcal{D}_n\left(\underline{r}\right) \mathcal{T}_{m,n}\left(\underline{r}_c\right) \mathcal{A}_n\left(\underline{r}'\right)\,, \tag{4.63}$$

with

$$\mathcal{D}_n\left(\underline{r}\right) = e^{-\imath \underline{k}_n\,\underline{r}}\,, \tag{4.64}$$

$$\mathcal{T}_{m,n}\left(\underline{r}_c\right) = \frac{-\imath k}{4\pi} \sum_{m=0}^{M} (-\imath)^m (2m+1) h_m^{(2)}(kr_c) P_m(\hat{k}_n\cdot\underline{r}_c)\,, \tag{4.65}$$

$$\mathcal{A}_n\left(\underline{r}'\right) = e^{-\imath \underline{k}_n\,\underline{r}'}\,. \tag{4.66}$$

and $\hat{k}_n = (\sin\theta_n\cos\phi_n, \sin\theta_n\sin\phi_n, \cos\theta_n)$, $\underline{k}_n = k\hat{k}_n$.

The solution of an integral equation requires the expansion of grad G as well. It can be obtained by deriving (4.64) with respect to the coordinates of the observation point $\underline{r}_o = (x_o, y_o, z_o)$. Considering that $\underline{r} = \underline{r}_o - \underline{r}_{oc} = (x_o - x_{oc}, y_o - y_{oc}, z_o - z_{oc}) = (x, y, z)$, it reads

$$\operatorname{grad} \mathcal{D}_n(\underline{r}) = (\partial_{x_o}\mathcal{D}_n, \partial_{y_o}\mathcal{D}_n, \partial_{z_o}\mathcal{D}_n) = (\partial_x\mathcal{D}_n, \partial_y\mathcal{D}_n, \partial_z\mathcal{D}_n) \;, \tag{4.67}$$

with

$$\partial_x\mathcal{D}_n = -\imath k \, \sin\theta_n \cos\phi_n \, e^{-\imath \underline{k}_n \underline{r}} \,, \tag{4.68}$$

$$\partial_y\mathcal{D}_n = -\imath k \, \sin\theta_n \sin\phi_n \, e^{-\imath \underline{k}_n \underline{r}} \,, \tag{4.69}$$

$$\partial_z\mathcal{D}_n = -\imath k \, \cos\theta_n \, e^{-\imath \underline{k}_n \underline{r}} \,. \tag{4.70}$$

4.4.2.2 Fast matrix-vector product

Again, the system matrix (3.37 a) can be formally approximated as in (4.1).

Let us consider the degrees of freedom $\underline{j}_k$ and $\underline{j}_l$ of $\underline{j}_s$ with associated the RWG basis functions (3.40) $\underline{\beta}_k(\underline{r}_o)$ and $\underline{\beta}_l(\underline{r}_s)$ that are nonzero vectors on the respective far groups Γ_o and Γ_s. For the sake of simplicity, we restrict the formal decomposition hereafter to the EFIE case (3.49) and in particular to the term that depends on the 3D Helmholtz Green function (4.54). Its contribution to $\boldsymbol{M}^{far}$ is denoted $\left(\boldsymbol{M}^{far}_{o,s}\right)_{k,l}$ and obtained by applying (4.63), it reads

$$\Re\left(\sum_{n=1}^{N_d} \boldsymbol{M}^{\mathcal{D}}_{o,k,n} \sum_{m=0}^{M} \boldsymbol{M}^{\mathcal{T}}_{m,n} \boldsymbol{M}^{\mathcal{A}}_{s,l,n} \right), \tag{4.71}$$

with

$$\boldsymbol{M}^{\mathcal{D}}_{o,k,n} = \int_{\Gamma_o} \underline{\beta}_k \mathcal{D}_n \, \mathrm{d}\Gamma \,, \quad \boldsymbol{M}^{\mathcal{A}}_{s,l,n} = \int_{\Gamma_s} \underline{\beta}_l \boldsymbol{\mathcal{A}}_n \, \mathrm{d}\Gamma \,, \tag{4.72 a,b}$$

and

$$\boldsymbol{M}^{\mathcal{T}}_{m,n} = \frac{\imath w \mu}{4\pi} \mathcal{T}_{m,n} \,. \tag{4.73}$$

Note that contribution of the term in (3.49) with grad G would be obtained in a similar way, and then added to (4.71).

The goal of (4.71) is once again to accelerate the product $\boldsymbol{M}^{far}\boldsymbol{Q}$ within an iterative process (see Section 4.2.2).

4.4.2.3 Operational count

Let us estimate the total operational count involved in the solution of an EFIE problem (Section 3.4.1) when applying FMM. For multipole expansions truncated at order M and a number of directions $N_d = 2M^2$ for $\hat{k}$, the total number of coefficients required to expand $\underline{a}$ and φ is $4N_d$ (aggregation and disaggregation). Let us consider N_g groups with $L = N/N_g$ unknowns each and a number of neighbour groups n. The number of operations involved in the direct computation between

the source group and the n neighbour groups requires $(n+1)L^2N_g = (n+1)LN$. The numerical evaluation of (4.72 b), aggregation operation, for N_d directions and N_g groups requires $4N_gN_dL = 4N_dN$. The number of plane wave translations (4.73) for N_g^2 source-observation pairs of groups is $4N_g^2N_d^2$. Finally, the plane wave reconstruction of the fields at the receiving groups (4.72 a), disaggregation operation, requires $4N_gN_dL = 4N_dN$. The total operational count is thus

$$(n+1)LN + 8N_dN + 4N_g^2N_d^2\,. \tag{4.74}$$

Minimising with respect to N_g yields to $N_g = \mathrm{cte}\,(N/N_d)^{2/3}$ and a computational cost of $\mathcal{O}(N^{4/3})$.

Chapter 5

Low frequency numerical tests

Contents

5.1 Introduction

In this chapter we present a series of low frequency (Laplace equation) numerical tests performed to validate the theoretical developments described in Chapter 4 and

their implementation. We consider several two-dimensional and three-dimensional test cases that may be modelled by numerical and physical coupled systems. Either a hybrid FE-BE analysis or a pure BE analysis is carried out for the electromagnetic problem. The FMM is applied to the expansion of the 2D and 3D Laplace equation to accelerate the solution of the BE part. The adaptive truncation scheme, elaborated in Sections 4.3.1.1 and 4.3.2.1, is applied. In case of FMM acceleration, the preconditioning (e.g. ILU decomposition) is based on the sparse matrix due to the BE near-field interactions (and the complete FE contribution for hybrid analyses).

The efficiency of the FMM is demonstrated through the study of the different numerical tests. Significant savings in computation time and storage requirements are achieved.

The first numerical test (Section 5.2) consists in the hybrid FE-BE analysis of a 2D eddy current problem. The aim of this test is to show that the adaptive truncation scheme significantly contributes to the computation time savings achieved with the FMM, particularly when dealing with moderate sized problems. The second numerical test (Section 5.3) concerns the hybrid modelling of a linear actuator taking into account saturation, the voltage supply and the mechanical equation. Updating the FMM acceleration (aggregation, disaggregation and translation) data for every new position of the moving part will prove to be simple and computationally cheap (only the translation data have to be updated). The third application (Section 5.4) considered deals with the hybrid FE-BE analysis of a 3D eddy current problem, in particular, the TEAM workshop problem 28. The transient behaviour of the electrodynamic levitation device is modelled taking into account the mechanical equation. The fourth numerical test (Section 5.5) models a microelectromechanical (MEM) switch by means of the FMM accelerated BE method. The results are validated and compared with those given by two commercial software packages.

5.2 Shielding problem

A linear time harmonic eddy current problem in $\mathbb{R}^2$ is considered. The magnetic field is computed using both a full FE model and a hybrid FE-BE model. We choose the 2D $\underline{b}$-conforming formulation and the 2D hybrid $\underline{b}$-conforming formulation described in Sections 2.5.1 and 2.6.3, respectively.

The full FE model is applied in a domain Ω comprising a domain Ω_s, a domain Ω_c, the surrounding air and a bounding ring to which a transformation method is applied in order to account for the free space extending to infinity [Brunotte *et al.*, 1992]. A current density $\underline{j} = j_s(x, y)\,\underline{1}_z$, directed along the z-axis, is given in the domain Ω_s. The rest of the exterior domain is current free. Eddy currents may appear in the domain Ω_c (with conductivity σ).

In the hybrid FE-BE model, the FE method is used in a domain Ω comprising solely the domains Ω_s and Ω_c. Its boundary is denoted Γ. The BE method accounts for the free space exterior to Ω extending to infinity. The BE part is either accelerated by means of the FMM or not. The adaptive truncation scheme for the 2D Laplace Green function is used (see Section 4.3.1.1).

Figure 5.1: Three conductors Ω_s and thin steel plate Ω_c

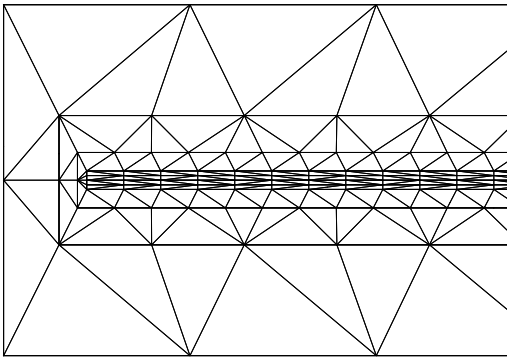

Figure 5.2: Detail of the discretisation of the domain Ω of the hybrid model

5.2.1 Description of the problem

The problem comprises three conductors carrying a three-phase current and a thin steel plate placed above the conductors. This is depicted in Figure 5.1. The plate serves as a protective shield (see flux lines in Figure 5.4).

The three copper conductors with square cross-section ($30\,\text{mm} \times 30\,\text{mm}$, $\mu = \mu_0$) carry imposed balanced sinusoidal currents of frequency $f = 50\,\text{Hz}$ and r.m.s. value $2\,\text{kA}$. The horizontal distance between the centres of the conductors is $125\,\text{mm}$. The three conductors constitute the source domain Ω_s.

The steel plate is $1\,\text{mm}$ thick and $1\,\text{m}$ wide. It is placed $100\,\text{mm}$ above the conductors. Its relative permeability $\mu_r = \mu/\mu_0$ and electrical conductivity σ are 1000 and $2\,10^6\,\text{S/m}$, respectively. The penetration depth in the plate equals $1/\sqrt{\pi f \mu \sigma} = 1.59\,\text{mm}$ at $f = 50\,\text{Hz}$.

Figure 5.2 shows a detail of the discretisation of the FE domain Ω in the hybrid FE-BE model. It comprises the steel plate and a layer of air around the plate. The plate Ω_c is discretised into four layers of triangular elements. The number of divisions along x is 500. Thanks to the three layers of air elements around the plate, the number of line segments on the BE contour Γ is reduced to 104 while retaining

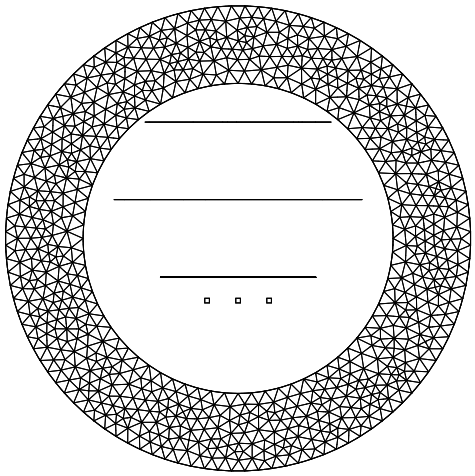

Figure 5.3: Discretisation of the FE transformation domain

a large number of divisions in the plate. The air layer also allows to avoid the oscillation problem that may occur when using piecewise constant basis functions $\beta_k(\xi)$ on an air-iron interface [Henrotte, 2000; Geuzaine *et al.*, 2001]. The hybrid FE-BE discretisation yields 4316 complex unknowns for the harmonic analysis: 4212 for a and 104 for q.

In the full FE model, the plate, the three conductors and a portion of the surrounding air are discretised by means of first order triangular elements. The discretisation of both the plate and the surrounding air layers coincides with the one in the hybrid model. The FE model is bounded by a ring (see Figure 5.3). On its outer boundary, the Dirichlet condition $a = 0$ is imposed. Two lines placed 0.5 m and 1 m above the plate, where the computed induction will be shown, are also depicted in Figure 5.3.

In order to allow a fair comparison of the hybrid model and the FE model with regard to both accuracy and computational cost, a sufficiently fine discretisation is adopted for the latter, resulting in 12844 complex unknowns for the harmonic analysis with a piecewise linear interpolation of the magnetic vector potential a.

5.2.2 Calculation results

The harmonic field calculations are first carried out with the FE model and the nonaccelerated hybrid FE-BE model. The flux pattern (real and imaginary part) obtained with the FE model is represented in Figure 5.4.

In Figure 5.5 the real and imaginary part of the x-component of the magnetic induction in the four layers of the plate are depicted for both resolution methods. The agreement is very good. The discretisation of the plate in four layers proves to be necessary: due to the eddy currents, the induction is seen to vary from one layer to another.

The y-component of the magnetic induction (real and imaginary part) above the plate at the distances of 0.5 m and 1.0 m is depicted in Figure 5.6. As expected,

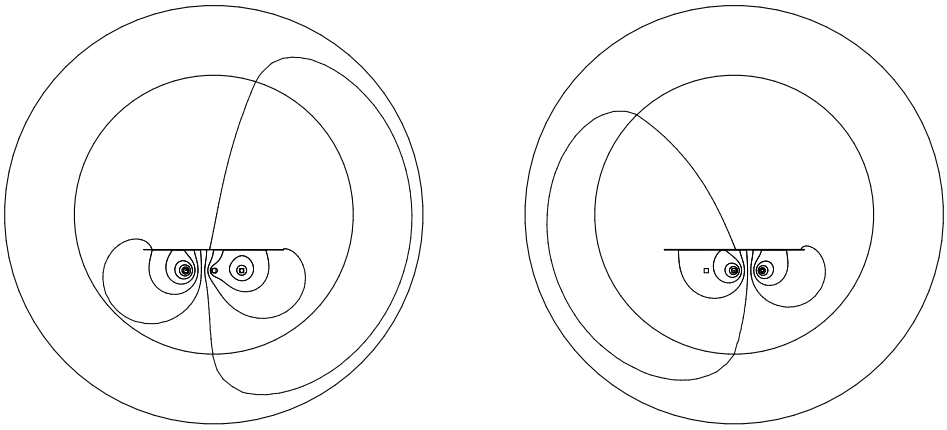

Figure 5.4: Real (left) and imaginary part (right) of the flux pattern

the curves achieved with the hybrid model are smoother due to the fact that in the BE formulation free space is automatically and exactly considered, while in the FE model the surrounded air is discretised and a transformation method is used to account for its extension to infinity.

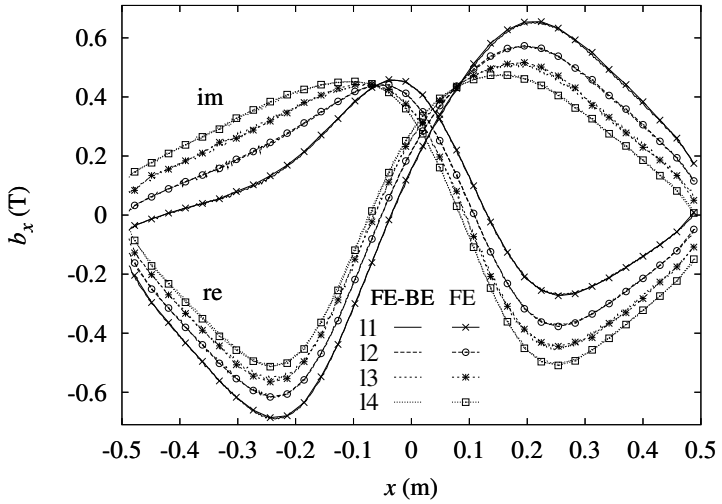

Figure 5.5: Induction b_x in the four layers (denoted l1, l2, l3, l4) in which the steel plate is discretised

The FMM is now applied to speed up the BE part of the hybrid model. The BE contour Γ is split up in 25 groups constituted by either 10 line segments (the two groups on the left and right edge of the plate) or 8 line segments (all the other groups). Two groups are considered to be far groups if there are at least two groups in between. This corresponds to $R_s/d \leq 1/6$ and $R_o/d \leq 1/6$, or, according to Figure 4.7 in Section 4.3.1, to a maximum truncation number $P_{max} = 8$ for $\varepsilon = 10^{-6}$. The classical law $P = \log_2(1/\varepsilon)$ leads to a truncation number of 20.

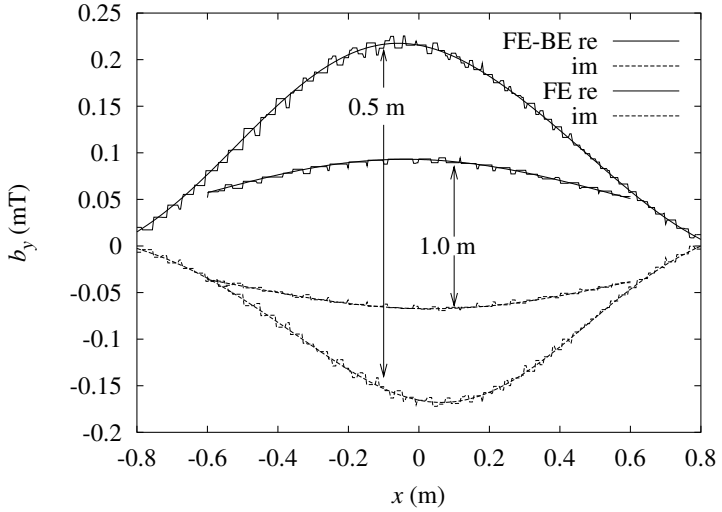

Figure 5.6: Induction b_y at 0.5 m and 1.0 m above the plate

The error of the induction in and above the plate obtained with the accelerated FE-BE hybrid model with respect to the nonaccelerated model is illustrated in Figures 5.7 and 5.8 . It is lower than 0.3 % in the plate, 0.06 % at 0.5 m above the plate and 0.033 % at 1.0 m above the plate.

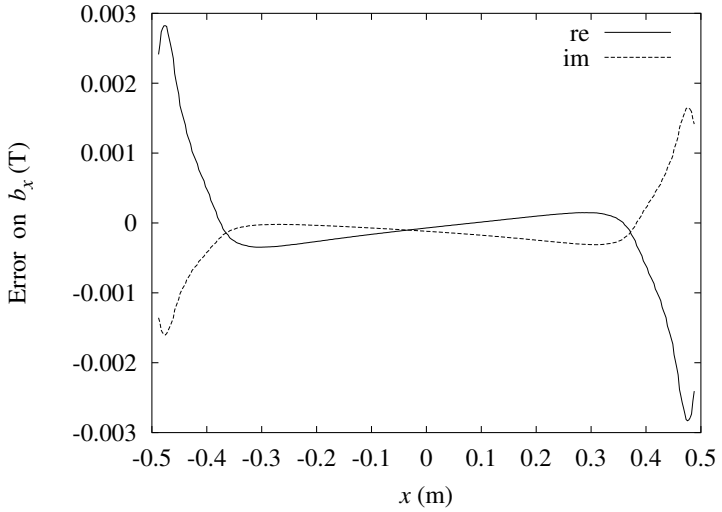

Figure 5.7: Error on the induction b_x in the steel plate due to the FMM acceleration

5.2.3 Computational cost

For all computations, the system of algebraic equations is solved by means of the iterative solver GMRES [Saad & Schultz, 1986]. To ensure convergence, an ILU-preconditioner is applied.

The total computation time on a 2 GHz Intel Pentium 4 Processor is 3.6 s for

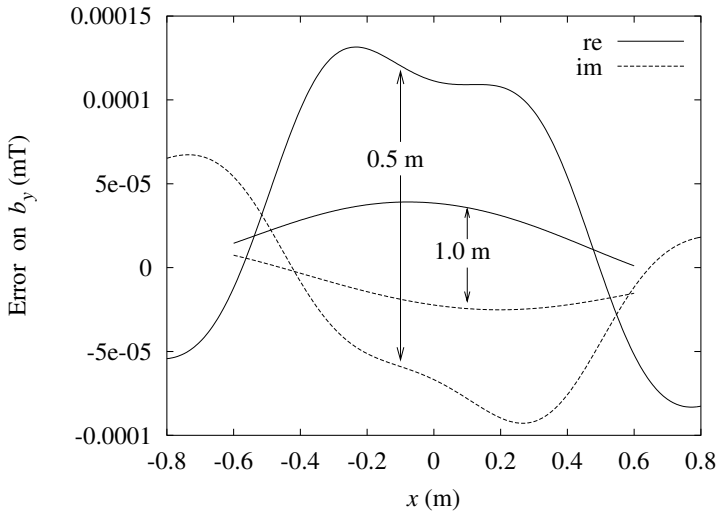

Figure 5.8: Error on the induction b_y at 0.5 m and 1.0 m above the steel plate due to the FMM acceleration

the FE model and 7.6 s for the hybrid model without FMM acceleration. Using the FMM with the adaptive truncation scheme ($P_{max} = 8$ and $P_{av} = 4$ for $\varepsilon = 10^{-6}$) results in a calculation time of 3.2 s. This is mainly due to the reduced time for the assembly (2.4 s vs 6.9 s), which constitutes approximately 75 % and 90 % of the total computation time for the accelerated and nonaccelerated hybrid model, respectively. When using a fixed truncation number $P = 20$, the application of the FMM to the hybrid model does not prove useful: the computation time increases to 12.4 s. By means of the adaptive truncation scheme, the solution of the system is thus achieved 4 times quicker.

The time spent on the iterative resolution of the system of algebraic equations is 1.2 s for the FE model and only 0.6 s for the accelerated hybrid model.

5.3 Electromechanical device

The two-dimensional modelling of a linear actuator is studied in detail. The 2D hybrid $\underline{b}$-conforming formulation developed in Section 2.6.3 is applied to the magnetostatic problem in $\mathbb{R}^2$. The FE method is used in a domain Ω comprising all saturable parts of the model and a domain Ω_s in which the current density $\underline{j} = j_s(x, y, t)\,\underline{1}_z$, directed along the z-axis, is given. The BE method provides a rigorous treatment for the free space exterior to Ω, the boundary of which is denoted Γ. Moreover, it allows to take into account movement without remeshing. The permanent magnets are considered as another source (see Section 1.3.2.2).

The transient phenomenon is characterised taking into account the nonlinear behaviour of materials, the voltage supply and the mechanical equation.

5.3.1 Electrical coupling of saturated hybrid models

We consider an electrical circuit which comprises a number of stranded conductors (e.g. coils) in the FE domain and a number of lumped components, viz voltage sources, resistive components and inductive components. By introducing loop currents associated with a set of independent current loops in the electrical circuit, Kirchhoff's current law automatically holds [Lombart & Meunier, 1993]. Adding the electrical circuit equations to the hybrid FE-BE system (2.58) in time domain, the coupled system of algebraic and differential equations can be written as

$$\begin{bmatrix} \boldsymbol{S} & \boldsymbol{C} & \boldsymbol{K} \\ \boldsymbol{D}^T & \boldsymbol{M} & 0 \\ 0 & 0 & \boldsymbol{R} \end{bmatrix} \begin{bmatrix} \boldsymbol{A} \\ \boldsymbol{Q} \\ \boldsymbol{I}_l \end{bmatrix} + \begin{bmatrix} \boldsymbol{T} & 0 & 0 \\ 0 & 0 & 0 \\ \boldsymbol{K}^{*T} & 0 & \boldsymbol{L} \end{bmatrix} \mathrm{d}_t \begin{bmatrix} \boldsymbol{A} \\ \boldsymbol{Q} \\ \boldsymbol{I}_l \end{bmatrix} = \begin{bmatrix} \boldsymbol{J}_{pm} \\ 0 \\ \boldsymbol{U} \end{bmatrix}, \tag{5.1}$$

where $\boldsymbol{S}$ and $\boldsymbol{T}$ are sparse FE matrices, $\boldsymbol{C}$ and $\boldsymbol{D}$ are partially dense matrices, $\boldsymbol{M}$ is a full BE matrix, $\boldsymbol{A}$ and $\boldsymbol{Q}$ are column matrices containing the coefficients of the magnetic vector potential and the equivalent magnetic current layer, $\boldsymbol{R}$ and $\boldsymbol{L}$ are square matrices that represent the resistive and inductive components respectively, $\boldsymbol{I}_l$ and $\boldsymbol{U}$ are vectors that contain the loop currents and the voltage sources respectively, $\boldsymbol{T}$ accounts for the eddy currents in conducting parts of the FE domain, $\boldsymbol{K}$ and $\boldsymbol{K}^*$ are due to the flux linkage of the conductors in the 2D FE model and $\boldsymbol{J}_{pm}$ contains the equivalent nodal currents due to the permanent magnets [Tsukerman *et al.*, 1993]. The end-winding inductance of the FE conductors (3D effect) can be taken into account by means of lumped elements in the electrical circuit.

For a given voltage excitation and given initial conditions, the system (5.1) can be solved in the time domain. The time discretisation is commonly performed with the so-called θ-method, which amounts to Crank-Nicholson method if $\theta = 1/2$, and to the backward Euler method if $\theta = 1$.

When saturation is included in the analysis, time stepping the system of algebraic and differential equations (5.1) produces a system of nonlinear equations for each time step. These nonlinear systems can be easily solved by means of the Newton Raphson (NR) method. The NR method linearises the nonlinear systems and an iterative method, e.g. GMRES, is applied.

In case of FMM, for every NR iteration the multiplications of $\boldsymbol{M}^{far}$ and $\boldsymbol{C}^{far}$ by the solution vector of the previous iteration $\boldsymbol{Q}$ are sped up when calculating the residual. Then for every GMRES iteration, the multiplications of $\boldsymbol{M}^{far}$ and $\boldsymbol{C}^{far}$ by a trial vector $\Delta\boldsymbol{Q}$ are also accelerated.

5.3.2 Electromechanical modelling

We consider a rigid part that moves inside an airgap (as in the application example below).

Some elements of the complete system matrix are time dependent due to the movement (BE part) and magnetic saturation (FE part). These elements must be recalculated for any new time step. Furthermore, for every time step, the nonlinear contributions vary within the NR iterative loop. In order to reduce computation

time, the whole system matrix is thus split up in three separate matrices. The contributions that remain constant throughout the simulation are calculated and stored. Those that are position dependent are recalculated and saved in a matrix for every time step. Finally, those that are due to the nonlinear materials are reevaluated for every time step and every NR iteration.

5.3.2.1 Mechanical equation

In the FE-BE simulation, the position of the moving body is either a given function of time or follows from the magnetic and other forces exerted on it. In the latter case, the mechanical equation has to be considered alongside the electromagnetic equations (5.1). If the movement is purely translational, it reads:

$$m\mathrm{d}_t\underline{v}(t) + \xi\underline{v}(t) + k\underline{x}(t) = \underline{F}(t), \quad \underline{v}(t) = \mathrm{d}_t\underline{x}(t), \tag{5.2}$$

where $\underline{x}(t)$ is the position, $\underline{v}(t)$ the speed, m the mass, ξ the viscous friction coefficient, k the elastic constant and $\underline{F}(t)$ the total applied force including the magnetic forces.

If the time step for a dynamic analysis is sufficiently small the mechanical state variables (e.g. the total magnetic force $\underline{F}$) can be regarded as constant for the solution of the electromagnetic equations in the considered time step and vice versa. Under this condition the electromagnetic and mechanical equations can be solved alternatively rather than simultaneously. We adopt this strategy referred to as "weak electromechanical coupling" [Henrotte *et al.*, 1994].

5.3.2.2 Computation of the magnetic force

The total magnetic force $\underline{F}$ exerted on the moving part can be calculated by integrating the Maxwell stress tensor $\underline{\underline{T}}$ along a contour enclosing it. This method is mesh dependent [Ren & Razek, 1990]. The Arkkio method is a variant of the Maxwell stress tensor method for torque calculation in rotating electrical machines [Arkkio, 1987]. The result obtained by the Arkkio method can be seen as the mean value of the torque calculated with the Maxwell stress tensor method over a family of concentric contours in the moving band.

If the FE domain Ω comprises an air layer S around the moving piece as depicted in Figure 5.12, a generalisation of the Arkkio method referred to as the eggshell method can be used as well [Henrotte, 2000; Henrotte *et al.*, 2003]. It amounts to a surface integral on the air layer S:

$$\underline{F} = l_z \int_S \frac{1}{\delta}\underline{\underline{T}}\,\hat{n}\,\mathrm{d}s \quad \text{with} \quad \underline{\underline{\mathrm{T}}} = \frac{1}{\mu_0}\left(\underline{\mathrm{b}}\,\underline{\mathrm{b}} - \frac{\mathrm{b}^2}{2}\underline{\underline{1}}\right), \tag{5.3 a,b}$$

where l_z is the axial length of the device, δ the local thickness of the FE air layer and $\hat{n}$ is the outward unitary normal vector.

When the FE-BE interface Γ coincides with a strong material discontinuity (i.e. it is located between two materials with very different μ such as air and iron),

unacceptable numerical oscillations may occur. The air layer required for the force calculation by (5.3 a) also allows to avoid the oscillation problem [Henrotte, 2000; Geuzaine *et al.*, 2001].

5.3.3 Description of the problem

We study an actuator developed by the firm E.I.B. (Électricité industrielle de Belgique). As shown in Figure 5.9, the actuator comprises a yoke, two permanent magnets, two coils and a moving piece.

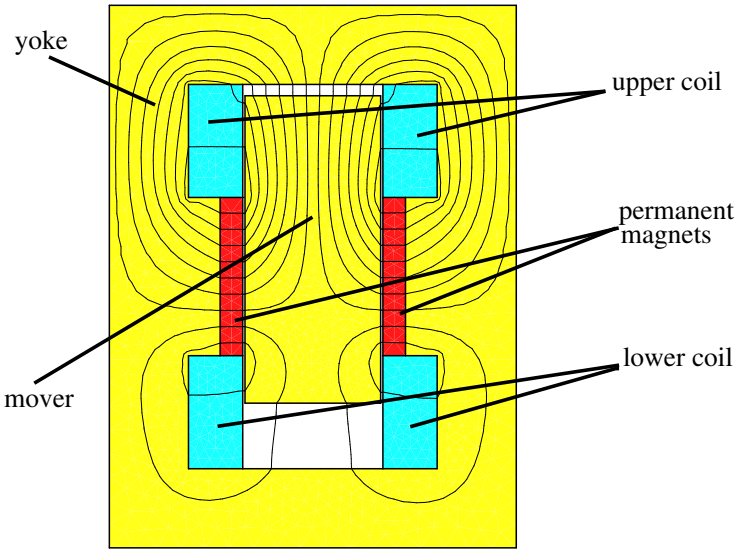

Figure 5.9: 2D model of a linear actuator, flux lines due to the permanent magnets

The airgaps above and below vary, depending on the position of the mover, between 0.3 mm and 15.7 mm. The two lateral gaps equal 0.5 mm. The permanent magnets have a constant horizontal remanent induction of $b_r = 0.8\,\mathrm{T}$ and a relative permeability of $\mu_r = 1.03$. The yoke and the mover are made of iron. Eddy currents in the magnets and in the laminated yoke and mover are neglected.

The permanent magnets constitute a magnetic lock that keeps the mover either in the upper or lower position tending to diminish the residual airgap. The mover is moved up or down by applying a voltage pulse to one of the coils. The commutation is facilitated by two springs. The vertical force they exert on the mover as well as the force due to the magnets are shown in Figure 5.10 as a function of position.

Both linear and nonlinear dynamic simulations are performed. For the linear analysis, the relative permeability of the iron is taken as $\mu_r = 1000$. For the nonlinear study, the nonlinear single-valued BH curve depicted in Figure 5.11 is adopted, and the iterative NR method is applied for every time step. The computational cost for both the nonaccelerated and the accelerated hybrid model will be discussed.

The FE domain Ω comprises the yoke, the mover, the permanent magnets and the coils. On its outer boundary, the Dirichlet condition $a = 0$ is imposed. In order

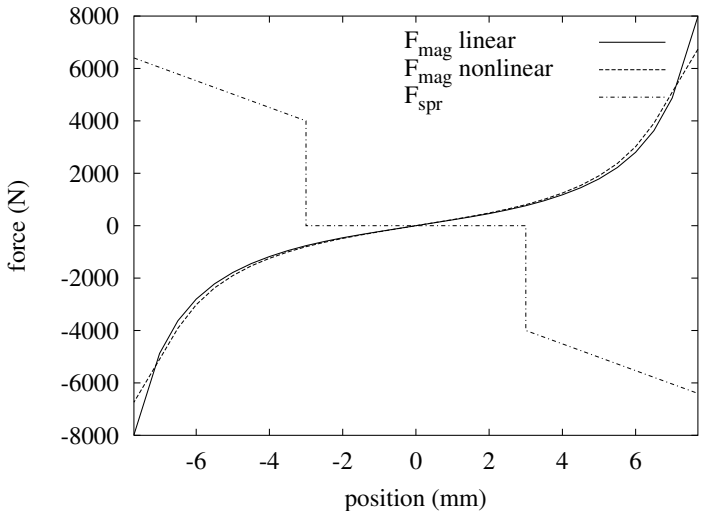

Figure 5.10: Magnetic force due to the permanent magnets and the spring force in function of the position of the mover. The mover is in the middle of the gap when $x = 0$

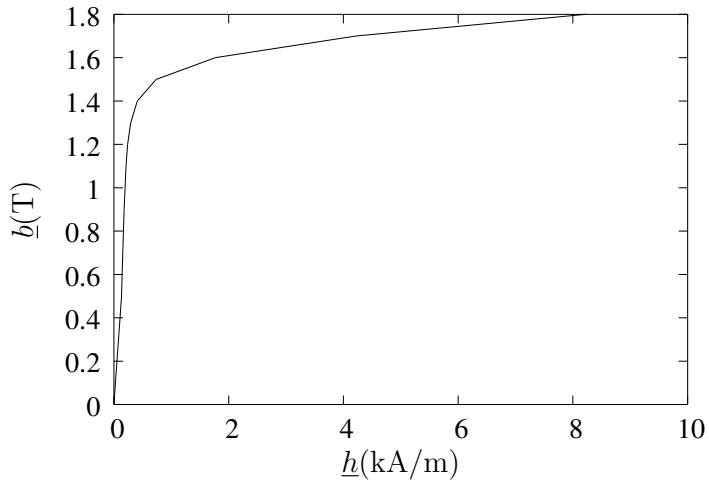

Figure 5.11: Nonlinear single-valued BH curve

to compute the magnetic force as mentioned in the previous section, an FE air layer of uniform thickness $\delta = 0.2$ mm is placed around the mover.

The BE domain is constituted by the outer contour of the air layer enclosing the moving piece, denoted Γ_1, and the outer boundary of the airgap, denoted Γ_2 (see Figure 5.12). The hybrid FE-BE discretisation, with 4083 triangular elements and 264 straight line segments, yields 2372 unknowns for the electromagnetic analysis (2108 for a and 264 for q). We adopt piecewise constant basis functions for q and evaluate the integrals (2.61) and (2.63) analytically.

When the single-level FMM is applied to speed up the BE part of the hybrid model, the contour Γ_1 (134 segments) and contour Γ_2 (130 segments) are split up in 26 and 21 groups respectively. This distribution was found to be optimal: using

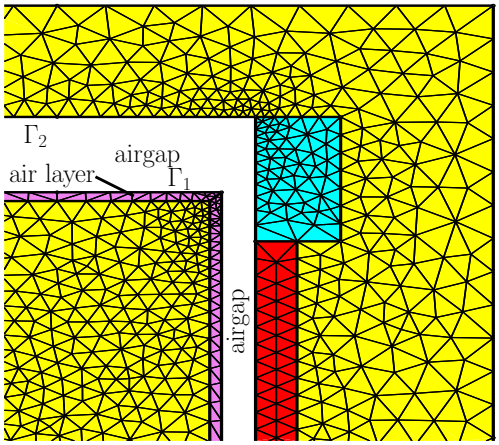

Figure 5.12: Detail of the discretisation of the FE air layer surrounding the moving piece. For the sake of visualisation, the airgap and the air layer have been scaled

more groups leads to a higher computation time for solving the system of equations while using less groups increases the assembly time. Two groups (on either Γ_1 or Γ_2) are considered to be far groups if there are at least two groups in between. This corresponds to $R_s/d \leq 1/6$ and $R_o/d \leq 1/6$, or, according to Figure 4.7, to a maximum truncation number $P_{max} = 8$ for $\varepsilon = 10^{-6}$. The classical law $P = \log_2(1/\varepsilon)$ leads to a truncation number of 20.

The voltage supply is included in the model by coupling a simple electrical circuit with the FE part of the hybrid model.

The rigid moving piece has a purely translational movement. Hence, the FMM disaggregation and aggregation integrals (4.12) are evaluated only once. As the BE domain comprises two contours Γ_1 and Γ_2 whose relative position varies, the FMM translation data (4.31) must be recalculated for every time step.

The system of algebraic and differential equations is time-stepped using the backward Euler scheme. A time interval of 50 ms (sufficiently long for achieving the commutation) has been studied with $\Delta t = 0.4\,\text{ms}$ (125 time steps). The mechanical equation and the electromagnetic system are solved alternatively obtaining the new position and the new magnetic force respectively. A magnetostatic calculation with only the permanent magnet excitation is carried out to supply the correct initial condition for the dynamic simulation.

5.3.4 Calculation results

At $t = 0$, the mover is in the upper position ($x = 7.7\,\text{mm}$) and a 15 V 10 ms voltage pulse is applied to the lower coil. The time evolution of the current in the lower coil for both the linear and nonlinear analysis is depicted in Figure 5.13. If the mover is maintained in the upper position, the coil behaves as an RL circuit and an exponential evolution of the current is expected and also observed. This case for both the linear and nonlinear analysis is also shown in Figure 5.13. The movement affects considerably the time variation of the current.

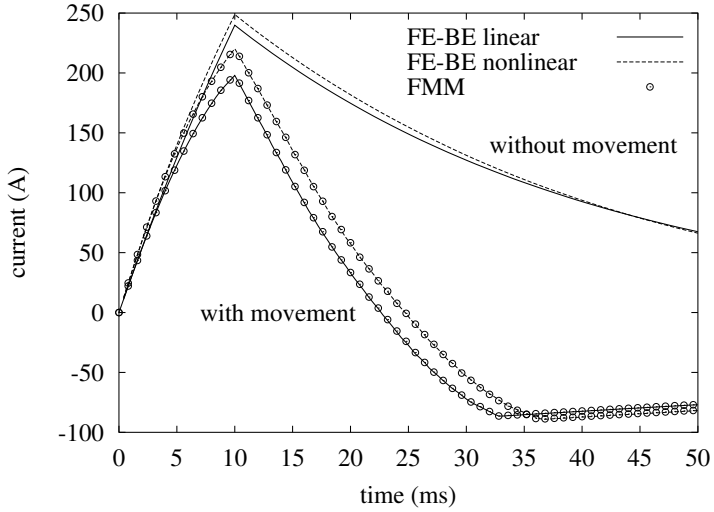

Figure 5.13: Evolution with time of the current in the lower coil when a 15 V 10 ms voltage pulse is applied (without and with movement)

Figures 5.14 and 5.15 show the position and speed of the mover in function of time. The mover reaches the lower position after 33 ms and 36 ms in the linear and nonlinear analysis respectively.

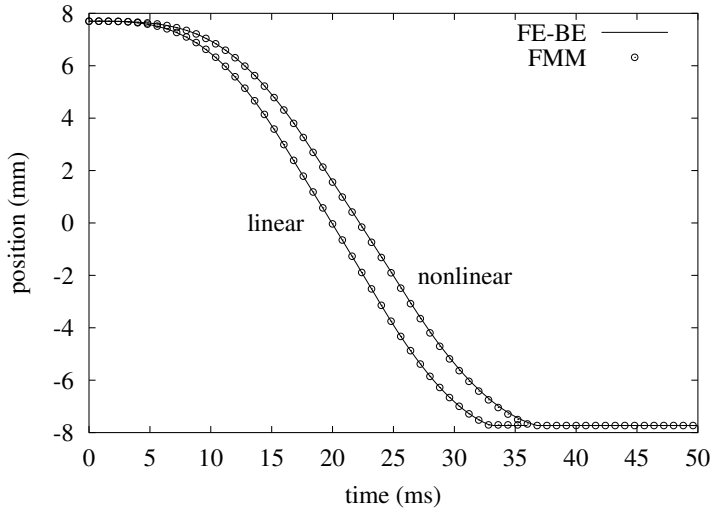

Figure 5.14: Position (mm) of the mover in function of time (ms) for the linear and nonlinear analysis with the FE-BE method (with or without FMM acceleration)

All results obtained with the accelerated FE-BE method present an excellent agreement with those of the nonaccelerated FE-BE.

5.3.5 Computational cost

All computations have been carried out on a 400 MHz MIPS R12000 Processor.

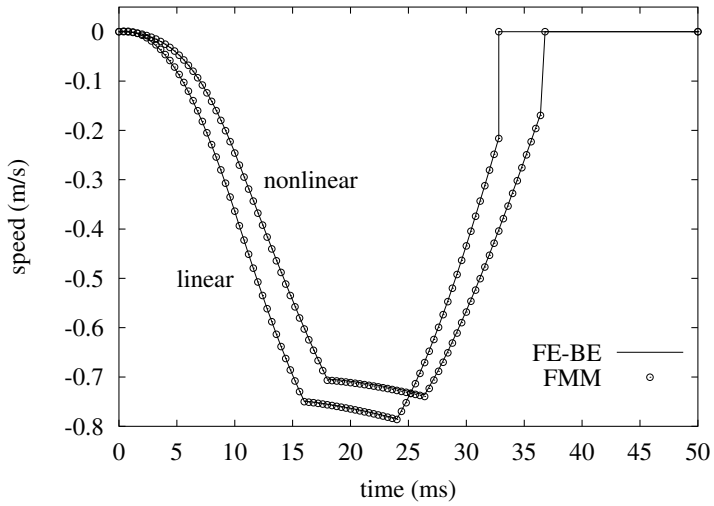

Figure 5.15: Speed (m/s) of the mover in function of time (ms) for the linear and nonlinear analysis with the FE-BE method accelerated or not by the FMM

The systems of algebraic equations are solved by means of the iterative solver GMRES [Saad & Schultz, 1986] with ILU-preconditioning. For the 2D problem at hand, when applying FMM acceleration, the preconditioning (based only on the sparse matrix comprising the FE contribution and the BE near field interactions) results in an increase of the number of GMRES iterations for solving the linear or linearised systems of equations, disadvantage which is largely outweighed by the fact that $\boldsymbol{M}^{far}$ and $\boldsymbol{C}^{far}$ are not evaluated explicitly.

Indeed, the linear calculation takes 1420 s without FMM and 470 s with FMM acceleration. For the nonlinear simulation, with 3 to 5 NR iterations per time step, the computation times are 2266 s without FMM acceleration and 990 s with the FMM acceleration. The reduction in computation time achieved by the FMM in the linear and nonlinear case is thus 70 % and 56 % respectively.

5.4 TEAM Workshop problem 28

We consider an eddy current problem in $\mathbb{R}^3$. The hybrid magnetodynamic $\underline{h}$–φ formulation described in Section 2.6.1 is used. The FE method is used in a domain Ω with boundary Γ while the BE method provides an exact treatment of the exterior space $\mathbb{R}^3\backslash\Omega$ and allows to consider movement without any tedious mesh manipulations (remeshing). The eddy current conducting part of Ω is denoted Ω_c and the nonconducting one Ω_c^C.

The transient behaviour is modelled taking into account the eddy currents and the mechanical equation.

5.4.1 Description of the problem

The electrodynamic levitation device of TEAM workshop problem 28 [Karl *et al.*, 1999] concerns a cylindrical aluminium plate ($\sigma = 3.40\ 10^7\,\mathrm{S/m}$, radius = 65 mm, thickness = 3 mm, mass = 0.107 kg) located above two coaxial coils carrying imposed sinusoidal currents of amplitude 20 A and frequency 50 Hz (see Figure 5.16). The inner and outer coils have $w_1 = 960$ and $w_2 = 576$ turns, respectively. The dimensions of the device are shown in Figure 5.17. The levitation height z refers to the distance between the lower circular end of the cylindrical plate and the upper sides of the coils ($z = 0$).

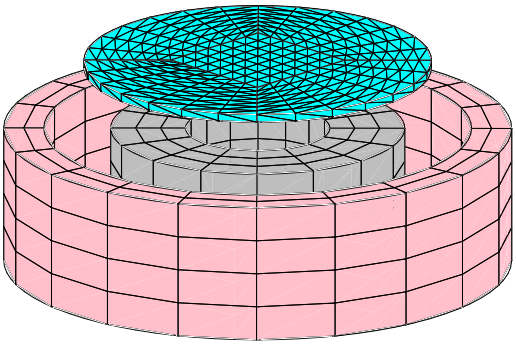

Figure 5.16: Levitation device model: cylindrical plate above two coaxial coils

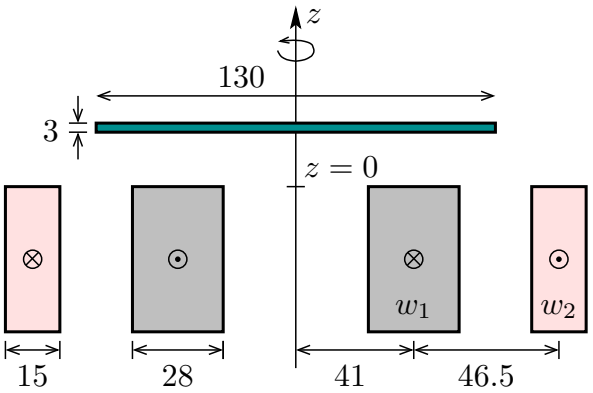

Figure 5.17: Dimensions in mm of the electrodynamic levitation device

At $t = 0$ the plate rests above the coils at a distance of $z = 3.8$ mm. For $t \geq 0$, sinusoidal currents flow in the coils in opposite directions.

The coils generate a time-varying magnetic field that induces eddy currents in the conducting plate Ω_c, which results in a vertical impulsive force $\underline{F}_{mag}$ on it. After some damped oscillations the plate reaches a stationary levitation height of $z = 11.3$ mm (measured). Due to the symmetry of the problem, we assume that the movement is purely translational.

The source magnetic field $\underline{h}_s$ is calculated by means of the Biot-Savart law (1.53). To this end, the inner and outer coils are discretised in 192 and 160 hexahedra

respectively (see Figure 5.16). The FE domain Ω can be thus restricted to the conducting plate Ω_c. We adopt edge basis functions for $\underline{h}$ and piecewise linear basis functions for q.

Different levels of mesh refinement are considered. When the FMM is applied, the surface Γ is split up into 36, 45, 60 or 77 groups depending on the discretisation (see Figure 5.18). Note that each group comprises elements on both sides of the plate.

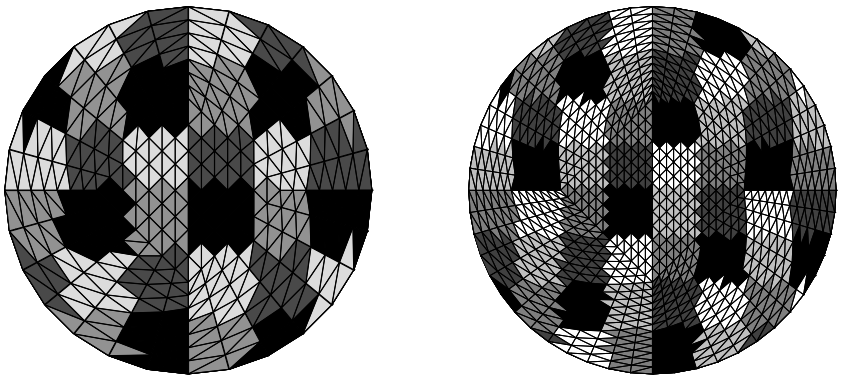

Figure 5.18: Distribution in 36 (right) and 60 (left) groups of the plate

The problem at hand deals with a purely translational movement of only one BE surface Γ. Hence, the FMM integrals (4.30) and (4.31) are independent of the position of the plate and are evaluated only once.

The system of algebraic and differential equations (2.39) and (2.40) is time-stepped along with the mechanical equation (5.2) using the backward Euler scheme. A time interval of $[0, 600\,\mathrm{ms}]$ is studied with either $\Delta t = 0.2\,\mathrm{ms}$ (3000 time steps) and $\Delta t = 0.4\,\mathrm{ms}$ (1500 time steps). We adopt the so-called weak electromechanical coupling (see Section 5.3.2.1).

The magnetic force $\underline{F}_{mag}$ exerted on conductors Ω_c can be calculated by means of Lorentz law:

$$\underline{F}_{mag} = \int_{\Omega_c} \underline{j} \times \underline{b} \; \mathrm{d}\Omega_c \,. \tag{5.4}$$

5.4.2 Calculation results

The transient behaviour of the levitation device is simulated using a hybrid FE-BE discretisation consisting of 1280 tetrahedra and 1344 triangles, which yields 1993 unknowns: 1473 for $\underline{h}$ and 520 for q. This is the coarsest mesh in Table 5.1. The optimal group distribution (for this particular mesh) is found to be 36 groups: employing more groups yields a higher computation time for solving the system of equations and more storage costs for the FMM data structures, while using less groups increases the assembly time and the memory requirements for the near BE part. The optimal number of FMM groups increases with the number of unknowns. The maximum and average truncation number are $P_{max} = 9$ and $P_{av} = 3$ for $R_{far} = 0.04$ and $\epsilon = 10^{-6}$.

Figure 5.19 presents a comparison between the measured levitation height vs time according to [Karl *et al.*, 1999] and computed results for $\Delta t = 0.2\,\text{ms}$ and $\Delta t = 0.4\,\text{ms}$ obtained by means of the FMM accelerated hybrid FE-BE technique . A better agreement is observed as the time step diminishes. For a given time step,

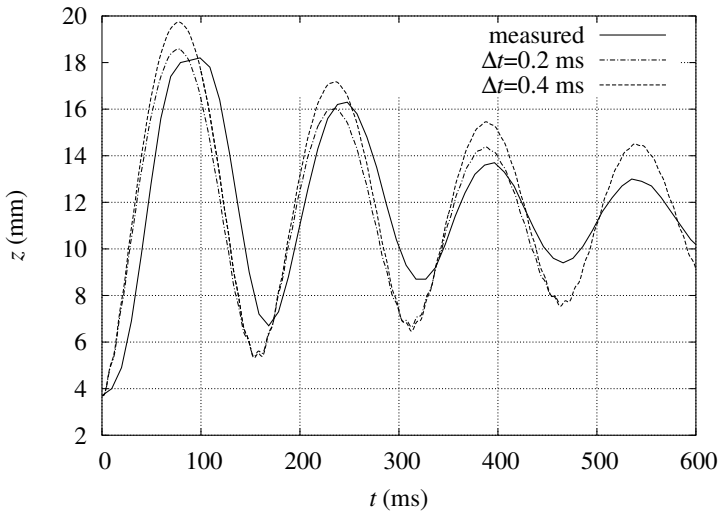

Figure 5.19: Measured and calculated levitation height vs time

a finer mesh is not observed to significantly improve the accuracy.

5.4.3 Computational cost

The system of algebraic equations is solved by means of the iterative solver GMRES [Saad & Schultz, 1986] with ILU-preconditioning on a 400 MHz MIPS R12000 Processor.

The CPU time per time step and the memory requirements for the different discretisations (with Γ split up into 36, 45, 60, 60, 60, 77 and 77 groups, respectively) are shown in Table 5.1. It illustrates the efficiency of the FMM as the number of BE unknowns increases. With the fourth mesh, e.g., the accelerated FE-BE analysis is roughly 16 times faster than the nonaccelerated one and the savings in memory approach 67 %. Furthermore, the use of the adaptive truncation scheme instead of a fixed truncation number ($P = 20$ for $\epsilon = 10^{-6}$) speeds up the solution of the electromagnetic system with roughly a factor two.

The grouping of the elements and the computation of the FMM data structures is done in a preprocessing that takes a few seconds, which is negligible in comparison to the total computational cost.

5.5 A shunt capacitive MEM switch

The present test case has been considered in the frame of a collaboration with the Katholieke Universiteit Leuven (KUL). The specifications of the MEM switch

Table 5.1: CPU time and memory requirements for different meshes

Unknowns		FE-BE		FE-BE + FMM	
FE	BE	CPU (hours)	mem (Mb)	CPU (hours)	mem (Mb)
1473	520	0.41	21	0.15	18
2433	848	1.49	42	0.30	24
3633	1256	4.97	71	0.52	35
5073	1744	16.03	150	0.98	51
6753	2314	45.24	326	1.84	70
8673	2960	117.41	514	2.65	94
10833	3688	-	-	4.53	158

together with some results obtained by means of different commercial software packages have been furnished by the departments ESAT-MICAS and ESAT-ELECTA.

Electrostatic parallel-plate actuators are widely used in many types of microelectromechanical systems (MEMS). MEM switches can be used in series or shunt mode and their contacts can be resistive or capacitive [Brown, 1998; Tilmans, 2002]. A shunt capacitive MEM switch consists of a metal armature (bridge) suspended over a bottom conductor, e.g. the centre conductor of a coplanar waveguide, mechanically anchored and electrically connected to the ground. A thin dielectric film is deposited on the bottom conductor (see Figure 5.20). When the bridge is up, the capacitance of the switch is very small and the RF signal freely passes through (the RF switch is on). By applying a bias voltage the switch is actuated: an electrostatic force occurs between the top and bottom electrodes and the bridge is pulled down, the capacitance increases and causes an RF short to ground (the RF switch is off) [Brown, 1998; Tilmans, 2002]. These actuators can be treated, in first approximation, as

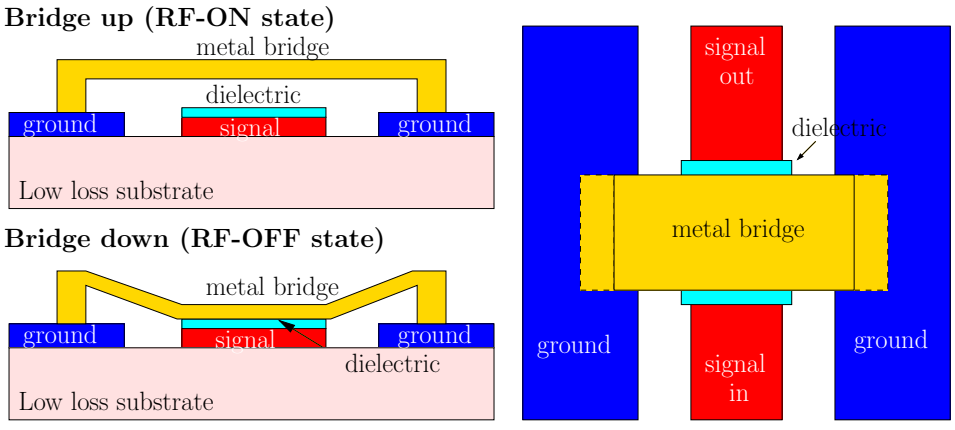

Figure 5.20: Electrostatically actuated capacitive shunt switch implemented on a CPW transmission line (side and top views)

lumped spring-mass systems with a single mechanical degree of freedom [Tilmans,

2002]. This analysis is helpful for physical insight, but disregards important effects such as the bending of the top plate and the stiction[1] between the bridge and the bottom contact [Brown, 1998]. The performance of RF MEM switches strongly depends on the deformation of the top electrode. A detailed knowledge of the exact deformation for an accurate estimate of the capacitance is thus crucial.

A BE approach is particularly suited for the analysis of the real electrostatic problem [Farina & Rozzi, 2001]. Indeed, the BE method provides a rigorous treatment for open problems and allows to consider the deformation without any remeshing. The elastic deformation of the top electrode (and the suspension beams) can be handled by means of a FE model. It depends directly on the electrostatic force exerted on the bridge and the material properties. The electrostatic field induces a force distribution, the value of which increases when the distance between the top and bottom plate diminishes. This interaction between the electrostatic and mechanical systems can be considered iteratively.

In this Section, we discuss the coupled mechanical-electrostatic analysis of a capacitive MEM shunt switch. Simulated results obtained by means of different software packages are briefly compared.

5.5.1 Description of the problem

The shunt capacitive MEM switch represented in Figure 5.21 is studied.

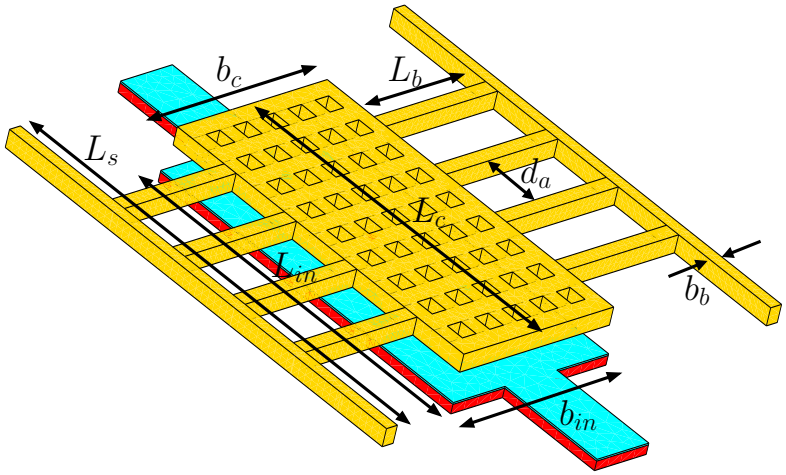

Figure 5.21: Geometry of the shunt capacitive MEM switch: $L_c = 475\,\mu$m, $b_c = 275\,\mu$m, $L_{in} = 485\,\mu$m, $b_{in} = 285\,\mu$m, $L_s = 625\,\mu$m, $L_b = 205\,\mu$m, $b_b = 20\,\mu$m and $d_a = 80\,\mu$m

It concerns a perforated top electrode (thickness = 4μ m) suspended by a set of

[1] Stiction is the force required to cause a body in contact with another to begin to move.

beams, and a bottom electrode (thickness = 0.5μ m) coated with a thin dielectric layer (thickness = 0.2μ m, $\varepsilon_r = 7$). The beam suspension allows a vertical movement with respect to the fixed bottom plate. The top plate is perforated to facilitate the under-etching of the structure. The dimension of the holes is $25\,\mu\text{m} \times 25\,\mu\text{m}$, with a pitch of $50\,\mu$m. The mechanical material constants of the top plate are $E = 70$ GPa and $\nu = 0.3$.

The BE method described in Section 3.4.4 with FMM acceleration is applied for solving the electrostatic problem while the mechanical problem is handled by a FE model. The behaviour of the switch is simulated using a discretisation consisting of 6544 triangles and 11151 tetrahedra, which yields 6544 degrees of freedom for the piecewise element constant charge q and 56331 degrees of freedom for the second order interpolation of the displacement u.

The optimal number of FMM groups (for this particular mesh) is found to be 35. The maximum and average truncation number are $P_{max} = 6$ and $P_{av} = 4$ for $R_{far} = 135\,\mu$m and $\epsilon = 10^{-6}$.

The electrostatic force $\underline{F}_e$ distribution on the surface of the electrode can be calculated as

$$\underline{F}_e(\underline{r}) = \frac{1}{2}\, q(\underline{r})\, \underline{e}(\underline{r})\,. \tag{5.5}$$

Introducing the electric field $\underline{e}$ on the surface of a conductor (3.70) in (5.5), the expression of $\underline{F}_e$ as a function of the charge distribution q is given by

$$\underline{F}_e(\underline{r}) = \frac{1}{2\,\varepsilon_0}\, q^2(\underline{r})\, \hat{n}\,. \tag{5.6}$$

The upper electrode is deformed by the electrostatic force exerted on it. The elastic equation has to be considered alongside the electrostatic equations. For linear elastic isotropic materials, it reads:

$$\boldsymbol{D}^T \underline{\underline{E}}\, \boldsymbol{D}\, \underline{u} + \underline{F} = 0\,, \tag{5.7}$$

where $\boldsymbol{D}$ is the differential operator matrix

$$\boldsymbol{D} = \begin{bmatrix} \partial_x & 0 & 0 \\ 0 & \partial_y & 0 \\ 0 & 0 & \partial_z \\ \partial_y & \partial_x & 0 \\ \partial_z & 0 & \partial_x \\ 0 & \partial_z & \partial_y \end{bmatrix} \tag{5.8}$$

with transpose $\boldsymbol{D}^T$, $\underline{\underline{E}}$ is the elasticity tensor, $\underline{u}$ is the displacement vector and $\underline{F}$ is the total force exerted. The elasticity tensor $\underline{\underline{E}}$ relates the stress tensor with the strain tensor. It depends on the Young modulus E and the Poisson ratio ν [Pilkey,

2002] and it reads

$$\underline{\underline{E}} = \frac{E}{(1+\nu)(1-2\nu)} \begin{bmatrix} 1-\nu & \nu & \nu & & & \\ \nu & 1-\nu & \nu & & \mathbf{0} & \\ \nu & \nu & 1-\nu & & & \\ & & & \frac{1-2\nu}{2} & 0 & 0 \\ & \mathbf{0} & & 0 & \frac{1-2\nu}{2} & 0 \\ & & & 0 & 0 & \frac{1-2\nu}{2} \end{bmatrix} . \tag{5.9}$$

The electrostatic and mechanical systems, (3.72) and (5.7), are solved iteratively obtaining the new electrostatic force distribution and the new displacement. The number of iterations required for sufficient convergence of the results (e.g. the capacitance) increases as the applied bias voltage approaches the pull-in voltage and the deformation of the top plate becomes greater.

5.5.2 Calculation results

The results obtained with GetDP [GetDP, 1997–2004] are compared with those given by the commercial software packages Coventor [Coventor, Inc., 2003] and FemLab [Femlab, 2003].

The zero-voltage capacitance $C_{V=0}$ and pull-in voltage V_{IN} calculated by GetDP are 0.36 pF and 14.2 V, respectively.

The deformation of the top electrode with a bias voltage of 11 V for the successive iterations is shown in Figure 5.22. Convergence is achieved after 9 iterations.

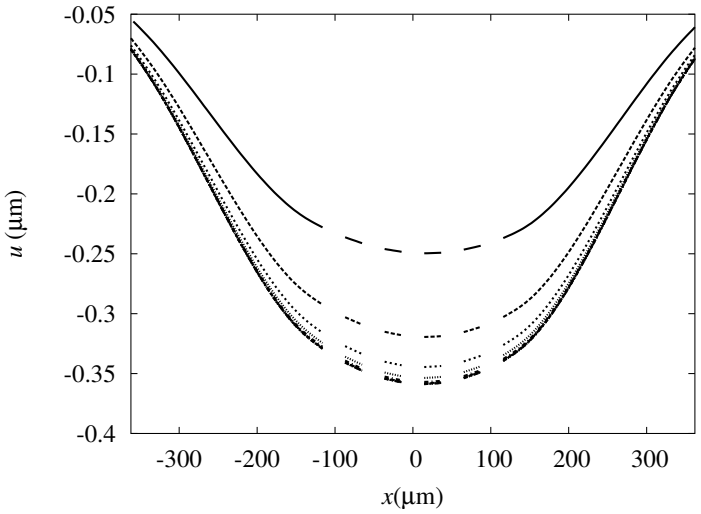

Figure 5.22: Convergence of the vertical displacement along a line through two short suspension beams and the perforated plate for an applied bias voltage of 11 V

In the simulations performed with the commercial programs, only a quarter of the geometry is considered. In the Coventor simulation, the electrostatic part is modelled by means of the BE method while the mechanical part is dealt with using

the FE method and second order elements. Symmetry boundary conditions are only taken into account for the mechanical problem.

In the FemLab computation, the whole electromechanical problem is solved by means of the FE method. Symmetry conditions are imposed for the electrostatic problem. With regard to the mechanical part, the elastic behaviour of the suspension (beams) is approximated by a stiffness constant [Brown, 1998; Tilmans, 2002]. For the face of the top electrode that is coupled with the suspension, the displacement is obtained by dividing the total electrostatic force by the stiffness constant.

The nominal capacitance $C_{V=0}$ obtained by Coventor and Femlab is 0.4 pF and 0.37 pF, respectively. The pull-in calculated voltage is 14.24 V for Coventor and 17.25 V.

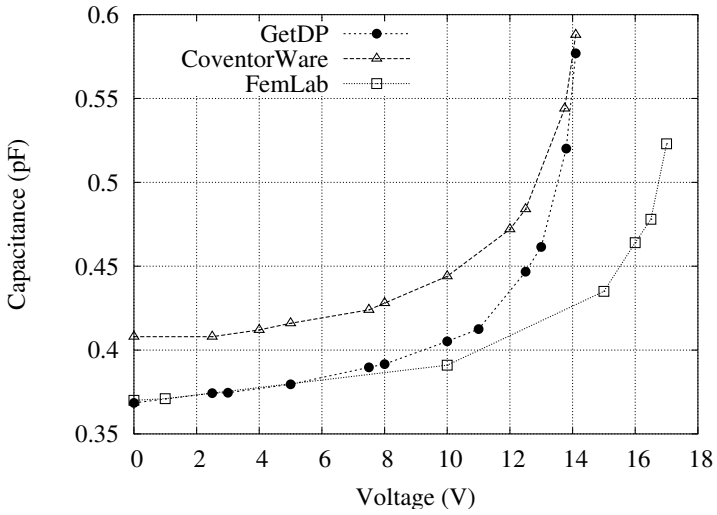

Figure 5.23: Calculated capacitance vs the applied bias voltage

The computed value of the capacitance as a function of the applied voltage is represented in Figure 5.23 for the three different solvers. The curves $C-V$ obtained with GetDP and FemLab agree well for low applied voltage, when the deformation is small. As the applied voltage increases, an accurate estimate of the displacement becomes critical, the approximation used in FemLab for the suspension does not suffice. On the contrary, the agreement between the curves obtained with GetDP and Coventor is better as the voltage increases. The influence of three quarters of the device, disregarded for the electrostatic computation in Coventor, seems to be more important for low applied voltages. However, the mechanical part is solved accurately in this case and contributes to enhance the results as the applied voltage increases.

Figure 5.24 shows the maximum vertical displacement of the top electrode as a function of the applied bias voltage. A good agreement between the values obtained by means of GetDP and Coventor is observed. The use of the approximation for the mechanical problem with a stiffness constant for modelling the suspension in the FemLab simulation explains again the divergence of the curves as the applied voltage augments.

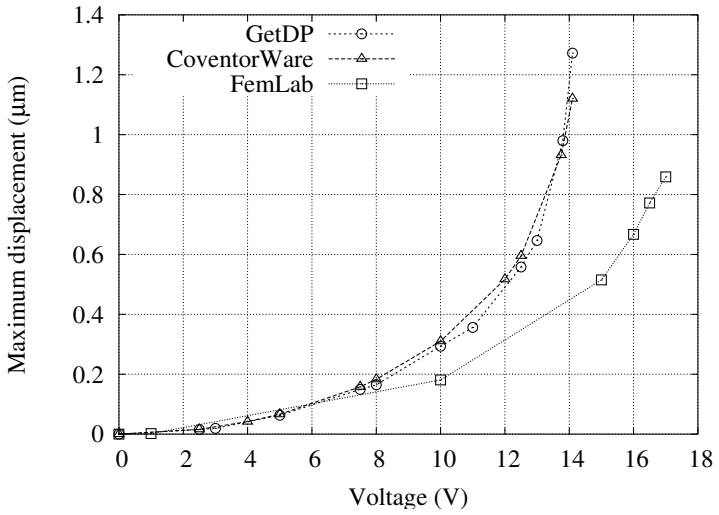

Figure 5.24: Maximum vertical displacement of the top electrode vs the applied bias voltage

Chapter 6

High frequency numerical tests

Contents

6.1 Introduction

In order to validate and evaluate the theoretical developments presented in Section 4.4 of Chapter 4, a series of two-dimensional and three-dimensional high frequency numerical tests are performed.

Sections 6.2 to 6.5 involve 2D and 3D scattering benchmark problems modelled by field integral equations (EFIE, MFIE and CFIE, see Section 3). A harmonic-time dependency is assumed and suppressed throughout. The complex formalism described in Section 1.3.1 is adopted.

The FMM is in all test cases applied to the expansion of either the 2D or 3D Helmholtz equation in order to accelerate the solution of a pure boundary element method. The grouping of the elements and the computation of the FMM data structures is done in a preprocessing step, the CPU time of which is negligible in comparison with the total computational cost.

In case of FMM, the preconditioning is based on the sparse matrix comprising the near-field interactions.

The approximate calculation times give an indication of the computational efficiency of the FMM accelerated BE method compared to the nonaccelerated BE method. Significant savings in storage requirements are also achieved.

In Sections 6.2 and 6.3, we consider a PEC cylinder and a PEC sphere illuminated by an incident plane wave, respectively. Results are compared to the analytical solution.

A thin wire placed in the vicinity of a perfectly electric conducting (PEC) square plate and illuminated by a plane wave is treated in Section 6.4. The input impedance of a dipole antenna located in front of a PEC sphere is calculated in Section 6.5. The solutions presented in the two latter sections are compared with those found in the literature.

6.2 Perfectly electric conducting cylinder

6.2.1 Description of the problem

A current source radiating in the presence of a PEC cylinder is one of the simplest 2D scattering problems for which an analytical solution can be obtained. We consider the scattering of a PEC cylinder of radius a illuminated by an incident plane wave polarised transversely to z. The incident plane wave can be expressed as

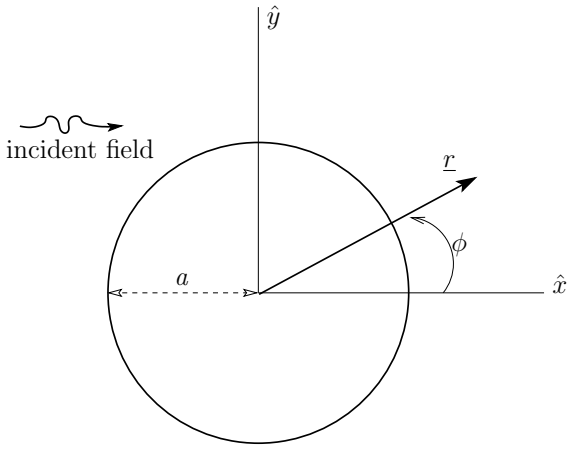

Figure 6.1: Plane wave incident on a perfectly electric conducting cylinder

$$\underline{h}_z^i = h_0 e^{-\imath kx} = h_0 \sum_{n=-\infty}^{\infty} \imath^{-n} J_n(kr)\, e^{\imath n\phi}\,, \quad \underline{e}_y^i = e_0 e^{-\imath kx} \tag{6.1}$$

with $h_0 = 1\,\mathrm{A/m}$, $e_0 = \eta_0 h_0\,\mathrm{V/m}$, k the wavenumber, $r = |\underline{r}|$, $\phi = \arg \underline{r} \in [0, 2\pi]$ as depicted in Figure 6.1, and $\eta_0 = 120\pi\,\Omega$ being the intrinsic impedance of free space. The total field is given by the sum of the incident and scattered fields, i.e.

$$\underline{h}_z = \underline{h}_z^i + \underline{h}_z^s = h_0 \sum_{n=-\infty}^{\infty} \imath^{-n} \left[J_n(kr) + b_n H_n^{(2)}(kr) \right] e^{\imath n\phi}\,, \tag{6.2}$$

with the coefficient $b_n = \dfrac{-J_n'(ka)}{H_n^{(2)'}(ka)}$.

Hereafter we replicate some analytical results [Harrington, 1961, Chapter 5]. When the incident plane wave is polarised transversely to z, the surface current on a PEC cylinder can be calculated analytically as

$$j_\phi = \frac{\imath 2 h_0}{\pi k a} \sum_{-\infty}^{\infty} \frac{\imath^{-n}\, e^{\imath n\phi}}{H_n^{(2)'}(ka)}\,, \tag{6.3}$$

where $H_n^{(2)'}$ is the derivative of $H_n^{(2)}$ (see (B.1) in Appendix B). The radar cross section (RCS) takes the form

$$\mathrm{RCS(dB)} = 10 \log \frac{4\pi}{\lambda^2} \lim_{r\to\infty} \left(r^2 \frac{|\underline{h}^s|^2}{|\underline{h}^i|^2} \right)\,, \tag{6.4}$$

where the ratio of the scattered to incident field

$$\frac{|\underline{h}^s|}{|\underline{h}^i|} = \sqrt{\frac{2}{\pi k a}} \left| \sum_{n=-\infty}^{\infty} \frac{J_n'(ka)}{H_n^{(2)'(ka)}\, e^{jn\phi}} \right|\,. \tag{6.5}$$

The problem is modelled by means of three different integral formulations (see Sections 3.4.1, 3.4.2 and 3.4.3). In any case, the current j is expanded in terms of the thin wire basis functions (3.44).

6.2.2 Calculation results

The scattering of a PEC cylinder of radius $a = 0.5\lambda$ illuminated by a plane wave is simulated using a BE discretisation consisting of 60 segments, which yields 120 real unknowns for j [1]. This is the coarsest mesh in Tables 6.1, 6.2 and 6.3. The surface current density on the PEC cylinder (real and imaginary part), calculated analytically and by means of the three integral equations (EFIE, MFIE and CFIE), is depicted in Figure 6.2. The agreement between the analytical solution and the numerical results is excellent.

The RCS of a PEC cylinder of radius $a = 0.5\lambda$ is also calculated analytically and using the three formulations mentioned above. A comparison of the results is shown in Figure 6.3. Again, the exact solution and the numerical solutions agree very well.

[1] As a rule of thumb, in high frequency problems, a suitable level of discretisation corresponds to a mesh with elements of dimension $\lambda/10$. In this chapter, we consider finer meshes for validating the efficiency of the FMM

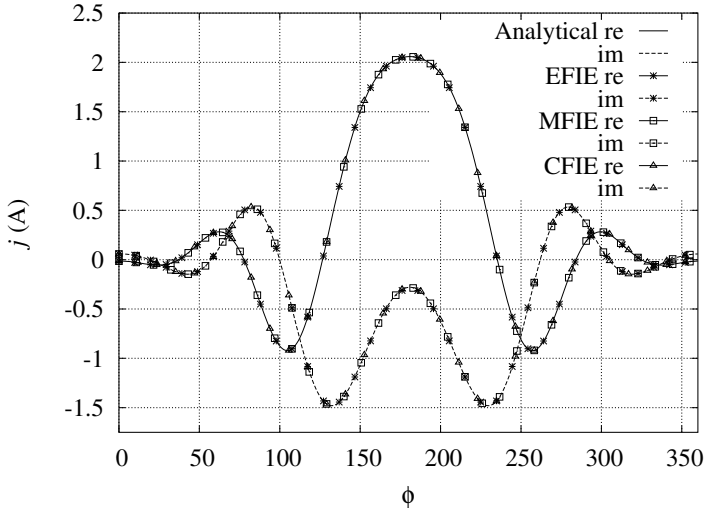

Figure 6.2: Real and imaginary part of the surface current on a perfectly electric conducting cylinder of radius $a = 0.5\lambda$

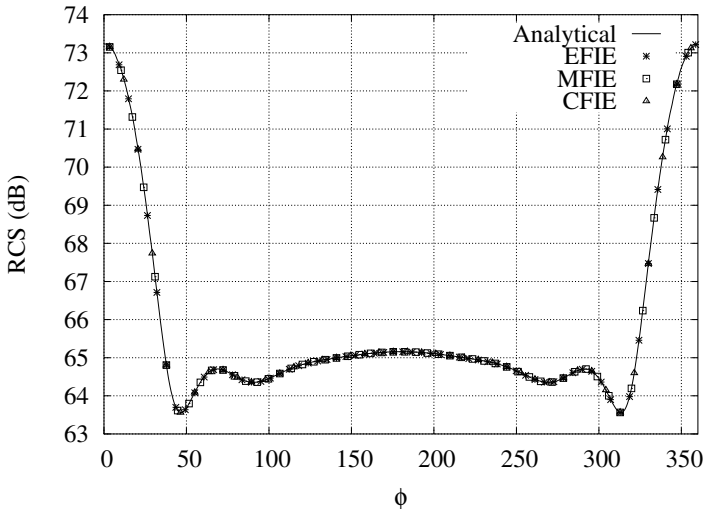

Figure 6.3: RCS a perfectly electric conducting cylinder of radius $a = 0.5\lambda$

6.2.3 Computational cost

All computations have been carried out on a 400 MHz MIPS R12000 Processor. The system of algebraic equations is solved by means of the iterative solver GMRES [Saad & Schultz, 1986] with ILU-preconditioning.

Several levels of mesh refinement have been considered. The CPU time and memory requirements for different discretisations and the EFIE, MFIE and CFIE formulations with and without FMM are shown in Tables 6.1, 6.2 and 6.3, respectively. The factor of reduction (in time and memory) attained with the FMM is shown as well.

Particular attention is paid to the data corresponding to the coarsest and finest

mesh, i.e. those arising the minimum and maximum number of unknowns, for every integral formulation.

For $N = 120$, when applying FMM the CPU time gets reduced by a factor of 2.8, 2.2 and 2.6, respectively, with the EFIE, MFIE and CFIE formulations. With respect to the memory requirements, they diminish in approximately 2 % for the EFIE and MFIE cases. The CFIE requires more memory since (3.66) implies more terms related to the Helmholtz equation and therefore more associated FMM data. However, the FMM achieves a better performance also with the CFIE analysis when a slightly increase in the number of unknowns occurs.

For $N = 2512$, the solution when applying FMM is achieved 26, 35.6 and 33 times faster than with the classical EFIE, MFIE and CFIE respectively. Concerning the memory needs, we obtain a 72 % reduction for all cases. This clearly illustrates the efficiency of the FMM as the number of unknowns increases.

For the sake of a quick comparison, Figures 6.4 and 6.5 bring together all the data in Tables 6.1, 6.2 and 6.3.

Table 6.1: CPU time (s) and memory requirements (Mb) – PEC cylinder case modelled by the EFIE formulation

	MoM		MoM + FMM		Reduction factor	
Unknowns	CPU	mem	CPU	mem	CPU	mem
120	1.10	3.13	0.39	3.09	2.8	1
208	3.37	3.88	0.93	3.25	3.6	1.2
312	7.94	5.75	1.93	3.65	4.1	1.6
416	15.40	6.84	3.41	4.06	4.5	1.7
624	44.38	15.86	7.73	5.76	5.7	2.7
832	109.37	20.86	13.96	7.07	7.8	2.9
1256	430.31	38.06	35.79	11.53	12	3.3
1392	606.92	43.13	42.38	12.81	14.3	3.3
1568	917.39	76.13	55.62	23.17	16.5	3.3
1792	1478.14	89.34	75.58	26.53	19.5	3.4
2088	2516.94	108.11	112.51	31.33	22.3	3.5
2512	4943.74	137.20	189.79	38.70	26	3.6

6.3 Perfectly electric conducting sphere

6.3.1 Description of the problem

We consider a PEC sphere of radius a illuminated by an incident plane wave propagating in the z direction. This is one of the simplest 3D scattering problems for which an analytical solution can be obtained.

Table 6.2: CPU time (s) and memory requirements (Mb) – PEC cylinder case modelled by the MFIE formulation

	MoM		MoM + FMM		Reduction factor	
Unknowns	CPU	mem	CPU	mem	CPU	mem
120	0.60	3.11	0.27	3.07	2.2	1
208	1.90	3.83	0.57	3.20	3.3	1.2
312	4.53	5.73	1.12	3.67	4	1.6
416	9.44	7.01	1.95	3.98	4.8	1.7
624	31.97	13.84	4.39	5.78	7.3	2.4
832	85.68	20.87	7.88	7.06	10.8	3
1256	381.98	38.07	21.57	11.51	17.7	3.3
1392	539.70	43.14	25.71	12.79	21	3.4
1568	834.54	76.14	34.64	22.17	24	3.4
1792	1368.77	89.39	48.20	24.48	28.4	3.6
2088	2365.39	108.15	73.98	29.28	32	3.7
2512	4817.73	137.25	135.29	38.72	35.6	3.7

Table 6.3: CPU time (s) and memory requirements (Mb) – PEC cylinder case modelled by the CFIE formulation

	MoM		MoM + FMM		Reduction factor	
Unknowns	CPU	mem	CPU	mem	CPU	mem
120	1.32	3.03	0.50	3.09	2.6	0.9
208	4.14	3.94	1.17	3.28	3.5	1.2
312	10.11	5.67	2.38	3.59	4.2	1.6
416	20.46	6.78	4.12	3.90	5	1.7
624	64.84	13.81	9.60	5.75	6.7	2.4
832	177.38	20.87	17.30	7.06	10.2	3
1256	767.95	38.06	48.13	11.47	16	3.3
1392	1116.35	58.06	56.41	17.59	19.7	3.3
1568	1685.43	76.13	73.76	23.12	22.8	3.3
1792	2753.16	89.37	103.69	26.50	26.5	3.4
2088	4771.52	108.08	157.78	31.26	30.2	3.5
2512	9513.41	137.19	287.66	38.68	33	3.5

The incident plane wave propagating in the z direction can be written as follows

$$e_x^i = e_0 e^{-\imath k_0 z}, \quad h_y^i = \frac{e_0}{\eta_0} e^{-\imath k_0 z}, \tag{6.6}$$

with $e_0 = \eta_0\,\mathrm{V/m}$, η_0 is the intrinsic impedance of free space.

The analytical solution of this problem can be found in [Harrington, 1961, Chapter 6]. The formulae of the induced surface current and the scattered field

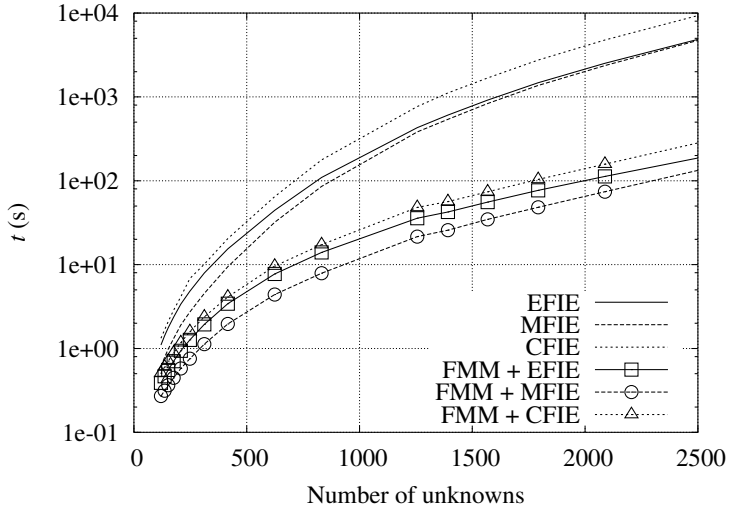

Figure 6.4: CPU time vs number of unknowns – PEC cylinder case

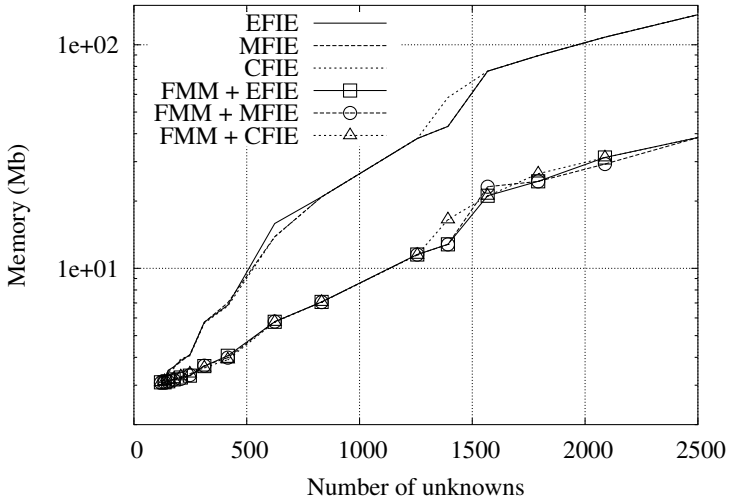

Figure 6.5: Memory requirements vs number of unknowns – PEC cylinder case

are reproduced hereafter. The surface current induced on the PEC sphere is given by

$$j_\theta = \frac{\imath}{\eta} e_0 \frac{\cos\phi}{ka} \sum_{n=1}^{\infty} a_n \left[\frac{\sin\theta P_n^{1'}(\cos\theta)}{\hat{H}_n^{(1)'}(ka)} + \frac{\imath P_n^1(\cos\theta)}{\sin\theta \hat{H}_n^{(1)}(ka)} \right], \tag{6.7}$$

$$j_\phi = \frac{\imath}{\eta} e_0 \frac{\sin\phi}{ka} \sum_{n=1}^{\infty} a_n \left[\frac{P_n^{1'}(\cos\theta)}{\sin\theta \hat{H}_n^{(1)'}(ka)} - \frac{\sin\theta P_n^{1'}(\cos\theta)}{\imath \hat{H}_n^{(1)}(ka)} \right], \tag{6.8}$$

with P_n^1 the Legendre function of the first kind degree n and order 1, $\hat{H}_n^{(1)}$ the alternative Hankel function of first kind and order n and the coefficient $a_n = \dfrac{\imath^{-n}(2n+1)}{n(n+1)}$. Note that the prime indicates the derivative of the corresponding Legendre and

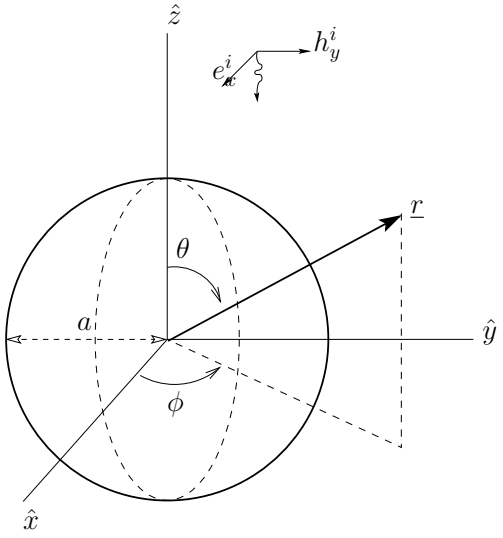

Figure 6.6: Plane wave incident on a perfectly electric conducting sphere

Hankel functions (see Appendix B). The scattered field reads

$$e_\theta^s = \frac{\imath e_0}{kr} e^{-\imath kr} \cos\phi \sum_{n=1}^{\infty} \imath^n \left[b_n \sin\theta P_n^{1'}(\cos\theta) - c_n \frac{P_n^1(\cos\theta)}{\sin\theta}) \right] , \tag{6.9}$$

$$e_\phi^s = \frac{\imath e_0}{kr} e^{-\imath kr} \sin\phi \sum_{n=1}^{\infty} \imath^n \left[b_n \frac{P_n^1(\cos\theta)}{\sin\theta} - c_n \sin\theta P_n^{1'}(\cos\theta) \right] , \tag{6.10}$$

where the coefficients b_n and c_n are given by

$$b_n = -a_n \frac{\hat{J}_n'(ka)}{\hat{H}_n^{(2)'}(ka)} \quad \text{and} \quad c_n = -a_n \frac{\hat{J}_n(ka)}{\hat{H}_n^{(2)}(ka)} . \tag{6.11}$$

Beware that the subscripts θ and ϕ refer to the corresponding spherical coordinates. The radar cross section (RCS) is calculated as follows

$$\mathrm{RCS(dB)} = 10 \log \frac{4\pi}{\lambda^2} \lim_{r\to\infty} \left(r^2 \frac{|\underline{e}^s|^2}{|\underline{e}^i|^2} \right) . \tag{6.12}$$

The 3D scattering problem has been modelled by three different integral equation formulations, the EFIE, MFIE and CFIE (Sections 3.4.1, 3.4.2 and 3.4.3). For all three formulations, the PEC sphere is discretised with plane triangles. We adopt RWG basis functions (3.40) for $\underline{j}$.

Different levels of mesh refinement are considered.

6.3.2 Calculation results

The scattering of a PEC sphere of radius $a = 0.2\lambda$ illuminated by a plane wave is simulated using a BE discretisation consisting of 1104 triangular elements which yields 2208 unknowns for $\underline{j}$.

Figure 6.7 represents a cut ($0 \leq \theta < 2\pi$, ϕ=0) of the surface current (real and imaginary part) induced by an incident plane wave on the PEC sphere. A very good agreement between the exact solution and the numerical results is observed.

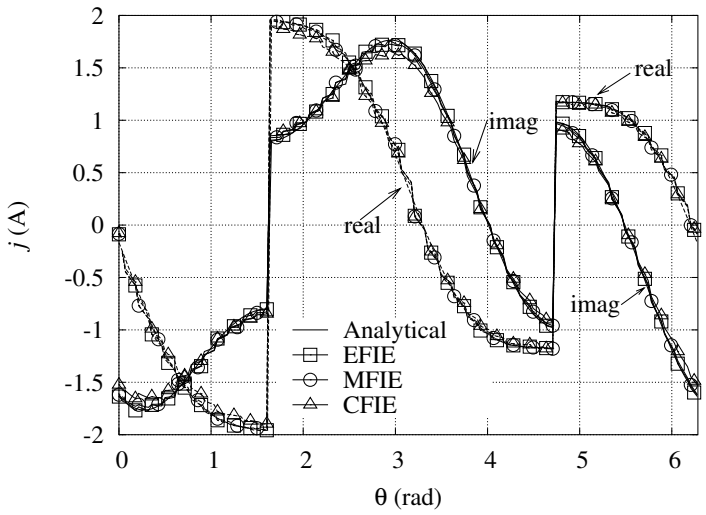

Figure 6.7: Real and imaginary part of the surface current (ϕ=0) on the perfectly electric conducting sphere with $a = 0.2\lambda$

The analytical RCS of the PEC sphere is compared with the calculated RCS using the EFIE, MFIE and CFIE formulations for $0 \leq \theta < \pi$ and $\phi = 0$ in Figure 6.8, and for $0 \leq \phi < \pi$ and $\theta = \pi/2$ in Figure 6.9. Again, the exact solution and the numerical solutions agree very well.

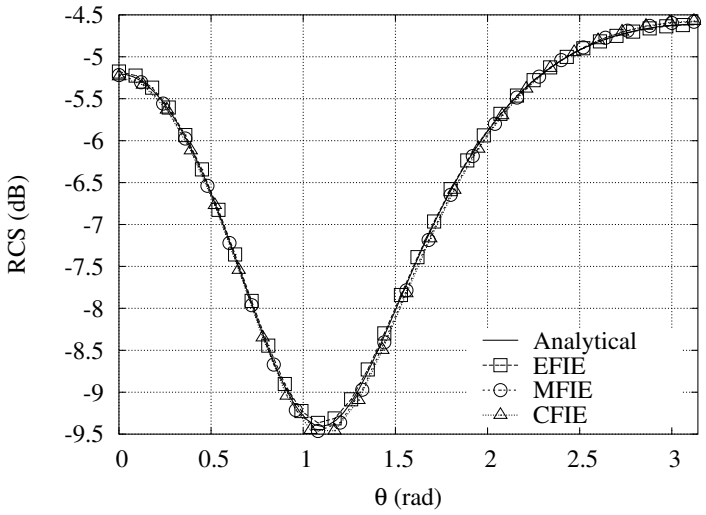

Figure 6.8: RCS ($\phi = 0$) of the perfectly electric conducting sphere with $a = 0.2\lambda$

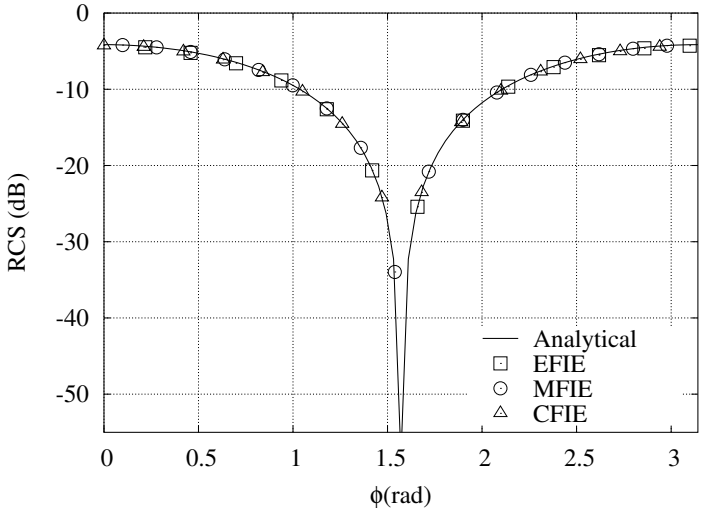

Figure 6.9: RCS ($\theta = \pi/2$) of the perfectly electric conducting sphere with $a = 0.2\lambda$

6.3.3 Computational cost

All computations have been carried out on a 400 MHz MIPS R12000 Processor. The system of algebraic equations is solved by means of the iterative solver GMRES [Saad & Schultz, 1986] with ILU-preconditioning.

Different discretisations have been considered. Tables 6.4, 6.5 and 6.6 gather all the data related to the CPU time and memory requirements for the different integral equations applied with and without FMM. The factor of reduction achieved with the FMM in both CPU time and memory is supplied as well.

We consider in particular the two extreme values of the number of unknowns for every integral formulation. For $N = 2208$, the solution when applying FMM is achieved 31, 26.3 and 38.6 times quicker than with the classical EFIE, MFIE and CFIE, respectively. With regard to the memory requirements, the FMM attains a reduction of 39 %, 43 % and 14 % for the EFIE, MFIE and CFIE cases respectively.

For $N = 6660$, the solution when applying FMM is achieved 42, 40.2 and 47.7 times quicker than with the classical EFIE, MFIE and CFIE respectively. Concerning the memory needs, the savings amount to 82 %, 85 % and 77 % with the EFIE, MFIE and CFIE cases respectively. This clearly indicates the efficiency of the FMM as the number of unknowns increases.

Figures 6.10 and 6.11 bring together all the data in Tables 6.4, 6.5 and 6.6. A comparison at a glance is then possible.

6.4 Wire scatterer in the vicinity of a square plate

6.4.1 Description of the problem

We consider a scattering problem in $\mathbb{R}^3$. It consists of a thin wire and a PEC square plate illuminated by a plane wave. The EFIE formulation described in Section 3.4.1

Table 6.4: CPU time (hours) and memory requirements (Mb) – PEC sphere case modelled by the EFIE formulation

	MoM		MoM + FMM		Reduction factor	
Unknowns	CPU	mem	CPU	mem	CPU	mem
2208	1.55	113.48	0.05	69.50	31	1.6
2880	3.69	164.81	0.11	84.87	34	2
4236	13.00	424.68	0.33	127.00	39	3.3
5076	22.71	540.45	0.57	156.34	40	3.4
6660	50.60	1230.48	1.22	220.09	42	5.6

Table 6.5: CPU time (hours) and memory requirements (Mb) – PEC sphere case modelled by the MFIE formulation

	MoM		MoM + FMM		Reduction factor	
Unknowns	CPU	mem	CPU	mem	CPU	mem
2208	0.79	116.19	0.03	50.50	26.3	2.3
2880	1.86	164.84	0.06	64.47	31	2.6
4236	6.34	424.69	0.18	103.32	35.3	4
5076	11.10	540.45	0.29	130.68	38.2	4.1
6660	25.32	1230.48	0.62	190.14	40.2	6.5

is chosen for modelling this problem.

Figure 6.12 shows the layout of the plate ($0.5\lambda \times 0.5\lambda$) and the wire (length = λ, thickness $a = 0.002\lambda$) together with the direction and polarisation of the plane wave. The wire is located perpendicular to and above the centre of one quadrant of the square plate. For the configuration and excitation considered, the field illuminating the wire is entirely due to scattering by the plate.

For simplicity, as the wire is sufficiently thin $a \ll \lambda$, we can adopt the thin wire approximation [Balanis, 1997, Chapter 7]. It consists in assuming that the electric field $\underline{e}$ produced on the surface of the wire by a surface current is the same as if the current were concentrated along a filament placed along the axis of the wire. Then the electric field on the surface of the wire would be obtained along a line parallel to the wire at a distance a from its axis.

6.4.2 Calculation results

The BE discretisation of the plate and the wire yields, with 392 triangles and 199 straight line segments, 1516 unknowns for $\underline{j}$. We adopt RWG basis functions (3.40) for the triangles and thin wire basis functions (3.44) for the segments. In order to apply the FMM, the plate is split in 49 groups and the wire in 7 groups. This group distribution was found to be optimal: using more groups leads to a higher computation time for solving the system of equations while using less groups increases the

Table 6.6: CPU time (hours) and memory requirements (Mb) – PEC sphere case modelled by the CFIE formulation

	MoM		MoM + FMM		Reduction factor	
Unknowns	CPU	mem	CPU	mem	CPU	mem
2208	2.32	116.14	0.06	100.20	38.6	1.2
2880	5.55	164.81	0.13	119.82	42.6	1.4
4236	19.05	424.67	0.42	171.70	45.3	2.5
5076	33.32	540.45	0.73	206.98	45.6	2.6
6660	77.88	1230.50	1.63	282.20	47.7	4.4

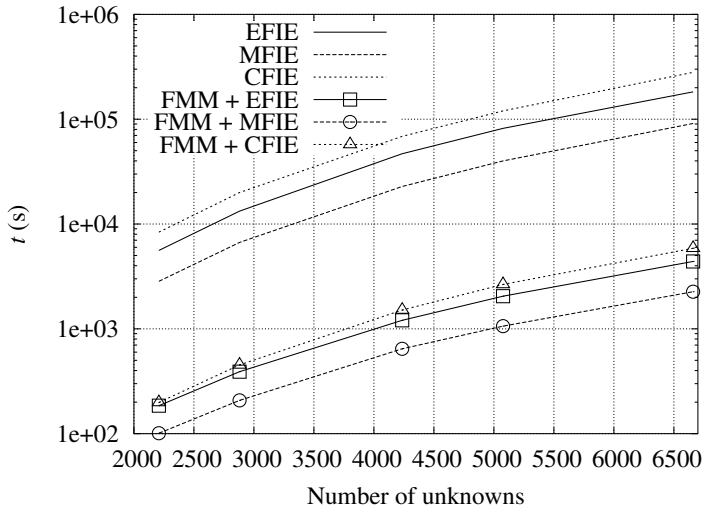

Figure 6.10: CPU time vs number of unknowns – PEC sphere case

assembly time. Two groups are considered to be far groups if there are at least two groups in between, which leads to $M = 7$ and $N_d = 98$ (see Section 4.4.2).

Figure 6.13 shows the real and imaginary part of the calculated current induced in the wire. For comparison and validation, the reference solution in [Rao, 1980, p. 125] is reproduced in Figure 6.14. Both results agree well.

The system of algebraic equations is solved by means of the iterative solver GMRES [Saad & Schultz, 1986] with ILU-preconditioning on a 2 GHz Intel Pentium 4 Processor.

The calculation takes 420 s without FMM and only 21 s with FMM, i.e. the FMM makes the resolution of the system 20 times faster. The efficiency of applying the FMM is also proved with respect to memory requirements: we need 38 Mb for the classical MoM calculation and 9 Mb for the FMM accelerated MoM calculation.

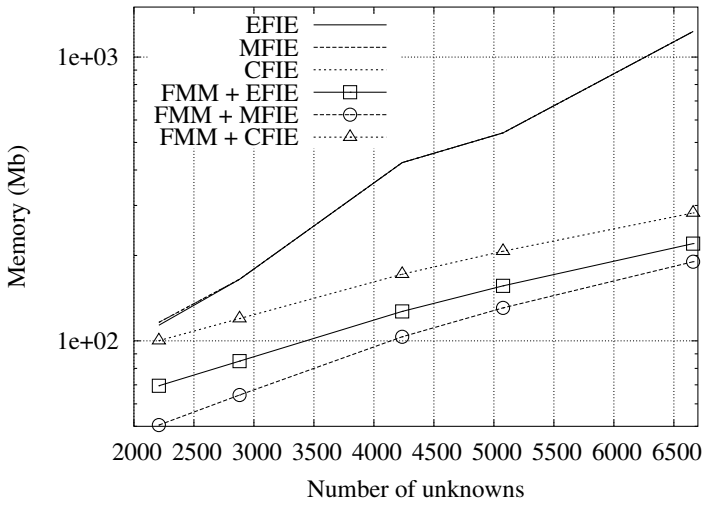

Figure 6.11: Memory requirements vs number of unknowns – PEC sphere case

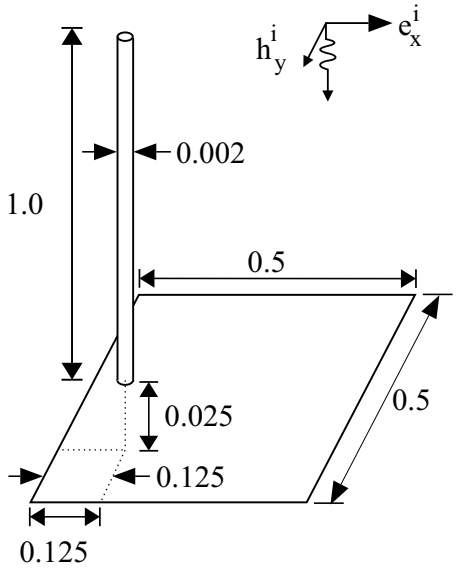

Figure 6.12: Wire/plate configuration and incident illumination

6.5 Dipole antenna near a conducting sphere

6.5.1 Description of the problem

We consider a scattering problem in $\mathbb{R}^3$. The problem under study, depicted in Figure 6.15, consists of a wire antenna (length $L = 12\,\text{cm}$, radius $a = 0.024765\,\text{cm}$) placed in the proximity of a PEC sphere (radius $r = 5.32\,\text{cm}$). The antenna is symmetrically located with respect to the equatorial plane of the sphere and driven by a voltage source at its centre, i.e. the antenna is a dipole. The distance from the centre of the sphere to the antenna is $d = 6.32\,\text{cm}$.

We model the problem by means of the EFIE formulation developed in Sec-

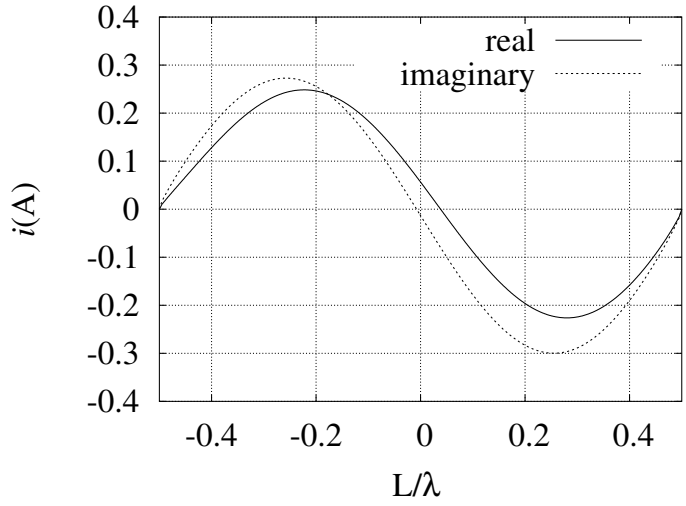

Figure 6.13: Real and imaginary part of the current induced in the wire – Our solution

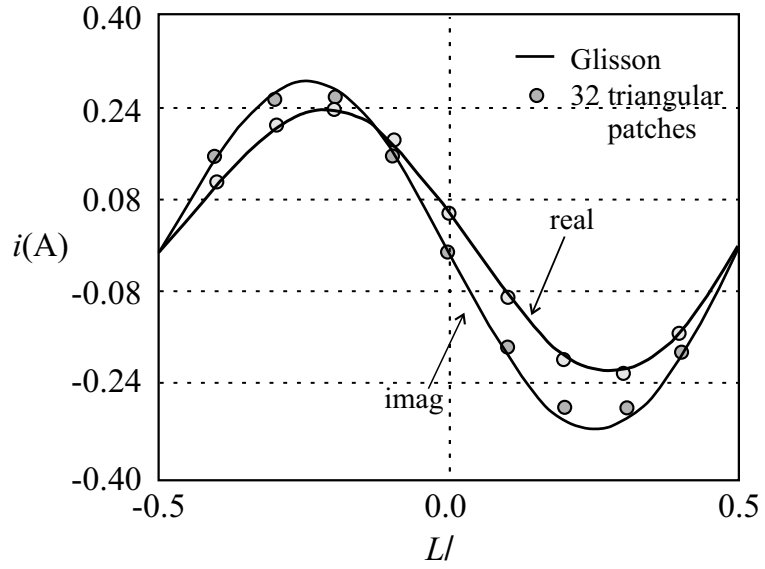

Figure 6.14: Real and imaginary part of the current induced in a wire – Reference solution from [Rao, 1980, p. 125]

tion 3.4.1. The FMM is then applied to the expansion of the 3D Helmholtz equation (4.57). The voltage source is modelled as a so-called *delta-gap* (see Appendix D).

We calculate the input impedance[2] of the dipole antenna for the range of frequencies $[0.8, 1.9]$ GHz around the resonance frequency of the dipole. For this range of frequencies, the thickness of the antenna a verifies $a \ll \lambda$ and the thin wire approximation [Balanis, 1997, Chapter 7] holds.

[2] An antenna can be represented by this equivalent impedance $Z = R + \imath X$, with R the resistance and X the reactance. Knowing this parameter will allow to match the antenna to a transmission line and other associated equipment only within a bandwidth.

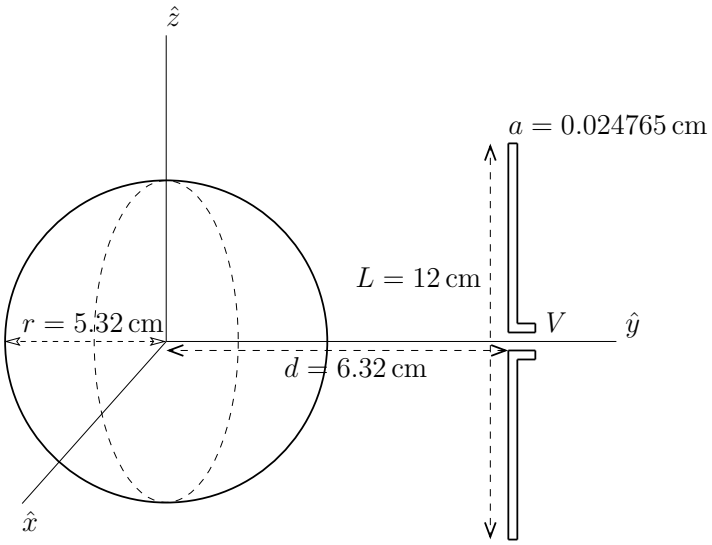

Figure 6.15: Layout of the dipole antenna and the perfectly electric conducting sphere

6.5.2 Calculation results

The problem is simulated using a BE discretisation of the dipole antenna and the PEC sphere consisting of 1224 triangles and 39 segments which yields 3748 complex unknowns for $\underline{j}$. We adopt RWG basis functions (3.40) for the triangles and thin wire basis functions (3.44) for the segments. When applying the FMM, the sphere and the antenna are split into 9 and 56 groups respectively. This group distribution was found to be optimal for the particular mesh described above: using more groups leads to a higher computation time for solving the system of equations while using less groups increases the assembly time. Again, two groups are considered to be far groups if there are at least two groups in between, which leads to $M = 7$ and $N_d = 98$ (see Section 4.4.2).

We calculate the conductance G and susceptance B ($1/Z = G + \imath B$) of the antenna dipole represented in Figure 6.15. The system of algebraic equations is then solved for different frequencies in the range $[0.8, 1.9]$ GHz. The obtained results have been verified against published results.

Figure 6.16 shows the conductance and susceptance as a function of frequency. In order to validate our solution, the results published in [Rao, 1980, p. 127] are reproduced in Figure 6.17. Both results agree well.

The system of algebraic equations is solved by means of the iterative solver GMRES [Saad & Schultz, 1986] with ILU-preconditioning on a 2 GHz Intel Pentium 4 Processor.

The calculation for one frequency takes 184 min without FMM and only 4.6 min with FMM. The system is then solved 40 times faster when the FMM acceleration is applied. The efficiency of applying the FMM is also proved with regard to memory requirements: we need 362 Mb for the classical MoM calculation and 112 Mb for the accelerated MoM calculation. The reduction of storage requirements amounts to

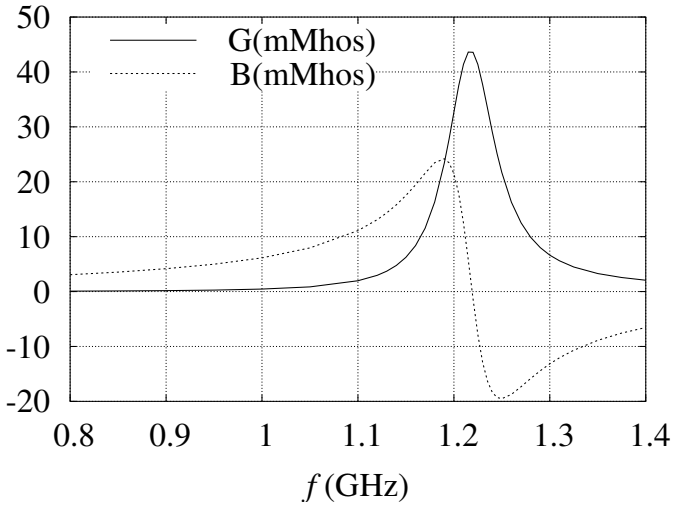

Figure 6.16: Variation of conductance and susceptance vs frequency of an antenna oriented parallel to the polar axis of a sphere. Our solution

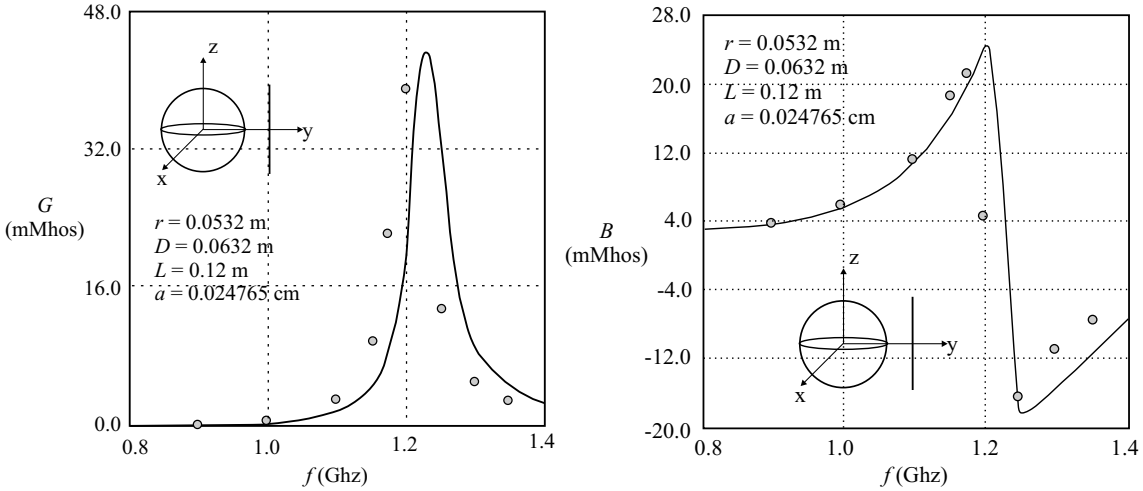

Figure 6.17: Variation of conductance (left) and susceptance (right) vs frequency of an antenna oriented parallel to the polar axis of a sphere. Reference solution from [Rao, 1980, p. 127](solid line)

69 %.

Conclusions

Contents

Fast solution methods have a definitive impact in the area of a computer-aided design of many technologies that rely on electromagnetism. We have studied, developed and applied one of these methods: the fast multipole method (FMM). The main achievements of this thesis are summarised hereafter, as well as the conclusions that can be drawn from the numerical tests, and some important future prospects.

Fast multipole method

The dense matrices (blocks) arising from a boundary element (BE) method (or from the BE part of a finite element-boundary element (FE-BE) hybrid method) in the system of algebraic equations significantly limit the size of the problem to be handled. The FMM permits to overcome this disadvantage by spatially decomposing the problem into groups of elements and determining the interactions between distant groups by means of multipole expansions of the Green functions (either the Laplace or Helmholtz Green function). This way the FMM allows to reduce the computational account and to speed up the solution of linear systems of equations resulting from the BE methods.

We have focused on low frequency problems (Laplace equation). The use of the FMM in scattering applications (Helmholtz equation) has already been extensively researched in the literature. Hence, we have not deliberately pursued to further investigate this kind of problems. Our contribution herein is reduced.

The multipole expansions of both the Laplace and Helmholtz Green functions have been presented in an original way, splitting them formally into matrices associated with the so-called FMM operations: aggregation, disaggregation and translation. The analytical expansions of the gradient of the Green functions (required in the formulations) have also been developed.

These expansions have to be truncated. In most cases, the conventional choice for the truncation number is too conservative. Indeed, if the distance between the

source point and its group centre and the distance between the observation point and its group centre are small compared to the distance between the two group centres, a smaller number of terms suffices. A novel adaptive truncation scheme for both the 2D and 3D Laplace Green function which takes those distances into account has been elaborated.

We have tackled some aspects relative to problems comprising moving parts. Updating the acceleration data (aggregation, disaggregation and translation) for every new position of the rigid moving parts has been proved to be simple and computationally cheap. Furthermore, the disaggregation and aggregation data do not vary in the particular case of purely translational movement. Only the translation data have to be modified.

Numerical tests

We have successfully tackled a range of numerical tests in both low and high frequency, which illustrates the power and versatility of the FMM. We would like to underline in particular the application of the FMM to the solution of 2D and 3D low frequency FE-BE hybrid models of problems comprising eddy currents, nonlinearities, movement and deformations. To the best of our knowledge, we have treated with the FMM problems comprising eddy currents and movement for the first time.

We have satisfactorily compared the results obtained by an accelerated FE-BE model (or a pure BE model) to those achieved by means of either a FE model or a nonaccelerated FE-BE model, to measurements found in the literature or to an analytical solution. In all considered cases, a very good agreement has been observed. The comparison of the results obtained by means of an accelerated FE-BE model and its nonaccelerated counterpart has shown the high accuracy of the method.

The considered applications have also demonstrated the effectiveness of the FMM with regard to memory requirements and computation time. Significant savings in those resources have been achieved. The grouping of the elements and the computation of the FMM data structures have been done in a preprocessing that takes a few seconds, which can be neglected in comparison with the total computational cost. We have observed an increase of the number of iterations with the application of the FMM. This is mainly due to the fact that the preconditioning disregards the far field interactions. It is worth mentioning that this rise is largely outweighed by the fact the so-called far matrices are never evaluated explicitly.

We would like to point out that the truncation scheme has proved to be specially useful when dealing with moderate sized problems. The use of a conventional truncation scheme would lead to computation costs similar to those required for a traditional BE computation. We have observed that the efficiency of the FMM increases considerably with the number of unknowns.

All the implemented tools are freely available on the Internet for further tests [GetDP, 1997–2004].

Future research

Many interesting prospects still remain. Several suggestions for future research lines are enumerated below:

- ✓ The extension of the truncation scheme developed for low frequency problems to high frequency cases would enhance the performance of the method. This extension could be straightforwardly undertaken.

- ✓ The implementation of a multilevel FMM would contribute to further accelerate the solution of the linear system of algebraic equations [Lu & Chew, 1994; Buchau *et al.*, 2000].

- ✓ The implementation of a parallelised FMM would lead to significantly improve its capabilities. The solution of the linear system of algebraic equations would be further speed up as well [Donepudi *et al.*, 2001]. Indeed, starting from the grouping scheme of the FMM it is obvious to compute the near-field interactions for each group separately and the parallelisation of the matrix-vector-product could be straightforwardly performed.

- ✓ The current implementation of boundary element methods does not allow to take advantage of possible symmetries. Moreover, the treatment of multiply connected domains by introducing cuts when applying a BE model has not yet been tackled. Including these features and accordingly adapting the FMM could also be carried out.

- ✓ We have tested the preconditioners available in [SPARSKIT, 1999]. Designing a better suited preconditioning technique would allow a better control of the number of iterations needed for a certain accuracy. In fact, when applying FMM the CPU time for each iteration step is relatively large in comparison to the total CPU time. Therefore, the reduction of the number of iteration steps reduces the computational costs noticeably. Furthermore, we have been confronted to the lack convergence of the iterative solver, specially when solving problems with small structures. A better preconditioning algorithm would help to ensure the convergence.

- ✓ The field computation in arbitrary points involves a postprocessing that can be accelerated by means of the FMM. Even though this postprocessing is not as cumbersome as finding the solution of the system, the application of the FMM could be very useful when dealing with a large number of field points.

Appendix A

Mathematical framework

A.1 Function spaces

Scalar and vector fields are defined at any point $\underline{x} = (x, y, z) \in \mathbb{R}^3$ and at any time instant $t \in \mathbb{R}$. For the sake of simplicity, the space-time dependence of the fields is generally omitted throughout this work, i.e. the scalar field $f(\underline{x}, t) = f(x, y, z, t)$ and the vector field $\underline{f}(\underline{x}, t) = \underline{f}(x, y, z, t)$ is thus often denoted by f and $\underline{f}$. In Cartesian coordinates, the vector field is denoted by $\underline{f} = (f_x, f_y, f_z)^T$ where f_x, f_y and f_z represent, respectively, its three components.

The domain of study is an open set Ω of $\mathbb{R}^3$, whose boundary is a closed surface Γ with exterior unit normal $\hat{n}$.

A.1.1 Square integrable field spaces

The spaces $L^2(\Omega)$ and $\boldsymbol{L}^2(\Omega)$ of square integrable scalar and vector fields on Ω, respectively, are defined by [Wait & Mitchell, 1985; Fowler, 1997]

$$L^2(\Omega) = \Big\{ u : \int_\Omega u^2(\underline{x})\, d\underline{x} < \infty \Big\}, \tag{A.1}$$

$$\boldsymbol{L}^2(\Omega) = \Big\{ \underline{u} : \int_\Omega \|\underline{u}(\underline{x})\|^2\, d\underline{x} < \infty \Big\}, \tag{A.2}$$

where $\underline{x}$ is a point of space, $d\underline{x}$ a volume element and $\|\underline{u}(\underline{x})\|$ represents the Euclidean norm of $\underline{u}(\underline{x})$. The scalar product of two elements $u, v \in L^2(\Omega)$ and $\underline{u}, \underline{v} \in \boldsymbol{L}^2(\Omega)$ is defined by

$$(u, v)_\Omega = \int_\Omega u(\underline{x})\, v(\underline{x})\, d\underline{x} \quad \text{and} \quad (\underline{u}, \underline{v})_\Omega = \int_\Omega \underline{u}(\underline{x}) \cdot \underline{v}(\underline{x})\, d\underline{x}. \tag{A.3}$$

The norm of an element $u \in L^2(\Omega)$ and $\underline{u} \in \boldsymbol{L}^2(\Omega)$ is defined by

$$\|u\|_{L^2(\Omega)} = (u, u)_\Omega^{1/2} = \Big[\int_\Omega u^2(\underline{x})\, d\underline{x} \Big]^{1/2}, \tag{A.4}$$

$$\|\underline{u}\|_{\boldsymbol{L}^2(\Omega)} = (\underline{u}, \underline{u})_\Omega^{1/2} = \Big[\int_\Omega \|\underline{u}(\underline{x})\|^2\, d\underline{x} \Big]^{1/2}. \tag{A.5}$$

If a space is normed, the distance between two elements $u, v \in L^2(\Omega)$ and $\underline{u}, \underline{v} \in \boldsymbol{L}^2(\Omega)$ is the norm of their difference, respectively, $d(u,v) = \|u - v\|$ and $d(\underline{u}, \underline{v}) = \|\underline{u} - \underline{v}\|$.

Two elements $u, v \in L^2(\Omega)$ ($\underline{u}, \underline{v} \in \boldsymbol{L}^2(\Omega)$) are said to be orthogonal if their scalar product is $(u,v)_\Omega = 0$ ($(\underline{u}, \underline{v})_\Omega = 0$). Two functional spaces are said to be orthogonal if all their elements are orthogonal.

Let E be a normed vector space. A sequence $\{u_n\}$ is called a Cauchy sequence if

$$\forall \epsilon > 0,\ \exists N \in \mathbb{Z}\ \Rightarrow d(u_m, u_n) < \epsilon \text{ if } m, n > N. \tag{A.6}$$

E is complete if every Cauchy sequence converges towards an element of E.

If E is a vector space equipped with a scalar product and if E is complete for the norm derived from this scalar product, then E is a Hilbert space.

The spaces $L^2(\Omega)$ and $\boldsymbol{L}^2(\Omega)$ are *Hilbert spaces* and can welcome physical fields, characterised by a finite energy.

The subspaces of $L^2(\Omega)$ and $\boldsymbol{L}^2(\Omega)$ for which all first order partial derivatives are also square integrable are known as the *Sobolev spaces* of scalar fields $H^1(\Omega)$ and vector fields $\boldsymbol{H}^1(\Omega)$, respectively. They are defined as

$$H^1(\Omega) = \Big\{ u \in L^2(\Omega) : \partial_x u, \partial_y u, \partial_z u \in L^2(\Omega) \Big\}, \tag{A.7}$$

$$\boldsymbol{H}^1(\Omega) = \Big\{ \underline{u} \in \boldsymbol{L}^2(\Omega) : \partial_x \underline{u}, \partial_y \underline{u}, \partial_z \underline{u} \in \boldsymbol{L}^2(\Omega) \Big\}. \tag{A.8}$$

Analogously, the Sobolev spaces $H^p(\Omega)$ and $\boldsymbol{H}^p(\Omega)$, $\forall p > 1$ are given by

$$H^p(\Omega) = \Big\{ u \in H^{p-1}(\Omega) : \partial_x u, \partial_y u, \partial_z u \in H^{p-1}(\Omega) \Big\}, \tag{A.9}$$

$$\boldsymbol{H}^p(\Omega) = \Big\{ \underline{u} \in \boldsymbol{H}^{p-1}(\Omega) : \partial_x \underline{u}, \partial_y \underline{u}, \partial_z \underline{u} \in \boldsymbol{H}^{p-1}(\Omega) \Big\}. \tag{A.10}$$

The Sobolev spaces are well adapted to variational problems.

For the sake of simplicity, the following notation is adopted for the integrals over a surface Γ of the scalar product of two functions:

$$\langle u, v \rangle_\Gamma = \int_\Gamma u(\underline{x})\, v(\underline{x})\, d\underline{x} \quad \text{and} \quad \langle \underline{u}, \underline{v} \rangle_\Gamma = \int_\Gamma \underline{u}(\underline{x}) \cdot \underline{v}(\underline{x})\, d\underline{x}. \tag{A.11}$$

A.1.2 Differential operators

The differential operators gradient, divergence and curl are of importance in many physical problems, and in particular for Maxwell's equations.

The grad operator in Cartesian coordinates for scalar fields f is classically defined as

$$\operatorname{grad} f = (\partial_x f, \partial_y f, \partial_z f)^T. \tag{A.12}$$

The Sobolev space that corresponds to the grad is thus

$$H(\mathrm{grad};\Omega) = \left\{u \in L^2(\Omega) : \mathrm{grad}\, u \in \boldsymbol{L}^2(\Omega)\right\}. \tag{A.13}$$

Note that $H(\mathrm{grad};\Omega) = H^1(\Omega)$

The classical definition of the curl and div operators for vector fields $\underline{f} = (f_x, f_y, f_z)^T$ are:

$$\mathrm{curl}\, \underline{f} = (\partial_y f_z - \partial_z f_y, \partial_z f_x - \partial_x f_z, \partial_x f_y - \partial_y f_x)^T, \tag{A.14}$$

$$\mathrm{div}\, \underline{f} = \partial_x f_x + \partial_y f_y + \partial_z f_z. \tag{A.15}$$

Based on the concepts of weak curl and div, we define the Hilbert spaces of stream functions and fluxes:

$$\boldsymbol{H}(\mathrm{curl};\Omega) = \left\{\underline{u} \in \boldsymbol{L}^2(\Omega) : \mathrm{curl}\, \underline{u} \in \boldsymbol{L}^2(\Omega)\right\}, \tag{A.16}$$

$$\boldsymbol{H}(\mathrm{div};\Omega) = \left\{\underline{u} \in \boldsymbol{L}^2(\Omega) : \mathrm{div}\, \underline{u} \in L^2(\Omega)\right\}. \tag{A.17}$$

We define the laplacian operator as well:

$$\Delta f = \nabla^2 f = \partial_x^2 f_x + \partial_y^2 f_y + \partial_z^2 f_z\,, \tag{A.18}$$

$$\Delta \underline{f} = \nabla^2 \underline{f} = (\nabla^2 f_x, \nabla^2 f_y, \nabla^2 f_z)\,. \tag{A.19}$$

A.1.3 de Rham complexes

The domains of the differential operators are built to satisfy $\mathcal{R}(\mathrm{grad}) \subset \mathcal{D}(\mathrm{curl})$, $\mathcal{R}(\mathrm{curl}) \subset \mathcal{D}(\mathrm{div})$, and $\mathcal{R}(\mathrm{div}) \subset L^2(\Omega)$, or, equivalently, $\mathrm{grad}\, H^1(\Omega) \subset \boldsymbol{H}(\mathrm{curl};\Omega)$, $\mathrm{curl}\, \boldsymbol{H}(\mathrm{curl};\Omega) \subset \boldsymbol{H}(\mathrm{div};\Omega)$ and $\mathrm{div}\, \boldsymbol{H}(\mathrm{div};\Omega) \subset L^2(\Omega)$. Therefore, the spaces $H^1(\Omega)$, $\boldsymbol{H}(\mathrm{curl};\Omega)$, $\boldsymbol{H}(\mathrm{div};\Omega)$ and $L^2(\Omega)$ form an algebraic structure called complex:

$$H^1(\Omega) \xrightarrow{\mathrm{grad}} \boldsymbol{H}(\mathrm{curl};\Omega) \xrightarrow{\mathrm{curl}} \boldsymbol{H}(\mathrm{div};\Omega) \xrightarrow{\mathrm{div}} L^2(\Omega) \tag{A.20}$$

If $\Omega = \mathbb{R}^3$, the sequence (A.20) is said to be exact since $\mathcal{R}(\mathrm{grad}) = \mathcal{K}(\mathrm{curl})$ and $\mathcal{R}(\mathrm{curl}) = \mathcal{K}(\mathrm{div})$. In this case, the image of $H^1(\mathbb{R}^3)$ in $\boldsymbol{H}(\mathrm{curl};\mathbb{R}^3)$ by the grad operator is exactly the kernel of the curl operator, which means that all curl-free fields are gradients. Analogously, the image of $\boldsymbol{H}(\mathrm{curl};\mathbb{R}^3)$ in $\boldsymbol{H}(\mathrm{div};\mathbb{R}^3)$ by the curl operator is exactly the kernel of the div operator, which means that all divergence-free fields can be expressed as the curl of some other fields.

If Ω is a bounded set of $\mathbb{R}^3$, the sequence is not exact any more, except for trivial topologies (for example if Ω is simply connected).

A.2 Green formulae

The generalised Green relation is given by

$$(\mathcal{L}u, v)_\Omega - (u, \mathcal{L}^* v)_\Omega = \int_\Gamma Q(u,v)ds, \quad \forall u \in \mathcal{D}(\mathcal{L}) \text{ and } \forall v \in \mathcal{D}(\mathcal{L}^*) \tag{A.21}$$

where $\mathcal{L}$ is a differential operator of order n defined on Ω, $\mathcal{L}^*$ is the adjoint of $\mathcal{L}$, and Q is a bilinear function of u and v and in their derivatives up to the order $n-1$.

The extensively used grad-div and curl-curl Green formulae are two particular cases of the the generalised Green relation (A.21). Let u be a function of $\Omega \mapsto \mathbb{R}$ and $\underline{v}$ a function of $\Omega \mapsto \mathbb{R}^3$.

Integrating the following vector analysis formula

$$\underline{v} \cdot \operatorname{grad} u + u \operatorname{div} \underline{v} = \operatorname{div} (u\underline{v}) \tag{A.22}$$

over Ω, and applying the divergence theorem, the Green formula of type grad-div is obtained:

$$(\underline{v}, \operatorname{grad} u)_\Omega + (\operatorname{div} \underline{v}, u)_\Omega = \langle u, \hat{n} \cdot \underline{v} \rangle_\Gamma, \quad \forall \underline{v} \in \boldsymbol{H}^1(\Omega) \text{ and } \forall u \in H^1(\Omega). \tag{A.23}$$

Let $\underline{w}$ be a function of $\Omega \mapsto \mathbb{R}^3$. Integrating the following vector analysis formula

$$\underline{v} \cdot \operatorname{curl} \underline{w} - \underline{w} \cdot \operatorname{curl} \underline{v} = \operatorname{div} (\underline{w} \times \underline{v}), \tag{A.24}$$

over Ω, and applying the divergence theorem, the Green formula of type curl-curl is obtained:

$$(\underline{v}, \operatorname{curl} \underline{w})_\Omega - (\operatorname{curl} \underline{v}, \underline{w})_\Omega = \langle \underline{v} \times \hat{n}, \underline{w} \rangle_\Gamma \quad \forall \underline{v}, \underline{w} \in \boldsymbol{H}^1(\Omega). \tag{A.25}$$

A.3 Strong and weak solutions

Let us consider the partial derivative problem

$$\mathcal{L}u = f \text{ in } \Omega, \tag{A.26}$$
$$\mathcal{B}u = g \text{ on } \Gamma, \tag{A.27}$$

where $\mathcal{L}$ is a differential operator of order n, $\mathcal{B}$ is a differential operator that imposes a boundary condition, the two functions f and g are defined in Ω and on Γ, respectively, and u is an unknown function defined on $\bar{\Omega}$. The system (A.26)-(A.27) constitutes a strong formulation. A function u that verifies (A.26)-(A.27) is called a strong solution.

A weak formulation of the same problem is given by

$$(u, \mathcal{L}^* v)_\Omega - (f, v)_\Omega + \int_\Gamma Q_g(v)\, ds = 0, \quad \forall v \in V(\Omega), \tag{A.28}$$

where $\mathcal{L}^*$ is defined by the generalised Green formula (A.21), Q_g is a linear form in v which depends on g and $V(\Omega)$ is a space of test functions (defined in relation with $\mathcal{L}^*$ and with the boundary condition (A.27)). A function u that satisfies (A.28) for all test functions $v \in V(\Omega)$ is called a weak solution.

The generalised Green formula (A.21) can be applied to (A.28) in order to switch from $\mathcal{L}^*$ to $\mathcal{L}$, which is in general equivalent to performing an integration by parts.

It is easy to verify that a strong solution is also a weak solution. On the other hand, proving that a weak solution is also a strong solution is not immediate because it has to be regular enough in order to be defined in a classical way. Weak formulations allow to prove the existence of a solution more easily than strong formulations and they are well adapted to finite element discretisations [Jonhson, 1987].

Appendix B

Some special functions

The following sections constitute a short reminder on some mathematical functions. For further details, see [Abramowitz & Stegun, 1970; Chew, 1995; Harrington, 1961].

B.1 Bessel functions

The Bessel equation of order m is given by

$$x^2 \frac{\mathrm{d}^2 y}{\mathrm{d}x^2} + x \frac{\mathrm{d}y}{\mathrm{d}x} + (x^2 - m^2)\, y = 0\,. \tag{B.1}$$

Solutions are the Bessel functions of the first kind $J_m(x)$, of the second kind $Y_m(x)$ (also called Weber's function) and of the third kind $H_m^{(1)}(x)$, $H_m^{(2)}(x)$ (also called Hankel functions). Each is a regular function of x throughout the x-plane cut along the negative real axis, and for fixed $x \neq 0$ each is an entire integral function of m.

Important features of the various solutions are: $J_m(x)$ ($\Re(m) \geq 0$) is bounded as $x \to 0$ in any bounded range of $\arg(x)$. $J_m(x)$ and $J_{-m}(x)$ are linearly independent except when m is an integer. $J_m(x)$ and $Y_m(x)$ are linearly independent for all values of m. $H_m^1(x)$ tends to zero as $|x| \to \infty$ in the sector $0 < \arg(x) < \pi$. $H_m^{(2)}(x)$ tends to zero as $|x| \to \infty$ in the sector $-\pi < \arg x < 0$. For all values of m, $H_m^{(1)}(x)$ and $H_m^{(2)}(x)$ are linearly independent.

The Hankel functions are related to the Bessel functions of the first and second kind as

$$H_m^{(1)}(x) = J_m(x) + \imath\, Y_m(x)\,, \tag{B.2}$$
$$H_m^{(2)}(x) = J_m(x) - \imath\, Y_m(x)\,. \tag{B.3}$$

Let us give the following important relations

$$J_{-m}(x) = (-1)^m J_m(x), \quad Y_{-m}(x) = (-1)^m Y_m(x) \tag{B.4}$$

and

$$H_{-m}^{(1)}(x) = (-1)^m H_m^{(1)}(x), \quad H_{-m}^{(2)}(x) = (-1)^m H_m^{(2)}(x)\,. \tag{B.5}$$

The Bessel function J_m can be put into an integral form. From formula [Abramowitz & Stegun, 1970, (9.1.21)], one can easily show that

$$J_m(x) = \frac{1}{2\pi}\int_0^{2\pi} e^{\imath x\cos\theta} e^{\imath m(\theta-\pi/2)}\mathrm{d}\theta\,. \tag{B.6}$$

The asymptotic behaviour of Bessel functions for large arguments is given by

$$J_m(x) \xrightarrow[x\to\infty]{} \sqrt{\frac{2}{\pi x}}\cos\left(x-\frac{\pi}{4}-\frac{m\pi}{2}\right), \tag{B.7}$$

$$Y_m(x) \xrightarrow[x\to\infty]{} \sqrt{\frac{2}{\pi x}}\sin\left(x-\frac{\pi}{4}-\frac{m\pi}{2}\right), \tag{B.8}$$

$$H_m^{(1)}(x) \xrightarrow[x\to\infty]{} \sqrt{\frac{2}{\imath\pi x}}\imath^{-m}\, e^{\imath x}\,, \tag{B.9}$$

$$H_m^{(2)}(x) \xrightarrow[x\to\infty]{} \sqrt{\frac{2\imath}{\pi x}}\imath^{m}\, e^{-\imath x}\,, \tag{B.10}$$

which place into evidence the wave character of the Hankel functions.

B.2 Spherical Bessel functions

The spherical Bessel functions are solutions of the differential equation

$$x^2\frac{\mathrm{d}^2y}{\mathrm{d}x^2}+2x\frac{\mathrm{d}y}{\mathrm{d}x}+[x^2-m(m+1)]\,y=0\,,\qquad m=0,\pm1,\pm2,\cdots\,. \tag{B.11}$$

Particular solutions are the spherical Bessel functions of the first kind,

$$j_m(x)=\sqrt{\frac{\pi}{2x}}J_{m+\frac{1}{2}}(x)\,, \tag{B.12}$$

the spherical Bessel functions of the second kind,

$$y_m(x)=\sqrt{\frac{\pi}{2x}}Y_{m+\frac{1}{2}}(x)\,, \tag{B.13}$$

and the spherical Hankel functions of the third kind,

$$h_m^{(1)}(x) \;=\; j_m(x)+\imath\, y_m(x)=\sqrt{\frac{\pi}{2x}}H^{(1)}_{m+\frac{1}{2}}(x)\,, \tag{B.14}$$

$$h_m^{(2)}(x) \;=\; j_m(x)-\imath\, y_m(x)=\sqrt{\frac{\pi}{2x}}H^{(2)}_{m+\frac{1}{2}}(x)\,. \tag{B.15}$$

It is worth mentioning the relations known as Rayleigh's formulae:

$$j_m(x) \;=\; x^m\left(-\frac{1}{x}\frac{\mathrm{d}}{\mathrm{d}x}\right)^m\frac{\sin x}{x}\,, \tag{B.16}$$

$$y_m(x) \;=\; (-x)^m \left(-\frac{1}{x}\frac{\mathrm{d}}{\mathrm{d}x}\right)^m \frac{\cos x}{x}\,. \tag{B.17}$$

The asymptotic behaviour of the functions j_m, y_m, $h_m^{(1)}$ and $h_m^{(2)}$ for large m is directly obtained from the asymptotic behaviour of J_m (B.7), Y_m (B.8), $H_m^{(1)}$ (B.9) and $H_m^{(2)}$ (B.10).

In some electromagnetic field problems, it is convenient to define the alternative spherical Bessel functions:

$$\hat{B}_m(x) = \sqrt{\frac{\pi x}{2}} B_{m+1/2}(x)\,, \tag{B.18}$$

where $\hat{B}_m(x)$ is given the same name and symbol as the corresponding arbitrary Bessel function $B_{m+1/2}$.

Some derivative and recurrence formulae are given by

$$\frac{\mathrm{d}B_m(x)}{\mathrm{d}x} = B_{m-1}(x) - \frac{m}{x}B_m(x)\,, \tag{B.19}$$

$$\frac{\mathrm{d}B_m(x)}{\mathrm{d}x} = -B_{m+1}(x) + \frac{m}{x}B_m(x)\,, \tag{B.20}$$

where $B_m(x)$ denotes an arbitrary solution to the Bessel equation (B.1).

B.3 Legendre polynomials

The Legendre polynomials $P_l(x)$ are real functions (polynomials of order l) defined in the interval $-1 \le x \le 1$. They arise from a power-series solution of the following second order differential equation, known as the Legendre equation:

$$\frac{\mathrm{d}}{\mathrm{d}x}\left[(1-x^2)\,\frac{\mathrm{d}}{\mathrm{d}x}P\right] + l\,(l+1)P = 0\,. \tag{B.21}$$

Some of the lower-degree Legendre polynomials are:

$$\begin{aligned} P_0(x) &= 1, \\ P_1(x) &= x, \\ P_2(x) &= \frac{1}{2}(3x^2-1), \\ P_3(x) &= \frac{1}{2}(5x^3-3x), \\ P_4(x) &= \frac{1}{8}(35x^4-30x^2+3). \end{aligned} \tag{B.22}$$

Note that they verify:

$$P_l(x) = (-1)^l\,P_l(-x) \qquad \text{and} \qquad P_l(1) = 1\,. \tag{B.23}$$

An alternative and sometimes convenient expression for the Legendre polynomials is given by Rodrigues' formula

$$P_l(x) = \frac{1}{2^l l!}\frac{\mathrm{d}^l}{\mathrm{d}x^l}(x^2-1)^l. \tag{B.24}$$

By convention, these polynomials are normalised to have the value unity at $x = 1$. They form a complete orthogonal set of functions on the interval $-1 \le x \le 1$. The orthogonality condition can be expressed as

$$\int_{-1}^{1} P_l(x)P_m(x)dx = \frac{2}{2l+1}\delta_{l,m}\,. \tag{B.25}$$

Since the Legendre polynomials form a complete set of orthogonal functions, any function $f(x)$ on the interval $-1 \le x \le 1$ can be expanded in terms of them. The Legendre series representation is:

$$f(x) = \sum_{l=0}^{\infty} \alpha_l P_l(x) \quad \text{where} \quad \alpha_l = \int_{-1}^{1} f(x)P_l(x)\mathrm{d}x\,. \tag{B.26}$$

Certain recurrence relations among Legendre polynomials of different order are useful in evaluating integrals, generating higher order polynomials from lower order ones, etc. From Rodrigues' formula it is a straightforward matter to show that

$$\frac{\mathrm{d}P_{l+1}}{\mathrm{d}x} - \frac{\mathrm{d}P_{l-1}}{\mathrm{d}x} - (2l+1)P_l = 0\,. \tag{B.27}$$

This result combined with Legendre differential equation (B.21) yields various recurrence relations:

$$(l+1)P_{l+1} - (2l+1)xP_l + lP_{l-1} = 0\,, \tag{B.28}$$

$$(x^2-1)\frac{\mathrm{d}P_l}{\mathrm{d}x} - lxP_l + lP_{l-1} = 0\,, \tag{B.29}$$

$$\frac{\mathrm{d}P_{l+1}}{\mathrm{d}x} - x\frac{\mathrm{d}P_l}{\mathrm{d}x} - (l+1)P_l = 0\,. \tag{B.30}$$

B.4 Associated Legendre functions

Let us consider the second order differential equation known as associated Legendre equation

$$\frac{\mathrm{d}}{\mathrm{d}x}\left[(1-x^2)\,\frac{\mathrm{d}}{\mathrm{d}x}P\right] + \left[l\,(l+1) - \frac{m^2}{1-x^2}\right]P = 0\,, \tag{B.31}$$

which has a finite solution on the interval $-1 \le x \le 1$ only if the parameter l equals zero or a positive integer and m takes the values $-l, -l-1, \cdots, 0, \cdots, l-1, l$. The solution of (B.31) is the so-called associated Legendre function of the first kind,

degree l and order m, $P_l^m(x)$. For positive m, it can be expressed as a function of the Legendre polynomials $P_l(x)$ as

$$P_l^m(x) = (-1)^m (1-x^2)^{m/2} \frac{\mathrm{d}^m}{\mathrm{d}x^m} P_l(x)\,. \tag{B.32}$$

Note that $P_l^m(x) = 0$ for $m > l$.

A definition valid for both positive and negative m is obtained by substituting $P_l(x)$ given by (B.24) in (B.32):

$$P_l^m(x) = \frac{(-1)^m}{2^l l!} (1-x^2)^{m/2} \frac{\mathrm{d}^{l+m}}{\mathrm{d}x^{l+m}} (x^2-1)^l\,. \tag{B.33}$$

Since the differential equation (B.31) depends only on m^2 and m is an integer, $P_l^{-m}(x)$ and $P_l^m(x)$ are proportional. It can be shown that

$$P_l^{-m}(x) = (-1)^m \frac{(l-m)!}{(l+m)!} P_l^m(x)\,. \tag{B.34}$$

The derivative of $P_l^m(x)$ can be calculated by means the following recursive relation [Abramowitz & Stegun, 1970, (8.5.2)]

$$(x^2-1)\frac{\mathrm{d}P_l^m(x)}{\mathrm{d}x} = (l+m)(l-m+1)(x^2-1)P_l^{m-1}(x) - mxP_l^m(x)\,. \tag{B.35}$$

For fixed m the functions $P_l^m(x)$ form an orthogonal set in the index l on the interval $-1 \le x \le 1$. The orthogonality relation is given by

$$\int_{-1}^{1} P_{l'}^m(x) P_l^m(x) dx = \frac{2}{2l+1} \frac{(l+m)!}{(l-m)!} \delta_{l',l}\,. \tag{B.36}$$

B.5 Spherical Harmonics

The functions $e^{\imath m\phi}$ constitute a set of complete orthogonal functions on the interval $\phi \in [0, 2\pi]$. The functions $P_l^m(\cos\theta)$, for each m, form a set of complete orthogonal functions in the index l on the interval $\theta \in [0, \pi]$. Therefore their product $P_l^m(\cos\theta)e^{\imath m\phi}$ form a complete orthogonal set on the surface of the unit sphere in the two indices l, m.

The spherical harmonics are thus defined for all $\theta \in [0, \pi]$ and $\phi \in [0, 2\pi]$ as

$$Y_l^m(\theta,\phi) = \sqrt{\frac{2l+1}{4\pi}\frac{(l-m)!}{(l+m)!}} P_l^m(\cos\theta)\, e^{\imath m\phi}\,, \tag{B.37}$$

verifying $Y_l^{-m}(\theta,\phi) = (-1)^m Y_l^{*m}(\theta,\phi)$, where * denotes the complex conjugate. Note that, for $m = 0$,

$$Y_l^0(\theta,\phi) = \sqrt{\frac{2l+1}{4\pi}} P_l(\cos\theta)\,. \tag{B.38}$$

An arbitrary function $f(\theta,\phi)$ can be expanded in spherical harmonics:

$$f(\theta,\phi) = \sum_{l=0}^{\infty} \sum_{m=-l}^{l} \alpha_l^m Y_l^m(\theta,\phi) \quad \text{with} \quad \alpha_l^m = \int Y_l^{*m}(\theta,\phi)\, f(\theta,\phi) \mathrm{d}\Omega \tag{B.39}$$

B.6 Addition theorems

B.6.1 Addition theorem for spherical harmonics

The addition theorem for spherical harmonics is the main analytical tool for generating the multipole expansions of the Laplace Green functions employed by the FMM.

Let us consider two arbitrary vectors $\underline{r}$ and $\underline{r}'$ with spherical coordinates (r, θ, ϕ) and (r', θ', ϕ'), respectively, forming an angle φ as shown in Figure B.1. The addition

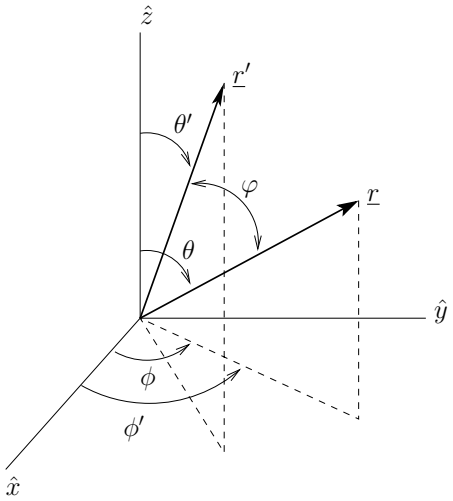

Figure B.1: Spherical coordinate system

theorem for spherical harmonics expresses a Legendre polynomial of order l and angle φ in terms of products of the spherical harmonics of the angles θ, ϕ and θ', ϕ'. It states that

$$P_l(\cos\varphi) = \frac{4\pi}{(2l+1)} \sum_{m=-l}^{l} Y_l^m(\theta,\phi)\, Y_l^{*m}(\theta',\phi') \;, \tag{B.40}$$

where $\cos\varphi = \cos\theta\cos\theta' + \sin\theta\sin\theta'\cos(\phi-\phi')$.

The potential at $\underline{r}$ due to a unit charge at $\underline{r}'$ can be expanded as

$$\frac{1}{|\underline{r}-\underline{r}'|} = \sum_{l=0}^{\infty} \frac{r_<^l}{r_>^{l+1}} P_l(\cos\varphi)\,, \tag{B.41}$$

with $r_<$ ($r_>$) the smaller (larger) of $|\underline{r}|$ and $|\underline{r}'|$. Introducing (B.40) in (B.41), the potential can be expressed in a completely factorised form as

$$\frac{1}{|\underline{r}-\underline{r}'|} = 4\pi \sum_{l=0}^{\infty} \sum_{m=-l}^{l} \frac{1}{2l+1} \frac{r_<^l}{r_>^{l+1}} Y_l^m(\theta,\phi)\, Y_l^{*m}(\theta',\phi') \;. \tag{B.42}$$

B.6.2 Addition theorems for (spherical) Bessel functions

The use of addition theorems arises in a number of solutions of scattering problems. They express wave functions in one coordinate system in terms of the wave functions of another coordinate system which is linearly translated from the first one. The addition theorems for (spherical) Bessel and Hankel functions are the main analytical tools for generating the multipole expansions of the Helmholtz Green functions employed by the FMM.

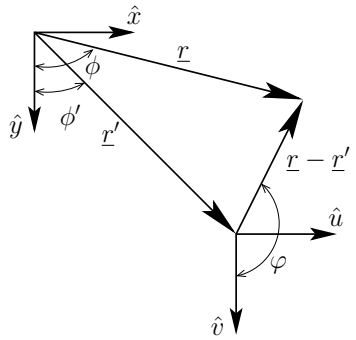

Figure B.2: Translation in the cylindrical coordinate system

The Graf formula [Abramowitz & Stegun, 1970, (9.1.79)] is the addition theorem for Bessel functions required for the expansion of the 2D Helmholtz Green function. It is given by

$$H_m\left(k\left|\underline{r}-\underline{r}'\right|\right)e^{\imath m\varphi}=\begin{cases}\sum\limits_{n=-\infty}^{+\infty} J_{n-m}\left(kr'\right)H_n\left(kr\right)e^{\imath n\phi-\imath(n-m)\phi'}, & r>r',\\ \sum\limits_{n=-\infty}^{+\infty} H_{n-m}\left(kr'\right)J_n\left(kr\right)e^{\imath n\phi-\imath(n-m)\phi'}, & r<r',\end{cases} \tag{B.43}$$

where $\underline{r}=(r,\phi)$, $r'=(r',\phi')$ are two vectors in cylindrical coordinates and $\varphi=\arg(\underline{r}-\underline{r}')$ is defined with respect to the new coordinate system (see Figure B.2). The conditions $r<r'$ and $r>r'$ imply the convergence of the expansions in the right-hand side of (B.43) [1].

The addition theorems for spherical Bessel and Hankel functions are required for expanding of the 3D Helmholtz Green function. The following identity, expressed in spherical coordinates (r,θ,ϕ) (see Figure B.1), is derived directly from these theorems [Abramowitz & Stegun, 1970, (10.1.45), (10.1.46)] and it serves as a starting point,

$$\frac{e^{-\imath kR}}{R}=\begin{cases}-4\pi\imath k\sum\limits_{l=0}^{\infty}\sum\limits_{m=-l}^{l} j_l(kr')\,Y_l^m(\theta',\phi')\,h_l(kr)\,Y_l^m(\theta,\phi)^*, & r>r'\\ -4\pi\imath k\sum\limits_{l=0}^{\infty}\sum\limits_{m=-l}^{l} h_l(kr')\,Y_l^m(\theta',\phi')\,j_l(kr)\,Y_l^m(\theta,\phi)^*, & r<r'\end{cases}, \tag{B.44}$$

[1] Equation (B.43) is satisfied for Hankel functions of the first kind $H_m^{(1)}$ and of the second kind $H_m^{(2)}$. The same applies to all the expressions in this appendix. The superscript indicating the kind is omitted.

with $R = |\underline{r} - \underline{r'}|$.

Appendix C

Limiting value of EFIE and MFIE

C.1 Integral in EFIE

This appendix deals with the value of the integral

$$I = \operatorname{grad} \int_{\Gamma} q(\underline{r}')\, G(\rho)\, \mathrm{d}\Gamma' \,, \tag{C.1}$$

as the observation point $\underline{r}$ approaches the smooth surface Γ, $\rho = |\underline{r} - \underline{r}'|$ is the distance from the source $\underline{r}'$ to the observation point $\underline{r}$. This integral appears in some forms of the EFIE considered in Section 3.4.1. It is safe to move the grad operator inside the integral when the observation point is not on Γ. The charge density $q(\underline{r}')$ is constant with regard to the unprimed coordinates which implies

$$\operatorname{grad}\left(q(\underline{r}')G(\rho)\right) = q(\underline{r}') \cdot \operatorname{grad} G(\rho) \,. \tag{C.2}$$

The integral is split into two integrals $I = I_{\Gamma\setminus\delta\Gamma} + I_{\delta\Gamma}$ as

$$I_{\Gamma\setminus\delta\Gamma} = \int_{\Gamma\setminus\delta\Gamma} q(\underline{r}') \operatorname{grad} G(\rho)\, \mathrm{d}\Gamma' \,, \quad \underline{r} \notin \Gamma \,, \tag{C.3}$$

$$I_{\delta\Gamma} = \int_{\delta\Gamma} q(\underline{r}') \operatorname{grad} G(\rho)\, \mathrm{d}\Gamma' \,, \quad \underline{r} \notin \Gamma \,. \tag{C.4}$$

Herein, $\delta\Gamma$ is a differential circular area with radius δ_0 and centred at $\underline{r}_0 \in \delta\Gamma$ (see Figure C.1). Let us consider that the observation point $\underline{r}$ is located at an infinitesimal distance from Γ, i.e. $\underline{r} = \underline{r}_0 + \varepsilon\hat{n}$, $\varepsilon \ll 1$. Introducing a local cylindrical coordinate system, we can express the source point as $\underline{r}' = \underline{r}_0 + \delta\cos\phi\,\hat{x} + \delta\sin\phi\,\hat{y}$ and $\rho = |\underline{r} - \underline{r}'| = \sqrt{\delta^2 + \varepsilon^2}$. If δ_0 is sufficiently small, the approximation $q(\underline{r}') \approx q(\underline{r}_0)$ is reasonable. Evaluating $\operatorname{grad} G$ and using $\mathrm{d}\Gamma' = \delta \mathrm{d}\phi\mathrm{d}\delta$, the integral $I_{\delta\Gamma}$ reads

$$I_{\delta\Gamma} \approx -\frac{q(\underline{r}_0)}{4\pi} \int_{\delta=0}^{\delta_0} \int_{\phi=0}^{2\pi} \left(\frac{1}{\rho} + \imath k\right) \underline{\rho}\, \frac{e^{-\imath k\rho}}{\rho^2} \delta \mathrm{d}\phi\mathrm{d}\delta \,. \tag{C.5}$$

Considering $k\rho \ll 1$ and $\underline{r} - \underline{r}' = \varepsilon\hat{n} - \delta\cos\phi\,\hat{x} - \delta\sin\phi\,\hat{y}$ leads to

$$I_{\delta\Gamma} \approx -\frac{q(\underline{r}_0)}{4\pi} \int_{\delta=0}^{\delta_0} \int_{\phi=0}^{2\pi} \frac{\varepsilon\hat{n} - \delta\cos\phi\,\hat{x} - \delta\sin\phi\,\hat{y}}{(\delta^2 + \varepsilon^2)^{\frac{3}{2}}}\, \delta \mathrm{d}\phi\mathrm{d}\delta \,. \tag{C.6}$$

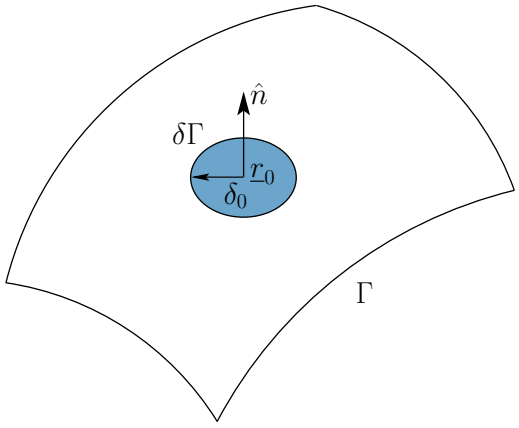

Figure C.1: Surface Γ with differential circular area $\delta\Gamma$

The integral along ϕ over the $\hat{x}$ and $\hat{y}$ components evaluate to zero. We get

$$I_{\delta\Gamma} \approx -\hat{n}\frac{q(\underline{r}_0)}{2}\int_{\delta=0}^{\delta_0}\frac{\varepsilon\delta}{(\delta^2+\varepsilon^2)^{\frac{3}{2}}}\mathrm{d}\delta = \hat{n}\frac{q(\underline{r}_0)}{2}\varepsilon\left(\frac{1}{\sqrt{\delta_0^2+\varepsilon^2}}-\frac{1}{\varepsilon}\right). \tag{C.7}$$

For $\varepsilon \to 0$, $\underline{r} \to \underline{r}_0$, and the above equation reduces to

$$I_{\delta\Gamma} \approx -\hat{n}\frac{q(\underline{r}_0)}{2}. \tag{C.8}$$

For $\delta \to 0$, $\delta\Gamma$ tends to a single point. For an observation point on the surface, (C.1) can thus be written as

$$I = -\hat{n}\frac{q(\underline{r})}{2} + \barint_{\Gamma} q(\underline{r}')\mathrm{grad}\, G(\rho)\,\mathrm{d}\Gamma'\,, \underline{r} \in \Gamma\,, \tag{C.9}$$

where the bar on the integral sign indicates that the point $\underline{r} = \underline{r}'$ is excluded from the integration.

C.2 Integral in MFIE

This appendix deals with the limiting value of the integral

$$I = \hat{n} \times \left(\mathrm{curl}\int_{\Gamma}\underline{j}(\underline{r}')\,G(\rho)\,\mathrm{d}\Gamma'\right), \tag{C.10}$$

as the observation point $\underline{r}$ approaches the surface Γ. The derivation hereafter closely follows the one in Section C.1, the same definitions hold. It is safe to move the curl inside the integral when the observation point $\underline{r}$ is not on Γ. The current density $\underline{j}(\underline{r}')$ is constant with respect to the unprimed coordinates which implies

$$\mathrm{curl}\left(\underline{j}(\underline{r}')G(\rho)\right) = -\underline{j}(\underline{r}') \times \mathrm{grad}\, G(\rho)\,. \tag{C.11}$$

The integral is separated into two integrals $I = I_{\Gamma\setminus\delta\Gamma} + I_{\delta\Gamma}$ as

$$I_{\Gamma\setminus\delta\Gamma} = -\hat{n} \times \int_{\Gamma\setminus\delta\Gamma} \underline{j}(\underline{r}') \times \operatorname{grad} G(\rho)\, \mathrm{d}\Gamma' \,, \quad \underline{r} \notin \Gamma \,, \tag{C.12}$$

$$I_{\delta\Gamma} = -\hat{n} \times \int_{\delta\Gamma} \underline{j}(\underline{r}') \times \operatorname{grad} G(\rho)\, \mathrm{d}\Gamma' \,, \quad \underline{r} \notin \Gamma \,. \tag{C.13}$$

The integral $I_{\delta\Gamma}$ is now considered further. When δ_0 is sufficiently small the approximation $\underline{j}(\underline{r}') \approx \underline{j}(\underline{r}_0)$ is reasonable. Evaluating $\operatorname{grad} G$ and using $\mathrm{d}\Gamma' = \delta \mathrm{d}\phi \mathrm{d}\delta$ yields

$$I_{\delta\Gamma} \approx \hat{n} \times \left(\frac{\underline{j}(\underline{r}_0)}{4\pi} \times \int_{\delta=0}^{\delta_0} \int_{\phi=0}^{2\pi} \left(\frac{1}{\rho} + \imath k \right) \underline{\rho}\, \frac{e^{-\imath k \rho}}{\rho^2}\, \delta \mathrm{d}\phi \mathrm{d}\delta \right) . \tag{C.14}$$

The integral in this expression was already treated in (C.5). Under the same suppositions, we obtain

$$I_{\delta\Gamma} \approx \hat{n} \times \left(\frac{\underline{j}(\underline{r}_0)}{2} \times \hat{n} \right) = \frac{\underline{j}(\underline{r}_0)}{2} \,. \tag{C.15}$$

For $\delta \to 0$, $\delta\Gamma$ tends to a single point. For an observation point on the surface, (C.10) can thus be written as

$$I = \frac{\underline{j}(\underline{r})}{2} - \hat{n} \times \barint_{\Gamma} \underline{j}(\underline{r}') \times \operatorname{grad} G(\rho)\, \mathrm{d}\Gamma' \,, \quad \underline{r} \in \Gamma \,, \tag{C.16}$$

where the bar on the integral sign indicates that the point $\underline{r} = \underline{r}'$ is excluded from the integration.

Appendix D

Source modelling

There are two main types of source models: the *delta-gap* voltage source [Balanis, 1997; Junker *et al.*, 1995] and the *frill generator* [Balanis, 1997; Fikioris *et al.*, 2003]. Both are depicted in Figure D.1.

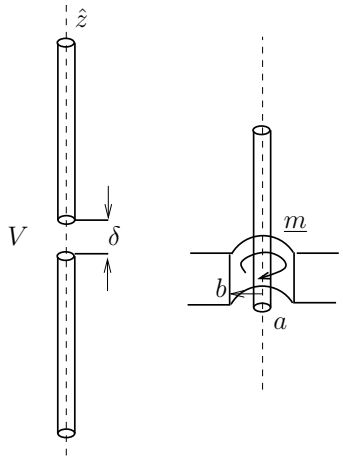

Figure D.1: Source modelling: delta-gap voltage source (left) and frill generator (right)

The delta-gap voltage source model assumes that the field generated within the gap is uniform. It is a good approximation for small spacings. The impressed field at the gap of the dipole is given by

$$\underline{e}_i = -\frac{V}{\delta}\hat{z}\,. \tag{D.1}$$

The source can be also modelled by an equivalent magnetic ring current which is usually referred to as frill generator. The frill generator model was introduced to calculate the fields from coaxial apertures [Tsai, 1972]. To use this model, the aperture is replaced with a circumferentially directed magnetic current:

$$\underline{m} = -\hat{n} \times \underline{e}_i = -\frac{V}{\delta}\hat{\phi}\,. \tag{D.2}$$

The fields generated on the surface of the wire (which can be approximated by those along its axis) can be computed using simple analytical expressions [Tsai, 1972; Balanis, 1997]. The inner radius a of the annular ring is usually the radius of the dipole wire. Since the dipole is fed by transmission lines, the outer radius b of the equivalent annular ring is found using the expression for the characteristic impedance of the transmission line. The field along the axis is given by

$$\underline{e}_i|_{axis} \approx -\frac{V}{2\ln(b/a)}\left[\frac{e^{-ik\sqrt{z^2+a^2}}}{\sqrt{z^2+a^2}} + \frac{e^{-ik\sqrt{z^2+b^2}}}{\sqrt{z^2+b^2}}\right]\hat{z}\,. \tag{D.3}$$

Bibliography

Abramowitz, M., & Stegun, I. A. (1970), *Handbook of Mathematical Functions*, Dover Publications.

Aksun, M. I., & Mittra, R. (1993), *Choices of expansion and testing funtiions for the method of moments applied to a class of electromagnetic problems*, IEEE Transactions on Microwave Theory and Techniques, **41**(3), 503–509.

Albanese, R., & Rubinacci, G. (1990), *Magnetostatic field computations in terms of two-component vector potentials*, International Journal for Numerical Methods in Engineering, **29**, 515–532.

Alpert, B., Beylkin, G., Coifman, R. R., & Rokhlin, V. (1993), *Wavelets for the fast solution of second-kind integral equations*, SIAM Journal of Scientific and Statistical Computing, **14**(1), 159–174.

Apalkov, D. M., & Visscher, P. B. (2003), *Fast multipole method for micromagnetic simulation of periodic structures*, IEEE Transactions on Magnetics, **39**(6), 3478–3480.

Arcioni, P., Bressan, Marco, & Perregrini, Luca. (1997), *On the evaluation of double surface integrals arising in the application of the boundary integral method to 3-D problems*, IEEE Transactions on Microwave Theory and Techniques, **45**(3), 436–439.

Arkkio, A. (1987), *Analysis of induction motors based on the numerical solution fo the magnetic field and circuit equatios*, Acta Polytechnica Scandinavica, 56.

Babuska, I., & Rheinboldt, W. C. (1979), *Adaptative approaches and reliability estimators in finite element analysis*, Journal of Computational Methods in Applied Mechanics and Engineering, **17/18**, 519–540.

Balanis, C. A. (1988), *Advanced Engineering Electromagnetics*, John Wiley & Sons.

Balanis, C. A. (1997), *Antenna Theory Analysis and Design*, John Wiley & Sons.

Balasubramanian, S., & Shanker, B. (2002), *Fast-integral-equation scheme for computing magnetostatic fields in nonlinear media*, IEEE Transactions on Magnetics, **38**(5), 3426–3432.

Barakat, K., & Webb, J. P. (2004), *A clustering algorithm for multi-level fast multipole methods*, IEEE Transactions on Magnetics, **40**(2), 1072–1075.

Barmada, S., Musolino, A., & Raugi, M. (2000), *Hybrid FEM/MOM formulation for eddy current problems with moving conductors*, IEEE Transactions on Magnetics, **36**(4), 827–830.

Beatson, R. K., Cherrie, J. B., & Mouat, C. T. (1999), *Fast fitting of radial basis functions: Methods baded on preconditioned GMRES iteration*, Advances in Computational Mathematics, **11**, 253–270.

Berenger, J. P. (1994), *A perfectly matched layer for the absorption of electromagnetic waves*, Journal of Computational Physics, **114**, 185–200.

Beylkin, G., Coifman, R. R., & Rokhlin, V. (1991), *Fast wavelet transforms and numerical algorithms I.*, Comm. Pure and Appl. Math., **44**, 141–183.

Bindiganavale, S. S., & Volakis, J. L. (1996), *Guidelines for using the fast multipole method to calculate the RCS of large objects*, Microwave and Optical Technology Letters, **11**(4), 190–194.

Bindiganavale, S. S., & Volakis, J. L. (1997), *A hybrid FE-FMM technique for electromagnetic scattering*, IEEE Transactions on Antennas and Propagation, **45**(1), 180–181.

Biró, O., & Preis, K. (1989), *On the use of the magnetic vector potential in the finite element analysis of three-dimensional eddy currents*, IEEE Transactions on Magnetics, **25**(4), 3145–3159.

Bossavit, A. (1988a), *Magnetostatic problems in multiply connected regions: some properties of the curl operator*, IEE Proceedings, **135, Pt. A**(3), 179–187.

Bossavit, A. (1988b), *Whitney Forms: a Class of Finite Elements for Three-Dimensional Computations in Electromagnetism*, IEE Proceedings, **135, Pt. A**(8), 493–499.

Bossavit, A. (1989), *Un nouveau point de vue sur les éléments mixtes*, Bulletin de la Société de Mathématiques Appliquées et Industrielles, **20**, 23–35.

Bossavit, A. (1993), *Électromagnétisme, en vue de la modélisation*, Springer-Verlag.

Bossavit, A. (1998a), *Computational Electromagnetism. Variational Formulations, Edge Elements, Complementarity*, Academic Press Inc.

Bossavit, A. (1998b), *A Rationale for "Edge-Elements" In 3-D Fields Computations*, IEEE Transactions on Magnetics, **24**(1), 74–79.

Bossavit, A. (2002), *Generating Whitney forms of polynomial degree one and higher*, To appear in IEEE Transactions on Magnetics, **38**(2).

Bossavit, A., & Vérité, J.-C. (1982), *A mixed FEM-BIEM method to solve 3D eddy current problems*, IEEE Transactions on Magnetics, **18**(2), 431–435.

Bossavit, A., & Vérité, J.-C. (1983), *The "TRIFOU" Code: Solving the 3-D Eddy-Currents Problem by Using H as State Variable*, IEEE Transactions on Magnetics, **19**(6), 2465–2471.

Bossavit, A., Vourdas, A., & Binns, K. J. (1989), *Correspondence on "Magnetostatics with scalar potentials in multiply connected regions"*, IEE Proceedings, **136, Pt. A**(5), 260–261.

Brebbia, C. A., & Walker, S. (1980), *Boundary Element Techniques in Engineering*, Newnes-Butterworth.

Brennan, C., & Cullen, P. J. (1998), *Application of the fast far-field approximation to the computation of UHF pathloss over irregular terrain*, IEEE Transactions on Antennas and Propagation, **46**(6), 881–890.

Brown, E. R. (1998), *RF-MEMS switches for reconfigurable integrated circuits*, IEEE Transactions on Microwave Theory and Techniques, **46**(11), 1868–1880.

Brunotte, X., Meunier, G., & Imhoff, J.-F. (1992), *Finite element modeling of unbounded problems using transformations : a rigorous, powerful and easy solution*, IEEE Transactions on Magnetics, **28**(2), 1663–1666.

Buchau, A., & Rucker, W. M. (2002), *Preconditioned fast adaptive multipole boundary-element method*, IEEE Transactions on Magnetics, **38**(2), 461–464.

Buchau, A., Huber, C. J., Rieger, W., & Rucker, W. M. (2000), *Fast BEM computations with the adaptive multilevel fast multipole method*, IEEE Transactions on Magnetics, **36**(4), 680–684.

Buchau, A., Rieger, W., & Rucker, W. M. (2001), *BEM computations using the fast multipole method in combination with higher order elements and the Galerkin method*, IEEE Transactions on Magnetics, **37**(5), 3181–3185.

Buchau, A., Hafla, W., Groh, F., & Rucker, W. M. (2003), *Improved grouping scheme and meshing strategies for the fast multipole method*, COMPEL, **22**(3).

Burkholder, R. J., & Kwon, D.-H. (1996), *High-frequency asymptotic acceleration of the fast multipole method*, Radio Science, **31**(5), 1199–1206.

Canning, F. X. (1990), *The impedance matrix-localization (IML) method for moment-method calculations*, IEEE Antennas and Propagation Magazine, **32**(5), 18–30.

Canning, F. X. (1993), *Improved impedance matrix localization method*, IEEE Transactions on Antennas and Propagation, **41**(5), 659–667.

Chen, K. (1998), *On a class of preconditioning methods for dense linear systems from boundary elements*, SIAM Journal on Scientific Computing, **20**(2), 654–698.

Chew, W. C. (1995), *Waves and Fields in Inhomogeneous Media*, IEEE Press.

Chew, W. C., Cui, T. J., & Song, J. M. (2002), *A FAFFA-MLFMA algorithm for electromagnetic scattering*, IEEE Transactions on Antennas and Propagation, **50**(November), 1641–1649.

Clemmow, P. C. (1950), *Some extensions to the method of integration by steepest descents*, Q. J. Mech. Appl. Math, **3**, 241–256.

Coifman, R., Rokhlin, V., & Wandzura, S. (1993), *The fast multipole method for the wave equation: A pedestrian prescription*, IEEE Antennas and Propagation Magazine, **35**(3), 7–12.

Coventor, Inc. (2003), *Accelerating MEMS Innovations*, http://www.coventor.com.

Darve, E. (2000), *The fast multipole method I: Error analysis and asymptotic complexity*, SIAM Journal on Numerical Analysis, **38**(1), 98–128.

Dautray, R., & Lions, J.-L. (1988), *Analyse mathématique et calcul numérique pour les sciences et les techniques*, Vol. 5, Spectres des Opérateurs, Masson.

Davey, K. (1989), *Analytical integration of linear three-dimensional triangular elements in BEM*, Applied mathematical modelling, **13**(August), 450–461.

Delves, L. M., & Walsh, J. (1974), *Numeric solution of integral equations*, Oxford University Press.

Donepudi, K. C., Jin, J.-M., Velamparambil, S., Song, J., & Chew, W. C. (2001), *A higher order parallelized multilevel fast multipole algorithm for 3-D scattering*, IEEE Transactions on Antennas and Propagation, **49**(7), 1069–1078.

Dular, P., Hody, J.-Y., Nicolet, A., Genon, A., & Legros, W. (1994), *Mixed finite elements associated with a collection of tetrahedra, hexahedra and prisms*, IEEE Transactions on Magnetics, **30**(5), 2980–2983.

Dular, P., Henrotte, F., Robert, F., Genon, A., & Legros, W. (1997), *A generalized source magnetic field calculation method for inductors of any shape*, IEEE Transactions on Magnetics, **33**(2), 1398–1401.

Dular, P., Legros, W., & Nicolet, A. (1998), *Coupling of local and global quantities in various finite element formulations and its application to electrostatics, magnetostatics and magnetodynamics*, IEEE Transactions on Magnetics, **34**(5), 3078–3081.

Dular, P., Geuzaine, C., & Legros, W. (1999), *A natural method for coupling magnetodynamic h-formulations and circuit equations*, IEEE Transactions on Magnetics, **35**(3), 1626–1629.

Dular, P., Kuo-Peng, P., Geuzaine, C., Sadowski, N., & Bastos, J. P. A. (2000), *Dual Magnetodynamic Formulations and their Source Fields associated with Massive and Stranded Inductors*, IEEE Transactions on Magnetics, **36**(4), 1293–1299.

Eibert, T. F., Sertel, K., & Volakis, J. L. (2000), *Hybrid finite element modelling of conformal antenna and array structures utilizing fast integral methods*, International Journal of Numerical Modelling, **13**, 81–101.

Emson, C. R. I., & Simkin, J. (1983), *An optimal method for 3-D eddy currents*, IEEE Transactions on Magnetics, **19**(6), 2450–2452.

Engheta, N., Murphy, W. D., Rokhlin, V., & Vassiliou, M. S. (1992), *The fast multipole method (FMM) for electromagnetic Scattering problems*, IEEE Transactions on Antennas and Propagation, **40**(6), 634–641.

Fang, J., & Wu, Z. (1995), *Generalized perfectly matched layer–an extension of Berenger's perfectly matched layer boundary condition*, IEEE Microwave and Guided Wave Letters, **5**(12), 451–453.

Farina, M., & Rozzi, T. (2001), *A 3D integral equation-based approach to the analysis of real-life MMICS–Application to Microelectromechanical systems*, IEEE Transactions on Microwave Theory and Techniques, **49**(12), 2235–2240.

Femlab. (2003), *Multiphysics in MATLAB*, http://www.femlab.com.

Fetzer, J., Kurz, S., & Lehner, G. (1997), *Comparison of analytical and numerical integration techniques for the boundary integrals in the BEM-FEM coupling considering workshop problem no. 13*, IEEE Transactions on Magnetics, **33**(2), 1227–1230.

Fetzer, J., Kurz, S., Lehner, G., & Rucker, W. M. (1999), *Analysis of an actuator with eddy currents and iron saturation: Comparison between a FEM and a BEM-FEM coupling approach*, IEEE Transactions on Magnetics, **35**(3), 1793–1796.

Fetzer, J., Kurz, S., Lehner, G., & Rucker, W. M. (2000), *Application of the BEM-FEM coupling and the vector Preisach model for the calculation of 3D magnetic fields in media with hysteresis*, IEEE Transactions on Magnetics, **36**(4), 1258–1262.

Fikioris, G., Lionas, J., & Lioutas, C. G. (2003), *The use of the frill generator in thin-wire integral equations*, IEEE Transactions on Antennas and Propagation, **51**(8), 1847–1854.

Forsman, K., & Kettunen, L. (1997), *Hybrid and Integral Formulations for 3D Eddy Current Problems*, IEEE Transactions on Magnetics, **33**(2), 1255–1258.

Forsman, K., Gropp, W., Kettunen, L., Levine, D., & Salonen, J. (1995), *Solution of dense systems of linear equations arising from integral-equation formulations*, IEEE Antennas and Propagation Magazine, **37**(6), 96–100.

Fowler, A. C. (1997), *Mathematical models in the applied sciences*, Cambridge University Press.

Geng, N., Sullivan, A., & Carin, L. (2001), *Fast multipole method for scattering from an arbitrary PEC target above or buried in a lossy half space*, IEEE Transactions on Antennas and Propagation, **49**(5), 740–748.

GetDP. (1997–2004), *GetDP, a general environment for the treatment of discrete problems*, http://www.geuz.org/getdp/.

Geuzaine, C. (2001), *High-Order hybrid finite element schemes for Maxwell's equations taking thin structures and global quantities into account*, Ph.D. thesis 212, University of Liège, Belgium, Faculty of Applied Sciences.

Geuzaine, C., Meys, B., Dular, P., & Legros, W. (1999a), *Convergence of High Order Curl-Conforming Finite Elements*, IEEE Transactions on Magnetics, **35**(3), 1442–1445.

Geuzaine, C., Dular, P., & Legros, W. (1999b), *Dual Formulations for the Modeling of Thin Conducting Magnetic Shells*, COMPEL, **18**(3), 385–397.

Geuzaine, C., Tarhasaari, T., Kettunen, L., & Dular, P. (2001), *Discretization Schemes for Hybrid Methods*, IEEE Transactions on Magnetics, **37**(5), 3112–3115.

Glisson, A. W., & Wilton, D. R. (1980), *Simple and efficient numerical methods for problems of electromagnetic radiation and scattering from surfaces*, IEEE Transactions on Antennas and Propagation, **28**(5), 593–603.

Golub, G. H., & Welsch, J. H. (1969), *Calculation of Gauss quadrature rules*, Mathematics of computations, **22**, 221–230.

Graglia, R. D. (1987), *Static and dynamic potential integrals for linearly varying source distributions in two- and three-dimensional problems*, IEEE Transactions on Antennas and Propagation, **35**(6), 662–669.

Graglia, R. D. (1993), *On the numerical integration of the linear shape functions times the 3-D Green's function or its gradient on a plane triangle*, IEEE Transactions on Antennas and Propagation, **41**(10), 1448–1455.

Graglia, R. D., Wilton, D. R., & Peterson, A. F. (1997), *Higher order interpolatory vector Bases for computational electromagnetics*, IEEE Transactions on Antennas and Propagation, **45**(3), 329–342.

Greengard, L., & Rokhlin, V. (1987a), *A Fast Algorithm for Particle Simulations*, Journal of Computational Physics, **73**(2), 325–348.

Greengard, L., & Rokhlin, V. (1987b), *Rapid evaluation of potential fields in three dimensions*, Technical report YALEU/DCS/RR-515, Department of Computer Science, Yale University, New Haven, CT.

Greengard, L., & Rokhlin, V. (1988), *On the efficient implementation of the fast multipole algorithm*, Technical report YALEU/DCS/RR-602, Department of Computer Science, Yale University, New Haven, CT, 1995.

Gürel, L., Sertel, K., & Sendur, I. K. (1999), *On the choice of basis functions to model surface electric current densities in computational electromagnetics*, Radio Science, **34**(6), 1373–1387.

Harrington, R. F. (1961), *Time-Harmonic Electromagnetic Fields*, McGraw-Hill.

Harrington, R. F. (1993), *Field computation by moment method*, IEEE Press.

Henrotte, F. (2000), *Modélisation des efforts électromagnétiques et de leurs effets dans des structures quelconques*, Ph.D. thesis 201, University of Liège, Belgium, Faculty of Applied Sciences.

Henrotte, F., Nicolet, A., Hedia, H., Genon, A., & Legros, W. (1994), *Modelling of electromechanical relays taking into account movement and electric circuits*, IEEE Transactions on Magnetics, **30**(5), 3236–3239.

Henrotte, F., Deliège, G., & Hameyer, K. (2003), *The eggshell method for the computation of electromagnetic forces on rigid bodies in 2D and 3D*, Proceedings of the 6th international symposium on electric and magnetic fields, EMF'2003, Aachen, Germany, October 6–9, 2003. Proceedings paper 3/2, pages 55–58, October.

Hsiao, G. C., & Kleinman, R. E. (1997), *Mathematical foundations for error estimation in numerical solutions of integral equations in electromagnetics*, IEEE Transactions on Antennas and Propagation, **45**(3), 316–328.

Jackson, J. D. (1998), *Classical Electrodynamics*, third edn., John Wiley & Sons.

Jiles, D. (1991), *Magnetism and magnetic materials*, Chapman and Hall.

Jin, J.-M., Volakis, J. L., & Collins, J. D. (1991), *A finite element-boundary integral method for scattering and radiation by two- and three-dimensional structures*, IEEE Antennas and Propagation Magazine, **33**(3), 22–32.

Jonhson, C. (1987), *Numerical solution of partial differential equations by the finite element method*, Cambridge University Press.

Junker, G. P., Kishk, A. A., & Glisson, A. W. (1995), *A novel delta gap source model for center fed cylindrical dipoles*, IEEE Transactions on Antennas and Propagation, **43**(5), 537–540.

Kameari, A. (1990), *Calculation of Transient 3D Eddy Current Using Edge-Elements*, IEEE Transactions on Magnetics, **26**(2), 466–469.

Karl, H., Fetzer, J., Kurz, S., Lehner, G., & Rucker, W. M. (1999), *Description of TEAM workshop problem 28: An electrodynamic levitation device*, http://ics.ec.lyon.fr/team.html.

Kettunen, L., Forsman, K., & Bossavit, A. (1998), *Discrete Spaces for Div and Curl-Free Fields*, IEEE Transactions on Magnetics, **34**(5), 2551–2554.

Kettunen, L., Forsman, K., & Bossavit, A. (1999), *Gauging in Whitney spaces*, IEEE Transactions on Magnetics, **35**(3), 1466–1469.

Kim, H., Ling, H., & Lee, C. (1996), *A fast moment method algorithm using spectral domain wavelet concepts*, Radio Science, **31**(5), 1253–1261.

Kittel, C. (1996), *Introduction to solid state physics*, seventh edn., John Wiley & Sons.

Koc, S., Song, J., & Chew, W. C. (1999), *Error analysis for the numerical evaluation of the diagonal forms of the scalar spherical addition theorem*, SIAM Journal on Numerical Analysis, **36**(3), 906–921.

Kotiuga, P. R. (1987), *On Making Cuts for Magnetic Scalar Potentials in Multiply Connected Regions*, Journal of Applied Physics, **63**(8), 3916–3918.

Kurz, S., Fetzer, J., Lehner, G., & Rucker, W. M. (1998), *A novel formulation for 3D eddy current problems with moving bodies using a lagrangian description and BEM-FEM coupling*, IEEE Transactions on Magnetics, **34**(5), 3068–3073.

Labreuche, C. (1998), *A convergence theorem for the multipole method for 2 dimensional scattering problems*, Mathematics of computation, **67**(222), 553–591.

Lacroux, G. (1989), *Les aimants permanents*, Lavoisier.

Lee, J.-F., Lee, R., & Burkholder, R. J. (2003), *Loop star basis functions and a robust preconditioner for EFIE scattering problems*, IEEE Transactions on Antennas and Propagation, **51**(8), 1855–1863.

Lombart, P., & Meunier, G. (1993), *A general purpose method for electric and magnetic combined problems for 2D, axisymmetric and transient systems*, IEEE Transactions on Magnetics, **29**(2), 1737–1740.

Lu, C. C., & Chew, W. C. (1993), *Fast algorithm for solving hybrid integral equations*, IEE Proceedings, Pt. H, **140**(6), 455–460.

Lu, C. C., & Chew, W. C. (1994), *A multilevel algorithm for solving a boundary integral equation of wave scattering*, Microwave and Optical Technology Letters, **7**(10), 466–470.

Lu, C. C., & Chew, W. C. (1995), *Fast far field approximation for calculating the RCS of large objects*, Microwave and Optical Technology Letters, **8**(5), 238–241.

Lu, N., & Jin, J.-M. (1996), *Application of fast multipole method to finite-element boundary-integral solution of scattering problems*, IEEE Transactions on Antennas and Propagation, **44**(6), 781–786.

Mautz, J. R., & Harrington, R. F. (1978), *H-field, E-field and combined field solutions for conducting bodies of revolution*, Arch. Electr. Uberstragung., **32**, 157–164.

Maxwell, J. C. (1891), *A Treatise on Electricity and Magnetism*, third edn., Clarendon Press.

Mayergoyz, I. D., Andrei, P., & Dimian, M. (2003), *Nonlinear magnetostatic calculations based on the fast multipole method*, IEEE Transactions on Magnetics, **39**(3), 1103–1106.

McLaren, A. D. (1963), *Optimal integration on a sphere*, Mathematics of Computation, **17**, 361–383.

Meys, B. (1999), *Modélisation des champs électromagnétiques aux hyperfréquences par la méthode des éléments finis. Application aux problème du chauffage diélectrique*, Ph.D. thesis, University of Liège, Belgium, Faculty of Applied Sciences.

Mur, G., & de Hoop, A. T. (1985), *A Finite-Element Method for Computing Three-Dimensional Electromagnetic Fields in Inhomogeneous Media*, IEEE Transactions on Magnetics, **MAG-21**(6), 2188–2191.

Nabors, K., & White, J. (1991), *FastCap: A multipole accelerated 3-D capacitance extraction program*, IEEE Transactions on Computer-Aided Design, **10**(11), 1447–1459.

Nabors, K., & White, J. (1992), *Multipole-accelerated capacitance extraction algorithms for 3-D structures with multiple dielectrics*, IEEE Transactions on Circuits and Systems – I: Fundamental Theory and Applications, **39**(11), 946–954.

Nabors, K., Kim, S., & White, J. (1992), *Fast capacitance extraction of general three-dimensional structures*, IEEE Transactions on Microwave Theory and Techniques, **40**(7), 1496–1506.

Nabors, K., Korsmeyer, F. T., Leighton, F. T., & White, J. (1994), *Preconditioned, adaptive, multipole-accelerated iterative methods for three-dimensional first-kind integral equations of potential theory*, SIAM Journal on Scientific Computing, **15**(3), 713–735.

Petersen, H. G., Smith, E. R., & Sølvason, D. (1995a), *Error estimates for the fast multipole method. I. The two-dimensional case.*, Proceedings of the Royal Society of London, serie A, **448**(March), 389–400.

Petersen, H. G., Smith, E. R., & Sølvason, D. (1995b), *Error estimates for the fast multipole method. II. The three-dimensional case.*, Proceedings of the Royal Society of London, serie A, **448**(March), 401–418.

Peterson, A. F. (1990), *The "interior resonance" problem associated with surface integral equations of electromagnetics: Numerical consequences and survey of remedies*, Electromagnetics, **10**(3), 293–312.

Peterson, A. F., Wilton, D. R., & Jorgenson, R. E. (1996), *Variational nature of galerkin and non-galerkin moment method solutions*, IEEE Transactions on Antennas and Propagation, **44**(4), 500–503.

Peterson, A. F., Ray, S. L., & Mittra, R. (1998), *Computational methods for electromagnetics*, IEEE Press.

Pilkey, Walter D. (2002), *Analysis and design of elastic beams: Computational methods*, John Wiley & Sons.

Ramo, S., Whinnery, J. R., & Duzer, T. Van. (1984), *Fields and Waves in Communication Electronics*, John Wiley & Sons.

Rao, S. M. (1980), *Electromagnetic scattering and radiation of arbitrarily-shaped surfaces by triangular patch modeling*, Ph.D. thesis, University of Mississippi.

Rao, S. M., & Wilton, D. R. (1990), *E-field, H-field, and Combined Field Solution for Arbitrary Shaped Three Dimensional Dielectric Objects*, Electromagnetics, **10**(4), 407–421.

Rao, S. M., Wilton, D. R., & Glisson, A. W. (1982), *Electromagnetic scattering by surfaces of arbitrary shape*, IEEE Transactions on Antennas and Propagation, **30**(3), 409–417.

Rao, S. M., Sarkar, T. K., & Harrington, R. F. (1984), *The electrostatic field of conducting bodies in multiple dielectric media*, IEEE Transactions on Microwave Theory and Techniques, **32**(11), 1441–1448.

Ren, Z., & Ida, N. (2000), *High-order elements of complete and incomplete bases in electromagnetic field computation*, IEEE Transactions on Magnetics, **36**(4), 1472–1478.

Ren, Z., & Razek, A. (1990), *Force calculation by Maxwell stress tensor in 3D hybrid finite element-boundary element integral formulation*, IEEE Transactions on Magnetics, **26**(5), 2774–2776.

Ren, Z., Bouillault, F., Razek, A., & Vérité, J.-C. (1988), *Comparison of Different Boundary Integral Formulations when Coupled with Finite Elements in Three Dimensions*, IEE Proceedings, **135, Pt. A**(8), 501–507.

Ren, Z., Bouillault, F., Razek, A., Bossavit, A., & Vérité, J.-C. (1990), *A New Hybrid Model Using Electric Field Formulation for 3D Eddy Current Problems*, IEEE Transactions on Magnetics, **26**(2), 470–473.

Ren, Z., Li, C., & Razek, A. (1992), *Hybrid FEM-BIM formulation using electric and magnetic variables*, IEEE Transactions on Magnetics, **28**(2), 1647–1650.

Rischmüller, V., Haas, M., Kurz, S., & Rucker, W. M. (2000), *3D transient analysis of electromechanical devices using parallel BEM coupled to FEM*, IEEE Transactions on Magnetics, **36**(4), 1360–1363.

Rokhlin, V. (1985), *Rapid solution of integral equations of classical potential theory*, Journal of Computational Physics, **60**(2), 187–207.

Rokhlin, V. (1990), *Rapid solution of integral equations of scattering theory in two dimensions*, Journal of Computational Physics, **86**(2), 414–439.

Rokhlin, V. (1993), *Diagonal forms of translation operators for the Helmholtz equation in three dimensions*, Applied and Computational Harmonic Analysis, 82–93.

Saad, Y., & Schultz, M. H. (1986), *GMRES: A Generalized Minimal Residual Algorithm for solving nonsymmetric linear systems*, SIAM Journal of Scientific and Statistical Computing, **7**(3), 856–869.

Sabariego, R. V., Gyselinck, J., Geuzaine, C., Dular, P., & Legros, W. (2003), *Application of the fast multipole method to the finite element - boundary element analysis of electromechanical devices*, COMPEL International Journal for Computation and Mathematics in Electrical and Electronic Engineering, **22**(3).

Sabariego, R. V., Gyselinck, J., Geuzaine, C., Dular, P., & Legros, W. (2004a), *Application of the fast multipole method to hybrid finite element–boundary element models*, Journal of Computational and Applied Mathematics, **168**, 403–412.

Sabariego, R. V., Gyselinck, J., Dular, P., Coster, J. De, Henrotte, F., & Hameyer, K. (2004b), *Coupled mechanical-Electrostatic FE-BE Analysis with FMM acceleration – Application to a shunt capacitive MEMS switch*, COMPEL International Journal for Computation and Mathematics in Electrical and Electronic Engineering, **23**(4), 876–884.

Sabariego, R. V., Sergeant, P., Gyselinck, J., Dular, P., Dupré, L., & Melkebeek, J. (2004c), *Fast 3D finite element - boundary element analysis of induction heaters with passive and active shielding*, Proceedings of Progress in Electromagnetics Research Symposium, PIERS 2004, Pisa (Italy), March 28-31, 470.

Sabariego, R. V., Gyselinck, J., Dular, P., Geuzaine, C., & Legros, W. (2004d), *Fast multipole acceleration of the hybrid finite element-boundary element analysis of 3D eddy current problems*, IEEE Transactions on Magnetics, **40**(2), 1278–1281.

Sarkar, T. K. (1985), *A note on the choice of weighting functions in the method of moments*, IEEE Transactions on Antennas and Propagation, **33**(4), 436–441.

Sarkar, T. K., Djordevic, A. R., & Arvas, E. (1985), *On the choice of expansion and weighting functions in the numerical solution of operator equations*, IEEE Transactions on Antennas and Propagation, **33**(9), 988–996.

Schelkunoff, S. A. (1964), *Electromagnetic waves*, D. Van Nostrand Company, Inc.

Sertel, K., & Volakis, J. L. (2000), *Incomplete LU preconditioner for FMM implementation*, Microwave and Optical Technology Letters, **26**(4), 265–267.

Sheng, X. Q., & Yung, E. K.-N. (2002), *Implementation and experiments of a hybrid algorithm of the MLFMA-enhanced FE-BI method for open-region inhomogeneous electromagnetic problems*, IEEE Transactions on Antennas and Propagation, **50**(2), 163–167.

Sheng, X. Q., Jin, J.-M., Song, J., Chew, W. C., & Lu, C.-C. (1998), *Solution of combined-field integral equation using multilevel fast multipole algorithm for scattering by homogeneous bodies*, IEEE Transactions on Antennas and Propagation, **46**(11), 1718–1726.

Song, J., & Chew, W. C. (1998), *The Fast Illinois Solver Code: requirements and scaling properties*, IEEE Computational Science and Engineering, **5**(3), 19–23.

Song, J., & Chew, W. C. (2001), *Error analysis for the truncation of multipole expansion of vector Green's functions*, IEEE Microwave and Wireless Components Letters, **11**(7), 311–313.

Song, J., Lu, C. C., & Chew, W. C. (1997), *Multilevel fast multipole algorithm for electromagnetic scattering by large complex objects*, IEEE Transactions on Antennas and Propagation, **45**(10), 1488–1493.

Song, J. M., & Chew, W. C. (1995), *Multilevel fast-multipole algorithm for solving combined field integral equations of electromagnetic scattering*, Microwave and Optical Technology Letters, **10**(1), 14–19.

SPARSKIT. (1999), *SPARSKIT: a basic tool-kit for sparse matrix computations*, http://www.cs.umn.edu/Research/arpa/SPARSKIT/sparskit.html.

Stratton, J. A. (1941), *Electromagnetic Theory*, McGraw-Hill.

Tilmans, H. A. C. (2002), *MEMS Components for Wireless Communications (invited paper)*, *Pages 1–34 of:* Proceedings EuroSensors XVI (CD-ROM only), September, 1–34.

Tsai, L. L. (1972), *A numerical solution for the near and far fields of an annular ring of magnetic current*, IEEE Transactions on Antennas and Propagation, **20**(5), 569–576.

Tsukerman, I. A., Konrad, A., Meunier, G., & Sabonnadière, J. C. (1993), *Coupled field-circuit problems: Trends and accomplishments*, IEEE Transactions on Magnetics, **29**(2), 1701–1704.

Van der Vorst, H., & Dekker, K. (1988), *Conjugate Gradient Type Methods and Preconditioning*, Journal of Computational Applied Mathematics, **24**, 73–87.

Vecchi, G. (1999), *Loop-star decomposition of basis functions in the discretization of the EFIE*, IEEE Transactions on Antennas and Propagation, **47**(2), 339–346.

Volakis, J. L., Özdemir, T., & Gong, J. (1997), *Hybrid finite-element methodologies for antennas and scattering*, IEEE Transactions on Antennas and Propagation, **45**(3), 493–507.

Wagner, R. L, & Chew, W. C. (1994), *A ray-propagation fast multipole algorithm*, Microwave and Optical Technology Letters, **7**(10), 435–438.

Wait, R., & Mitchell, A. R. (1985), *Finite Element Analysis and Applications*, John Wiley & Sons.

Wandzura, S. (1991), *Optimality of Galerkin method for scattering computations*, Microwave and Optical Technology Letters, **4**(5), 199–200.

Webb, J. P., & Forghani, B. (1993), *Hierarchal Scalar and Vector Tetrahedra*, IEEE Transactions on Magnetics, **29**(2), 1495–1498.

Welij, J. S. (1985), *Calculation of eddy currents in terms of h on hexahedra*, IEEE Transactions on Magnetics, **21**(6), 2239–2241.

Wilton, D. R., Rao, S. M., Glisson, A. W., Schaubert, D. H., Al-Bundak, O. M., & Butler, C. M. (1984), *Potential integrals for uniform and linear source distributions on polygonal and polyhedral domains*, IEEE Transactions on Antennas and Propagation, **32**(3), 276–281.

Yuan, X., Lynch, D. R., & Strohbehn, J. W. (1990), *Coupling of finite element and moment methods for electromagnetic scattering from inhomogeneous objects*, IEEE Transactions on Antennas and Propagation, **38**(3), 380–385.

Zienkiewicz, O. C., Kelly, D. W., & Bettess, P. (1977), *The coupling of the finite element method and boundary solution procedures*, International Journal for Numerical Methods in Engineering, **11**, 355–375.

Author Index

Generated on 17th October 2010